YA-94: A Conceptual Approach to Designing a New Close Air Support Aircraft

a project presented to
The Faculty of the Department of Aerospace Engineering
San José State University

in partial fulfillment of the requirements for the degree
Master of Science in Aerospace Engineering

by

Alexander H. Nuyn

May 2022

approved by

Mr. Sean Montgomery
Faculty Advisor

ABSTRACT

YA-94: A Conceptual Approach to Designing
A New Close Air Support Aircraft

Alexander Hillary Nuyn

The following project describes the conceptual approach of designing a new close air support (CAS) aircraft, the YA-94, succeeding the A-10 Thunderbolt II 'Warthog' in the aspect of performance, payload, and operational cost. This new aircraft will solely have a mission for CAS only and not that of a multi-role fighter like the F-35. This design was achieved using similar methods provided by Raymer's textbook, *Aircraft Design: A Conceptual Approach, Sixth Edition*, and Roskam's book series, *Airplane Design*, which analyzed various components – such as the fuselage, wing, weight and sizing estimates, and tail. MATLAB was the primary program used to calculate and analyze various sizing requirements following Raymer's/Roskam's provided methods. The RDSwin computer program was also used to calculate, iterate, and verify various aircraft design variables. XFLR5 and AVL, aerodynamic software, were used to analyze the YA-94's stability and controls, especially during trim or OEI conditions. Significant efforts were made to reduce the operational costs of this new CAS aircraft resulting in a lower cost per hour than the A-10. Featured specifications for this aircraft includes some of the following: maximum external payload capacity of 16,000 lbs, a combat radius of 250 nmi when fully loaded, two-seater cockpit, maximum climb rate of 10,000 ft/min, cruise speed of 350 knots, and using the same GE TF34 turbofan engines and GAU-8 gatling cannon both found on the A-10.

ACKNOWLEDGEMENTS

Table of Contents

List of Figures

List of Tables

List of Acronyms/Abbreviations

Acronyms/Abbreviations	Definition
AC	Air conditioner/aerodynamic center/alternating current
AM	Additive Manufacturing
AoA	Angle of attack
APU	Auxiliary power unit
AR	Aspect ratio
AVL	Athena Vortex Lattice
CAD	Computer-aided design
CAS	Close air support
CG	Center of gravity
CLS	Contractor Logistics Support
CPFH	Cost per flying hour
CTOL	Convention takeoff and landing
DEEC	Digital electronic engine control
DOC	Direct operating cost
DoD	Department of Defense
FAA	Federal Aviation Administration
FHPB	Flying-hour program budgeting
FOB	Forward operating base
FOD	Foreign object debris
FOV	Field of view
ft	foot/feet
GE	General Electric
hp	Horsepower
hrs	hours
HVAC	Heating, ventilation, and air conditioning
in	inches
JDAM	Joint direct attack munition
kg	kilogram
km	Kilometer
KPH	Kilometers per hour
lbf	Pounds force
lbs	pounds
LCC	Life-cycle cost
LOC	Line of sight
m	meters
MPH	Miles per hour
MSL	Mean sea level
MTOW	Maximum takeoff weight
N	Newtons
kN	Kilo-newtons
NACA	National Advisory Committee for Aeronautics airfoils
nmi	Nautical miles
OA-X	Observation, attack, concept

OBOGS	Onboard Oxygen Generating System
OC	Operational cost
OEI	One engine inoperative
PL	Payload
RDDMC	Research, development design, and manufacturing costs
RDTE	Research, development, testing, and engineering
RIO	Radar intercept officer
ROC	Rate of climb
SFC	Specific fuel consumption
SL	Sea level
STOL	Short takeoff and landing
STVOL	Short takeoff vertical landing
TOP	Takeoff parameter
TOW	Takeoff weight
US	United States
USAF	United States Air Force
WWII	World War 2

List of Symbols

Symbols, Coefficients, and Parameters

Symbol	Definition	Units (Imperial | Metric)
AR	Wing Aspect Ratio	-----
a	Acceleration	$ft/_{s^2} \mid m/_{s^2}$
b	Wingspan	$ft \mid m$
C	Coefficient	-----
c	Chord length	$ft \mid m$
$\bar{c}$	Mean aerodynamic chord	$ft \mid m$
c'	Chord length flap extended	$ft \mid m$
d	Diameter	$ft \mid m$
e	Oswald span efficiency	-----
FF	Form factor	-----
G	Climb gradient	-----
g	Gravity constant	$ft/_{s^2} \mid m/_{s^2}$
h	Height	$ft \mid m$
I_{xx}	Inertia moment about x-axis	$lbf \cdot ft \cdot s^2 \mid kg \cdot m^2$
I_{yy}	Inertia moment about y-axis	$lbf \cdot ft \cdot s^2 \mid kg \cdot m^2$
I_{zz}	Inertia moment about z-axis	$lbf \cdot ft \cdot s^2 \mid kg \cdot m^2$
K	Variable constant factor	-----
L/D	Lift-to-Drag Ratio	-----
l	Length	$ft \mid m$
M	Mach number	-----
M	(Pitching) Moment	$ft \cdot lbs$
$\dot{m}$	Mass flow rate	$lbm/s \mid kg/s$
N	Yaw moment	$ft \cdot lbs$
n	Load Factor	-----
P	Roll rate	deg/s
Q	Interference factor	-----
$\bar{q}$	Dynamic Pressure	$\frac{lbs}{ft \cdot s^2} \mid \frac{kg}{m \cdot s^2}$
S	Wing Area	$ft^2 \mid m^2$
s	Distance	$ft \mid m$
T	Thrust force	$lbf \mid kN$
T/W	Thrust-to-Weight Ratio	-----
t/c	Airfoil thickness ratio	-----
U	Speed	$\frac{ft}{s} \mid \frac{m}{s}$
V	Velocity	$\frac{ft}{s} \mid \frac{m}{s}$
W	Weight	$lbs \mid kg$
W/S	Wing Loading	$lbs/ft^2 \mid kg/m^2$

Greek Symbols

α	Angle of attack	degrees
γ	Flight path angle	degrees

Δ	Incremental difference	-----
ζ	Damping ratio	Radians
θ	Angle	degrees
Λ	Sweep angle	degrees
λ	Taper ratio	-----
μ	Dynamic viscosity	$slug/_{ft \cdot s} \mid kg/_{m \cdot s}$
π	pi	3.14…
ρ	density	$lbs/ft^3 \mid kg/m^3$
σ	ratio	-----
τ	Time constant	seconds
$\dot{\psi}$	Turn rate	deg/sec

Subscripts

$(\ )_c$	Component	
$(\ )_{c4}$	Quarter chord location	
$(\ )_D$	3D drag	
$(\ )_d$	2D drag	
$(\ )_e$	Empty	
$(\ )_f$	Final/Fuselage/Flap/Friction	
$(\ )_i$	Iterative/increment	
$(\ )_L$	3D lift	
$(\ )_{LE}$	Leading-edge	
$(\ )_l$	2D lift	
$(\ )_m$	(Pitching) moment	-----
$(\ )_{max}$	Maximum value	
$(\ )_{MTOW}$	Max takeoff weight	
$(\ )_{ref}$	Reference	
$(\ )_{reqd}$	Required	
$(\ )_T$	Due to thrust	
$(\ )_{VS}$	Variable sweep	
$(\ )_{VT}$	Vertical tail	
$(\ )_W$	Wing	
$(\ )_{wet}$	Wetted area	
$(\ )_{wm}$	Windmilling	
$(\ )_0$	Initial value	
$(\ )_1$	Steady	

Chapter 1 – Introduction

1.1   General Overview

Close air support, or CAS, is a predominant method to display air superiority. It is a military action in supporting ground forces using aerial strikes from an aircraft. CAS was first used back in the First World War when the British designed the first ground-attack aircraft, a modified F.E 2b fighter capable of carrying 20 lb bombs and mounted machine guns [1]. After exhausting their ammunition, the planes would rearm and refuel before returning to the battle zone to provide additional CAS. This tactic was later judged critical in places where infantry was pinned down [2].

The evolving battlefield required CAS to evolve with it, introducing more designated aircraft to fulfill the CAS roles. In modern-day, these include various military helicopters, the Lockheed AC-130 gunship, and the A-10 Thunderbolt II. First introduced back in October 1977, the A-10, also known as the Warthog, was manufactured by Fairchild Republic and was designed solely for providing CAS for friendly ground troops, attacking armored vehicles, and providing quick-action support against enemy ground forces [3]. The A-10 is still in service for the U.S. Air Force, with its service life extended to 2040 with no planned retirement date [4]. This project aims to explore a conceptual design of a new CAS aircraft for the new modern battlefield while possibly improving the range and payload aspects of the A-10.

1.2   Literature Review

Close air support is a crucial and dangerous tactic needed in the armed forces requiring specific aircraft designed for this type of mission. This section covers the details of CAS, the outlook for designing aircraft for this role, and the current aircraft fulfilling this mission with their respective features.

1.2.1   CAS

In terms of military tactics, described in a joint publication by the U.S. Department of Defense (DoD), CAS is defined as an air action where fixed or rotary-winged aircraft perform airstrikes against hostile targets near friendly forces [5]. This required detailed integration of each air mission with the fire and movement of the following forces: attacks with aerial bombs, glide bombs, missiles, rockets, aircraft cannons, and even directed-energy weapons (e.g., lasers). CAS requires excellent coordination with friendly ground forces due to how closely performed these attacks are. From the perspective of a land-force commander, air power's most significant contribution is in weakening and impeding enemy forces before they reach friendly troops. An article from Task and Purpose reaffirms this insight. This partnership approach between ground and airborne forces is the most suitable against the largest number of adversaries. It can easily be adjusted toward greater prominence for either partner [6].

Several opportunities are made available with CAS. One key finding in military operations is the increased Army's interest in air attacks. Currently, the Army seeks to become more strategically deployable and agile on the battlefield, thus reducing the weight of ground-based munitions such as artillery brigades and increasing Army requests for CAS and air interdiction [6].

The opportunities for effective partnering of air and ground forces are likely to grow significantly in the future. It is recommended that the Army and the Air Force collaborate and develop new concepts and technologies to speed up this process. This includes a new aircraft with updated technology that would effectively designate targets while ensuring essential oversight of friendly ground forces remains roaming over the battlefield [6]. The DoD realized CAS is not just a critical tactic but a crucial partnership between ground and air forces to overcome great adversaries they might face.

1.2.2   Future Of Attack Aircraft

As mentioned before, with the state of ground combat evolving every day, the concept of CAS must evolve with it. This evolution includes communication systems, integration methods, weapons, and even the aircraft itself. In a notable event, described in *The Light Aircraft* by Weisgerber, jet-powered fighters have been a constant presence, striking critical targets and carrying out other missions during the US-led wars in Afghanistan and Iraq [7]. However, the sounds of thunderous jet engines could be competing with the return of the high-pitched wail of the turboprop. Based on this article, the U.S. Air Force (USAF) is currently deciding whether to bring the return of light, prop-driven attack aircraft. In other words, the fleet of military aircraft may see a mix of both prop-driven and jet-powered aircraft sortied for irregular conflicts. This

change stems from two significant findings. First, it has become more noticeable that Air Force pilots are dropping fewer bombs and performing more armed overwatch missions. Moreover, second, the degradation of high-performance aircraft has become more prominent in brutally fast-paced operations since 2001. One year in Southwest Asia is equivalent to five to seven years of real-time degradation.

Therefore, the USAF believes the inclusion of turboprop-driven light attack aircraft may solve this problem. It could reduce billions annually from USAF's operation and maintenance costs. In addition, compared to jet fighters, light attack aircraft consume much less fuel allowing them to fly for hours without refueling. The article also noted that these light attack aircraft are desired to be two-seater aircraft. It is known that a pilot's situational awareness is often reduced during a two-ship tasking as one aircraft is frequently getting gas from a tanker while the other aircraft performs the CAS mission. Air Combat Command determined that this creates an unacceptable burden of responsibility for low-time, inexperienced wingmen. Therefore, if an aircraft provides a two-seater design, the rear controller could manage forward air control, strike coordination and reconnaissance, air interdiction, and joint terminal attack controller training. At the same time, the primary pilot can concentrate on their primary task, which is close air support and armed reconnaissance. As one field grade officer opined, this would allow lieutenants and captains to gain their needed combat experience and get better at what they do.

In addition to the USAF's desired design aspect of a future attack aircraft, the Military Institute of Science and Technology at Dhaka performed a design and optimization study for ground attack aircraft [8]. This report suggests minimum mission requirements that a newly conceptualized attack aircraft must meet to be considered an attack aircraft. These requirements were extracted from a market analysis, regarded as applicable requirements for aircraft design: a minimum range of 1,080 nautical miles, maximum Mach number of 0.65, a ceiling flight of 45,000 ft, payload capability of 16,000 lbs, and a load factor ranging between +4 to -3.

Their configuration involved a bullet-shaped fuselage, low-wing design, an H-tail, high bypass turbofan engines for propulsion, and retractable landing gear. The fuselage requires a minimum fuel volume capacity of 187 ft^3 and a single pilot on board. Therefore, their fuselage design had an overall length of 49 ft and a diameter of 5 ft. The wing design is needed to produce enough lift to carry out the entire mission requirement while having enough strength to carry fuel, payload, and engines onboard. Thus, the team selected a NACA-2415 airfoil which yielded an ideal lift coefficient of 1.1 and a net maximum lift coefficient of 1.5. As for the tail design, an "H" tail was selected to obscure the hot exhaust gases produced by the engines to prevent heat-seeking devices from locking on. A high bypass turbofan was chosen as it was the best option for a subsonic attack aircraft, with both engines mounted aft and over the fuselage with pylons. Finally, retractable landing gear allows their aircraft to be more aerodynamically efficient.

When comparing their aircraft to the existing A-10, it had an overall smaller fuselage length with a reasonably longer wingspan. Unfortunately, it resulted in a lower take-off weight with a difference of roughly 5,000 lbs. The thrust-to-weight ratio is slightly higher, with a value of 0.39 compared to the A-10's thrust-to-weight ratio of 0.36. The study declared the design a noteworthy success. Figure 1.1 shows their final aircraft design, which undoubtedly has a similar look to the A-10.
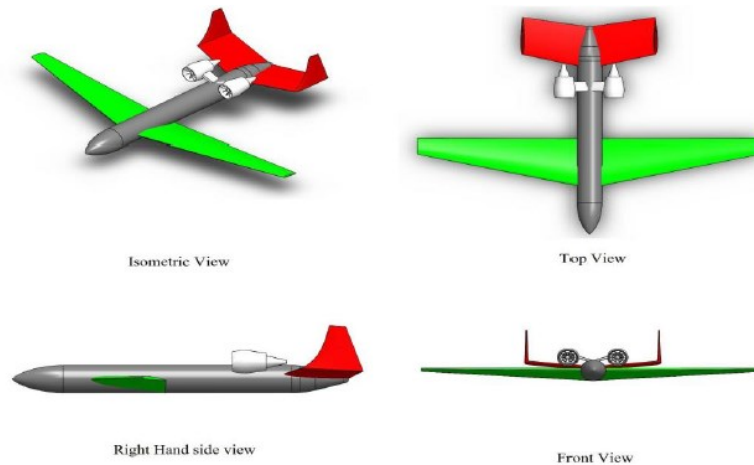
Figure 1.1 – CAD model of Shohan, et al. final aircraft design [8]

1.2.3 Mission Profile of Typical CAS Aircraft

The general mission profile for air superiority can be seen in Figure 1.2 provided by Raymer [9]. This is only a general representation of a typical military aircraft providing close air support, whether from an AC-130 gunship or a B-2 stealth bomber. The attack aircraft would take off from its assigned forward operating base (FOB) and climb to its cruising altitude. As it arrives at its operation area, it would descend to its required supporting altitude. From this position, the aircraft would drop its ordinance, perform standard air-to-ground attacks, or cruise above allied ground troops providing overhead reconnaissance. Once the aircraft's mission is complete, it ascends back to its cruising altitude. It returns to its original FOB or another allied airfield, possibly loitering nearby before landing.
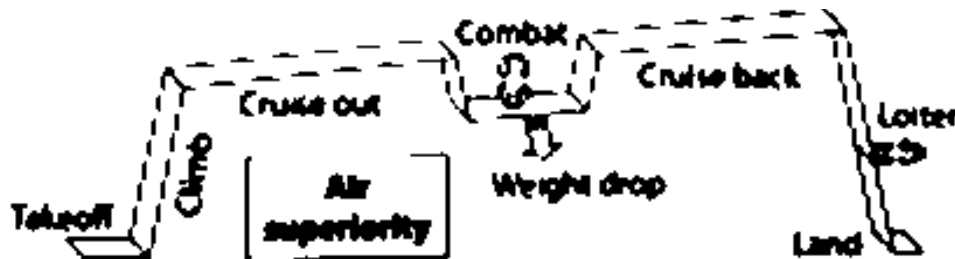
Figure 1.2 – General mission profile of reference [9]

This is the general concept of an attack aircraft's mission profile described by Raymer as described above. A further breakdown of this mission profile is detailed later in the following chapters regarding the conceptual aircraft.

1.2.4   Comparative Aircraft for CAS

This section covers the comparable aircraft currently or will be available for light or heavy CAS missions. This section divides into two parts: the Light-class and the Heavy-class of attack aircraft.

1.   Light-class attack aircraft

Currently, the USAF is looking into registering light attack aircraft to their growing arsenal of military aircraft. These aircraft have an official designation of Observation, Attack, Concept (OA-X) aircraft, including the Beechcraft AT-6 Wolverine, the Embraer Super Tucano, and the Textron AirLand Scorpion.

Table 1.1 lists each aircraft's mission specifications and features with images of each aircraft seen in Figure 1.3, Figure 1.4, and Figure 1.5.

Table 1.1 – Light-class attack aircraft mission specifications

Aircraft:	AT-6 Wolverine [10] [11]	Super Tucano [12] [13]	Scorpion [14]
Powerplant	Single, Turboprop Diesel Engine, 1600 hp	Single, Turboprop Diesel Engine, 1604 hp	2x Turbofans, 4000 lbf thrust each
External Armament Payload Capacity	4110 lbs (1864 kg)	3300 lbs (1500 kg)	6200 lbs (2800 kg)
Crew	2	2	2
Max Range	1725 nmi		1600 nmi (w/o external fuel), 2200 nmi (w/ external fuel
Combat Range		300 nmi	130 nmi
Max Speed	Mach 0.67		Mach 0.67
Cruise Speed		280 knots	
Max Takeoff Weight	10,000 lbs (4535 kg)	11,905 lbs (5400 kg)	22,000 lbs (9980 kg)
Endurance	4.5 hrs (internal), 7.5 hrs (4 external tanks)	8.4 hrs	5 hrs

Figure 1.3 – Beechcraft AT-6 Wolverine [10]

Figure 1.4 – Embraer EMB 314 Super Tucano [15]

Figure 1.5 – Textron AirLand Scorpion [16]

The American AT-6 Wolverine is a multi-mission, light attack, and armed reconnaissance aircraft. It features a low cantilever wing, a two-seat enclosed cockpit, and a 1600 hp turboprop engine. Similarly, the Super Tucano is another light attack aircraft from Brazil with the capability of providing light CAS. It also features a low cantilever wing and a

two-seat configuration enclosed cockpit design. A single turboprop engine with the capability of 1604 hp is used to generate thrust for the Super Tucano. Finally, and unquestionably different than the two previously mentioned, the Scorpion is an American jet aircraft capable of light attack, intelligence, surveillance, and reconnaissance duties. It also features a two-seat configuration cockpit with a cantilever high-wing instead. The Scorpion includes twin turbofan engines, each capable of 4000 lbf of thrust.

Looking at these three aircraft, the first notable distinct feature of the Scorpion is its jet-powered capability. This allows the aircraft to carry much more payload and accelerate at a higher rate than the two turboprop-driven aircraft. However, its combat and max range is lower since jet propulsion consumes much more fuel faster. Thus, both the AT-6 and Super Tucano can travel much further and longer than their jet counterparts. All three aircraft advertise a two-seater configuration which is beneficial to the lead pilot's situational awareness as described in the previous section, Future of Attack Aircraft.

2. Heavy-class attack aircraft

Many jet fighters are currently or have been designed for CAS roles. This section examines three unique jet fighter aircraft with CAS missions kept in mind: the Lockheed Martin F-35, the Sukhoi Su-25, and the Fairchild Republic A-10. Table 1.2 lists the mission specification and other notable features of each aircraft. Figure 1.6, Figure 1.7, and Figure 1.8 present images of each aircraft.

Table 1.2 – Heavy-class attack aircraft mission specifications

Aircraft:	F-35 Lightning II [17]	Su-25 Frogfoot [12]	A-10 Thunderbolt II [3]
Powerplant	Single Turbofan, 25,000 lbf, 40,000 lbf w/ afterburner	2x Turbojet, 9930 lbf thrust each	2x Turbofans, 9065 lbf thrust each
Internal/External Armament Payload Capacity	5700 lbs/15,200 lbs	0 lbs/9700 lbs	0 lbs/16,000 lbs
Crew	1	1	1
Max Range	1500 nmi (internal fuel)	540 nmi	2240 nmi w/ ferry
Combat Range	669 nmi, 760 nmi (air-to-air config)	400 nmi (SL, 9700 lbs PL, 2 external tanks)	250 nmi (CAS), 252 nmi (anti-armor)
Max Speed	> Mach 1.6	Mach 0.77	Mach 0.57
Cruise Speed		500 knots	300 knots
Max Takeoff Weight	70,000 lbs	42,550 lbs	50,000 lbs
Endurance			

Figure 1.6 – Lockheed Martin F-35 Lightning II [18]

Figure 1.7 – Sukhoi Su-25 Frogfoot [19]

Figure 1.8 – Fairchild Republic A-10 Thunderbolt II [20]

The F-35 is an American fifth-generation stealth fighter designed for multi-role combat purposes, including air superiority and CAS missions. It is a single-seater, blended wing body aircraft featuring a single turbofan engine capable of 25,000 lbf of thrust and afterburner effects allowing a maximum thrust to 40,000 lbf [17]. Depending on its variant, it could include a center lift-fan enabling the F-35 to perform Short Takeoff and Landing (STOL) or Vertical Takeoff and

Landing (VTOL) duties. This gives the F-35 much more operating capabilities in various environments. The Su-25 is a Soviet Union variant of an attack aircraft designed solely for CAS or anti-armor missions. It also features a single-seat cockpit configuration but is equipped with twin turbojet engines. Its overall configuration is a standard jet aircraft with a high-wing cantilever design and T-shaped empennage. Finally, the last aircraft of comparison is the American A-10 Thunderbolt II, also solely designed for CAS missions in the Cold War era. It is a single-seat aircraft with a cantilever low-wing design and an H-shaped tail. Two turbofan engines are driven, each producing 9065 lbf of thrust, mounted above the fuselage with pylons [3].

Each aircraft is designed significantly differently while capable of providing CAS as intended. The F-35 is a fifth-generation fighter and much newer than the Su-25 and A-10. Due to its high thrust capability, it can carry much more payload, internally and externally, and travel faster than the speed of sound (supersonic). In addition, since its overall design is a blended wing body, the F-35 is stealthy and can launch coordinated attacks before adversaries can see them coming. Moreover, since it is a multi-role fighter, the F-35 can do more than just CAS missions. However, due to its high-end specs, the F-35 is very expensive and must be flown sparingly. This issue is further discussed in a later section.

On the other end of the spectrum, the Su-25 and A-10 are solely designed as attack aircraft during the Cold War. Both feature twin jet engines and similar maximum takeoff weight. One difference between the two is their payload capability. Although the A-10 has a lower thrust capability, it can carry more external payloads. Another notable design difference is their tails. The Su-25 features a conventional tail, while the A-10 has an H-shaped tail. One benefit of the H-shaped tail is that it allows much more stable flight, mainly when diving to perform its attack run. Another benefit is that it reduces the heat signature from its twin engines. This would allow some counterplay against heat-seeking weaponry. Both aircraft are still in service in their respective armed forces but are undoubtedly becoming outdated to more modern and sophisticated aircraft.

1.2.5   Engine Comparison Study

This section covers the comparable jet engines currently available or used for known aircraft capable of CAS missions. Specifications of these engines can be seen in Table 1.3 with images in Figure 1.9 through Figure 1.12.

Table 1.3 – Engine variants and specifications

Engines:	TFE731 [21]	Tumansky R-13 [22]	GE TF34 [23]	PW F135 [24]
Class	Geared Turbofan	Turbojet	Twin-shaft, High Bypass Turbofan	Two-spool, Axial Flow, Augmented Turbofan
Length	49.7 inch	181.3 inch	100 inch	220 inch
Diameter	39.4 inch	43.1 inch	49 inch	46 inch
Max thrust	3500-4750 lbf	8970 lbf (dry), 14,320 lbf (wet)	9000 lbf	27,000 lbf (dry), 43,000 lbf (wet)
Specific Fuel Consumption (SFC)	0.469-0.517 lb/lbf/hr	0.93 lb/lbf/hr (idle), 2.09 lb/lbf/hr (wet)	0.371 lb/lbf/hr	
Thrust to Weight Ratio	4.7-5.3	5.4	6.28	7.47
Afterburner	No	Yes	No	Yes
Application	Textron Scorpion	Sukhoi Su-25	Fairchild Republic A-10	Lockheed Martin F-35

Figure 1.9 – Honeywell TFE731 turbofan engine [25]

Figure 1.10 – Tumansky R-13 engine [26]
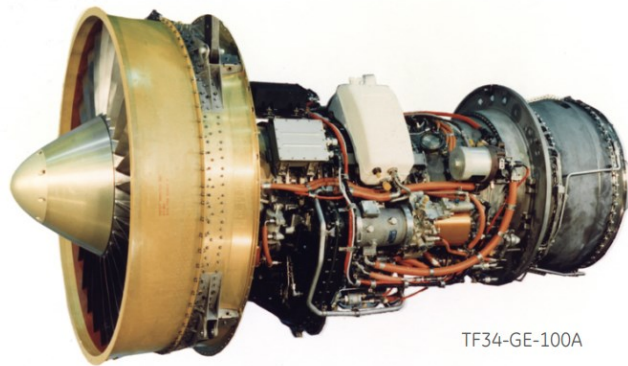
Figure 1.11 – General Electric TF34 engine [23]
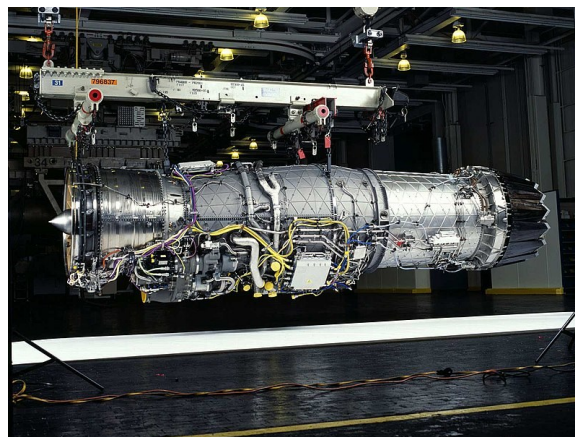
Figure 1.12 – Pratt & Whitney F135 engine [27]

The TFE731 is a geared turbofan engine commonly used on business jet aircraft. It was initially designed by Garrett AiResearch and later produced by Honeywell Aerospace, with its design based on the core of the TSCP700. The design featured two critical factors: low fuel consumption and low noise profile. Since the -50R variant, 70 improvements were made, including improved core and low-pressure spool technologies, new digital electronic engine

control (DEEC), and a complete nacelle and thrust reverser system [25]. The R-13 is a Soviet turbojet engine, a successor to the R-11 engine, designed by Sergei Alekseevich Gavriov, having a two-spool axial-low turbojet featuring a new five-stage high-pressure compressor, new combustion chamber, new afterburner, and greater use of titanium components [22]. The General Electric TF34 is a high bypass military turbofan engine that delivers the highest thrust-to-weight ratio, lowest specific fuel consumption, and the quietest operation in its class. 2,100 TF34 engines have been produced, accumulating over 13 million engine flight hours spanning combat and peacetime missions [23]. Finally, the F135 is a fifth-generation mixed-flow after-burning turbofan engine. There are two variants of this engine, a Conventional Take-Off and Landing (CTOL) variant and a two-cycle Short Take-Off Vertical Landing (STVOL) variant, which includes a forward lift fan [28].

The R-13 is the only turbojet engine presented in this group and has a thrust-to-weight ratio that is approximately the average of the other three turbofan engines. Because it is a turbojet, it has a very high SFC and thus requires additional fuel to operate. This explains why the Su-25 requires ferry tanks to achieve only a maximum range of 500 nmi. Though powerful in its time, the R-13 is not a very efficient engine compared to the GE TF34 engine, which was produced in a similar timeline.

The TFE731 and TF34 engines are turbofan engines and do not feature afterburning capabilities. The TFE731 is much smaller than the TF34 and can only produce roughly half the maximum thrust compared to its competitor. Although with a lower thrust output, the TFE731 has a higher SFC. Finally, the TF34 has a favorable thrust-to-weight ratio given its lower SFC. Overall, the TFE731 is smaller and lighter but less efficient than the TF34 in output.

Finally, the F135 by Pratt & Whitney is the longest out of the bunch, with a much higher thrust output and higher thrust-to-weight ratio. The SFC for the F135 is unknown, but the media has mentioned multiple times how expensive the fuel cost is for operating such an engine. Pratt & Whitney is currently cooperating with the US Navy on a two-block improvement plan. The first block involves a 7-10% increase in thrust and a 5-7% lower fuel burn. The plans include better cooling technology for turbine blades, increasing the engine's longevity, and substantially reducing maintenance costs. Block two works with the US Air Force's Adaptive Engine Transition Program to introduce technology for an engine rated at 45,000 lbs of thrust in a sixth-generation fighter [29]. Though the F135 is much newer and more advanced than the previous three and shows a promising future, it is yet to be seen as a favorable and applicable engine for future aircraft.

1.2.6   Flight Operations Cost

Another aspect of the design that must be investigated is the operational cost of the aircraft. A basic understanding of how the cost is determined for an aircraft is reviewed in this section to give a better sense how to approach the cost evaluation of the new designed aircraft. Chapter 22 – Cost Analysis will give a detail breakdown of the actual cost analysis of the designed aircraft later presented in this report.

There are two types of costs to consider: (1) the research, development, design, and manufacturing costs (RDDMC), including testing and production launch costs, and (2) the operational cost (OC) [30]. Military aircraft use life-cycle cost (LCC) rather than direct operating cost (DOC), mainly used for commercial aircraft. It is the cost involved for the entire fleet from "cradle to grave," including disposal. This is important since military operations have no cash flowing back (e.g., paying customers) [31]. A typical LCC for a military aircraft is listed below in Table 1.4.

Table 1.4 – Life cycle cost of military aircraft [31]

RDDMC	Production	In-service	Disposal
Engineering	Parts manufacture	Operation	Scrapping
Ground testing	Assembly	Maintenance	Complete disposal
Technology demo	Tooling	Ground Support	
Prototype flight test	Deliveries	Training	
Tech support		Post-design services	
Publication		Administration	

Only the OC portion of the LLC is investigated for this section of this project, specifically the cost per flying hour (CPFH). CPFH is a very complex subject as it depends on the purpose of giving such a value. Therefore, there is no single value or answer when discussing an aircraft's CPFH.

According to a report from the RAND Corporation, the term CPFH has been used in different contexts in DoD [32]. These different contexts include its usage in budgeting for the services' flying-hour programs, reimbursable rates for customers who use DoD aircraft, responding to requests for information outside DoD, and cross-system comparisons.

In terms of flying-hour program budgeting (FHPB), it is the idea that if one wishes to adjust flying hours incrementally (up or down), how much must the FHPB change? Or vice versa. Thus, CPFH used in FHPB is intended to capture only elements of cost that are directly variable with flying hours. This calculation can be seen in equation (1.1), where DLRs represent the depot level reparable variable of the aircraft.

$$CPFH_{FHPB} = Fuel + \frac{Consumables + DLRs}{Flying\ Hours} \tag{1.1}$$

Another usage of CPFH is for flying-hour reimbursable billing rates, basically, how much other DoD, other federal, other customers, and foreign military should be charged on a per-flight-hour basis. The typically prescribed rates for DoD customers usually include costs found in FHP CPFH and depot maintenance costs and, if applicable, variable contractor logistics support (CLS) costs. As for other federal agencies and foreign military sales, these rates cover the DoD rate's cost categories and allocation of crew salaries. CPFH can also be applied for public rates, including all the abovementioned costs plus an allocation for asset utilization (depreciation) and unfunded civilian retirement costs. These rates are summarized in their respective calculations found in equations (1.2) through (1.4).

$$CPFH_{Reimb} = CPFH_{FHPB} + \frac{Depot\ Maintenance + Variable\ CLS^3}{Flying\ Hours} \qquad (1.2)$$

$$CPFH_{Other\ Fed\ Agency} = CPFH_{Reimb} + \frac{Allocation\ of\ Crew\ Salary\ Cost}{Flying\ Hours} \qquad (1.3)$$

$$CPFH_{Public} = CPFH_{Other\ Fed\ Agency} + \frac{Depreciation + Allocate\ of\ Unfunded\ Retire\ Costs}{Flying\ Hours} \qquad (1.4)$$

Many from Congress and media requesting information on operations and support cost of an aircraft are also given in CPFH. These requests typically involve the question: How does the CPFH of one aircraft compare to another? Or what does it cost to fly a particular aircraft? The individual responsible for responding to the inquiry would either choose the $CPFH_{Reimb}$ or the $CPFH_{FHPB}$ definitions, given the circumstance.

The F-35 costs \$42,000 per hour of flight during its assigned missions, compared to the A-10, which only costs \$19,000-20,000 per hour of flight [33]. That is a massive difference, especially when performing the same close air support mission. Of course, the Air Force prefers to use the A-10 to perform its routine CAS missions while using the F-35 for much more demanding missions to offset its high cost. Gen. Mark Welsh, former chief of staff, suggests that an aircraft designed for CAS should be priced between \$4,000 and 5,000 per hour [34]. Only the aircraft of the OA-X project is known to have a flight cost as envisioned by Gen. Welsh and the Air Force [33]. Assuming these given costs are defined as $CPFH_{FHPB}$, it can be assumed that one of the main contributing factors to the CPFH is fuel consumption. Therefore, engine designs are further investigated to help reduce this cost throughout this project.

1.3   Objectives

The purpose of this project is to explore the following possibilities:
- Reduce the cost of the flight for a CAS mission.
- Use the same engines found on the A-10 to maintain fuel efficiency while still compensating the recoil force from the GE GAU-8 gatling cannon.
- Integrate a second pilot on board to assist in reducing the workload of the primary pilot during CAS missions.

Currently, the flight operation cost of the A-10 is between \$19,000 and 20,000 per hour of flight [34]. The project investigates various design configurations, study similar attack aircraft, and build the aircraft based on findings to reduce operational costs. It is also desired to use the same efficient engines found on the A-10 while ensuring the new aircraft does not create too much drag reducing the existing engine's overall thrust capabilities. These engines need to stay powerful enough to compensate the 45 kN recoil force of the gatling cannon [35]. Each of the A-10's engines currently produce 40.3 kN of installed thrust [36]. Therefore, each time the gun fires, the aircraft's thrust is halved. It is desired to maintain this effect or improve it through aerodynamics and increase the installed thrust capabilities. Finally, the intent of including a second pilot would reduce the workload of the primary pilot by assisting them in communicating

with friendly forces, determining the location of suppression, and planning an interception of flight with ease. Hopefully, the extra hand onboard would overshadow the additional weight onboard when performing the weight analysis throughout the project.

1.4   Methodology

The conceptual design will require understanding the mission, knowing similar aircraft, and following methods described in "Aircraft Design: A Conceptual Approach" by Raymer and "Airplane Design" by Roskam to arrive at the final conceptual design. In the initial stages, the role and objectives of CAS must be understood to know the types of weapons to carry, maneuvers that would be performed during the mission, and the average required response times to assist friendly ground forces. The overall mission profile diagram depicts the aircraft's main objectives. A compilation of existing known aircraft with CAS capability will then be put together for reference, with a trade study to follow. This database would assist in gathering required estimates of the new conceptual aircraft, including required take-off weight, empty weight, payload weight, lift-to-drag ratio, and wing aspect ratio. Also, an overview of desired engines will be investigated and help determine the desired thrust and fuel efficiency.

Once the required estimated values have been determined, performance sizing will follow similar methods presented by Raymer and Roskam while assuming a jet-fighter class type. The final desired values will be obtained through iteration using various computer programs including the RDSwin program, XFLR5, and AVL. Additional required designs and analyses will continue through the outlined methods of Raymer and Roskam. Physical design aspects of the conceptual aircraft will also be completed, such as the cockpit, fuselage, wing, tail, and avionics systems.

Chapter 2 – Mission Specifications

2.1   Mission Specification

Moving forward, the conceptual aircraft of this project will be designated as YA-94. Table 2.1 outlines the YA-94's required capabilities and performance.

Table 2.1 – YA-94's mission specifications

General Characteristics			
Crew Size	2		
Max External Payload Weight	16,000 lbs	7,300 kg	
Powerplant	2x Engines		
Performance			
Max Speed	400 knots (Mach 0.6)	460 MPH	740 KPH
Combat Radius	250 nmi	288 miles	463 km
Cruise Speed	350 knots (Mach 0.52)	400 MPH	645 KPH
Stall Speed	120 knots	138 MPH	222 KPH
Service Ceiling	50,000 ft	15,240 m	
Cruising Altitude	30,000 ft	9,144 m	
Takeoff Distance*	2,000 ft	610 m	
Landing Distance*	2,000 ft	610 m	
Sustain Turn Rate | G-Loading	≥5°/sec | 2-Gs		
Instant Turn Rate | G-Loading	≥20°/sec | 6-Gs		
Turn Radius	2,000 ft	610 m	
Rate of Climb	4,000 ft/min	1,220 m/min	
Armament/Miscellaneous			
GE GAU-8 Cannon (unloaded | loaded)	620 lbs | 4,029 lbs	282 kg | 1,800 kg	
External Hardpoints	11		
Aerial refueling capable	Yes		

*Required distance during ground run only

The YA-94 is suggested to carry similar external provisions as the A-10 and carry any combination respected to its mission. Weapon and equipment types and their singular weight values are shown in Table 2.2 to understand the aircraft's payload capability. The basic loadout configuration can be seen in Appendix A. Later section lays out specific armament combinations per the mission profile model. It must be noted that the USAF requires the new CAS aircraft to have a ground roll distance of no more than 3,000 ft [37]. It will be later determined in this report and additional iterations that the YA-94 exceeds this requirement and thus a ground roll for both takeoff and landing is only stated at 2,000 ft in the above table.

Table 2.2 – Armament types and weights

	Max Quantity	Weight (Per Unit)	
Rockets			
LAU-61/LAU-68 Rocket Pod	4	463 lbs/316 lbs	210 kg/143 kg
LAU-131 Rocket Pod	6	160 lbs	72.5 kg
Missiles			
AIM-9 Sidewinder	2	188 lbs	85 kg
AGM-65 Maverick	6	210-304 lbs	95-138 kg
Bombs			
Mk 80 Unguided	1-2	250-2,000 lbs	113-907 kg
Mk 77 Incendiary	2	750 lbs	340 kg
Cluster	2	750 lbs	340 kg
Paveway Laser-guided	1-2	250-2,000 lbs	113-907 kg
Joint Direct Attack Munition (JDAM)	1	2,000 lbs	907 kg
Wind Corrected Munition Dispenser (WCMD)	1	1,000 lbs	454 kg
Other			
Flares Pod	1	28 lbs	12.7 kg
ECM Pod	1	440 lbs	200 kg
Targeting Pod	1	450 lbs	204 kg
Drop Tanks	2	600 US gal	2,300 L

2.2   Mission Profile

Figure 2.1 represents the typical mission profile the YA-94 will accomplish. It is similar to the mission profile of an A-10 or any other attack aircraft. In segment 1, the aircraft taxi and takeoffs from a Forward Operating Base (FOB) runway. In segments 2 and 3, the aircraft climbs to its cruising altitude, where it would level out and cruise until it reaches its operations area. Depending on the distance, the YA-94 may require aerial refueling during segment 3. This is to avoid carrying unnecessary fuel and reduce the risks of fires. As it reaches segment 4, the aircraft lowers to its operating altitude and provides air support as necessary. Segment 4 may vary in support requests. Three different close air support mission profiles are covered in the following parts: anti-personnel support, anti-armor support, and armed reconnaissance. Once the air support has achieved its objective, the aircraft begins segment 5, regaining its cruising altitude and returning to its original FOB or another allied airbase. During segment 5, the aircraft may require another aerial refueling before returning. Segments 6 and 7 cover the aircraft's descent and landing, respectively. The aircraft may require loitering during segment 6, awaiting further instructions before making its landing approach.
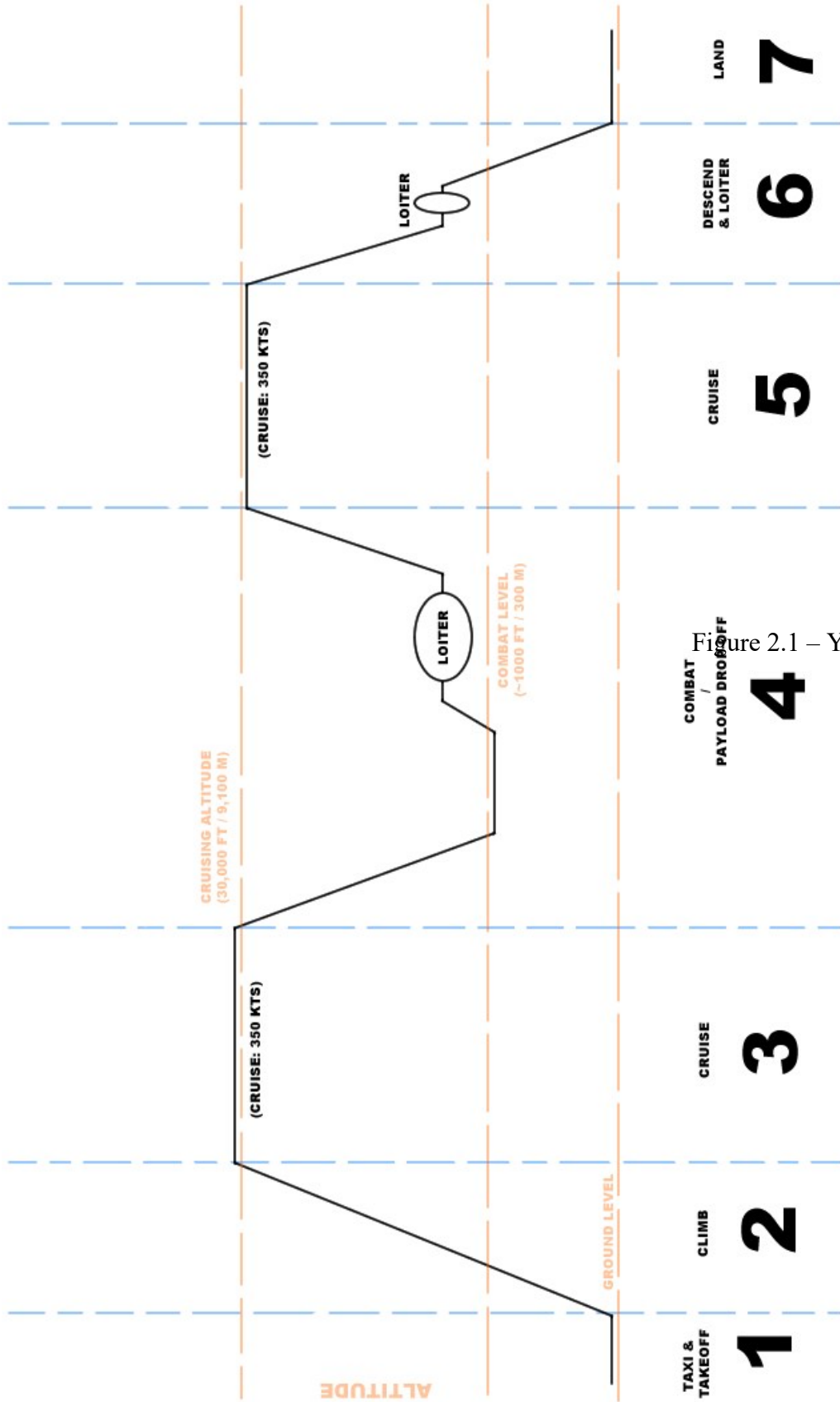
Figure 2.1 – YA-94 general mission profile

2.2.1   Anti-Personnel Support Mission Profile

The mission profile for Anti-Personnel Support is seen in Figure 2.2. As segment 4 begins, the YA-94 would lower its altitude and drop its weapon payload at marked locations designated by a ground controller. The external payload for this sortie may include the following combination: Rocket pods, lightweight unguided bombs, incendiary bombs, cluster bombs, or a lightweight Paveway laser-guided bomb. In addition, the YA-94 may also include a flare pod or an ECM pod in case of hostile anti-air ordinance. Table 2.3 provides a sample loadout for this mission, including total armament quantity and weight.

Once all external weaponry payload has been deployed, the aircraft may begin performing strafe runs along the enemy lines, as needed, with its onboard gatling cannon. When completed, and if needed, the aircraft could loiter for an additional amount of time before returning home.
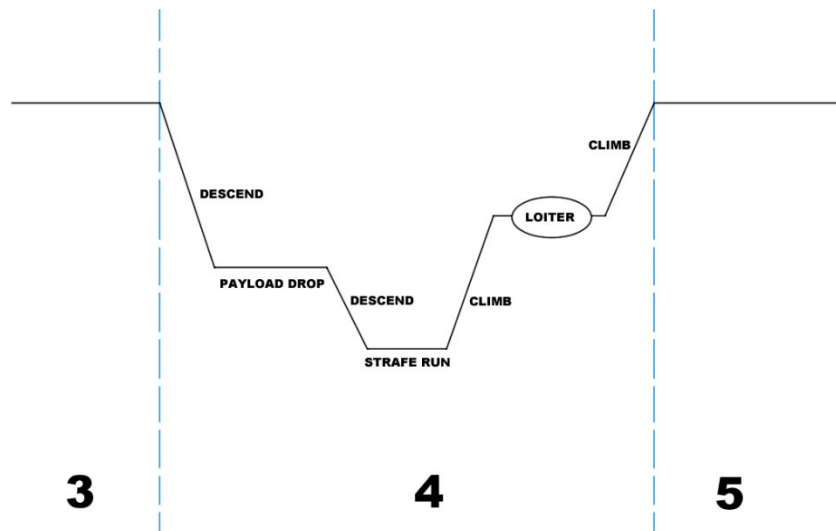
Figure 2.2 – Anti-personnel mission profile segment

Table 2.3 – Anti-personnel loadout sample

	Quantity	Weight (Per Unit)	
Rockets			
LAU-61/LAU-68 Rocket Pod	2	463 lbs	210 kg
Bombs			
Cluster	4	750 lbs	340 kg
Paveway Laser-guided	2	250 lbs	113 kg
Other			
Flares Pod	1	28 lbs	12.7 kg
ECM Pod	1	440 lbs	200 kg
Gun Loaded	Yes	4,029 lbs	1,800 kg
	Req'd Hardpoints	**Total Weight**	
	10	8,930 lbs	4,050 kg

2.2.2   Anti-Armor Support Mission Profile

During an Anti-Armor Support mission, where enemies may have tanks or other armored vehicles, the aircraft may repel the hostile forces with a combination of the following: Maverick missiles, a heavy-weight unguided bomb, a heavy-weight laser-guided bomb, a JDAM, or a WCMD. The YA-94 may also carry along flare or ECM pods to counter enemy fire. During this profile segment, depicted in Figure 2.3, the aircraft drops all its necessary payload as called out per the ground controller and most likely returns to base immediately. The aircraft has carried a much heavier payload, increasing fuel consumption, and may not stay within the zone for an extended amount of time. This is determined to be the most critical mission profile for the aircraft.
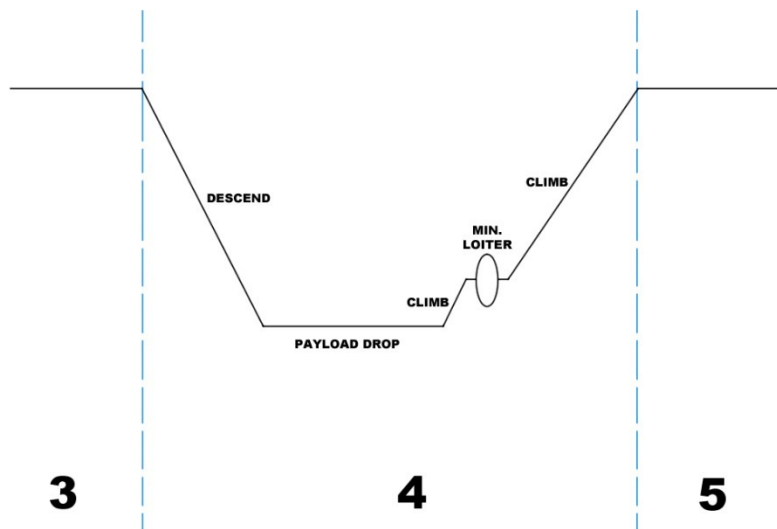
Figure 2.3 – Anti-armor mission profile segment

Table 2.4 – Anti-armor loadout sample

	Quantity	Weight (Per Unit)	
Missiles			
AGM-65 Maverick	6	304 lbs	138 kg
Bombs			
Mk 82 Unguided	3	500 lbs	227 kg
Paveway Laser-guided	2	2,000 lbs	907 kg
Joint Direct Attack Munition (JDAM)	1	2,000 lbs	907 kg
Other			
ECM Pod	1	440 lbs	200 kg
Targeting Pod	1	450 lbs	204 kg
Gun Loaded	Yes	4,029 lbs	1,800 kg
	Req'd Hardpoints	**Total Weight**	
	10	14,200 lbs	6,440 kg

2.2.3   Armed-Reconnaissance Mission Profile

Finally, Figure 2.4 portrays a typical profile segment for Armed-Reconnaissance. The aircraft would descend to an observable cruising altitude during this mission segment and provide overhead reconnaissance for allied ground forces. This would last for an extended time while occasionally providing air interdictions. Since the aircraft would be loitering for quite some time, fuel drop tanks are most likely to be carried along to extend the flight duration. Tanks would be required to drop off before engaging to increase the aircraft's performance. Other external payload necessities are shown in Table 2.5, including rocket pods, Maverick missiles, light-weight unguided bombs, a flare pod, or an ECM pod. The payload would need to be light to increase the aircraft's endurance for this profile segment.
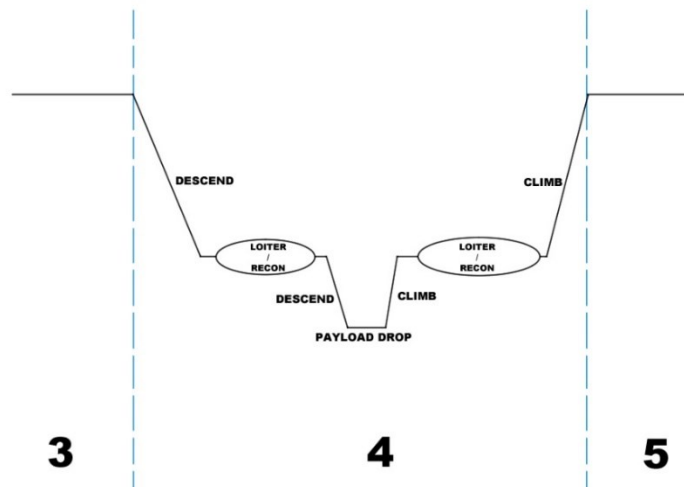
Figure 2.4 – Armed-reconnaissance mission profile segment

Table 2.5 – Armed recon loadout sample

	Max Quantity	Weight (Per Unit)	
Rockets			
LAU-131 Rocket Pod	2	160 lbs	72.5 kg
Missiles			
AGM-65 Maverick	6	304 lbs	138 kg
Bombs			
Mk 80 Unguided	2	250 lbs	113 kg
Paveway Laser-guided	1	250 lbs	113 kg
Other			
Flares Pod	1	28 lbs	12.7 kg
Drop Tanks	2	600 US gal	2,300 L
Gun Loaded	Yes	4,029 lbs	1,800 kg
	Req'd Hardpoints	**Total Weight**	
	10	11,000 lbs	5,000 kg

2.3   Critical Mission Requirements

Table 2.6 lists the following critical mission requirements that must be considered when designing the YA-94. These are the minimum requirements this aircraft must fulfill to be considered design-worthy.

Table 2.6 – YA-94 mission requirements

Combat Radius	250 nmi	288 miles	463 km
Armament Payload*	16,000 lbs		7,300 kg
Crew Size	Two persons		
Cruise Speed	350 knots	400 MPH	645 KPH
Aerial Refuel	Yes		
Loiter/Armed-Recon	≥ 30 Minutes		
Carry GAU-8 Cannon**	4,029 lbs		1,800 kg

*Weight includes ammo
**Cannon considered part of structures weight

2.4   Measure of Merit

Besides the aircraft's mission requirements, it is desired that the YA-94 meet additional design characteristics to aid in the final design process. These additional conditions are known as measures of merit, qualifying and quantifying the demand for the aircraft. Below is a list of measures of merit for the YA-94, ranked from most to least significant.

1. **Affordable CFPH**. Somewhere between $7,000 to $15,000 per hour of flight.
2. **Low heat signature**. Engines should be mounted high, allowing engine exhaust to cool off and prevent/reduce heat-seeking lock-ons by adversaries.
3. **Low empty weight**. Helps in reducing fuel consumption, allowing lower operation costs. It is desired between 25,000 to 30,000 pounds.

Chapter 3 – Weight Sizing

3.1   Introduction

Weight and sizing determine how big and heavy the aircraft must be to perform the critical mission and carry the desired payload. This initial calculation determines the wing and propulsion sizing for the required mission profile. This chapter shall walk through the initial sizing approach of the YA-94 to calculate its final takeoff, empty, and fuel weights. This is accomplished by providing an estimated takeoff weight per the payload carried during the mission and then iterating using Raymer's and Roskam's methods. Different values are obtained between the two methods and require an average to determine the final design weight values. Two different loadout missions were also investigated to determine the correct weight to accommodate the varying the loads the aircraft may be armed with. Throughout the chapter, the anti-personnel mission profile was used as an example to show how sensitive the initial guess weight value can be and later why the heavier critical mission profile must be used instead.

3.2   Weight Estimates

3.2.1   Takeoff- and Empty-Weight Fractions

Table 3.1 yields a database of similar aircraft with their respective maximum takeoff, design takeoff, and empty weights. This establishes an initial weight guess for the YA-94.

Table 3.1 – Database of comparable mission aircraft

Aircraft	Role	Max Takeoff Weight	Design Takeoff Gross Weight	Empty Weight
Fairchild Republic A-10 Thunderbolt II	CAS	50,000 lbs (22,700 kg)	30,384 lbs (13,782 kg)	24,959 lbs (11,321 kg)
Sukhoi Su-25	CAS	42,549 lbs (19,300 kg)	31,835 lbs (14,440 kg)	21,605 lbs (9,800 kg)
Lockheed Martin F-35 Lightning II	Multirole Fighter	70,000 lbs (31,751 kg)	49,540 lbs (22,471 kg)	29,300 lbs (13,290 kg)
Textron AirLand Scorpion	Light Attack/Recon	22,000 lbs (9,979 kg)	17,800 lbs (8074 kg)	12,700 lbs (5,761 kg)
McDonnell Douglas F-4E Phantom II	Interceptor	61,795 lbs (28,060 kg)	41,500 lbs (18,824 kg)	30,328 lbs (13,757 kg)
General Dynamics F-16 Fighting Falcon	Multirole Fighter	42,300 lbs (19,187 kg)	26,500 lbs (19,187 kg)	18,900 lbs (8,573 kg)

Studying Table 3.1 and having the A-10 as the lead aircraft of reference, the YA-94 takeoff weights are approximated as follows:

$$W_{MTOW} = 50,000 \ lbs$$
$$W_0 = 32,600 \ lbs$$

W_0 represents the design takeoff weight of the aircraft. It is determined with the following equation:

$$W_0 = W_{crew} + W_{payload} + W_{fuel} + W_{empty} \tag{3.1}$$

The weight of both the crew and payload is known as they are givens per the design requirements and dependent on the mission type. The YA-94 is projected to carry a crew of 2 and a similar payload capability to the A-10. To keep the calculations and weights simple an anti-personnel mission was assumed, therefore $W_{crew} = 460 \, lbs$ and $W_{payload} = 9,000 \, lbs$. This only leaves the fuel and empty weights unknown.

The empty weight can be estimated using Figure 3.1. This graph, however, gives an approximation in terms of an empty weight fraction $\left(\frac{W_e}{W_0}\right)$. Another approach would be referencing Table 3.2 and using equation (3.2), where A is a multiplier based on aircraft type, C is the negative slope found in Figure 3.1, and K_{VS} is the variable-sweep constant. In this case $K_{VS} = 1.00$ since the aircraft being designed has a fixed sweep. Using the initial guess of W_0 and a design of a jet fighter, the empty weight fraction can be initially approximated as 0.573.
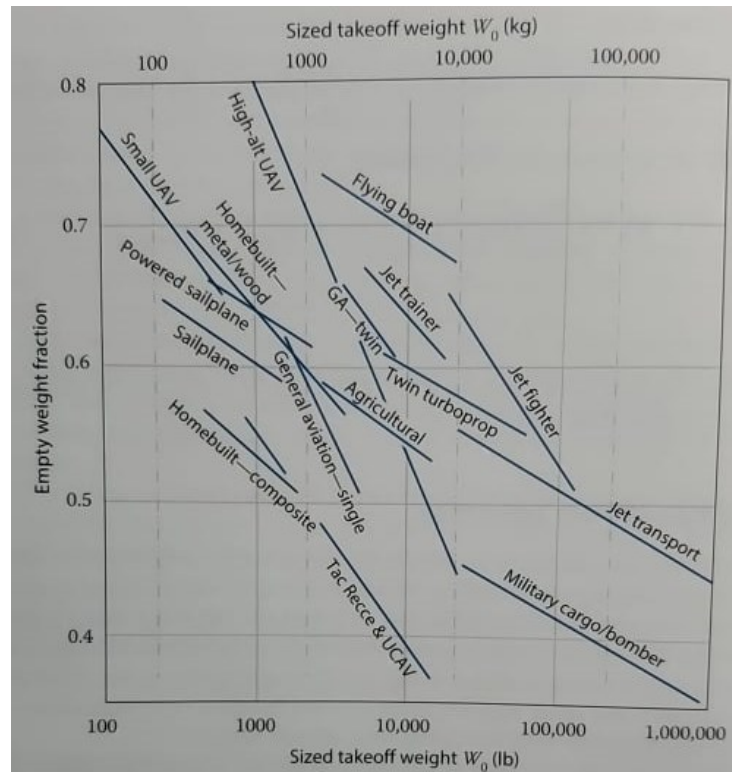
Figure 3.1 – Empty weight fraction trends [9]

Table 3.2 – Empty weight fraction vs. W_0 [9]

	A	{A-metric}	C
Sailplane – unpowered	0.86	{0.83}	-0.05
Sailplane – powered	0.91	{0.88}	-0.05
Homebuilt – metal/wood	1.19	{1.11}	-0.09
Homebuilt – composite	1.15	{1.07}	-0.09
General aviation – single engine	2.36	{2.05}	-0.18
General aviation – twin engine	1.51	{1.4}	-0.10
Agricultural aircraft	0.74	{0.72}	-0.03
Twin turboprop	0.96	{0.92}	-0.05
Flying boat	1.09	{1.05}	-0.05
Jet trainer	1.59	{1.47}	-0.10
Jet fighter	2.34	{2.11}	-0.13
Military cargo/bomber	0.93	{0.88}	-0.07
Jet transport	1.02	{0.97}	-0.06
UAV – Tac Recce & UCAV	1.67	{1.47}	-0.16
UAV – high altitude	2.75	{2.39}	-0.18
UAV - small	0.97	{0.93}	-0.06

$$\frac{W_e}{W_0} = A W_0^C K_{VS} \tag{3.2}$$

3.2.2 Fuel-Fraction Estimations

Estimating fuel cannot be determined through simple statistical means. Instead, the aircraft to be designed must be "flown" over its required mission. In this case, each fuel weight fraction requires calculation over each segment of the mission profile. The overall mission profile includes the combat segment presented in Figure 2.2. Historical values of warmup, takeoff, climbing, and landing weight fractions can be used as initial estimates to simplify the work, and these values are in Table 3.3. This only leaves the mission profile's cruise, loiter, and combat segments.

Table 3.3 – Historical mission-segment weight fractions [9]

Mission Segment	(W_i/W_{i-1})
Warmup and takeoff	0.970
Climb	0.985
Landing	0.995

For the remaining segments, the SFC and L/D are estimated. Assuming the propulsion of a high-bypass turbofan engine, the SFC during cruise and loiter can be assumed as 0.5/hr (14.1 mg/Ns) and 0.4/hr (11.3 mg/Ns), respectively. The L/D can be estimated using Figure 3.2, resulting in an approximated L/D of 15, assuming a comparison with the A-6. These values are then plugged into equations (3.3) and (3.4).

Equation (3.3) calculates the fuel fraction during the cruising segment where R is the range, C is the specific fuel consumption (SFC), V is the aircraft's velocity, and L/D is the lift-to-drag ratio. (3.4) calculates the fuel fraction during the loiter segment, where E is the endurance or loiter time. It must be noted that C and L/D vary with speed and altitude. Furthermore, the YA-94 is designed to drop ordinance during combat, making things more complicated. Therefore, the aircraft will experience very different performance characteristics between its mission profile's first and second half.

$$\frac{W_i}{W_{(i-1)}} = \exp\left(\frac{-RC}{V(L/D)}\right)$$ (3.3)

$$\frac{W_i}{W_{(i-1)}} = \exp\left(\frac{-EC}{V(L/D)}\right)$$ (3.4)
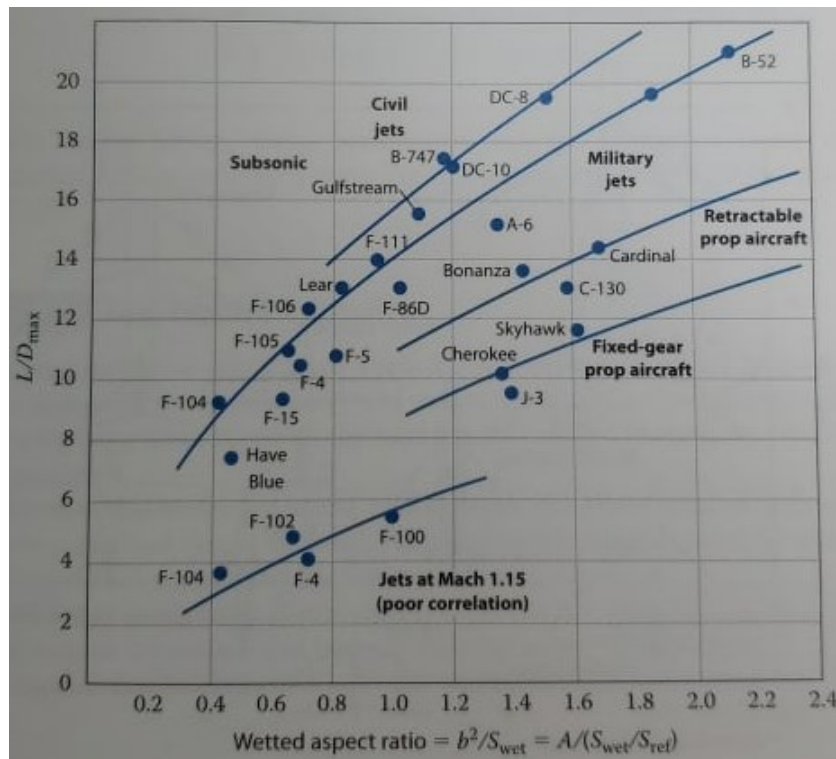
Figure 3.2 – Maximum lift-to-drag ratio trends [9]

Once all weight fractions from each segment are determined, they are multiplied together, determining the total mission weight fraction W_x/W_0. This value can then be plugged into equation (3.5) to estimate the total fuel fraction. An assumption of a 6% allowance for reserve and trapped fuel is made using the 1.06 multiplier.

$$\frac{W_f}{W_0} = 1.06\left(1 - \frac{W_x}{W_0}\right)$$ (3.5)

3.3   Takeoff Weight Calculation

Once all empty- and fuel-weight fractions are estimated, the gross takeoff weight is iteratively found using equation (3.6). This is done by guessing the gross takeoff weight, calculating the statistical empty-wight fraction, and calculating the gross takeoff weight. If the result does not match the initial guess value, a value between the two is used for the next guess.

$$W_0 = \frac{W_{crew} + W_{payload}}{1 - \left(W_f/W_0\right) - \left(W_e/W_0\right)} \tag{3.6}$$

3.3.1   RDSWin Program (Raymer's Method)

The entire iterative process is done through the RDSWin program. To show why choosing the correct mission profile is important, a mission profile for Anti-Personnel is chosen with the following inputs shown in Table 3.4 provide the program's initial sizing. It will be later shown that the program well underestimates the required weight for the aircraft. Values in each segment are also calculated and viewed in Appendix B.

Table 3.4 – Initial sizing inputs for RDSWin

Initial Sizing Inputs	Imperial Units	Metric Units
Takeoff Weight	50,000 lbs	22,700 kg
Weight of Crew | Cargo | Passengers | Misc.	460 | 8,900 | 0 | 0 lbs	208 | 4,100 | 0 | 0 kg
Class	Jet Fighter	
Fudge Factor	1.0	
Cf_e	Air Force Fighter	
S_{wet}/S_{ref}	4.92	
Parasitic Drag Fudge Factor	1.0	
Wing Aspect Ratio	6.00	
Oswald Span Efficiency (e)	0.80	
Wing Loading	$90\ lbf/ft^2$	$440\ kg/m^2$
Propulsion	Jet Propulsion	
Thrust-to-Weight ratio | SFC	0.35 | 0.371/hr	
Afterburner	No	
# of engines	2	
Range	500 nmi	

The final weights were determined from the inputted table values as listed below. However, it must be realized when using this program, the phase of dropping the payload or dispensing the ammo midflight was not considered. Therefore, the following calculated values are very rough estimates for the YA-94:

- **Takeoff weight:** 32,000 lbs (15,000 kg)
- **Empty weight:** 19,600 lbs (8,900 kg)
- **Fuel weight:** 3,300 lbs (1,500 kg)

These values, however, are only for a typical CAS mission, and weight values must be calculated for a more critical mission. Therefore, an Anti-Armor mission was also analyzed, changing the initial takeoff weight to 50,000 lbs (22,700 kg) and the cargo weight to 16,000 lbs (7,300 kg). Again, the RDSWin program does not take into consideration of payload drop. The following weight values are obtained as follows:

- **Takeoff weight:** 50,700 lbs (23,000 kg)
- **Empty weight:** 29,000 lbs (13,200 kg)
- **Fuel weight:** 5,200 lbs (2,400 kg)

The empty weight between the two missions differs significantly. An average between the two mission profiles is calculated to obtain the best estimate. This gives a more reasonable weight size for the YA-94 when using RDSWin.

- **Takeoff weight:** 41,400 lbs (18,800 kg)
- **Empty weight:** 24,300 lbs (6,400 kg)
- **Fuel weight:** 4,250 lbs (1,900 kg)

3.3.2   Roskam's Method

On the other hand, Roskam's method considers payload drop-off and ammo dispensation during a strafing run. Derived methods from Roskam's *Part I: Preliminary Sizing of Airplanes* for a jet fighter was used in a MATLAB program to determine the same weight categories calculated from RDSWin. The MATLAB script for each mission type with a single iteration sample for an Anti-Personnel mission can be referenced in Appendix C.

The following assumptions were made when performing this method:

- The constant lift-to-drag ratio of 15 was used across all flight scenarios, except during the cruise. A factor of .866 was used in the lift-to-drag ratio during cruise phases.
- Constant SFC is used across the entire mission profile.
- 150 nmi range was considered for both cruise-in and cruise-out phases. 100 nmi range was considered during the dash-out and dash-in phases. This brings a total range of 500 nmi.
- Cruise velocities were considered at 350 knots.

With these assumptions, the following final weight values for Anti-Personnel were calculated:

- **Takeoff weight:** 26,000 lbs (11,800 kg)
- **Empty weight:** 16,200 lbs (7,350 kg)
- **Fuel weight:** 3,400 lbs (1,540 kg)

As for a more critical mission, the final weight values were calculated:

- **Takeoff weight:** 58,000 lbs (26,300 kg)
- **Empty weight:** 32,600 lbs (14,800 kg)
- **Fuel weight:** 7,600 lbs (3,450 kg)

Once again, the two mission profiles caused a significant difference between the two empty-weight values. An average of the weight values will also be calculated for the Roskam method.

- **Takeoff weight:** 42,000 lbs (19,000 kg)
- **Empty weight:** 24,400 lbs (11,000 kg)
- **Fuel weight:** 5,500 lbs (2,500 kg)

3.4   Conclusion

It is concluded that the Roskam method gives a much more realistic weight measurement compared to Raymer's method. However, Roskam's values have significant margins between the two mission profiles, and the average is assumed to be slightly misleading. Therefore, the MTOW is estimated closely to the known MTOW of 50,000 lbs found on the A-10 as it is predicted that the YA-94 can carry the same payload weight. Both the Raymer and Roskam methods calculate a similar empty weight average and were rounded down to 24,000 lbs to allow additional payloads and storage onboard. Finally, the fuel weight is underestimated by both methods when compared to the A-10. Therefore, the final value is increased to 8,600 lbs, close to the fuel weight found on the A-10.

- **Max takeoff weight:** 50,000 lbs (22,700 kg)
- **Empty weight:** 24,000 lbs (10,900 kg)
- **Fuel weight:** 8,600 lbs (3,900 kg)

Chapter 4 – Wing and Propulsion Sizing

4.1   Introduction

This chapter investigates the performance requirements and sizing constraints of the YA-94. The relationships between the aircraft's thrust-to-weight ratio (T/W) and wing loading (W/S) parameters are investigated to constrain various design aspects of the aircraft. Constraining these aspects helps appropriately size the required wing area (S) and engine size (T). This is to avoid, for example, oversizing the wing which could lead to unnecessary additional skin friction drag. Or under sizing the engines which could later lead to the aircraft underperforming climb or turn requirements. The following performance constraints are analyzed and used to determine the desired sizing factors of S and T:

- Stall Speed
- Takeoff Distance
- Landing Distance
- Cruise and Climb Estimates
- Rate of Climb Estimate
- Instantaneous and Sustained Turning Estimates

When all constraints have been calculated, their values (in terms of T/W and W/S) are consolidated and plotted on a Matching Graph determining the aircraft's desired wing and propulsion sizing while meeting all desired performance constraints listed above. The following results are determined through a MATLAB code using very conservative values and estimates while also being replicated using RDSWin, which gives closer to realistic values. These inputs, outputs, and processes can be found in Appendix D, section 27.0.

4.2   Sizing per Stall Speed

The first main contributor to the YA-94's performance is its stall speed. This is the minimum speed an aircraft must maintain to remain airborne. Also, this speed determines the aircraft's approach speed which determines the required landing distance.

Equation (4.1) estimates the stall speed while determining the required wing loading for this constraint. V_{stall} is the estimated stall speed of the aircraft, ρ is the density of the air the aircraft is traveling through, and $C_{L_{max}}$ is the maximum lift coefficient the aircraft's wing shall produce.

$$W/S = \frac{1}{2}\rho V_{stall}^2 C_{L_{max}} \tag{4.1}$$

Per the USAF's comments, when looking into "tomorrow's A-10," it is desired that the aircraft flies at low altitudes at low speeds, anywhere between 150 to 300 knots. However, a stall speed at 120 knots is chosen with the maximum lift coefficient values set at 1.5, 1.6, and 1.7 for

the clean configuration. The following wing loading values are produced in Table 4.1 and plotted in Figure 4.1.

Table 4.1 – Wing loading required during stall

V_{stall}	**120 knots**		
$C_{L_{max}} =$	**1.5**	**1.6**	**1.7**
$\left(\dfrac{W}{S}\right), \left(\dfrac{lbs}{ft^2}\right)$	78.72	83.97	89.21
$\left(\dfrac{W}{S}\right), \left(\dfrac{kg}{m^2}\right)$	384.34	409.98	435.56
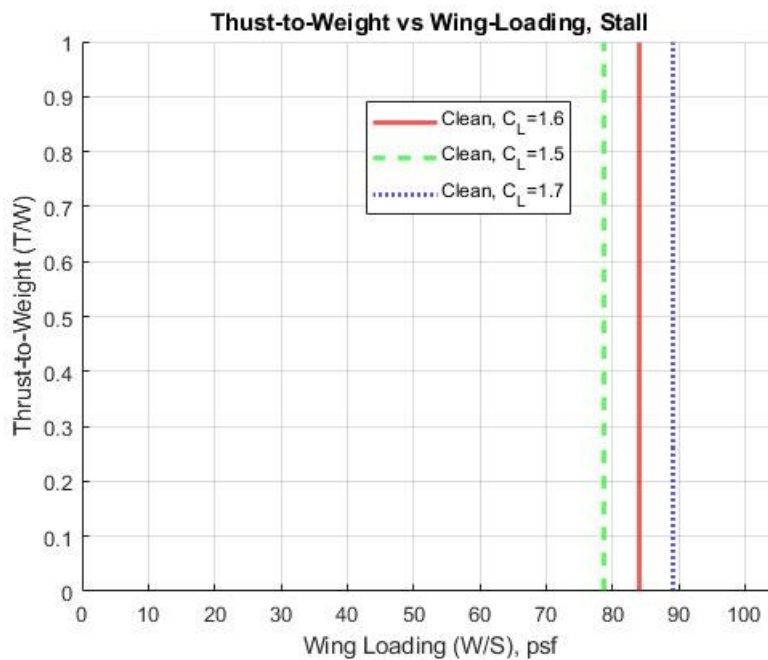
Figure 4.1 – Required wing-loading at stall speed

The wing loading at $C_{L_{max}} = 1.6$ is chosen as the stall condition due to the possible higher MTOW than the A-10. Therefore, a bigger wing is predicted for the YA-94. For interpretation, it is desired to have a wing loading left of the vertical plotted line suggesting a larger wing design either at this specified or lower values of W/S at $C_{L_{max}} = 1.6$.

4.3   Sizing per Takeoff Distance

The following constraint is the aircraft's takeoff distance. This is determined by the relationship between the aircraft's W/S and T/W. The takeoff distance involves the required distance the aircraft must travel to become airborne and the required distance to clear a minimum 50 ft obstacle for military aircraft, as described by both Raymer and Roskam. A diagram of this takeoff is seen in Figure 4.2.
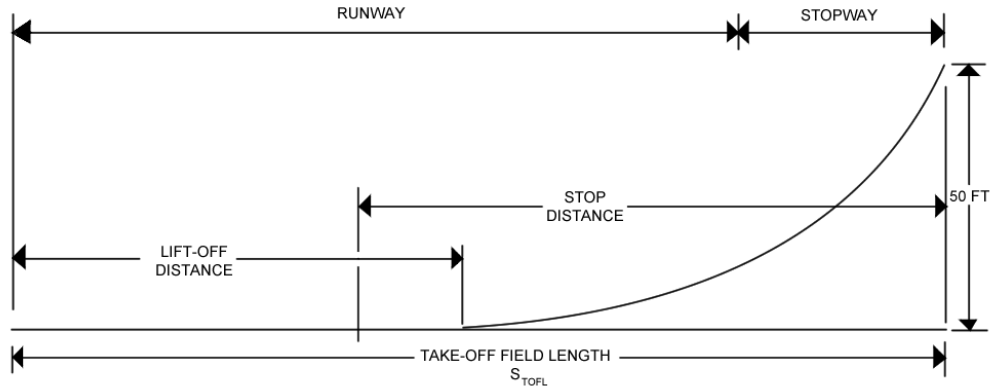
Figure 4.2 – Takeoff diagram [38]

The takeoff constraint in terms of W/S and T/W can be determined with equation (4.2), where TOP is the takeoff parameter, σ is the air density ratio between the operating altitude and sea level standard atmosphere conditions, and $C_{L_{TO}}$ is the lift coefficient during takeoff.

$$T/W = \frac{W/S}{TOP * \sigma * C_{L_{TO}}} \tag{4.2}$$

The following assumptions were used to determine the above relationship to size the desired takeoff distance:

- $C_{L_{TO}}$ values of 1.6, 1.8, and 2.0
- TOP of $180\frac{lbs^2}{ft^2}$
- Density ratio $\sigma = \frac{\rho_{sea\ level}}{\rho_{sea\ level}} = \frac{0.0024}{0.0024} = 1.0$
- W/S values of 10, 20, 40, 60, 80, 100, 120, 140 $\frac{lbs}{ft^2}$

The TOP was estimated using Figure 4.3 at 3,700 ft, which includes the total distance on ground and in air. Per the USAF, a takeoff distance is desired to be 3,000 ft, assuming this only pertains to ground roll. Sea level altitude at standard atmosphere conditions was considered resulting a density ratio of 1.0.
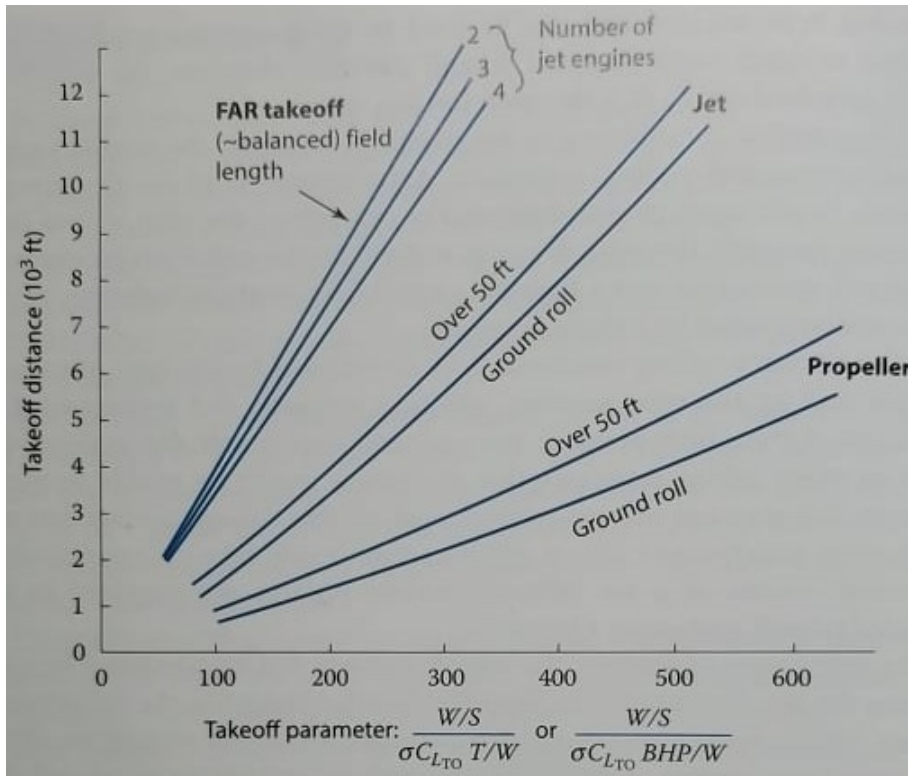
Figure 4.3 – Takeoff distance estimation [9]

A tabulation of the T/W values is shown in Table 4.2, with their respective plots shown in Figure 4.4.

Table 4.2 – Required thrust-to-weight ratio for takeoff

$\frac{W}{S},\left(\frac{lbs}{ft^2}\right)$	$\frac{W}{S},\left(\frac{kg}{m^2}\right)$	$C_{L_{max}} =$	1.6	1.8	2.0
10	48.8		.0347	.0309	.0278
20	97.6		.0694	.0617	.0556
40	195.3		.1389	.1235	.1111
60	293.0	$\frac{T}{W} =$	.2083	.1852	.1667
80	390.6		.2778	.2469	.2222
100	488.2		.3472	.3086	.2778
120	585.9		.4167	.3704	.3333
140	878.9		.4861	.4321	.3889
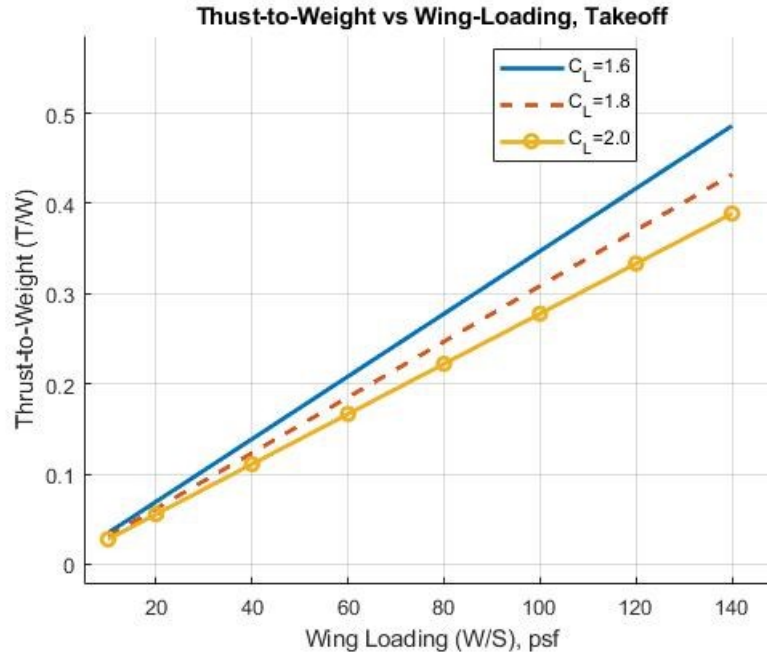
Figure 4.4 – Required T/W and W/S for takeoff

It is desired to constrain the aircraft above and to the left of the plotted lines. This indicates a large wing size with little thrust during takeoff. For comparison, if the YA-94 has a similar wing-loading as the A-10 at $100\ lbs/ft^2$ with a $C_{L_{max}}$ of 1.8, the YA-94 would only require a T/W of 0.35, close to the A-10's T/W of 0.36.

When analyzing with RDSWin, it was determined that the YA-94 would require a ground roll at 2,742 ft during takeoff. This aligns very well with the USAF takeoff requirement under 3,000 ft. It will be later determined through further iteration, the YA-94 is capable of taking off under 2,000 ft during the ground roll phase.

4.4 Sizing per Landing Distance

The landing distance is only dependent on the aircraft's W/S. This relationship is determined by equation (4.3), where the required W/S during landing is only a product of the W/S at stall (from equation (4.1)) and the ratio between the aircraft's landing weight W_{land} to its takeoff weight W_0.

$$\frac{W}{S} = \left(\frac{W}{S}\right)_{stall} * \frac{W_0}{W_{land}} \tag{4.3}$$

The following assumed values were used to determine the above relation:

- Landing weight $W_{land} = 26{,}368\ lbs$ assuming all external payload dropped, 75% of ammo dispensation, and 50% of fuel used up
- Takeoff weight $W_0 = 50{,}000$ as determined back in Chapter 3

35

The following W/S variations are determined with the listed assumptions above. The following W/S variations are determined in Table 4.3 and plotted in Figure 4.5.

Table 4.3 – Maximum wing loading required for landing

$C_{L_{max}}$	1.6	1.8	2.0
$\left(\dfrac{W}{S}\right)_{land}, \left(\dfrac{lbs}{ft^2}\right)$	126.44	142.25	158.05
$\left(\dfrac{W}{S}\right)_{land}, \left(\dfrac{kg}{m^2}\right)$	617.33	694.53	771.67
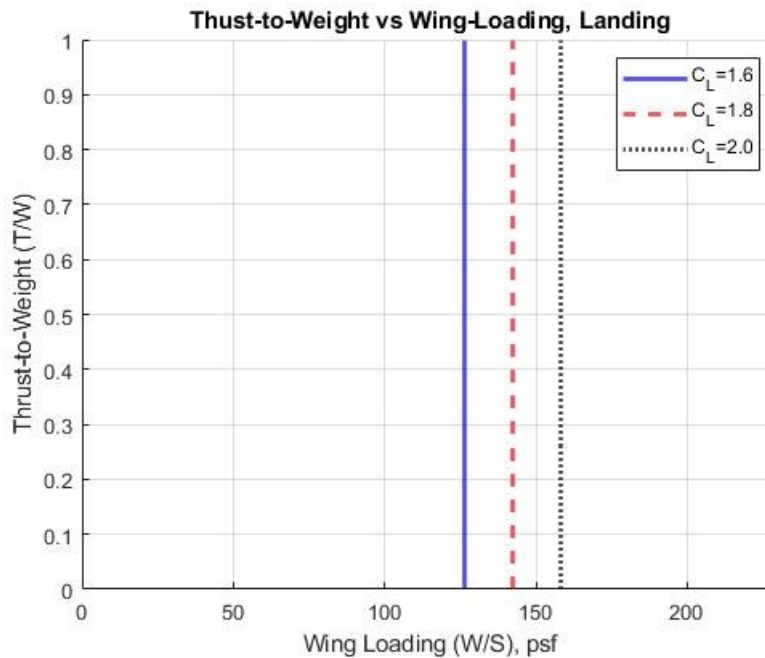
Figure 4.5 – Required W/S for landing

This plot constrains how small the wing size can be regardless of generated thrust during landing. Therefore, it desired to size the wing left of the plotted vertical lines at or below the desired W/S.

Using the same wing-loading comparison of the A-10 and a $C_{L_{max}}$ of 2.0, the required landing distance can be estimated using equation (4.4), resulting a total landing distance of 2,348.5 ft (715.8 m). S_a in equation (4.4) is the required horizontal obstacle-clearance distance, 450 ft for military aircraft, to avoid a 50 ft height obstacle.

$$S_{land} = 80\left(\frac{W}{S}\right)\left(\frac{1}{\sigma C_{L_{max}}}\right) + S_a \tag{4.4}$$

When analyzing with RDSWin with the same $C_{L_{max}}$ the total required landing distance comes out to 3,170 ft (966 m), including both distances traveled in air and on the ground.

4.5   Climb Estimates

Climbing requirements constrains both wing and engine sizing together requiring relationship analysis between T/W and W/S. The required thrust for the climb is based on the aircraft's climb gradient, defined in equation (4.5), the ratio between the vertical rate-of-climb (ROC) velocity and the projected horizontal velocity during the climb.

$$G = \frac{ROC}{V_{velocity}} \tag{4.5}$$

Per both Roskam and Raymer methods, horizontal velocity is estimated 30% above the aircraft's stall speed. For the vertical portion, it is desired by the USAF that the aircraft can climb at least 4,000 feet per minute at an altitude of 5,000 ft. For comparison, the A-10 can climb at 6,000 feet per minute. To understand the relationship between the thrust required and the vertical ROC, a set of vertical ROC values were used to determine various climb gradients G: 4000, 5000, and 6000 feet per minute.

With the various gradients determined, they are plugged into equation (4.6) to determine the required T/W at each vertical ROC. Additional estimations were made as follows:

- Horizontal Dynamic Pressure $q_{climb} = 103.85 \frac{lbs}{ft*s}$ at 30% above stall speed and an altitude of 5,000 ft.
- Zero-lift drag coefficient $C_{D_0} = 0.015$
- Wing aspect ratio $AR = 6$
- Oswald efficiency $e = 0.80$ at clean configuration

$$\frac{T}{W} = G + \left(\frac{q_{climb} * C_{D_0}}{W/S} + \frac{W/S}{q_{climb}\pi ARe} \right) \tag{4.6}$$

This relationship is then plotted as seen in Figure 4.6.
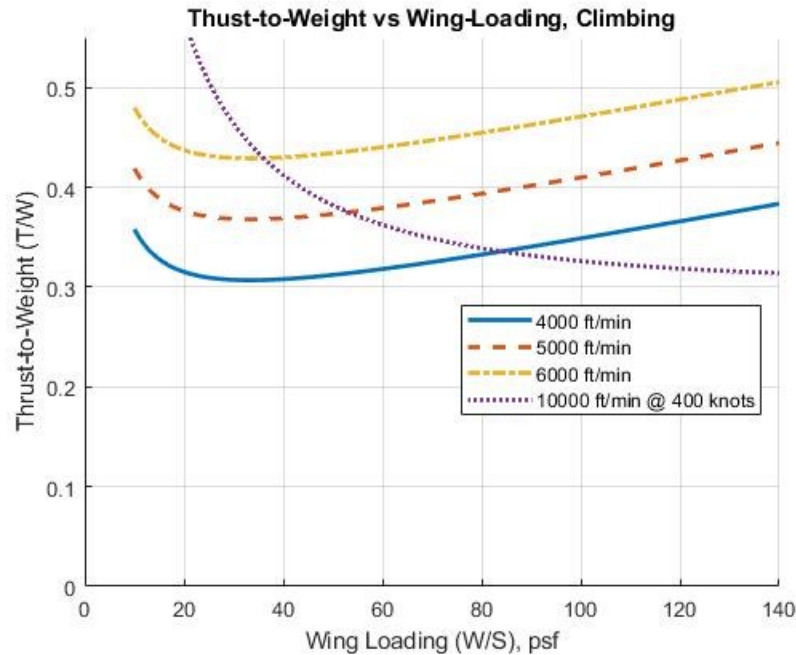
Figure 4.6 – Required thrust for climb

Depending on wing size, the engine size is constrained above the plotted values from the above figure. As W/S increases, the T/W decreases exponentially, then gradually increases to the right. This implies that a smaller wing is recommended while only needing to increase the engine slightly. When compared to the A-10's clime rate capability of 6,000 ft/min, the YA-94 needs to produce a T/W of roughly 0.47 at a W/S value of $100 \ lbs/ft^2$. This T/W value is higher than the estimated T/W of 0.35. Therefore, a ROC of 4000 ft/min is chosen instead as it meets both T/W estimate and ROC requirement by the USAF.

Later determined and explained in section 20.4, when adjusting the horizontal dynamic pressure to the aircraft's maximum speed of 400 knots and a ROC of 10,000 ft/min, it can be seen a T/W of only 0.33 is required at the designed W/S of 85 lbs/ft². Therefore, the YA-94 is capable of higher ROC when travelling at higher speeds, depicted by the purple dotted line in Figure 4.6. However, the 4000 ft/min is kept as critical for sizing purposes.

4.6   Cruise Estimates

Cruise speed is another essential constraint to the YA-94's performance, more apparent when determining the aircraft's range capability. The cruise speed is a factor based on both the W/S and T/W. This relationship is presented in equation (4.7).

$$\frac{T}{W} = \frac{q_{cruise} * C_{D_0}}{W/S} + \frac{W/S}{q_{cruise} * \pi * AR * e} \tag{4.7}$$

The following assumptions were made to determine the above equation:

- Dynamic pressure of $q = 155.08 \frac{lbs}{ft-s}$ at 30,000 ft above MSL and cruising at 350 knots.
- Zero-lift drag coefficient $C_{D_0} = 0.015$
- Wing aspect ratio $AR = 6.0$
- Oswald efficiency $e = 0.80$ at clean configuration

At various W/S values, the equation is plotted in Figure 4.7.
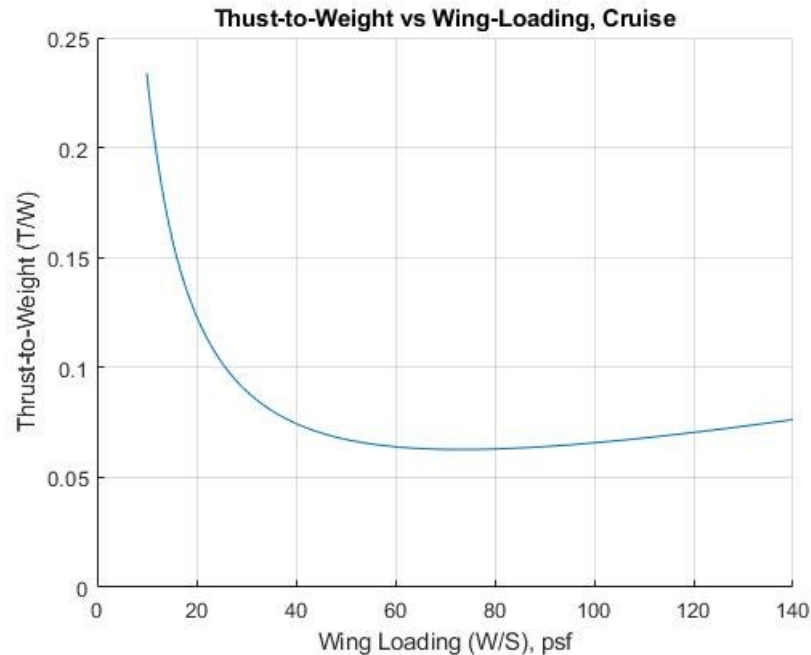
Figure 4.7 – Required T/W and W/S for cruise

Figure 4.7 constrains the maximum wing size and minimum engine size of the YA-94 to achieve the required cruise speed. Thus, it is desired to be above and to the right of the plotted line. The required thrust decreases exponentially and gradually increase as the wing reduces in size.

4.7 Turning Estimates

Two turn types are required in a military aircraft, including the instantaneous and the sustained turning maneuvers. The instantaneous turn is an aircraft's maximum turn capability at any given moment, sacrificing energy and altitude in the process. A sustained turn is how well and tightly the aircraft can maintain the turn rate for an extended time without sacrificing altitude and energy. Both maneuvering types need a very tight turn radius for an attack aircraft. This allows the aircraft to provide continuous support for ally ground troops and remain nearby between each attack.

The aircraft's maximum lift or overall structural integrity determines the maximum instantaneous turn. In other words, only the W/S of the aircraft needs consideration. Equation (4.8) determines the required W/S where n is the load factor acting on the wing. Per the USAF

requirements in a new attack aircraft, it is desired to have the capability to pull 6-Gs at 20 degrees per second quickly. This turn rate determines the required tangential velocity solved in (4.9), solving the required dynamic pressure during the turn. Figure 4.8 shows the required W/S to manage such a turn at different combat maximum C_L while using the listed assumptions and estimations.

$$\frac{W}{S} = \frac{q_{turn} * C_{L_{max},combat}}{n} * \frac{W_0}{W_{combat}} \tag{4.8}$$

$$V_{turn} = \frac{g\sqrt{n^2 - 1}}{\dot{\psi}} \tag{4.9}$$

- Gravity acceleration $g = 32.2\frac{ft}{s^2}$
- Turn rate $\dot{\psi} = 20°/sec$
- Combat Weight $W_{combat} = 0.85 * W_0$
- Dynamic pressure of $q_{sturn} = 354\frac{lbs}{ft-s}$ at SL, standard atmosphere condition
- Load factor $n = 6\ Gs$
- Combat Max lift coefficient $C_{L_{max},combat} = 1.5, 1.6, 1.7$

As for sustained turning, it is based on only the T/W of the aircraft. It is desired that YA-94 can perform a sustained turn of at least 2-Gs. It can also be estimated that the Oswald efficiency reduces by 30% or more of its initial clean values. Equation (4.10) determines the necessary relationship for the desired sustained turn capability.

$$\frac{T}{W} = 2n * \sqrt{\frac{C_{D_0}}{\pi * AR * e}} \tag{4.10}$$

The listed estimates were used in the above relationship:

- Load factor $n = 2\ Gs$
- Zero-lift drag coefficient $C_{D_0} = 0.015$
- Wing aspect ratio $AR = 6.0$
- Oswald efficiency is 50%, 60%, and 70% of $e = 0.80$ at clean configuration

This relationship is plotted in Figure 4.8, constraining each turn maneuver's minimal wing and engine size. Maintaining a sustained turn requires a large enough engine to provide great thrust over time, and the wing also needs to be large enough to handle the high loading experienced during an instantaneous turn.
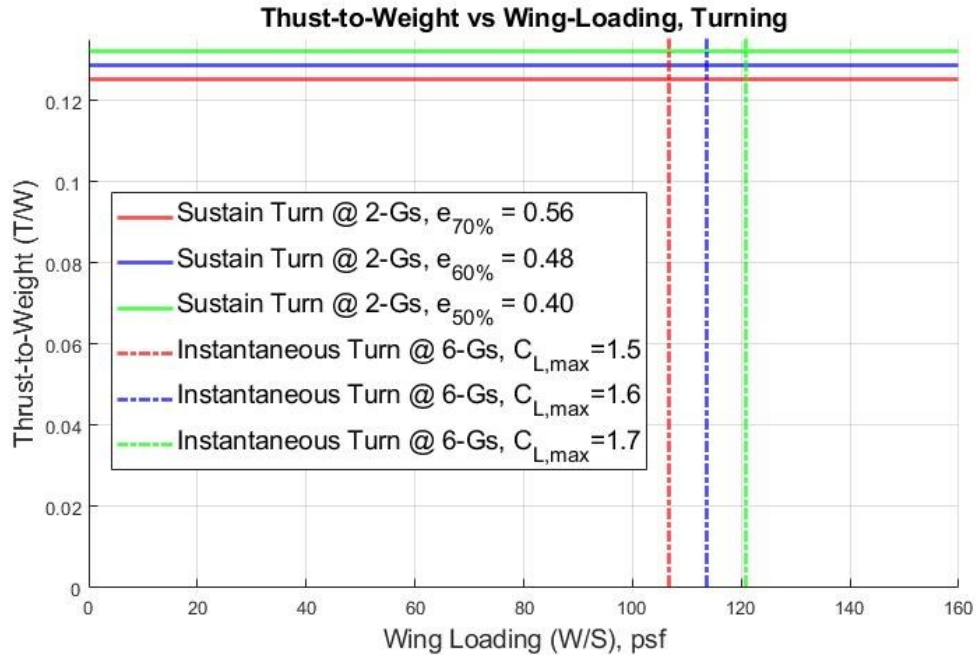
Figure 4.8 – Required T/W and W/S for instantaneous and sustained turning

The sustained turn is attainable and well under the required T/W values determined in the previous sections. The instantaneous turn constraint is also achievable allowing the wing to be smaller than the A-10 if needed. Therefore, all predicted turn rates and loadings are attainable in this design.

4.8   Matching Graph

After establishing all required constraints in relations between thrust-to-weight ratio and wing-loading, the above results are compiled into a single plot called a Matching Graph, as seen in Figure 4.9. The calculations and steps to generate this graph can be referred in Appendix D – MATLAB Code: Wing-Loading and Thrust-to-Weight Ratio Relations. This graph assists in determining the required or desired size of the wing and propulsion systems for the YA-94. Figure 4.9 displays only the constraints at required values with the design point and region indicated. Thus, the desired sizing of the aircraft has an estimated wing-loading of $85 \ lbs/ft^2$ and a thrust-to-weight ratio capability of around 0.35.
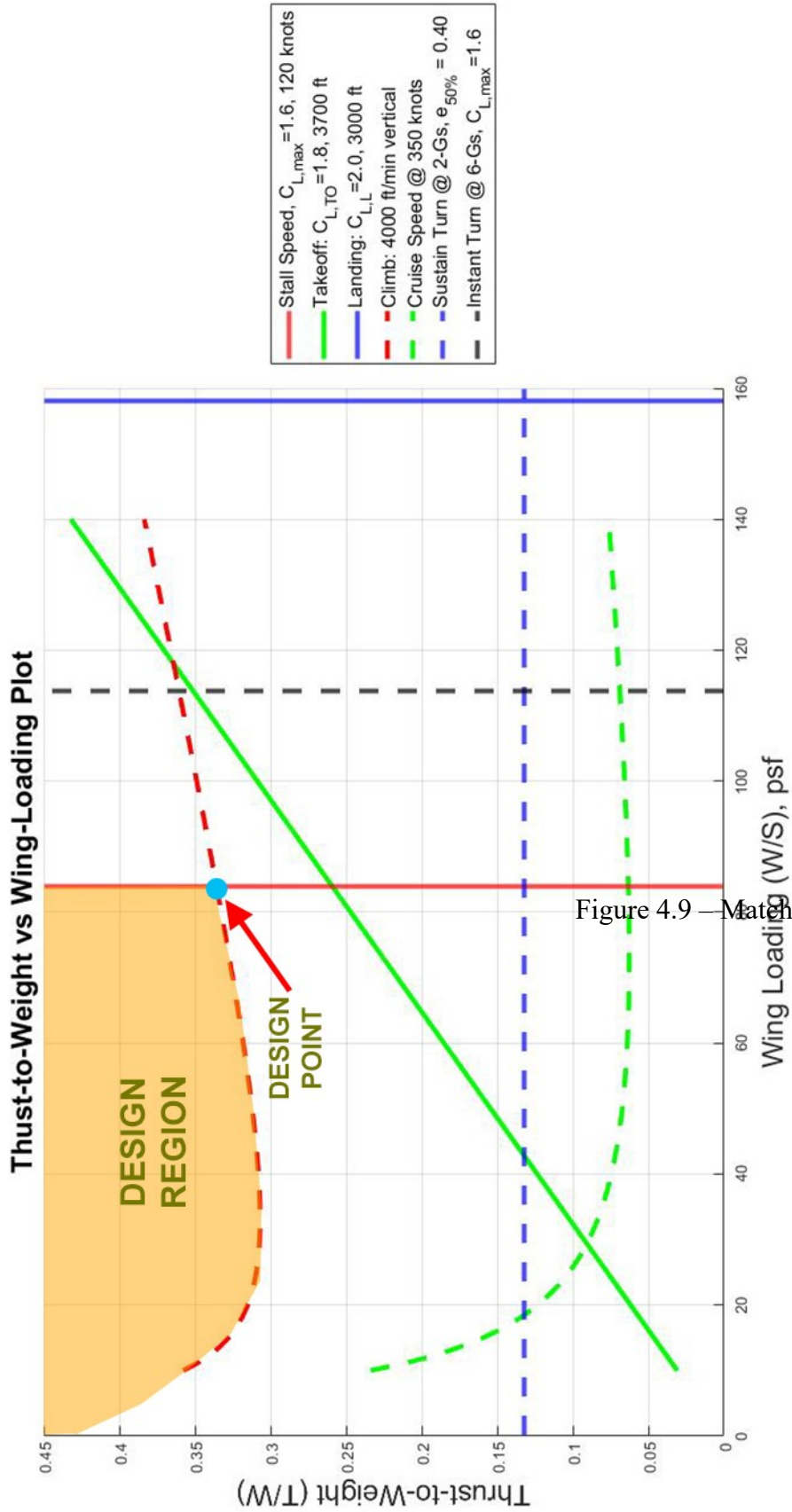
Figure 4.9 – Matching graph of all constraints

4.9   Conclusion

As seen in Figure 4.9, though all constraints must be calculated to determine the proper sizing of the wing and propulsion systems for the aircraft, not all constraints are significant to the design. For example, the required wing-loading for landing is to the right, signifying a smaller wing can be used while meeting the wing-loading required for stall. In addition, the plot for cruise and sustained turning is well in the lower T/W regions of the plot. Therefore, the required thrust for both aspects is not of great concern.

As for the constraints with significant effects on the YA-94's design, the takeoff constraints, for example, plays a significant role. A T/W of roughly 0.34 is required to achieve the takeoff distance and stall speed. For comparison, the T/W on the A-10 is 0.36. Therefore, assuming the same W_0, the YA-94 would require an additional 5.7% decrease in engine size suggesting that the same engine from the A-10 can be used. Another constraint that must be taken into consideration is the instantaneous turn. To achieve a 6-G load turn at 20 deg/sec, the aircraft requires a maximum wing loading of 115 lbs/ft^2. This suggests a similar wing size of the A-10 can be used for the YA-94.

In conclusion, the following constraints have been determined as important for the design process and referenced for sizing purposes when configuring the aircraft:

- Takeoff
- Stall Speed
- Climb
- Instantaneous Turn

Chapter 5 – Conceptual Aircraft Configuration

5.1   Introduction

Chapter 5 discusses selecting the configuration of the wing, empennage, landing gear, propulsion, gun placement, external payload placement, fuel tanks, and cockpit layout. Most of these features are determined based on the constraints discussed in Chapter 4. Other features are observed further and determined based on past aircraft configurations covered in the comparative study section. A final concept design of the YA-94 is presented at the end of this chapter.

5.2   Comparative Study

Table 5.1 compiles all previous aircraft discussed in Chapter 1 and briefly looks into their configuration setup. Images of the tabulated aircraft can be referenced back in Chapter 1.

Table 5.1 – Similar CAS aircraft configuration comparison

Aircraft:	AT-6	EMB 314	Scorpion	F-35	Su-25	A-10
Wing Location	Low-Wing	Low-Wing	High-Wing	Blended Wing-Body	High-Wing	Low-Wing
Crew Size	2	2	2	1	1	1
Landing Gear	Tricycle	Tricycle	Tricycle	Tricycle	Tricycle	Tricycle
# of Engines	1	1	2	1	2	2
Engine Type	Turboprop	Turboprop	Turbofan	Turbofan	Turbojet	Turbofan
Tail	Conventional	Conventional	Twin-Tail	Twin-Tail	Conventional	H-Tail
Service Introduction	2001	2003	Under Development	2015	1981	1977

5.3   Discussion

Each CAS aircraft listed in Table 5.1 has at least two similar configuration traits. One significant aspect is the choice to be designed as a conventional aircraft instead of an exotic design. Cockpit, empennage, wings, and landing gear are all placed in similar locations along the fuselage, which is found on other aircraft outside the CAS role. However, each aircraft differs in its detailed configuration. This section shall discuss the pros and cons of each configuration layout.

5.3.1 Wing Placement

- Low Wing [9]

    Low wings are wings mounted at the bottom of the aircraft's fuselage. One of their main advantages is the increased storage for the landing gear. Since the wing box is already strong on its own, it can absorb gear loads. Another advantage is the ground clearance for the underbelly of the fuselage, which reduces the aft-fuselage upsweep needed to attain the required takeoff angle of attack. However, the landing gear must be lengthened, increasing its overall weight with such a ground clearance. Additionally, a dihedral angle is required for low wings to avoid the wingtip striking the ground during an undesirable landing.

- High Wing [9]

    A high wing mounts to the upper fuselage allowing the fuselage to be placed closer to the ground while giving sufficient ground clearance for jet engines and propellers without the need for excessive landing-gear lengths. Furthermore, this placement minimizes the wing tips' chances of striking the ground at a nose-high rolled altitude. One disadvantage is the wings obscuring the pilot's visibility during a turn, usually in the direction of the aircraft's maneuver. Another is the increased fuselage size and weight. Since the wings are mounted high, the fuselage structure must be strengthened to support the landing-gear loads.

- Blended Wing-Body (BWB) [39] [40]

    BWB is a configuration with no clear decisive line between the wings and the fuselage. As in the name, the wing and body structures are smoothly blended, allowing a reduced wetted area and skin drag allowing increased fuel efficiency. In addition, the BWB aircraft is capable of stealth flight as it has much smoother surfaces around the aircraft, reducing its overall radar signature. However, the disadvantage of this design is that it has a higher empty weight for a given payload and is thus not economical for short missions. This design is very complex to design and maintain, especially when stealth is an important feature.

5.3.2 Tail Design

There are many variations in empennage designs, as shown in Figure 5.1. However, for a CAS aircraft, only a limited amount of tail designs may be considered applicable for its mission. The conventional, twin, dual/H, and pelikan tail designs are considered and discussed below.
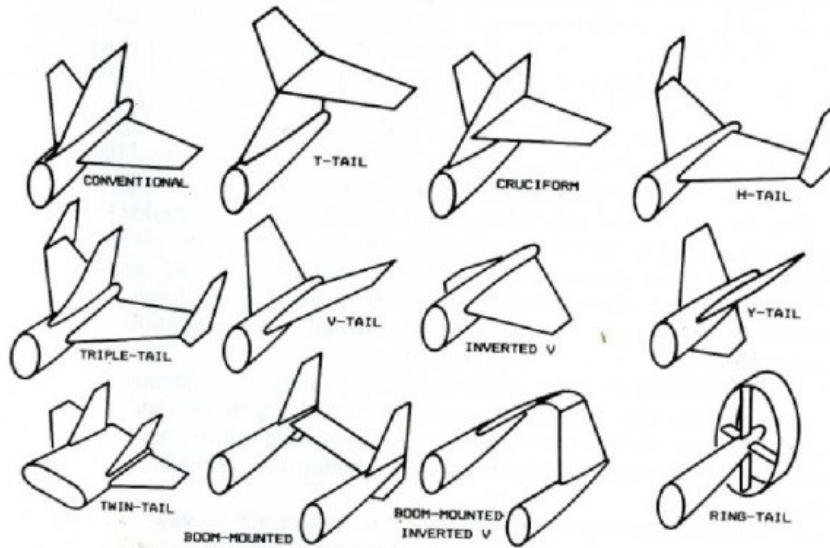
Figure 5.1 – Various Empennage Configurations [41]

- Conventional

    This is the most common tail form for many aircraft as they are easier to manufacture and maintain. As a bonus, they are very lightweight for their design. Unfortunately, the vertical stabilizer must be designed very tall to sustain yaw stability which increases the radar cross-section of the aircraft. Likewise, there are no redundancies since there is only a single vertical stabilizer. This is crucial for fighter aircraft during combat as yaw stabilization is challenging to maintain if it were to be damaged. [42]

- Twin-Tail

    The twin-tail is the next typical tail design for various modern-day air superiority aircraft. This is because they help reduce the aircraft's overall radar cross-section. These tails are much shorter than the conventional design while maintaining the same, or perhaps better, yaw stability control. This tail design also provides redundancy in case one rudder becomes damaged. However, to operate two vertical stabilizers would require additional hydraulic systems, increasing weight, and required maintenance. [42]

- Dual/H-Tail

    The dual-tail, commonly referred to as the H-tail, is similar to the twin-tail design, featuring two separate vertical stabilizers. The main difference is that the vertical stabilizers are located on the ends of the horizontal stabilizer on an H-tail. This allows for better aerodynamic performance due to the endplate effect. Typically, as air flows over the horizontal surface, a bit of air tends to spill out to the side of the surface. Endplates stabilize the flow over the horizontal surface, providing more yawing stability than the twin-tail design. In addition, this design allows smaller, lighter, and more aerodynamically efficient horizontal stabilizers. [41] [42]

- Pelikan Tail

    The pelikan tail is an experimental tail design shown in Figure 5.2 and was first applied to Northrop Grumman's YF-23. This tail design allows only the need for two control surfaces to achieve pitch, yaw, and roll. This gave greater pitch control at high angles of attack, and two tail surfaces would have a much lower radar signature than the standard four surfaces found on many fighter aircraft. However, using two larger control surfaces suggested a considerable weight penalty. This design would require bigger hydraulic pumps and cylinders to operate, dramatically increasing the aircraft's overall weight by hundreds of pounds. [43]

Figure 5.2 – Pelikan tail design [41]

5.3.3   Crew-Cockpit Size

In many cases, fighter aircraft include a single pilot or two, the other being a Radar Intercept Officer (RIO). In most modern fighter aircraft, only a single pilot is required due to advancements in technology, allowing the single pilot to multitask. With only one pilot on board, there are dramatic weight savings for additional internal equipment to be installed or higher external payload capacity. However, in a CAS mission and discussed back in Chapter 1, a wingman would be required since the pilot in the primary attack aircraft will reduce their situational awareness over time. The wingman would only be required to assist in forwarding communications with various controllers. This results in wasted energy, time, and money maintaining a second aircraft in the air while further producing low-time, inexperienced wingmen. If not for the CAS mission, the second aircraft could be used in more meaningful tasks while giving airmen in that aircraft the required flying experience they need.

In contrast, a fighter aircraft with a pilot and an RIO allows the pilot to focus on the mission's objective, in this case, providing CAS for allied troops. The RIO will assist in all forward communications and designating targets, relieving the pilot of the extra burden of such activities. This helps increase the pilot's situational awareness while increasing accuracy and effectiveness when engaging their target. Nevertheless, including an RIO on board increases the weight while reducing the internal capacity of the aircraft. This includes installing an additional ejection seat, extending the internal length of the cockpit, and additional electronics the RIO may need onboard.

5.4   Configuration Discussion

After understanding the advantages and disadvantages of the listed configuration designs above, the YA-94 configuration is proposed and discussed in the following subsections:

- Low wing, straight
- H-tail
- Tandem cockpit
- Tricycle landing gear
- High-mounted, twin turbofan engines

5.4.1   Low Wing, Straight

A low wing configuration is chosen for this design as it allows underbelly clearances required to mount external armament underneath its fuselage as the YA-94 is required to carry as much external payload as it can where available. This wing configuration also allows for a smaller fuselage as it does not require absorbing high loads from the main landing gear while maintaining an overall aerodynamic fuselage. In addition to the low wing configuration, the wings themselves are a straight design. Since this aircraft is for subsonic flight, swept wings are unnecessary and nonbeneficial. An inverted gull wing design was also considered but scrapped due to the risk of increased weight and complex geometry as it has both an anhedral and dihedral outline.

5.4.2   H-Tail

The H-tail design is the chosen tail configuration for the YA-94. This allows the aircraft to have excellent yaw stability, especially when diving and engaging enemy targets on the ground, as accuracy is crucial. In addition, since the engines are mounted above the fuselage, discussed later, the H-tail provides a lower heat signature. When viewed at the aircraft's rear at any slight angle, the hot exhaust from the engine is blocked from view due to the twin vertical stabilizers and the extended horizontal stabilizer. This makes it difficult for heat-seeking armament to maintain a perfect lock on the aircraft. Since this aircraft flies at low altitudes and low speeds during combat, this is a required safety feature for the pilots on board. In addition to safety, since there are two vertical stabilizers, this provides redundancy if one becomes damaged during combat, allowing the pilot to fly away with some control remaining.

5.4.3   Tandem Cockpit

A crew of two is considered for the design. As mentioned before, regardless of how modern avionics allows easier multi-tasking, reducing the workload of the primary pilot is still helpful and allows them to focus on providing CAS. The primary pilot only needs to fly the aircraft and engage the target with an RIO on board. The RIO can take care of the rest, such as locating targets and communicating with controllers for effective engagement. This crew setup also provides another redundancy set if the primary pilot becomes impaired or unconscious during combat. The RIO can take over flying the aircraft and possibly save the pilots and the aircraft.

5.4.4   Tricycle Landing Gear

The choice of a tricycle landing gear configuration is due to it being typical for modern military aircraft. This configuration allows a much clearer view from the cockpit than the conventional or tail gear configuration. This landing gear grants the aircraft's tail to be lifted above the ground allowing enough clearance for the aircraft to perform aggressive high angles of attack during takeoff. The aircraft's center of gravity (CG) is also moved forward of the main landing gear in this configuration. This nearly eliminates ground looping, where a fixed-wing aircraft is rapidly rotated in the yawing plane while speeding on the ground. If this occurs, one wing could rise with the other striking the ground, and in severe cases, the wing could dig into the ground, causing the aircraft to swing violently or even cartwheel [44]. Since the YA-94 requires sorting quickly, this configuration provides another safety net when the aircraft is rapidly taking off from the runway.

5.4.5   High-Mounted, Twin Turbofan Engines

The design decision for the engines' placement was to be mounted above the fuselage and towards the rear. Due to operating environments, engines mounted high are less susceptible to becoming damaged from ingesting foreign object debris (FOD) along the runway. This allows the aircraft to operate at various locations where the runway is not considered "clean" [45]. As mentioned previously, the heated exhaust from the engines travels over the H-tail reducing its heat signature with the engines mounted high and above the tail.

As for the engines themselves, they are of turbofan design. They are much more fuel-efficient for jet aircraft while providing sufficient thrust to arrive at their area of operation much quicker. Two of these engines must provide redundancy if one becomes damaged during combat. Also, two engines need to provide enough thrust to compensate for the recoil force of the gatling gun mounted on the aircraft.

5.5   Proposed Configuration Concept

Considering the above configuration selection, Figure 5.3 provides a conceptual sketch of the YA-94. Figure 5.4, Figure 5.5, and Figure 5.6 show the internal layout of major components such as landing gear storage, gun placement, etc.

Another configuration decision to note is that the gun is placed ahead of the cockpit, assisting in balancing the aircraft along the forward and aft direction. Fuel tanks are placed close to the aircraft's center to mitigate potential damage from enemy fire. Eleven external hardpoints will be available on the aircraft to maximize external storage capacity.
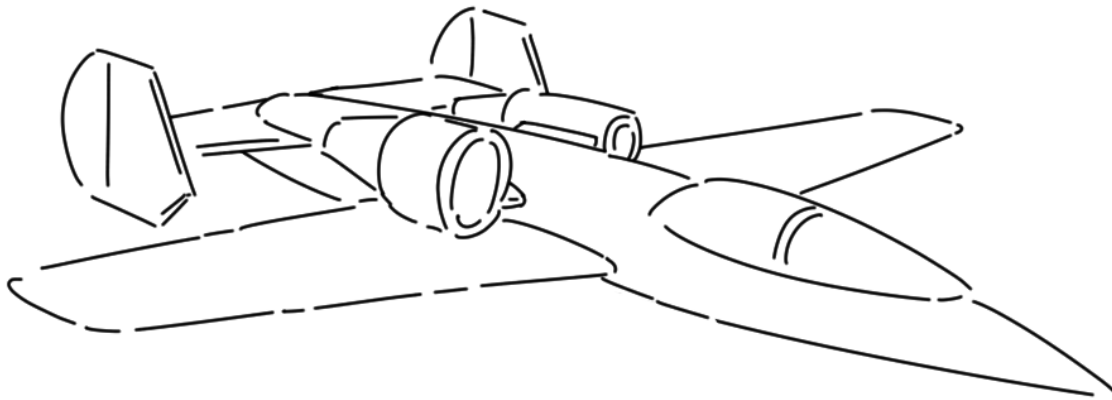
Figure 5.3 – Conceptual sketch of the YA-94
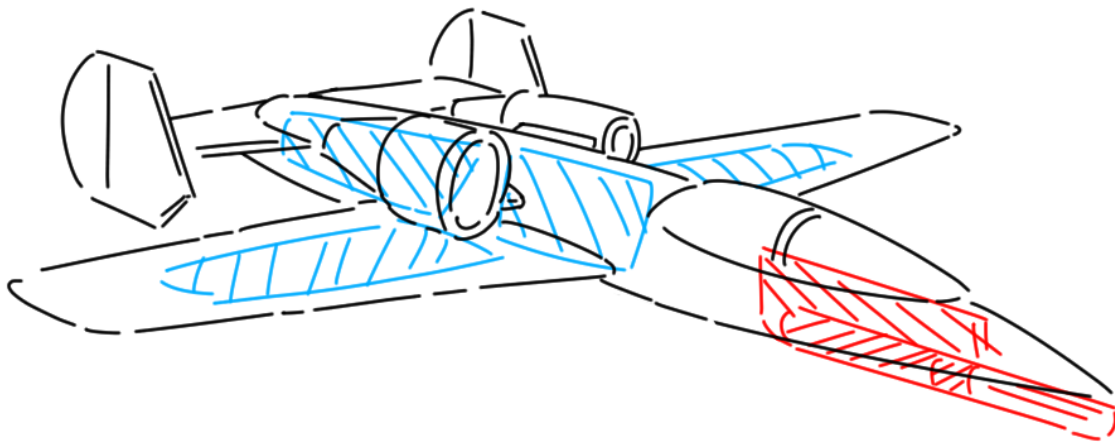
Figure 5.4 – Fuel tank (blue) and gun (red) placement on YA-94
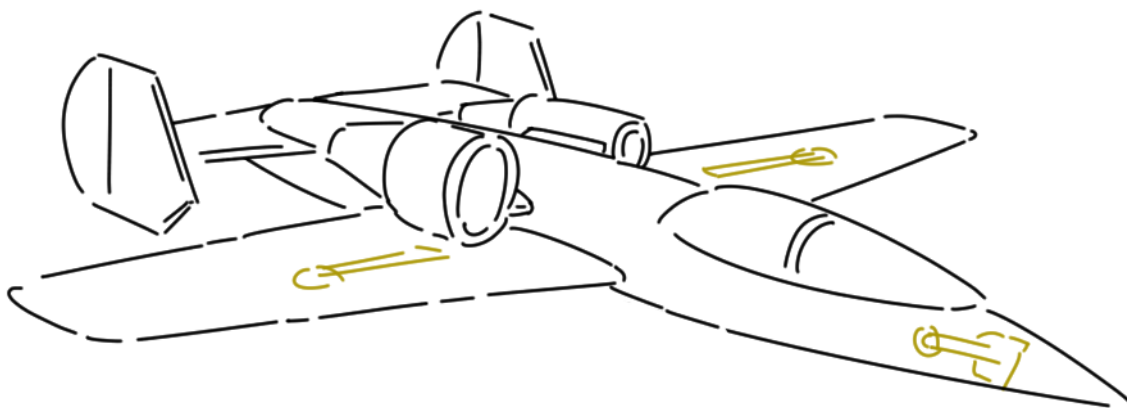
Figure 5.5 – Landing gear placement on YA-94
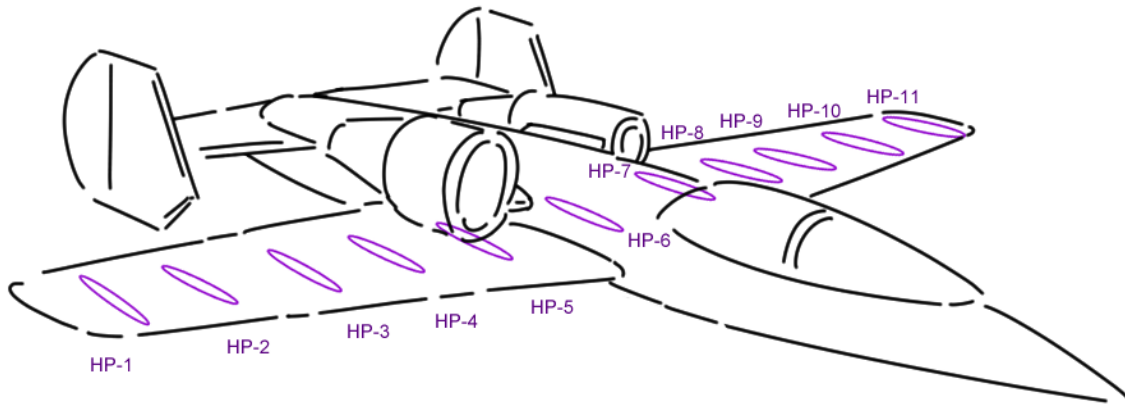
Figure 5.6 – Hardpoint locations on YA-94

5.6   Final Concept

After further analysis and final adjustments to the aircraft's overall design, Figure 5.7 presents the final design of the YA-94, modeled in Creo Parametric. The design analysis and adjustments are described in the following chapters.
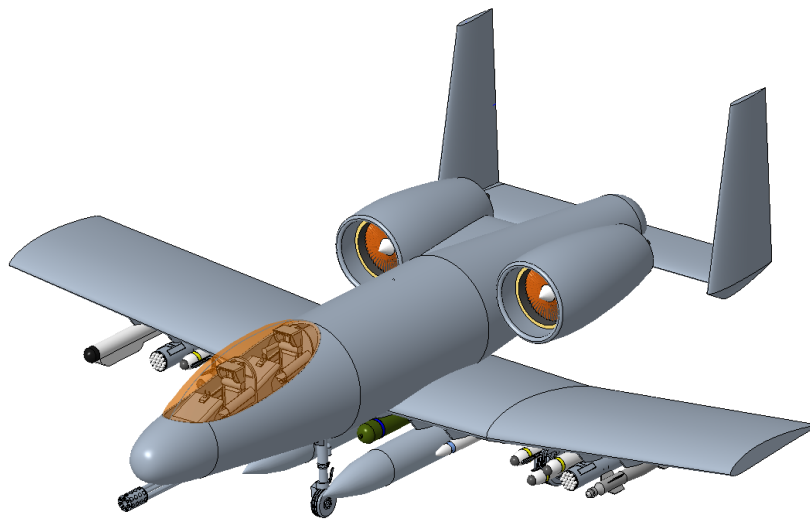
Figure 5.7 – YA-94 final CAD concept

Chapter 6 – Propulsion System Design

6.1   Introduction

Chapter 6 discusses the choices of engines, the down-selection process, and the chosen engine's specifications, such as maximum thrust capability and specific fuel consumption (SFC). Installed thrust analysis was performed and discussed to confirm the chosen engine for the aircraft. In addition, the integration of the chosen engine is discussed, including its position and start-up feature.

6.2   Turbofan Engines and Downselection

Two turbofan engine models were considered after browsing through various engine manufacturing catalogs. One of them was the TF-34-GE-100A turbofan by General Electric, and this is the original engine currently used on the A-10. An image of this engine can be seen below in Figure 6.1. The next engine of choice was the CF34-8C5B1 turbofan, also by General Electric, as seen in Figure 6.2. Table 6.1 presents and compares both engines' specifications.

Figure 6.1 – General Electric TF34-GE-100A turbofan engine

Figure 6.2 – General Electric CF34-8C5B1 turbofan engine

Table 6.1 – Engine specification comparison

	TF34-GE-100A		CF34-8C5B1	
Max thrust (lbf | kN, uninstalled)	9,065	40.3	13,790	61.3
Bypass ratio	6.5		5	
Max diameter (in | cm)	52	132.1	49	124.5
Fan diameter (in | cm)	46	116.8	46.2	117.3
Length (in | cm)	100	254	128	325.1
Dry weight (lbs | kg)	1,440	653.2	2,400	1088.6
SFC (lbm/lbf/hr | kg/N/hr)	0.371	.0378	0.670	.0683

When performing the weight sizing back in Chapter 3 – Weight Sizing, it was predicted that about 8000 lbs of fuel were required onboard (excluding external drop tanks) with an initial guess of the TF34's SFC. Therefore, the TF34 engine was chosen to be also used on the YA-94. Though the CF34 provides much higher thrust capability, the SFC is double what is present in the TF34. Therefore, additional fuel will be required resulting in a much heavier aircraft. The following section will discuss the installed thrust analysis of the TF34 to confirm it was the correct engine of choice.

6.3   Installed Thrust Analysis

Both Raymer's and Roskam's methods determined the TF34's installed thrust. Determining this thrust will confirm whether this engine is suited for this aircraft's mission specifications.

6.3.1   Raymer's Installed Thrust

It is estimated that the reference pressure recovery of a subsonic engine is 1.0. With the selected engine being a podded nacelle, the actual recovery pressure due to its very short duct is estimated to be 0.98. Knowing these recovery pressures, equation (6.1) can be used to estimate the thrust loss due to installation where C_{ram} is the inlet ram recovery correction factor, typically between 1.2 to 1.5. This results in a 2.70% thrust loss due to nacelle installation.

$$\% \, Thrust \, Loss = C_{ram}\left[\left(\frac{P_1}{P_0}\right)_{ref} - \left(\frac{P_1}{P_0}\right)_{actual}\right] \times 100\% \tag{6.1}$$

Another component of thrust loss to consider is the loss due to bleed air. Using the given manufacturing data of the engine's mass flow, equation (6.2) can be used to estimate the thrust loss due to bleed air, where C_{bleed} is the bleed correction factor (approximated as 2.0) and $\dot{m}_{bleed}$ is the bleed mass flow rate, typically ranging between 1-5% of the engine mass flow rate. When using the equation assuming a 5% bleed mass flow rate, the thrust loss due to bleed air results in 10.0%.

$$\% \ Thrust \ Loss = C_{bleed} \left[\frac{\dot{m}_{bleed}}{\dot{m}_{engine}} \right] \times 100\% \tag{6.2}$$

Therefore, a single TF-34 turbofan engine loses 12.7% of its maximum thrust when installed, thus only producing a maximum thrust of 7,913.74 lbf (35.2 kN). With the YA-94 being a twin-engine aircraft, the YA-94 can produce a maximum installed thrust of 15,800 lbf (70.3 kN).

6.3.2   Roskam's Installed Thrust

Roskam's predictions also confirmed whether the TF-34 is a suitably selected engine. To begin, the power extraction from the engine must be determined. This includes power from the electrical, mechanical, and pneumatic power systems. Both electrical and mechanical power extraction can be estimated at 100 shp for each. As for the pneumatic power extraction, it can be estimated using equation (6.3) where $\dot{m}_{bleed}/\dot{m}_a$ is the pneumatic total engine mass flow ratio, estimated to be .04 from historical data for attack jet fighters. The pneumatic power extraction required for the YA-94 is 434.9 shp.

$$P_{pneum} = \left(\frac{\dot{m}_{bleed}}{\dot{m}_a} \right) \left(\frac{T_{reqd} U_1}{550} \right) \tag{6.3}$$

With power extraction determined, equation (6.4) can be used to determine available installed thrust at each given speed where the following variables are defined below.

$$T_{av} = T_{\underline{tst}\atop av} \left(1 - 0.35 K_t M_1 \left(1 - \eta_{\underline{inl}\atop inc} \right) \right) - 500 \left(\frac{P_{extr}}{U_1} \right) \tag{6.4}$$

where:
- $T_{\underline{tst}\atop av}$ = Available uninstalled thrust
- M_1 = Flight mach number
- $\eta_{\underline{inl}\atop inc}$ = inlet efficiency
- P_{extr} = Total power extraction
- K_t = Effect of mach number factor

The above equation is plotted in Figure 6.3. This illustrates that as the aircraft speeds up, the available install thrust increases. Therefore, at the maximum speed of 400 knots with both engines running, the installed thrust is 17,257 lbf (76.76 kN). This is much more than what was predicted using Raymer's method and still meets the thrust requirement when performing a sustained turn as calculated in the previous sub-section. For maximum performance, the Roskam value will be used for installed thrust predictions.
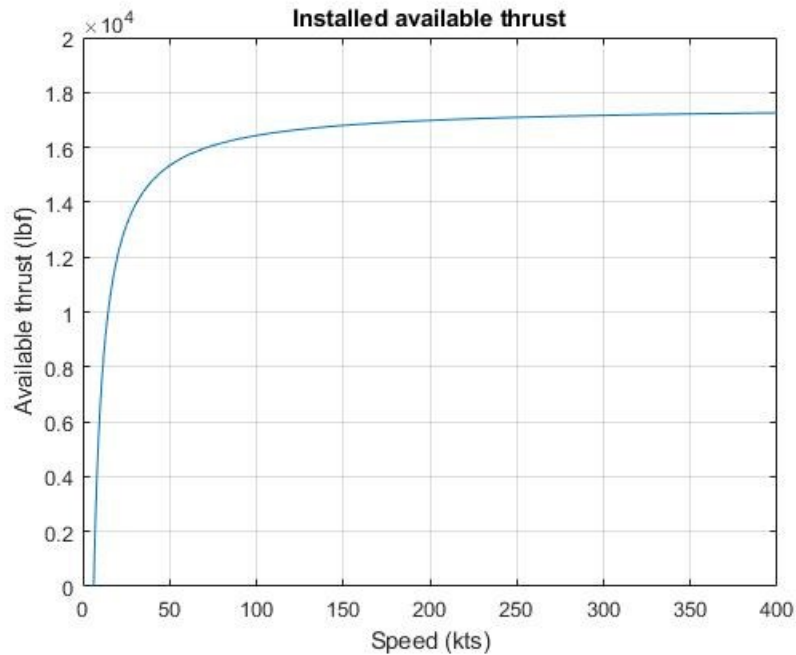
Figure 6.3 – Available installed thrust per aircraft speed

6.4   Propulsion System Integration

Both TF-34 turbofan engines will be mounted high above the fuselage and located aftward. As described in section 5.4.5, mounting the engines high will allow cleaner airflow into the inlets reducing the chances of ingesting FOD. Therefore, the YA-94 can operate on rougher airfields and runways if necessary.

With the engines located aftward, this allows for counterbalancing the heavy gun and large cockpit at the nose of the aircraft. Also, with the H-tail located behind the two engines, the heat exhaust can be easily concealed, making heat-seeking devices difficult to maintain lock-on.

Finally, an auxiliary power unit will be integrated alongside the engines. This will allow onboard startups and not require an external power generator to start the engines before the flight. An internal illustration of the engine integration can be seen below in Figure 6.4.
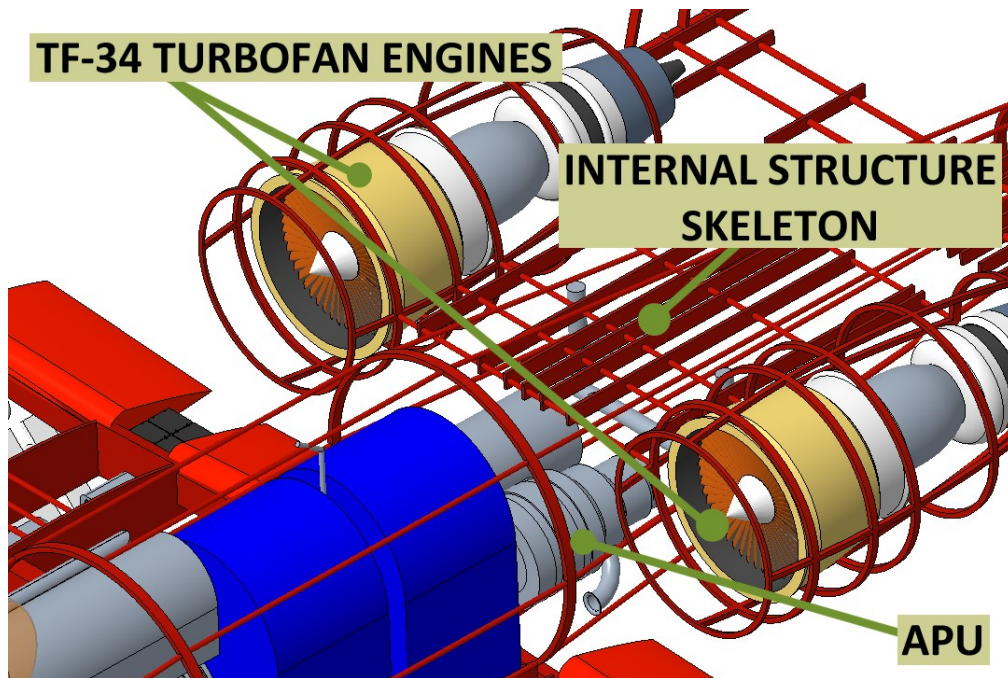
Figure 6.4 – Internal propulsion integration illustration

6.5   Conclusion

This chapter presented two engine model choices which were later downselected in favor of the TF-34 turbofan engine by General Electric, the same engine used on the A-10. Both Raymer and Roskam methods were used to analyze and justify the choice of the engine by confirming the required and available installed thrust during a sustained turning maneuver. It was also decided to integrate the engines at the aft end of the aircraft to balance the aircraft longitudinally while providing an internal APU to allow self-startup without using an external power generator resource.

Chapter 7 – Fuselage Design

7.1   Introduction

This chapter discusses the YA-94's fuselage design using preliminary estimates of mission weights and performance constraints calculated in previous chapters. The following factors were considered for the design:

- Maximum Takeoff Weight
- Fuel Weight and Storage
- Nose Landing Gear Location
- Wing Placement
- Engine Placement
- Gun Placement
- Tandem Seat Configuration

The chapter will detail the cockpit layout, seating arrangement, and the overall fuselage configuration, including fuel tank storage, gun, and avionic equipment locations.

7.2   Cockpit Design

7.2.1   Seating Layout

Figure 7.1 portrays a typical tandem cockpit configuration used in military jets. This layout could be seen on the F-14 Tomcat, F/A-18 Super Hornet, and F-4 Phantom, to name a few. However, this configuration is now mainly reserved for jet trainers rather than fighter aircraft.
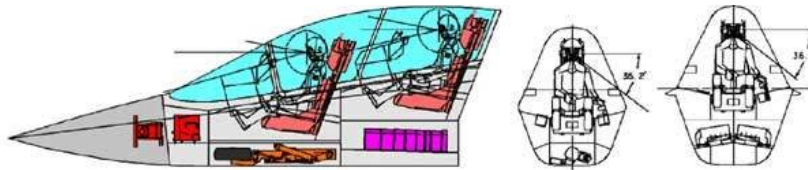
Figure 7.1 – Tandem cockpit configuration [46]

As mentioned in previous chapters, this configuration allowed the primary pilot to operate the aircraft and provide effective CAS. The co-pilot assists in managing other controls that the primary pilot would usually use, shifting focus away from the task at hand. In addition to the tandem configuration, both locations will include their ejection seat. The typical dimensions of these seats can be seen in Figure 7.2.
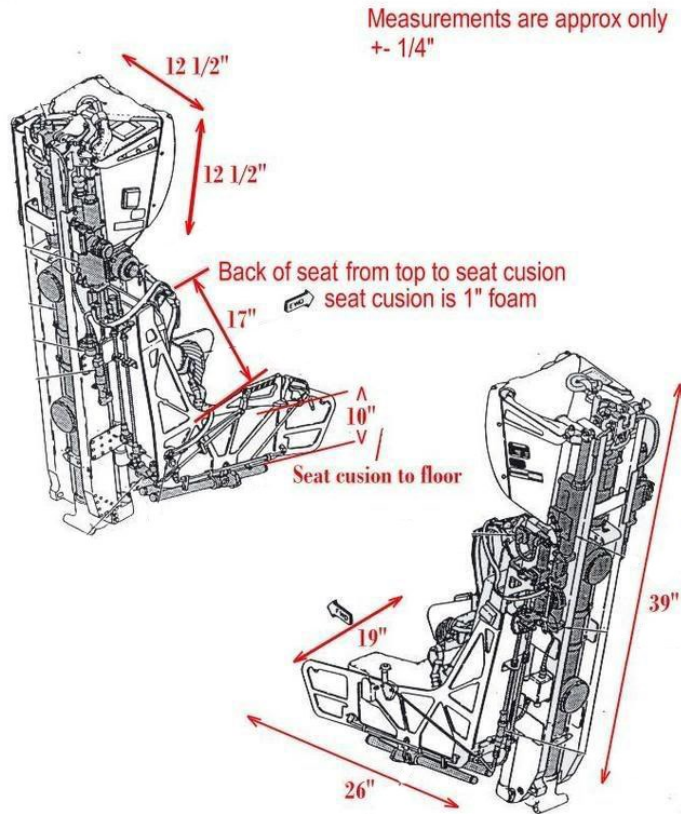
Figure 7.2 – Typical ejection seat dimension [47]

7.2.2 Pilot Field of Vision and Accessibility

After determining the pilot's seating location, it is vital to determine the pilot's visibility and accessibility and adjust as necessary. Visibility for the crew is crucial during takeoff and landing and especially during combat, as there will be times the pilots would require to identify friendly and hostile locations physically. Figure 7.3 illustrates the pilot's primary field of vision (FOV), defined as looking without moving the head.
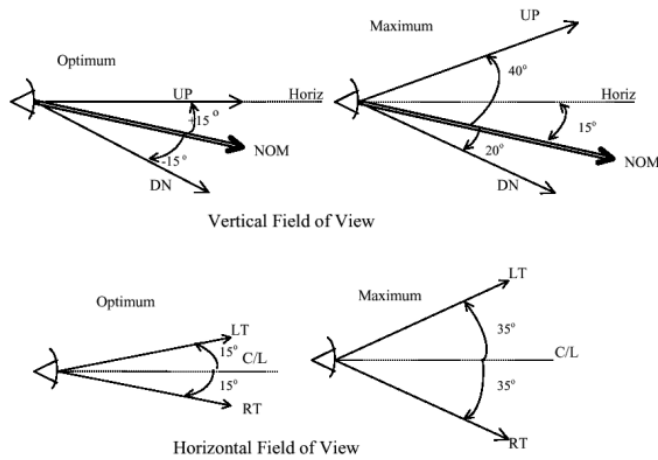
Figure 7.3 – Primary FOV – vertical and horizontal [48]

Realistically, the pilot will move their head to face or locate their target, not just their eyes. Therefore, to maximize their FOV, a bubble canopy design will be used to enclose the cockpit, similar to the canopy found on the F-16 (Figure 7.4).

Figure 7.4 – F-16 bubble canopy [49]

The pilots will be required to see outside their canopy and their instruments within the cockpit. All consoles provide a glare shield to prevent the sun from blinding the pilot's instruments onboard, ensuring displays are easy to read. Of course, this glare shield must not protrude too much, blocking the displays themselves. Figure 7.5 shows this required line-of-sight (LOS) between the console dashboard and displays.
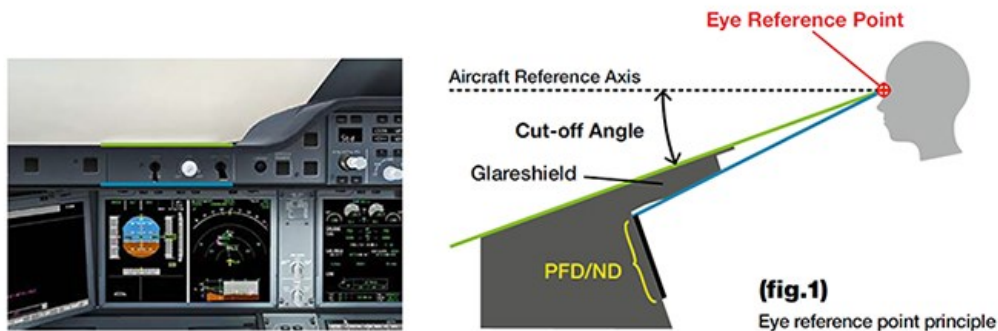
Figure 7.5 – Flight console accessibility [50]

It is also important to note that pilots between 5ft 2in (1.6 m) to 6ft 3in (1.9 m) shall access all of the aircraft's controls in the cockpit. This requirement stipulates from EASA CS 25.777, ensuring that the design fits most pilots. [50]

The final seating layout can be seen in Figure 7.6, including subsystems located around the cockpit area: main gun, ammo drum, nose gear, radar, and titanium "bathtub." Figure 7.7 and Figure 7.8 present each pilot's LOS when seated in the aircraft. Overall, with a bubble canopy, the pilot has almost a complete 360° FOV.
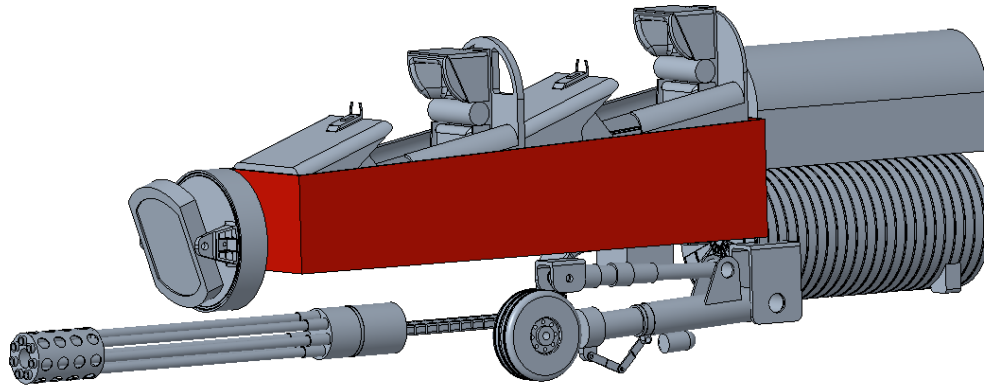
Figure 7.6 – Internal cockpit configuration
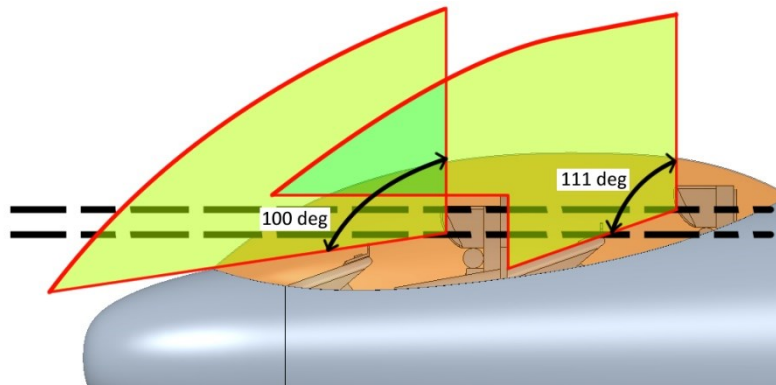
Figure 7.7 – Cockpit FOV and LOS angles (right view)
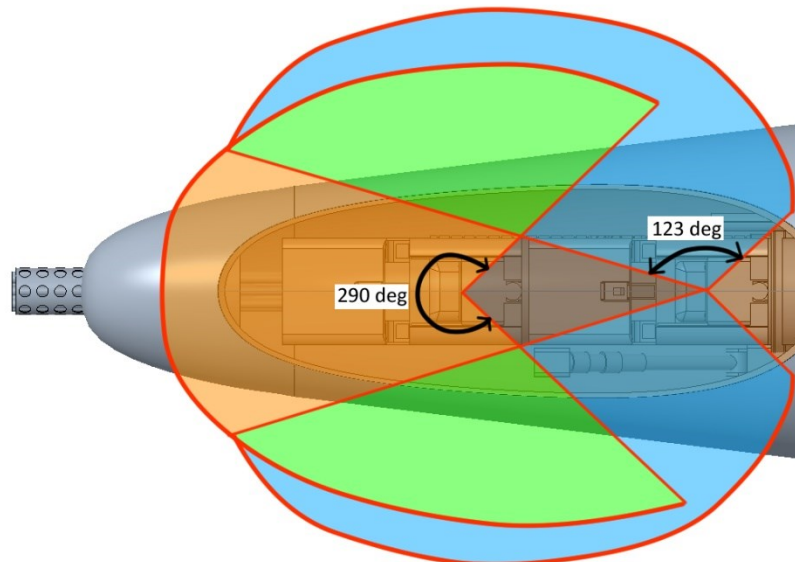
Figure 7.8 – Cockpit FOV and LOS angles (top view)

7.3   Fuselage Design

The fuselage design uses a similar approach presented by Roskam. Important geometric parameters of the fuselage are presented in Figure 7.9. This allows size estimation of the overall fuselage, including its length, diameter, tail clearance, and internal storage capacity.
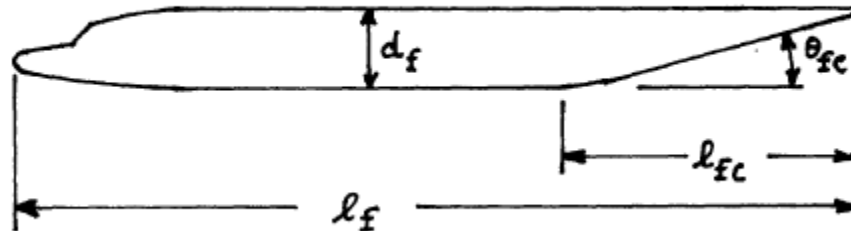
Figure 7.9 – Fuselage geometric parameters [38]

Each parameter determines its required dimensions to the surrounding sizing parameters. Each variable parameter represents the following:

- l_f = overall length of the fuselage
- d_f = overall diameter of the fuselage
- l_{fc} = length of fuselage clearance
- θ_{fc} = angle of fuselage clearance

The relationship between these parameters can be seen in Figure 7.1. For this project, the Fighter category is referenced for estimated fuselage measurements.

Table 7.1 – Definition of geometric fuselage parameters [38]

Airplane Type	l_f/d_f	l_{fc}/d_f	θ_{fc} (deg)
Homebuilt	4 – 8	3	2 – 9
Single Engine	5 – 8	3 – 4	3 – 9
Twins	3.6 – 8	2.6 – 4	6 – 13
Agricultural	5 – 8	3 – 4	1 – 7
Business Jets	7 – 9.5	2.5 – 5	6 – 11
Regionals	5.6 – 10	2 – 4	15 – 19
Jet Transports	6.8 – 11.5	2.6 – 4	11 – 16
Mil. Trainers	5.4 – 7.5	3	Up to 14
Fighters	7 – 11	3 – 5	0 – 8
Mil. Transports, Bombers, and Patrol Airplanes	6 – 13	2.5 – 6	7 – 25
Flying Boats	6 – 11	3 – 6	8 – 14
Supersonics	12 – 25	6 – 8	2 – 9

7.3.1 Fuselage Geometry

The initial estimation of the fuselage is begun with its overall length. This is calculated with equation (7.1), where a and C are statistical multiplicities to determine the fuselage length based on the aircraft's takeoff weight.

$$L_f = a * W_0^C \tag{7.1}$$

The a and C values can be determined in Table 7.2. For this project, the Jet Fighter category will be used.

Table 7.2 – Fuselage length vs. W_0 (lb or {kg}) [9]

	a	C
Sailplane – unpowered	0.86 {0.383}	0.48
Sailplane – powered	0.71 {0.316}	0.48
Homebuilt – metal/wood	3.68 {1.35}	0.23
Homebuilt – composite	3.50 {1.28}	0.23
General aviation – single engine	4.37 {1.6}	0.23
General aviation – twin engine	0.86 {0.366}	0.42
Agricultural aircraft	4.04 {1.48}	0.23
Twin turboprop	0.37 {0.169}	0.51
Flying boat	1.05 {0.439}	0.40
Jet trainer	0.79 {0.333}	0.41
Jet fighter	0.93 {0.389}	0.39
Military cargo/bomber	0.23 {0.104}	0.50
Jet transport	0.67 {0.287}	0.43

Using a takeoff weight of 50,000 lbs (22,680 kg), the overall length of the fuselage comes out to be 63 ft (19.2 m). The A-10 has an overall length of 53 ft (16.2 m). However, after arranging the internal components of the aircraft, it was determined that the fuselage only needed to be 50 ft in length. See section 7.3.2 for internal arrangement details.

Using the above ratios provided in Table 7.2, the other geometric parameters can be calculated, assuming $l_f/d_f = 6.25$, $l_{fc}/d_f = 2.19$, and $\theta_{fc} = 6.2°$.

- Fuselage diameter: $d_f = \dfrac{l_f}{l_f/d_f} = \dfrac{50}{6.25} = 8\ ft\ (2.33\ m)$
- Tail length clearance: $l_{fc} = \dfrac{l_{fc}}{d_f} * d_f = 2.19 * 8 = 17.52\ ft\ (9.33\ m)$

A CAD model of this determined fuselage can be seen in Figure 7.10.
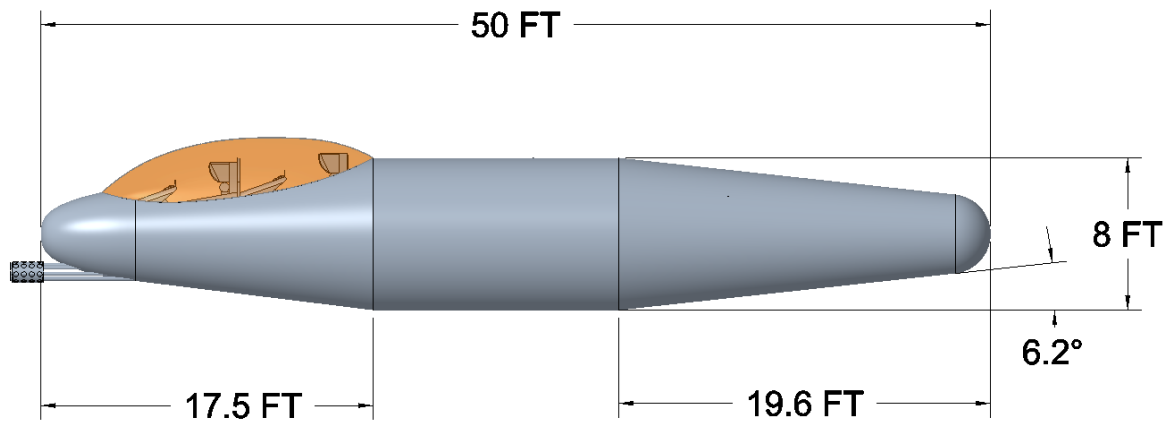
Figure 7.10 – YA-94 fuselage geometry

7.3.2   Fuselage Internal Arrangements

Figure 7.11 presents the internal arrangement of the YA-94 with its internal subsystems numbered and referenced in Table 7.3.
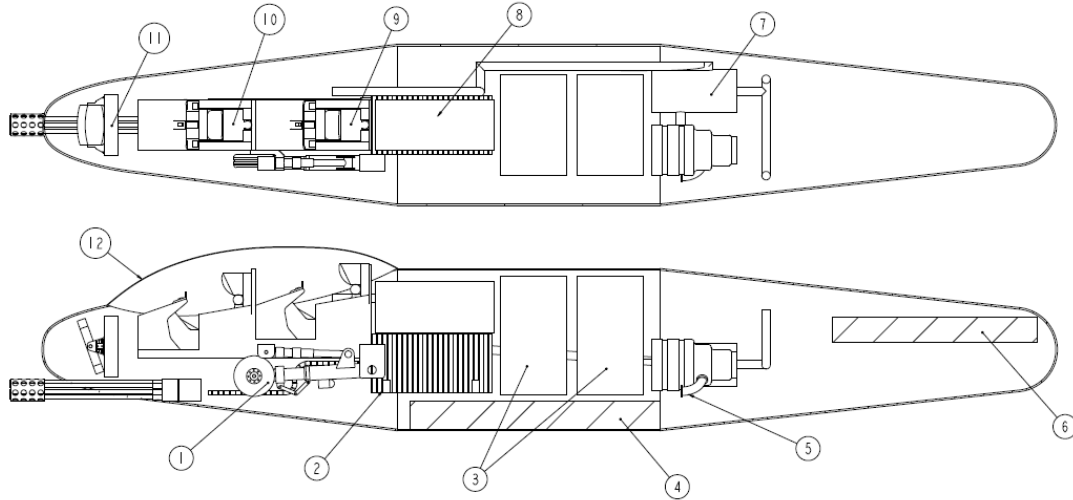
Figure 7.11 – YA-94 internal arrangement

Table 7.3 – Internal components

Find No.	Component Name
1	Nose Gear
2	GAU-8 Gatling Cannon and Ammo Drum
3	Internal Fuel Tanks
4	Wing Box
5	APU
6	Horizontal Tail box
7	AC unit
8	Avionics and Equipment
9	RIO Ejection Seat
10	Pilot Ejection Seat
11	Nose Radar
12	Canopy Glass

As shown, most of the components are located forward of the aircraft. This is to balance the aircraft longitudinally since both engines are mounted aftward. The ammo drum and fuel tanks must be located near the aircraft CG. They are components that will vary in weight during the entire flight process, thus mitigating any dramatic shifts in the aircraft's overall CG location.

The fuel tanks are mounted vertically above the fuselage centerline to allow the wing box to sit below. This placement will be further discussed in Chapter 8.

7.3.3   Weapon Placement

A standard air-to-air gun such as the M61A1 can produce a recoil force of 2 tons (18 kN). The GAU-8 (Figure 7.12) can produce roughly five times that recoil force when fired. Therefore, to prevent sudden yawing motion from firing, the gun is located near the aircraft's centerline [9]. Like the A-10, the YA-94's nose gear is offset to the gun's left to allow a clear LOS for the gun's barrels.
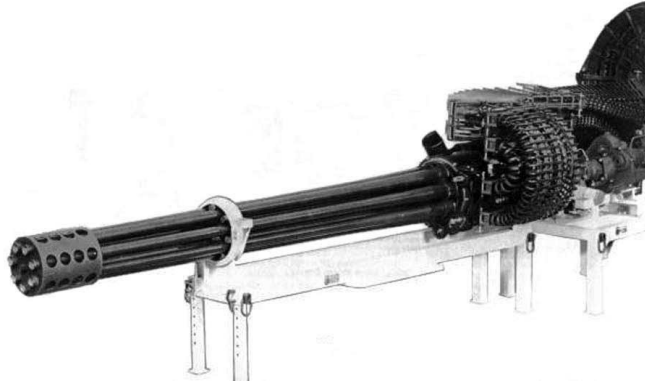
Figure 7.12 – General Electric GAU-8/A avenger gatling gun [51]

Due to its length, the pilots are seated above the gun's barrel and feeding mechanism. The ammo drum is placed behind both pilots, further into the fuselage. This will reduce exposure from incoming enemy fire, which could pre-detonate the ammo if not well protected.

As discussed in Chapter 5, the YA-94 will have 11 hardpoints along its wingspan to allow the mounting of various munitions and external devices. Eight of these are located along the wings themselves, and this leaves 3 of them located on the fuselage. Therefore, it is suggested that the three hardpoints be located directly below the wing box along the fuselage belly. This will provide structural integrity when mounting heavy external ordinances.

7.4   Conclusion

This chapter presented the detailed design approach for the cockpit and fuselage. Roskam's methods were used to estimate the overall fuselage dimensions based on provided dimension ratios for fighter aircraft. Internal arrangements of significant components were also discussed to predict the aircraft's CG location. Visualization of these arrangements and designs was done using Creo Parametric.

Chapter 8 – Wing Design

8.1   Introduction

Chapter 8 discusses the YA-94's wing design taking into consideration of the following factors from previous chapters:

- Maximum takeoff weight
- Fuel storage
- Maximum lift coefficient per flight condition
- Stall speed
- Landing gear storage

The chapter will detail the wing planform design, airfoil selection process, high-lifting device design, internal fuel storage, and main landing gear storage.

8.2   Wing Planform

8.2.1   Wing Planform Design Criteria

The YA-94 is designed for low-speed to subsonic flight regimes. Therefore, a straight wing planform design was chosen. A straight wing also allows easier mounting of external payloads. Since the location of the quarter chord is constant along the entire wingspan, the payload can be mounted roughly parallel to this chord line as well. Therefore, during payload drop, the overall aircraft's CG will only shift slightly, maintaining the aircraft's balance throughout the flight.

A straight wing will allow more accessible aerodynamic analysis, allowing easier design processes for its control surfaces. Finally, a straight wing allows all the air to flow over the entire wing parallel to the direction of flight. This will assist in easier landings at lower speeds and air densities while increasing lift in a shorter amount of time during takeoff reducing the required length for a runway.

8.2.2   Wing Planform Design

The wingspan and aspect ratio was estimated for the YA-94 using the specifications of the A-10 for reference. These values are then used to calculate other values presented in Table 8.1. Figure 8.1 and Figure 8.2 shows the top and front view of the wing noting relevant dimensions.

Table 8.1 – Wing design specification

Parameter	Value (Imperial | Metric)	
Reference Wing Area (S, ft^2 | m^2)	600	55.74
Aspect Ratio (AR)	6	
Wing Span (b, ft | m)	60	18.29
Mean Aerodynamic Chord ($\bar{c}$, ft | m)	10.03	3.06
Aerodynamic Center Lateral Location ($\bar{y}$, ft | m)	14.55	4.43
Taper Ratio (λ)	0.82	
Leading Edge Sweep Angle ($\Lambda_{L.E.}$, deg)	3.81°	
Quarter Chord Sweep Angle ($\Lambda_{c/4}$, deg)	0°	
Polyhedral Deflection (deg | deg)	0°	7°	
Geometric Twist (deg)	2°	
Incidence Angle (deg)	0°	
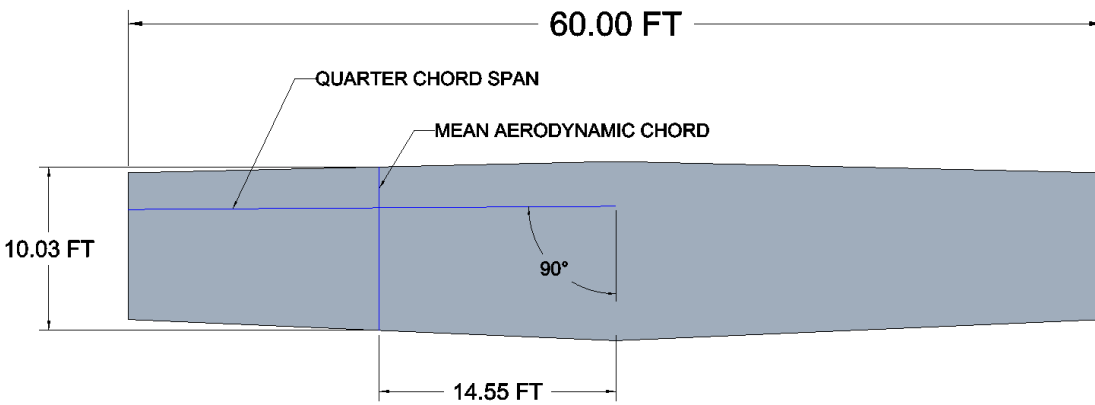
Figure 8.1 – Wing planform design
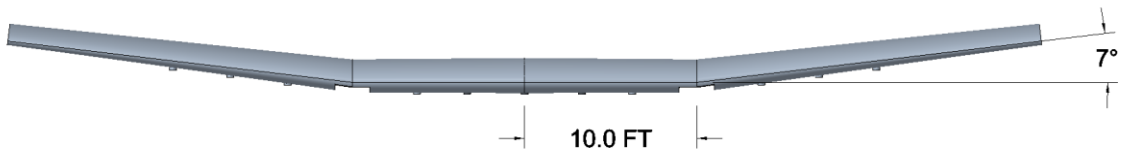
Figure 8.2 – Front wing design

8.3 Airfoil Selection and Analysis

The desired airfoil must provide enough lift to carry heavy payloads during takeoff and combat. A thicker airfoil may be used since the aircraft will only fly at most Mach 0.6, subsonic speed. It was discovered that the A-10 features an aerodynamic twist design, using two different airfoils at its root and tip. However, these two airfoils only differ in thickness ratios. This was to bring structural efficiency while maintaining consistent aerodynamics along the wing's span.

67

Heavier external payloads such as drop tanks will be located closer to the root side of the wing to prevent dramatic shifts in the CG if asymmetric dropping occurs. Lighter payloads will be mounted at the outermost part of the wing; thus, having least effects on the CG location during drop sequence.

Table 8.2 presents the two selected airfoils with their respective specifications, where NACA 4418 will be used at the root, and NACA 4415 will be used at the tip. Following the table are diagrams of the two selected airfoils.

Table 8.2 – Wing airfoil details

Parameter	Value
NACA 4418	
Airfoil Camber	4%
Airfoil Thickness (t/c)	18%
NACA 4415	
Airfoil Camber	4%
Airfoil Thickness (t/c)	15%
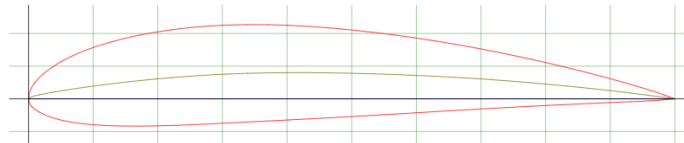
Figure 8.3 – NACA 4415 diagram
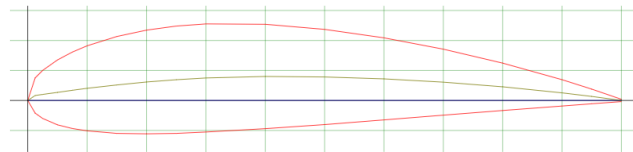
Figure 8.4 – NACA 4418 diagram

In Chapter 4, it was desired to have a wing clean maximum lift coefficient of 1.6. Equation (8.1) determined the airfoils' Reynold's numbers at the root or tip to ensure the selected airfoils provided the required lift.

$$R_{n_{r\ or\ t}} = \rho V c_{r\ or\ t} / \mu \tag{8.1}$$

where:
- $\rho = air\ density$
- $V = air\ speed$
- $c_{r\ or\ t} = chord\ length\ at\ root\ or\ tip\ of\ wing$
- $\mu = dynamic\ air\ viscosity$

Figure 8.5 will then be used to determine the maximum 2D lift coefficient, which in turn will be used in equation (8.2) to determine the analytical maximum wing lift coefficient, where

k_λ is the taper ratio factor. k_λ in this case is estimated to be 0.88. The final values of the determined airfoils are listed in Table 8.3.
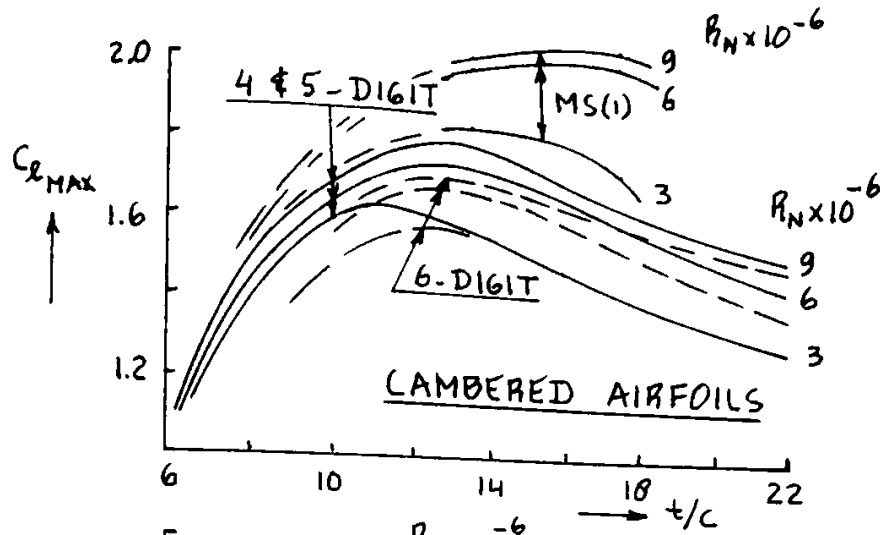
Figure 8.5 – Effect of thickness ratio and Reynold's number on $C_{L_{max}}$ [38]

$$C_{L_{maxw}} = \frac{k_\lambda \left(c_{l_{maxr}} + c_{l_{maxt}} \right)}{2} \tag{8.2}$$

Table 8.3: Wing airfoil specification

Parameter	Value
Maximum Mach Number	0.6
Minimum Reynolds Number (Re)	1.20E+07
Maximum Reynolds Number (Re)	1.46E+07
C_{lmax} at root	1.75
C_{lmax} at tip	1.70
Clean C_{Lmax} Required/Predicted	1.6
Analytical Clean C_{Lmax}	1.56

As seen in Table 8.3, the analytical maximum lift coefficient of the wing is 1.56. However, it is determined acceptable and close enough when compared to the predicted maximum lift coefficient of 1.6.

8.3.1   Additional Geometry Features

In addition to the aerodynamic twist, the wing will also feature a geometric twist and a polyhedral span design. A geometric twist of -2° at the wingtip is applied, providing a wash-out effect which would reduce the chance of stall at the tips of the wing when flying at lower speeds and higher angles of attack. The polyhedral feature was chosen to maximize roll stability at the tips while maintaining high lift closer to the root of the wing.

8.4 High-Lift Devices

8.4.1 High-Lift Devices Design Criteria

High-lift devices will be necessary during takeoff and landing to create additional lift when traveling at lower speeds. The required incremental lift produced at each flight condition is calculated using equations (8.3) and (8.4), knowing the maximum lift coefficient at takeoff and landing are 1.8 and 2.0, respectively.

$$\Delta C_{L_{max_{TO}}} = 1.05(C_{L_{max_{TO}}} - C_{L_{max}}) \tag{8.3}$$

$$\Delta C_{L_{max_{L}}} = 1.05(C_{L_{max_{L}}} - C_{L_{max}}) \tag{8.4}$$

Using the analytical maximum lift coefficient determined in the previous section, Table 8.4 lists the incremental lift that the high-lift devices must produce. Adding the incremental values to the maximum lift coefficient of 1.56, the required lift coefficients by the deployed flaps are determined as listed.

Table 8.4 – High lift devices design criteria

Parameter	Value
ΔC_L Takeoff	0.25
ΔC_L Landing	0.46
Design Takeoff C_{Lmax}	1.81
Design Landing C_{Lmax}	2.02

8.4.2 High-Lift Devices Design

Knowing the incremental lift values are high, a fowler-flap design was chosen as the high-lift device for the YA-94, similar to what is used on the A-10. The geometry of the flaps can be seen in Figure 8.6 with the decision to have two pairs of fowler flaps, one pair on each side. This is to avoid collision of wing-mounted payloads. Both Roskam and Raymer methods were used separately to analyze this design
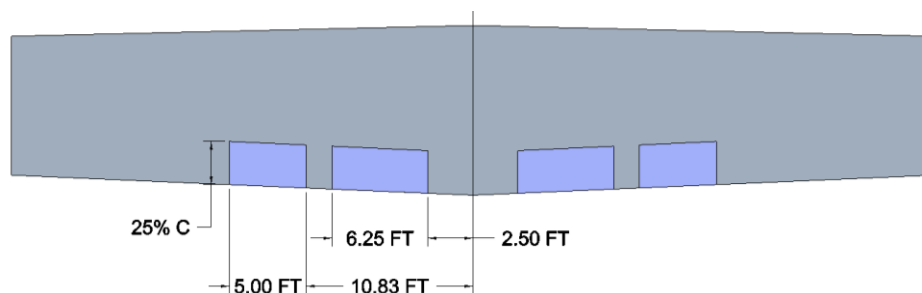
Figure 8.6 – Flap planform geometry

8.4.2.1 Flap Design – Roskam's Method

To ensure the sizing of the flaps produces the required incremental lift, equation (8.5) is used to estimate the incremental lift coefficient based on a defined flap area as defined in Figure 8.7.

$$\Delta C_{l_{max}} = \Delta C_{L_{max}} \left(\frac{S}{S_{wf}} \right) / K_\Lambda \tag{8.5}$$

where:
- S_{wf} = flap wing area (defined in Figure 8.7)
- K_Λ = flap sweep correction factor
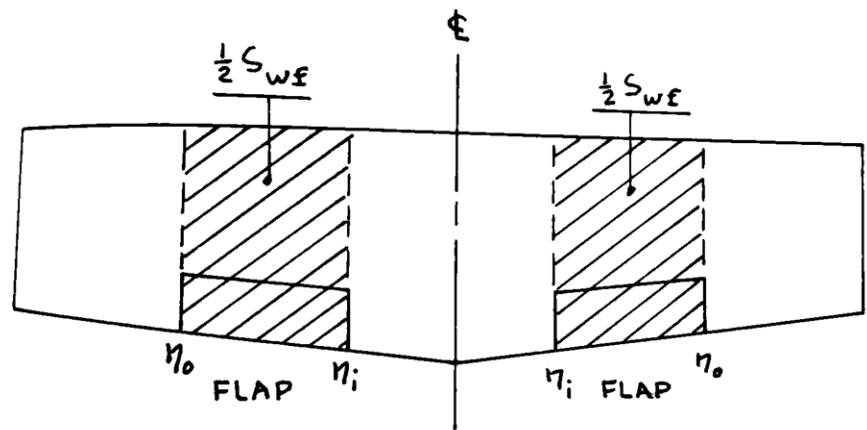
Figure 8.7 – Flap area definition [38]

Knowing the sweep correction factor of .92 and total flap area of 233.58 ft², Table 8.5 lists the maximum produced lift increments needed by the defined flaps illustrated above in Figure 8.6

Table 8.5 – Required flap lift coefficient increments

	Takeoff	Landing
$\Delta C_{l,max}$	0.59	1.09

Next, the incremental lift coefficient based on the given flap's chord length ratio c_f/c (0.25 in this case) and deflection δ_f must be determined. This is done by using equation (8.6) for fowler flaps.

$$\Delta c_l = c_{l_\alpha} * \alpha_{\delta_f} * \delta_f \tag{8.6}$$

where:
- c_{l_α} = unflapped section lift curve sloped, assumed to be 2π
- α_{δ_f} = lift effectiveness parameter (defined in Figure 8.8)
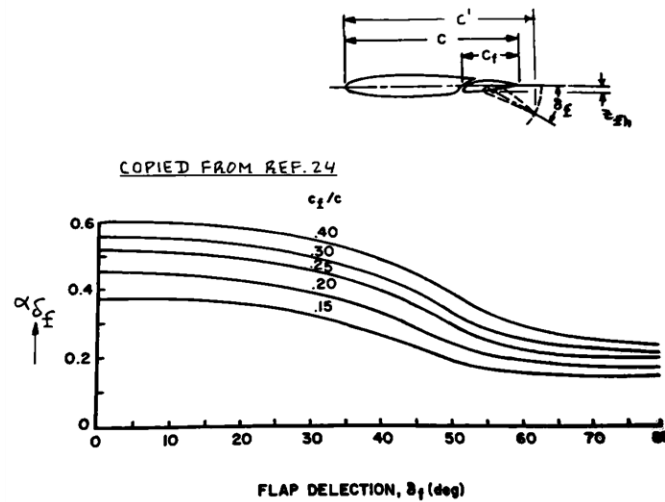
Figure 8.8 – Section lift effectiveness parameter

Assuming a flap defection of 15° for takeoff and 40° for landing, Table 8.6 lists the produced incremental lift coefficients by the designed fowler flaps.

Table 8.6 – High lift devices design

	Takeoff	Landing
Deflection angle (deg)	15°	40°
Δc_l	0.84	1.97

Using Roskam, the designed fowler flaps meet and over exceed the needed incremental lift during takeoff and landing conditions. These values seem unrealistic and require further analysis with Raymer's method.

8.4.2.2 Flap Design – Raymer's Method

To verify the selected airfoils, equation (8.7) is used to determine the clean max lift coefficient where $\Lambda_{0.25c} = 0°$ since there is no sweep along the wing's quarter chord span. The $C_{l_{max}}$ in this case is the average of both airfoil's $C_{l_{max}}$. This results in a $C_{L_{max}}$ of 1.55, close enough to the required clean coefficient of 1.6.

$$C_{L_{max}} = 0.9 C_{l_m} cos\Lambda_{0.25c}$$

(8.7)

Equation (8.8) is used to determine the incremental lift provided by the flaps. Table 8.7 is referenced to estimate the 2D incremental lift coefficient of the flaps. Again, fowler flaps are selected in this case. Table 8.8 lists the flap settings and the obtained incremental lifts. Figure 8.9 illustrates the generic chord increase due to fowler flaps.

Table 8.7 – Approximate lift coefficients of high-lift devices [9]

High-lift Device	$C_{l_{max}}$
Flaps	
Plain and split	0.9
Slotted	1.3
Fowler	$1.3c'/c$
Double slotted	$1.6c'/c$
Triple slotted	$1.9c'/c$

$$\Delta C_{L_{max}} = 0.9\Delta C_{l_{max}} \left(\frac{S_{flapped}}{S_{ref}}\right) cos\Lambda_{H.L.} \tag{8.8}$$

Slotted Fowler flap
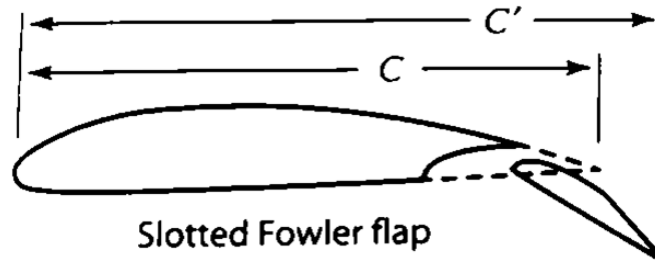
Figure 8.9 – Fowler flap chord length design

Table 8.8 – Fowler flap design settings

	Imperial	Metric
C	10.8 ft	3.30 m
Takeoff		
c'_{TO}	10.7 ft	3.26 m
Deflection	15.0°	
$\Delta C_{L_{max}}$	0.35	
Landing		
c'_{land}	12.9 ft	3.93 m
Deflection	40.0°	
$\Delta C_{L_{max}}$	0.54	

As a result, Raymer's method meets the lift requirements while determining a much lower lift increment than Roskam's. Therefore, Raymer's values are considered for the design as they seem more in line with the predicted lift increments in section 8.4.1.

8.5   Wing Lateral Control Surface Design

Below in Figure 8.10 is the wing aileron design for the YA-94. Figure 8.10 displays the ailerons (green) with respect to the primary wing spars and flaps (yellow) to ensure fitting. As shown, there is sufficient room for the designed control surfaces.
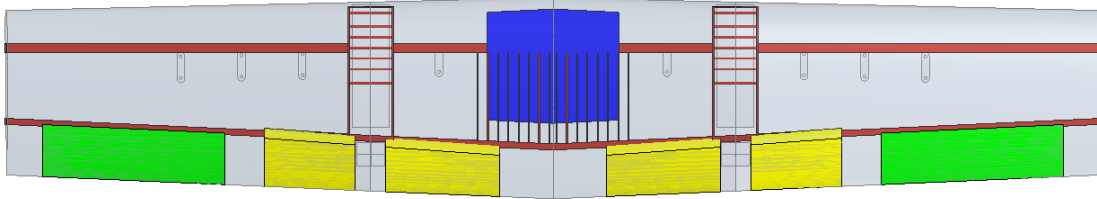
Figure 8.10 – Internal wing and control surface diagram

8.6   Internal and External Storage Design

The YA-94 will carry roughly 80% of its fuel within the fuselage as it provides the most protection from incoming enemy fire. The remaining 20% will be located close to the root side of the wing. Figure 8.11 illustrates the internal wing tank (blue) with 29.1 ft^3 (0.82 m^3) volume. This allows the wing to carry 1,410 lbs (640 kg) of fuel.
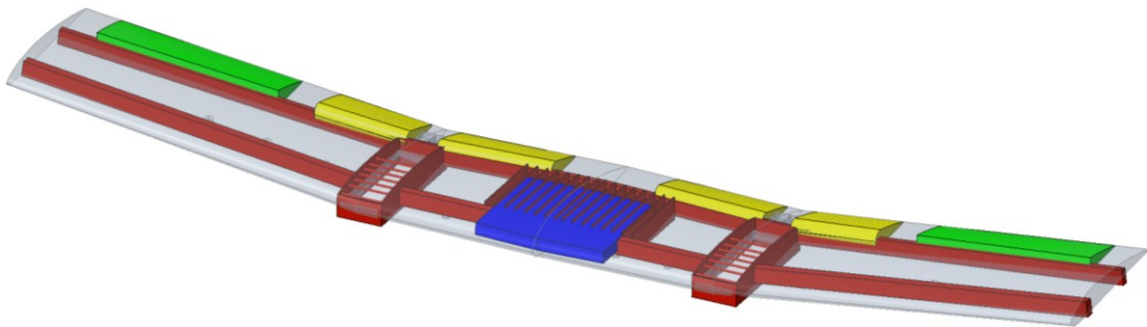
Figure 8.11 – Internal wing fuel tank location

In addition to internal storage, the wing is also designed to provide 11 hardpoints for external payload storage. Figure 8.12 provides a view of the hardpoint locations with pylons attached.
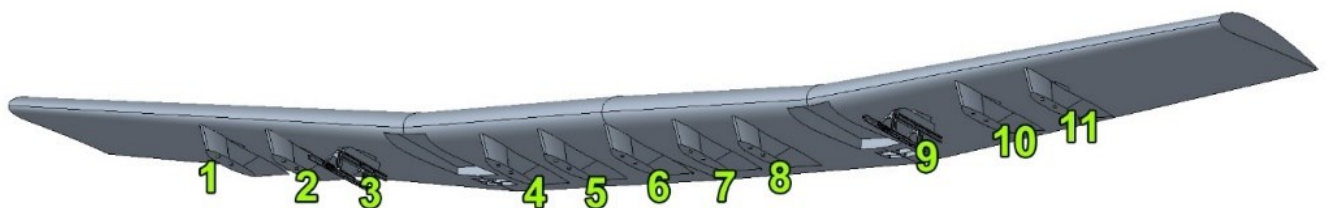
Figure 8.12 – Wing hardpoint locations

8.7   Conclusion

Illustrated in Figure 8.13 is the final wing design with all flap and control surfaces shown and dimensioned. Also, details of each airfoil cross-section type demonstrate how the wing tapers and transitions from one airfoil to the other.
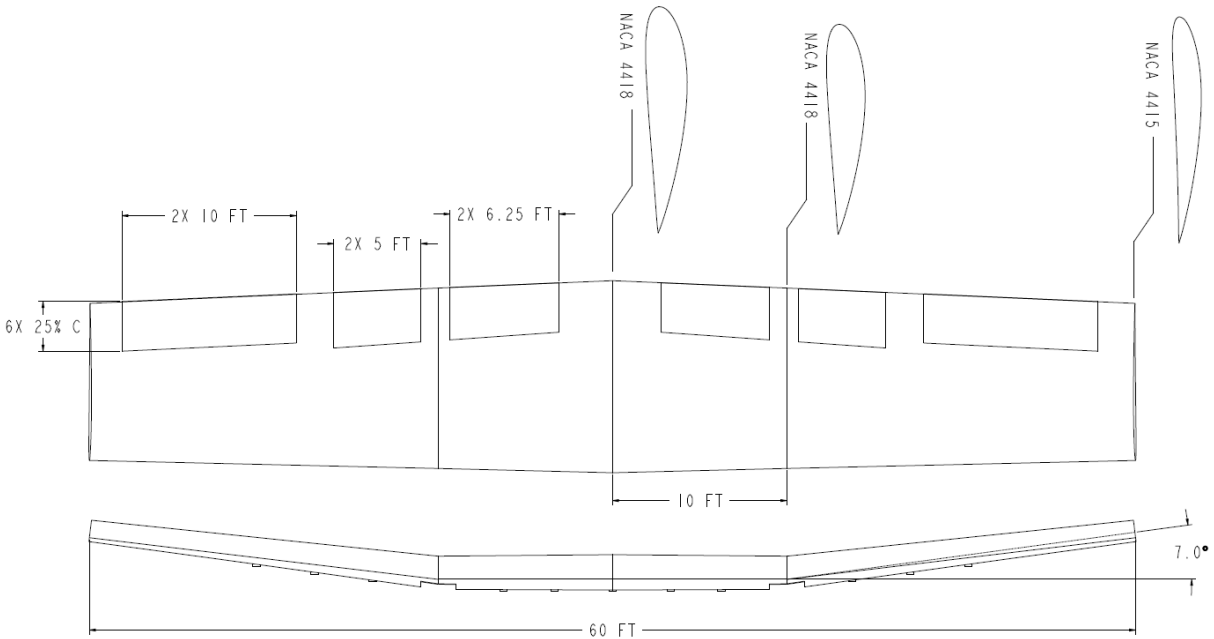
Figure 8.13 – Final wing design diagram

Overall, the current wing design meets all required specifications for cruise, takeoff, and landing. All flaps and aileron sizing fit within the specified wing geometry while allowing sufficient room for major internal structures and fuel tanks. Eleven external hardpoints have also been successfully added to the underside of the wing to allow flexible combinations of ordinance types per mission condition.
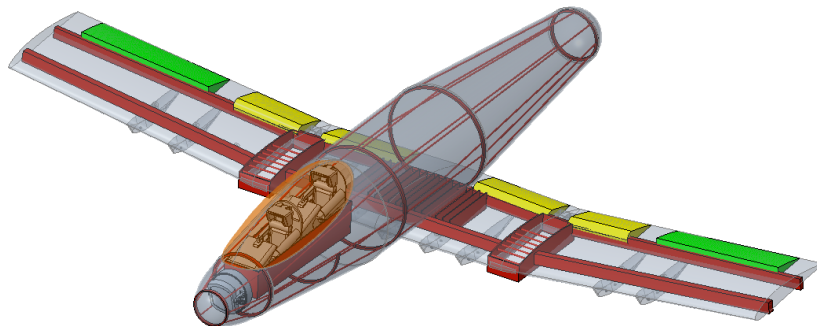
Figure 8.14 – Wing integration design

Chapter 9 – Empennage Design

9.1   Introduction

As previously discussed in Chapter 5, it was determined that the YA-94 would use an H-tail design due to both its stability and passive countermeasure features. This chapter will present the design and analysis of the YA-94's empennage, including:

- Empennage location
- Airfoil selection
- Horizontal tail sizing and design
- Vertical tail sizing and design
- Control surface design

9.2   Overall Empennage Design

The H-tail design features excellent yaw stability, especially during a high-speed and steep-dive maneuver. In addition, it provides a passive ability to reduce the aircraft's heat signature, preventing heat-seeking weapons from establishing lock-on. Figure 9.1 presents the general location of the empennage, measured between the wing's quarter chord line to the the horizontal tail quarter chord line.
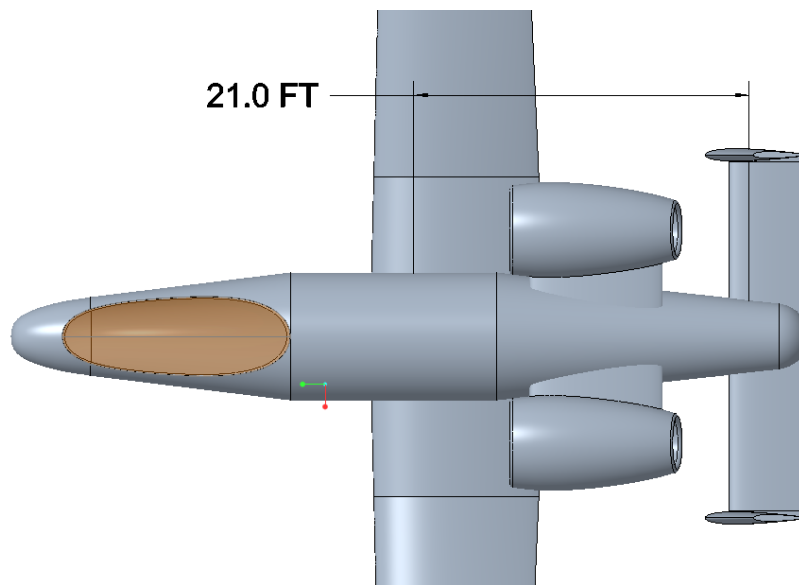
Figure 9.1 – Top view, empennage location reference

It is determined that no incidence or dihedral angle will be applied to the empennage. This will keep manufacturing and design costs low due to its simplicity. Tapering and sweep angles are also not employed in this design to keep the horizontal plane as large as possible due to the short lever arm for pitching.

9.3 Empennage Airfoil Selection

A symmetric airfoil was chosen for the empennage design, using the NACA 0012 airfoil, as seen in Figure 9.2. The airfoil has zero camber with a maximum thickness-to-chord ratio of 12%. This airfoil was chosen as it is one of the most commonly used airfoil profiles for various aircraft empennages.

Figure 9.2 – NACA 0012 airfoil

9.4 Horizontal Stabilizer Design

Following Raymer, equation (9.1) was used to estimate the planform area of the horizontal stabilizer. Table 9.1 provides typical tail volume coefficients to estimate and use in equation (9.1). In this case, the jet fighter category was used.

Table 9.1 – Typical tail volume coefficients [9]

	Typical Values	
	Horizontal c_{HT}	Vertical c_{VT}
Sailplane	0.50	0.02
Homebuilt	0.50	0.04
General aviation – single engine	0.70	0.04
General aviation – twin engine	0.80	0.07
Agricultural	0.50	0.04
Twin turboprop	0.90	0.08
Flying boat	0.70	0.06
Jet trainer	0.70	0.06
Jet Fighter	0.40	0.07-0.12
Military cargo, bomber	1.00	0.08
Jet transport	1.00	0.09

$$S_{HT} = \frac{c_{HT}\bar{C}_W S_W}{L_{HT}} = \frac{(0.38)(10.03ft)(600ft^2)}{21ft} = 108.9 \ ft^2 \tag{9.1}$$

where:
- $\bar{C}$ = wing mean chord
- S_W = wing planform area
- L_{HT} = distance between the aerodynamic center of the wing and horizontal stabilizer

After solving the equation, it was determined that the planform area would need to be 108.9 ft^2 (10.1 m^2). Using basic rectangular geometry and assuming a constant chord length of

5 ft along the span, the horizontal stabilizer requires a span of 21.8 ft (6.6 m). Figure 9.3 shows the final planform design of the horizontal stabilizer.
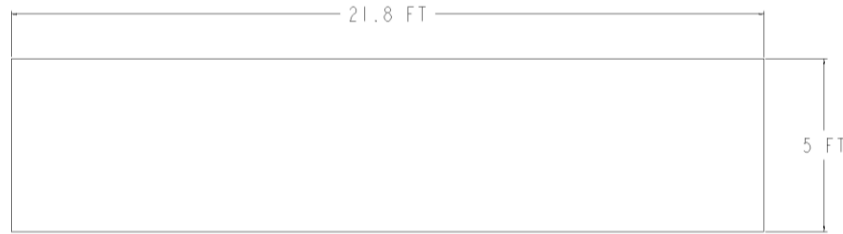
Figure 9.3 – Horizontal stabilizer planform design

Table 9.2 – Horizontal tail design specification

Parameter	Value (Imperial | Metric)	
Reference HT Area (ft² | m²)	108.9	10.12
Volume Coefficient (C_{HT})	0.38	
Aspect Ratio (AR)	4.36	
HT Span (ft | m)	21.8	6.64
Root Length (ft | m)	5	1.52
Tip Length (ft | m)	5	1.52
Mean Aerodynamic Chord (ft | m)	5	1.52
Taper Ratio (λ, deg)	1.00	
Leading Edge Sweep Angle (deg)	0°	
Quarter Chord Sweep Angle (deg)	0°	
Incidence Angle (deg)	0°	
Dihedral Angle (deg)	0°	

9.5   Vertical Stabilizer Design

Similar to how the horizontal stabilizer was designed, equation (9.2) is used instead to determine the required planform area of the vertical stabilizer while referencing Table 9.1.

$$S_{VT} = \frac{c_{VT}b_W S_W}{L_{VT}} = \frac{(0.07)(60ft)(600ft^2)}{20.89ft} = 60.3 \, ft^2 \tag{9.2}$$

where:
- b_W = wingspan
- S_W = wing planform area
- L_{vT} = distance between the aerodynamic center of the wing and vertical stabilizer

Assuming a tail volume coefficient of 0.07, a total planform area of $120.6 \, ft^2$ ($11.2 \, m^2$) is required for the vertical stabilizer. Therefore, each vertical stabilizer will have an area of $60.3 \, ft^2$ ($5.6 \, m^2$). Again, using basic trapezoidal geometry and assuming a tip chord length of 3.5 ft (1.1 ft) and a root chord length of 6.5 ft (2.0 m), the height of a single vertical stabilizer comes out to 12.1 ft (3.7 m). Figure 9.4 shows the planform design of the vertical stabilizer.
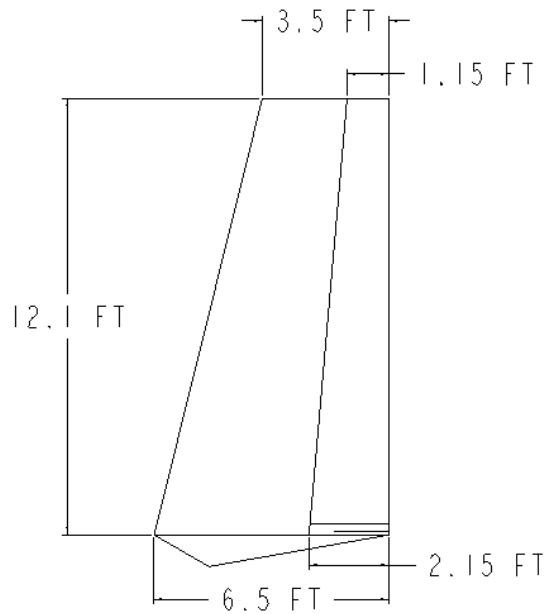
Figure 9.4 – Vertical stabilizer planform design

Table 9.3 – Vertical tail (single) design specification

Parameter	Value (Imperial | Metric)	
Reference VT Area (ft^2 | m^2)	60.3	5.60
Volume Coefficient (C_{VT})	0.54	
Aspect Ratio (AR)	4.36	
VT Height (ft | m)	12.1	3.69
Root Length (ft | m)	6.5	1.98
Tip Length (ft | m)	3.5	1.07
Mean Aerodynamic Chord (ft | m)	5.15	1.57
Taper Ratio (λ)	0.54	
Leading Edge Sweep Angle (deg)	13.9°	
Quarter Chord Sweep Angle (deg)	10.5°	
Incidence Angle (deg)	0°	
Dihedral Angle (deg)	90°	

9.6   Longitudinal and Directional Control Design

Figure 9.5 illustrates the empennage control surfaces (colored in blue) with respect to the internal structure. Both horizontal and vertical control surfaces make up 33% of the chord length of each of their respective stabilizers.
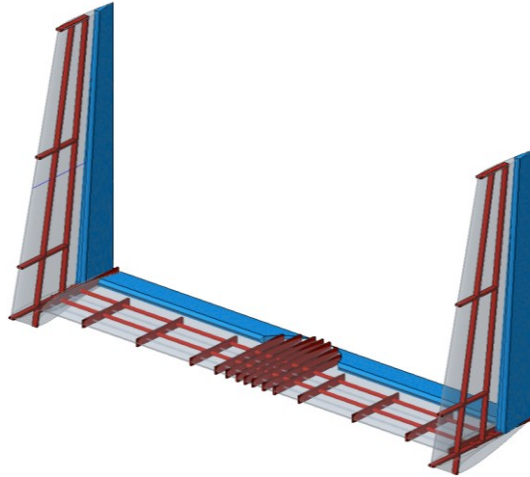
Figure 9.5 – Empennage internal structure and control surface design

9.7   Conclusion

The H-tail empennage provides excellent yaw stability, especially when descending at steep angles and high speeds. Raymer's method was used to determine the sizing of the overall empennage structure. Empennage control surfaces are estimated to be 33% of the chord length while also fitting within the designed internal structure. Figure 9.6 presents the empennage integrated into the overall aircraft design.
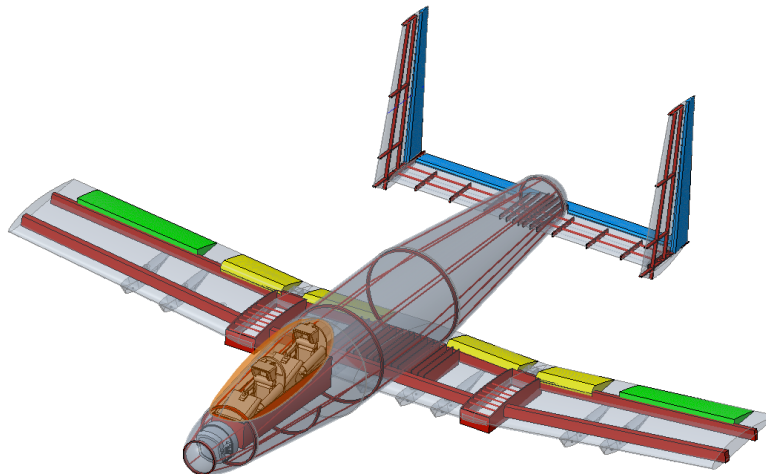
Figure 9.6 – Empennage integration design

Chapter 10 – Landing Gear Design

10.1   Introduction

Chapter 10 introduces the landing gear design for the YA-94. The design process discusses the following features:

- Design and arrangement
- Storage
- Clearances

10.2   Design

10.2.1 Arrangement

As determined in Chapter 5, a tricycle landing gear scheme was chosen as the design approach for the YA-94. This will provide sufficient ground clearance, especially when mounting underwing payload systems. In addition, the landing gear system will be fully retractable to help reduce the overall drag of the aircraft. Figure 10.1 presents the overall design layout of the main and nose landing gear.

The wheelbase of the landing gear is presented in Figure 10.2. It must be noted that the nose gear is not center-aligned between the main gear, and this is to compensate for the gun located at the center front of the nose.

Figure 10.1 – Landing gear design layout
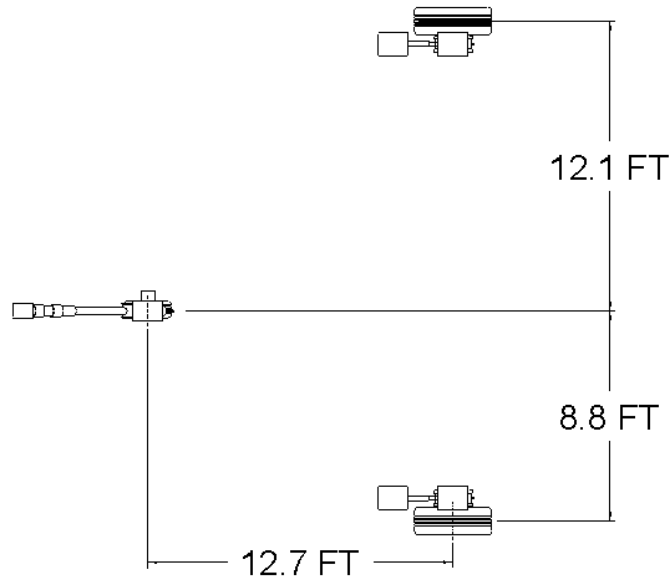
Figure 10.2 – Landing gear wheelbase layout

10.2.2 Landing Gear Sizing

The sizing of tires, wheels, and retraction system can be seen in Figure 10.3. The chosen tire type is the Flight Eagle tire from Goodyear, as it has a speed rating of 210 mph (338 kph) which is well above the takeoff and landing speed [52]. Tire sizing of main gear is based on equation (10.1) using jet fighter values provided in Table 10.1(gives in inches). Table 10.2 presents main and nose gear wheel size. Per Raymer, it is estimated that the nose wheel is 60% of the main wheel size. The design of the retraction system references the A-10's existing retracting gear system.
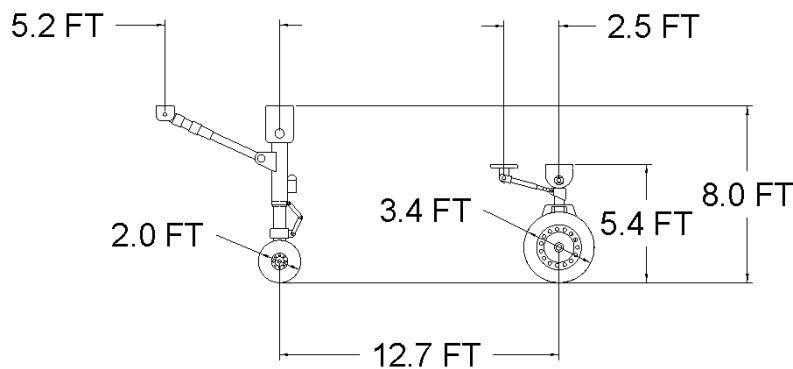
Figure 10.3 – Landing gear sizing

$$Diameter \ or \ width = AW_W^B \tag{10.1}$$

where:

- $W_W = Weight \ on \ wheel, typically \ 90\% \ of \ MTOW$

Table 10.1 – Statistical tire sizing [9]

Aircraft Type	Diameter		Width	
	A	B	A	B
General aviation	1.51	0.349	0.1750	0.312
Business twin	2.69	0.251	1.170	0.216
Transport/bomber	1.63	0.351	0.1043	0.480
Jet fighter/trainer	1.59	0.302	0.0980	0.497

Table 10.2 – YA-94 tire size

	Diameter		Width	
Main wheel	3.4 ft	1.04 m	1.2 ft	0.37 m
Nose wheel	2.0ft	0.61 m	0.7 ft	0.21 m

As for tire pressure, it is recommended by Raymer to be about 200 psi (1380 kPa) when operating on major military airfields.

10.2.3 Retraction and Storage

The landing gear system retracts forward, similar to the A-10's landing gear system. Commonly, the main gear would stow into the fuselage or sideways into the wing, as seen on WWII fighter planes. However, due to the payload mounts located across the entire wingspan, there is only enough room to retract forward, with the aftward retraction considered a risk. With the gear deploying backward, it can act as a failsafe in case of hydraulic pressure loss. This is done by the forward motion of the aircraft which keep the gears deployed due to drag and friction when rolling on the ground.

Figure 10.4 and Figure 10.5 illustrates the landing gear in its stowed condition. The main gear will be mounted to the main and trailing edge wing spar since the wing box is designed to withstand high loads. As mentioned before, the nose gear retracts to the side of the cockpit. Front "nose caps" are added to the wing's leading edge to provide aerodynamic efficiency to the main landing gear as the wheel cannot retract completely into the wing, thus causing additional unnecessary drag.
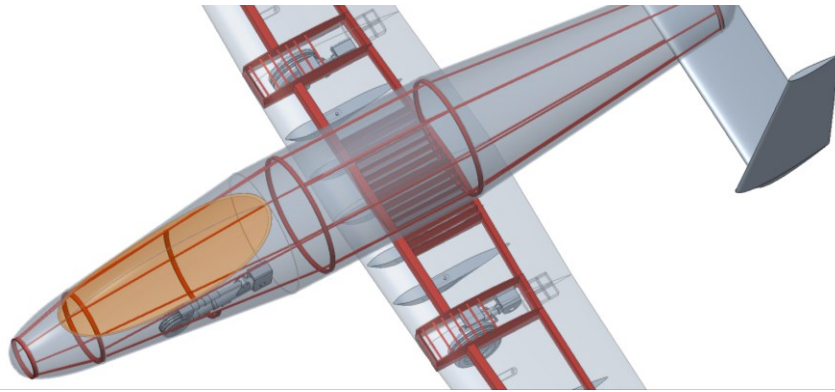
Figure 10.4 – Landing gear stowed (top view)
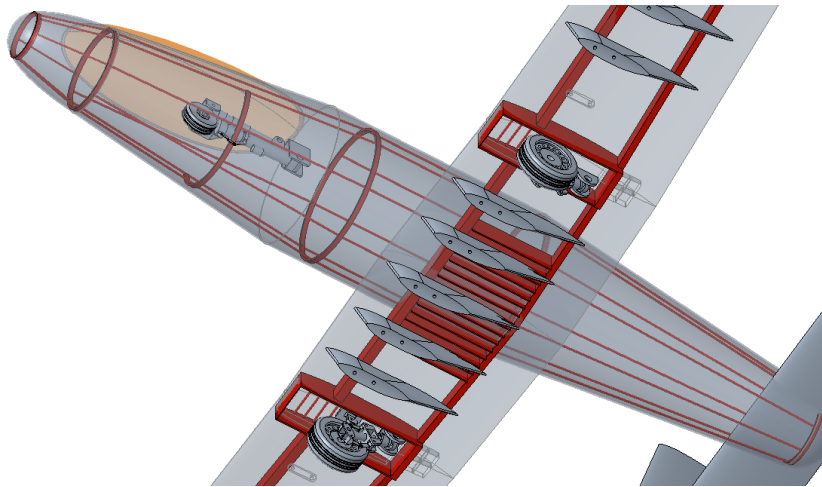
Figure 10.5 – Landing gear stowed (bottom view)

10.3   Clearance Analysis

The following section discusses various safety clearance angles and distances achieved by the designed landing gear regarding the aircraft's CG. It must be noted that the weight and balance and the CG location of the YA-94 were analyzed and determined ahead of the initial landing gear design, and this analysis will be later discussed in chapter 11.

10.3.1 Tip-Back Clearance
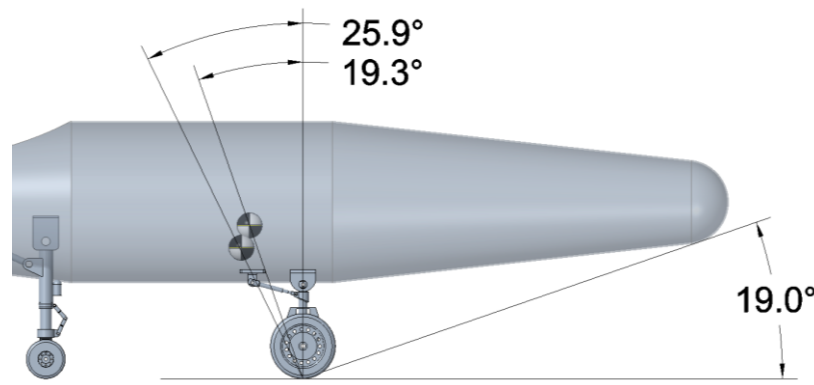
Figure 10.6 – Tip-back angle and clearance

As shown in Figure 10.6, the tail has a maximum 19-degree tip-back angle clearance. This is above the 15-degree requirement presented by Raymer, allowing the pilots more than enough clearance to pull the nose up during takeoff or landing without having the tail striking the ground. The CG location at 25.9° presents when the aircraft is fully loaded while the CG location at 19.3° presents the aircraft being close to empty. With angles greater than 15°, the CG is guaranteed in front of the main landing gear at all loading conditions.

10.3.2 Wing Tip Strike Clearance
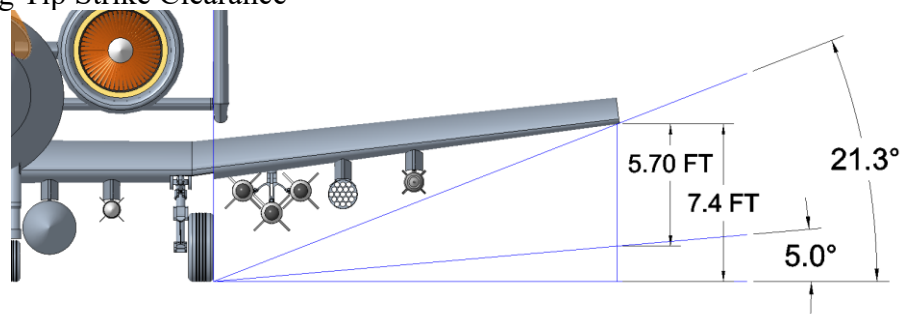
Figure 10.7 – Wing-tip strike clearance angles

Figure 10.7 confirms the clearance of the wingtip if the aircraft were to roll near the ground. Per Raymer, it is recommended for the wing tip to have a minimum clearance of 6 inches above the ground if rolled by 5-degrees, and there is more than enough clearance if such a situation occurs. In addition, in a critical situation, if the wingtip were to touch the ground, the external payloads mounted on the far end of the wing are cleared from striking.

10.3.3 Overturn Angle
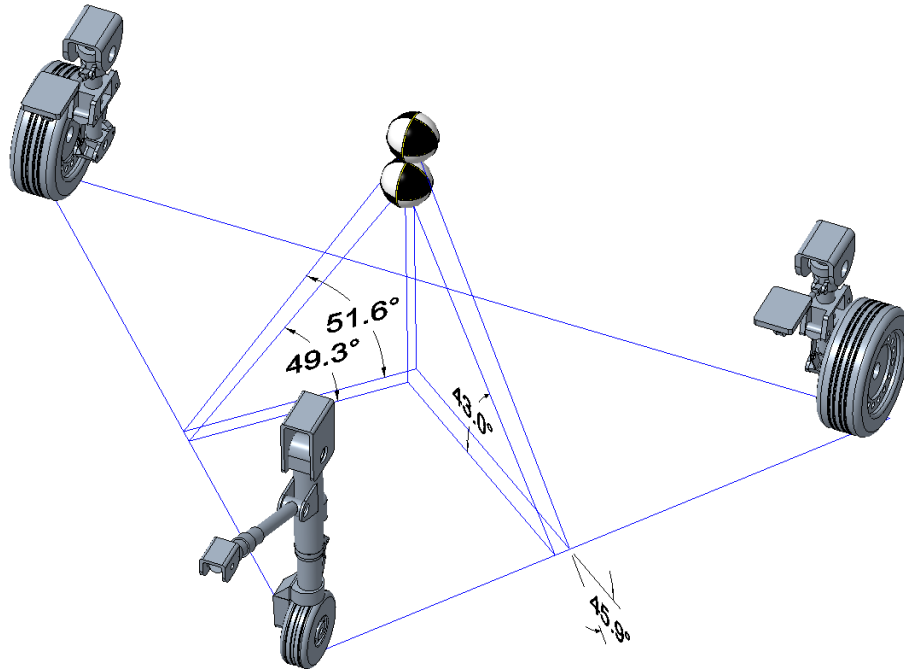
Figure 10.8 – Overturn angles

Per Raymer, the overturn angle in either direction is recommended to be under 63-degrees. Figure 10.8 illustrates that this requirement is met by measuring angles when the CG is located at the highest point (45.9° port side and 51.6° starboard side) and when the CG is located forward most (43.0° port side and 49.3° starboard side). Since the nose gear is offset to one side to allow clearance for the main gun, both sides must be measured to ensure the aircraft does not tip on either side when turning left or right.

10.3.4 Ground Clearance

1.3 FT   4.6 FT
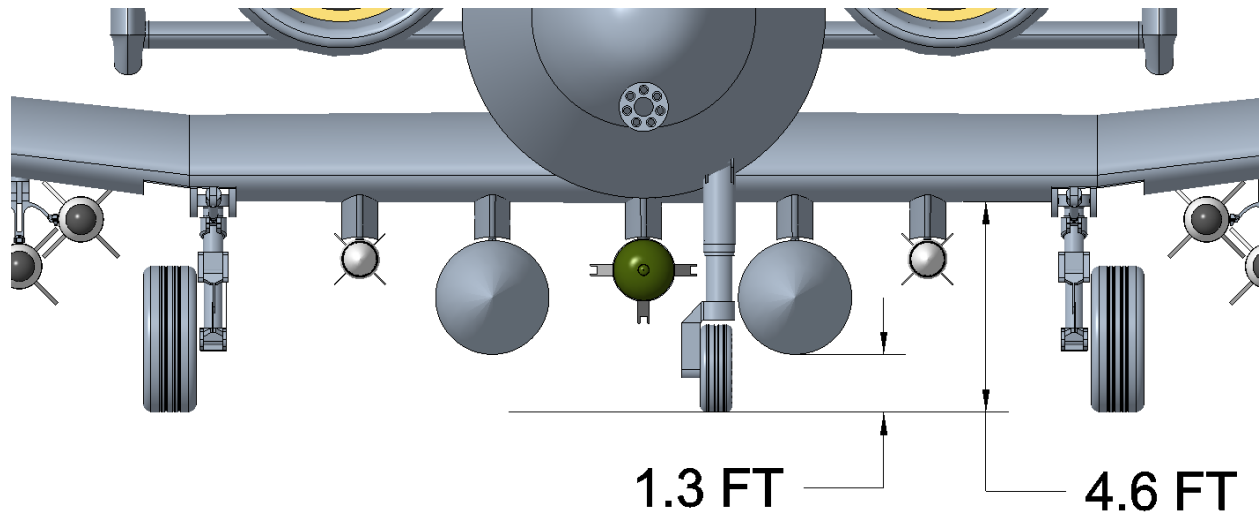
Figure 10.9 – Ground clearance

As shown in Figure 10.9, there is sufficient ground clearance for external payloads mounted below the wing. In reference to FAA requirements, there must be a minimum clearance of 7-inches, which is widely exceeded, as shown in the image above.

10.4   Conclusion

The current landing gear design satisfies all safety clearances based on the above illustrations. The landing gear system uses the existing design from the A-10 while using recommended tires by Goodyear. Figure 10.10 presents the thus far aircraft design with the landing gear system fully integrated.

Figure 10.10 – YA-94 with landing gear fully integrated (deployed)

Chapter 11 – Weight and Balance

11.1 Introduction

This chapter presents the weight and balance analysis of the YA-94. The following aspects of the aircraft are determined:

- Component weight breakdown
- Actual fuel weight
- CG location
- CG envelope diagram

11.2 Component Weight Breakdown

Various component weights of the YA-94 were estimated based on provided equations from Raymer, Section 15.3.1, for fighter and attack aircraft [9]. See Appendix E for equations and input values used for this design. Three tables show the weight breakdown of major weight categories that make up the total empty weight: structure, propulsion, equipment, and useful load. The empty weight resulted in 24,112 lbs (10,937 kg). Locations were determined through Creo, referencing an arbitrary point located 300 inches in front and 100 inches below the tip of the aircraft's nose. Figure 11.1 presents these CG point locations of all detailed components within the aircraft.

Table 11.1 – Structure group weight and location breakdown

	Weight lbs	X-Location ft	Y-Location ft	Z-Location ft
STRUCTURES GROUP	16151.396	40.710	-0.005	8.338
Wing	3252.677	41.657	0.000	6.186
Horiz. Tail	474.144	61.690	0.000	8.333
Vert. Tail (L)	1066.528	61.483	-11.358	12.868
Vert. Tail (R)	1066.528	61.483	11.358	12.868
Fuselage	4889.094	38.093	0.000	8.758
Main Lndg Gear - (L)	423.451	41.807	-9.846	4.443
Main Lndg Gear - (R)	423.451	41.807	9.846	4.443
Nose Lndg Gear	276.256	27.781	-1.563	7.189
Engine Mounts	55.168	50.745	0.000	10.825
Engine Section	33.099	50.833	0.000	10.833
GAU-8 Avenger Canon	1963.000	32.547	0.179	7.957
Pylons	378.000	41.018	0.000	4.828
AGM Rack (L)	50.000	39.979	-13.750	4.628
AGM Rack (R)	50.000	39.979	13.750	4.628
Ti Bathtub	1750.000	25.394	0.000	8.987

Table 11.2 – Propulsion group weight and location breakdown

	Weight	X-Location	Y-Location	Z-Location
	lbs	ft	ft	ft
PROPULSION GROUP	4110.455	48.751	-0.013	10.812
Engine (L)	1440.000	51.101	-6.667	10.833
Engine (R)	1440.000	51.101	6.667	10.833
Tailpipe	0.000	0.000	0.000	0.000
Engine Cooling	402.549	47.500	0.000	10.833
Oil Cooling	76.856	47.500	0.000	10.833
Engine Controls	39.336	24.505	0.000	9.678
Starter	41.906	46.492	-1.255	7.995
Fuel System	669.809	41.108	0.000	10.949

Table 11.3 – Equipment group weight and location breakdown

	Weight	X-Location	Y-Location	Z-Location
	lbs	ft	ft	ft
EQUIPMENT GROUP	3850.788	34.126	0.004	0.001
Flight Cntrls/Instru./Furnish	1223.483	24.505	0.000	9.678
Hydraulics	253.743	40.000	0.000	6.250
Electrical	810.862	40.000	0.000	9.000
Avionics	1082.191	33.938	0.000	10.717
Air Conditioning	230.509	45.538	1.632	8.300
APU installed	250.000	46.492	-1.255	7.995

Table 11.4 presents the weight breakdown of the useful load groups, including the two pilots on board, fuel, and various external ordnance payloads. A maximum takeoff weight of 50,000 lbs (22,680 kg) is used to determine the available fuel onboard after taking the difference between the max takeoff weight and the empty and payload weights.

Table 11.4 – Useful load group weight and location breakdown

	Weight lbs	X-Location ft	Y-Location ft	Z-Location ft
USEFUL LOAD GROUP	25887.360	39.843	0.024	5.598
Pilot with equipment	230.000	23.750	0.000	10.000
RIO with equipment	230.000	29.583	0.000	10.417
Left Wing Payload	6863.000	40.470	-7.974	3.781
Drop Tank	3880.800	40.161	-3.333	3.292
MK82 Bomb	500.000	40.808	-6.250	4.135
AGM-65 Maverick 3x Rack	1386.000	40.992	-13.750	3.935
LAU-61 Rocket Pod	470.000	39.897	-17.083	4.823
GBU-12 Pavway	510.000	40.510	-20.417	5.417
Flare Pods (4x)	116.200	45.240	-10.000	5.347
Center Payload	3066.000	35.391	0.000	6.632
Gun Ammo	2066.000	32.547	0.000	7.957
CBU-87 Cluster Bomb	1000.000	41.268	0.000	3.896
Right Wing Payload	6893.000	40.480	8.028	3.775
Drop Tank	3880.800	40.161	3.333	3.292
MK82 Bomb	500.000	40.808	6.250	4.135
AGM-65 Maverick 3x Rack	1386.000	40.992	13.750	3.935
LAU-61 Rocket Pod	470.000	39.897	17.083	4.823
ECM	540.000	40.641	20.417	5.257
Flare Pods (4x)	116.200	45.240	10.000	5.347
Burn In-Flight Payload	8605.360	41.124	0.000	7.892
Fuel (weight available)	8595.360	41.113	0.000	7.888
Oil	10.000	50.745	0.000	10.825
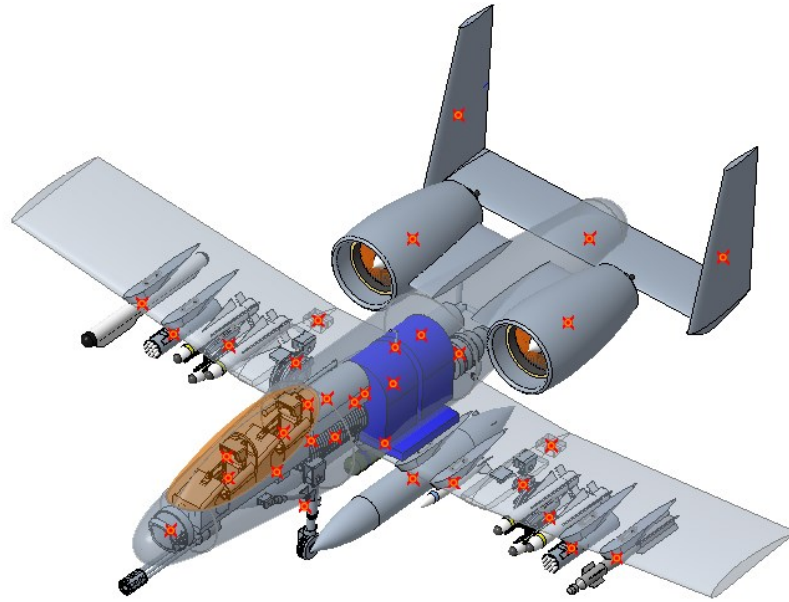
Figure 11.1 – Component CG point locations

11.3 Center of Gravity Location

The above weight and location data is used to determine the moment arms about each of the three-dimensional axes and then used to solve the center of mass for the entirety of the aircraft. Table 11.5 presents the CG location of the aircraft in various scenarios. The MTOW CG location was also modeled using the determined location values to confirm its location in the aircraft, illustrated in Figure 11.2.

Table 11.5 – YA-94 CG location per various loadings

	Weight lbs	X-Location ft	Y-Location ft	Z-Location ft
MTOW CG	**50,000**	**40.4**	**0.0**	**6.5**
Payload-Out CG	33,200	40.9	0.0	7.6
Empty CG	24,100	41.0	0.0	7.4
Fuel-Out, Payload-On CG	41,400	40.3	0.0	6.2
Drop Tank Release	42,200	40.5	0.0	6.0
Payload Release	28,880	40.8	0.0	7.5
Clean, 10% Fuel	25,440	40.8	0.0	7.5
Clean Flight with Fuel Only	33,200	40.9	0.0	7.6
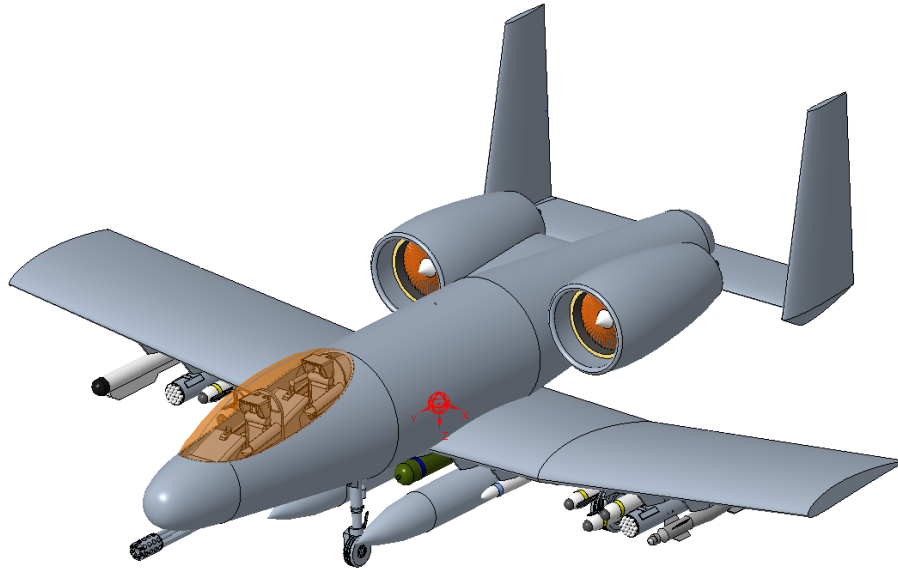
Figure 11.2 – MTOW CG location modeled

Mass was also added to the 3D models to allow Creo to compute the CG location per its given geometries and volumes. The table presents Creo's pre-determined CG location, and the locations closely match the analytical values above with a foot difference in the vertical location. This is due to missing detailed components which were not modeled and present in the current CAD model iteration.

Table 11.6 – Creo computed MTOW CG location

	X-Location ft	Y-Location ft	Z-Location ft
Creo Est. CG	40.4	0.0	7.6

11.3.1 CG Envelope

Using the known mass and CG data, the aircraft was also modeled into XFLR5. This computes the neutral point location of the aircraft, located 42.7 ft (13.0 m) from the chosen arbitrary reference point. This value can be used to determine the aft and forward limits of the CG location. Typically, the aft limit is estimated to be 10% in front of the neutral point location, while the forward limit is 30% in front. These limit locations are defined as percentage-based along the wing's MAC length. The neutral point is located at 52.3% of the wing's MAC, making the forward limit 22.3% and the aft limit 42.3% along with the wing's MAC.

To visualize and verify that the CG location of the aircraft fits within the limits mentioned above, a CG envelope was generated using the various CG locations presented in Table 11.5. This provides an overview of the aircraft's stability throughout the flight regime, from takeoff to combat and landing. Figure 11.3 presents the various flight points of the YA-94.
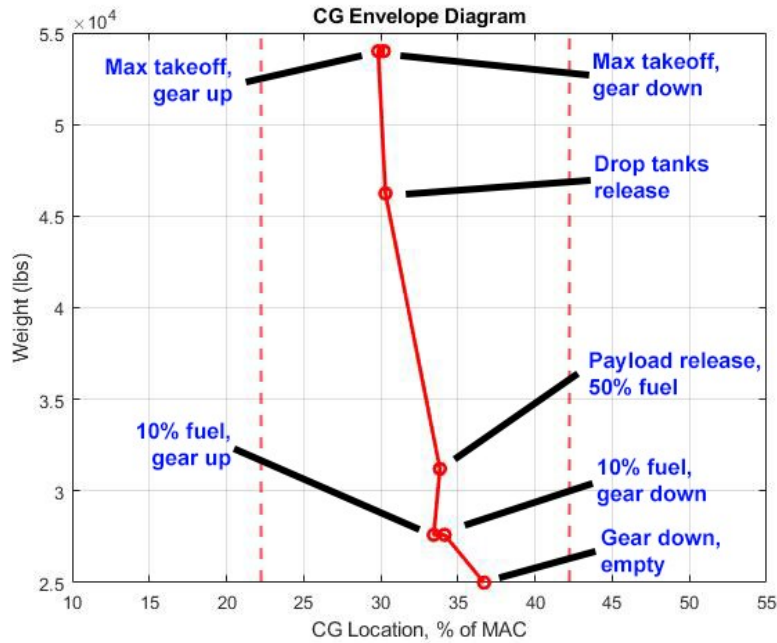
Figure 11.3 – CG envelope along wing's MAC length

As can be seen, the change in CG location stays within the defined limits, therefore, verifying the stability of the aircraft for each changing condition throughout the mission.

11.4   Conclusion

After a detailed weight breakdown of the significant components of the aircraft, the calculated fuel weight aligns closely with the predicted fuel weight; 8,595.4 lbs (3,898.8 kg) compared to RDSWin, which was estimated to be 8,538.3 lbs (3,873 kg). In addition, the CG location of the aircraft was confirmed in multiple ways, with all methods resulting in similar locations. Creating the CG envelope diagram confirms the stability of the aircraft longitudinally during various flight scenarios.

Chapter 12 – Stability Analysis

12.1 Introduction

Chapter 12 introduces the stability analysis of the YA-94 using a combination of Raymer's method and simulation in XFLR5. The following topics are analyzed and discussed:

- Static margin
- Modal analysis

12.2 Static Margin

The static margin is defined as the aircraft's static longitudinal stability and controllability. With the neutral point previously determined using XFLR5 in Chapter 11, equation (12.1) can then be used to determine the static margin, where x_{NP} is the location of the neutral point, x_{CG} is the location of the center of gravity, and x_{MAC} is the mean aerodynamic chord length. This results in a positive static margin of 22.34% at MTOW.

$$SM = \frac{x_{NP} - x_{CG}}{x_{MAC}} \times 100\% = \frac{42.66ft - 40.42ft}{10.03ft} \times 100\% = 22.34\% \tag{12.1}$$

The mass inertia moments at this location are determined using the three equations below, where b is the wingspan, W is the takeoff weight, L is the fuselage length, g is the gravitational constant, and $\bar{R}_i$ are the gyration radii in the x, y, and z directions. The gyration radii for a jet fighter are defined in Table 12.1. The inertia moment of the aircraft can be seen in Table 12.2. For comparison, Creo was also used to confirm the mass moments of inertia per its given mass and geometry.

$$I_{xx} = \frac{b^2 W \bar{R}_x^2}{4g} \tag{12.2}$$

$$I_{yy} = \frac{L^2 W \bar{R}_y^2}{4g} \tag{12.3}$$

$$I_{zz} = \left(\frac{b+L}{2}\right)^2 \frac{W \bar{R}_z^2}{4g} \tag{12.4}$$

Table 12.1 – Radii of gyration for jet fighter [9]

$\bar{R}_x$	$\bar{R}_y$	$\bar{R}_z$
0.23	0.38	0.52

Table 12.2 – Moments of inertia

Moments of Inertia	I_{xx}	I_{yy}	I_{zz}
$(slug \cdot ft^2)$	73,928.57	140,139.75	317,531.06
$(kg \cdot m^2)$	100,247.14	190,029.50	430,572.11

Table 12.3 – Creo moments of inertia

Moments of Inertia	I_{xx}	I_{yy}	I_{zz}
$(slug \cdot ft^2)$	95,389.06	143,741.37	214,587.65
$(kg \cdot m^2)$	129,330.20	194,887.13	290,941.79

The analytical and Creo values are somewhat similar, within the same factor of 10. The values themselves, however, differ by a marginal amount. Moving forward, the analytical values are used in future calculations. The determined moments of inertia are then used in XFLR5 to determine the aircraft's longitudinal and lateral stability modes.

12.3   Modal Analysis

Using XFLR5 with the known inertia moments, weight, and CG location, the longitudinal stability mode was analyzed and generated the following frequencies in Table 12.4. This can be visually interpreted in Figure 12.1. A root-locus plot was also generated, as seen in Figure 12.2. All points lie on the left-hand side of the graph dictating that the aircraft's longitudinal modes are stable.

Table 12.4 – Longitudinal mode values

	Short Period (Red)	Phugoid Period (Blue)
Natural Frequency (Hz)	0.573	0.011
Damped Natural Frequency (Hz)	0.536	0.011
Damping Ratio ζ	0.353	0.004
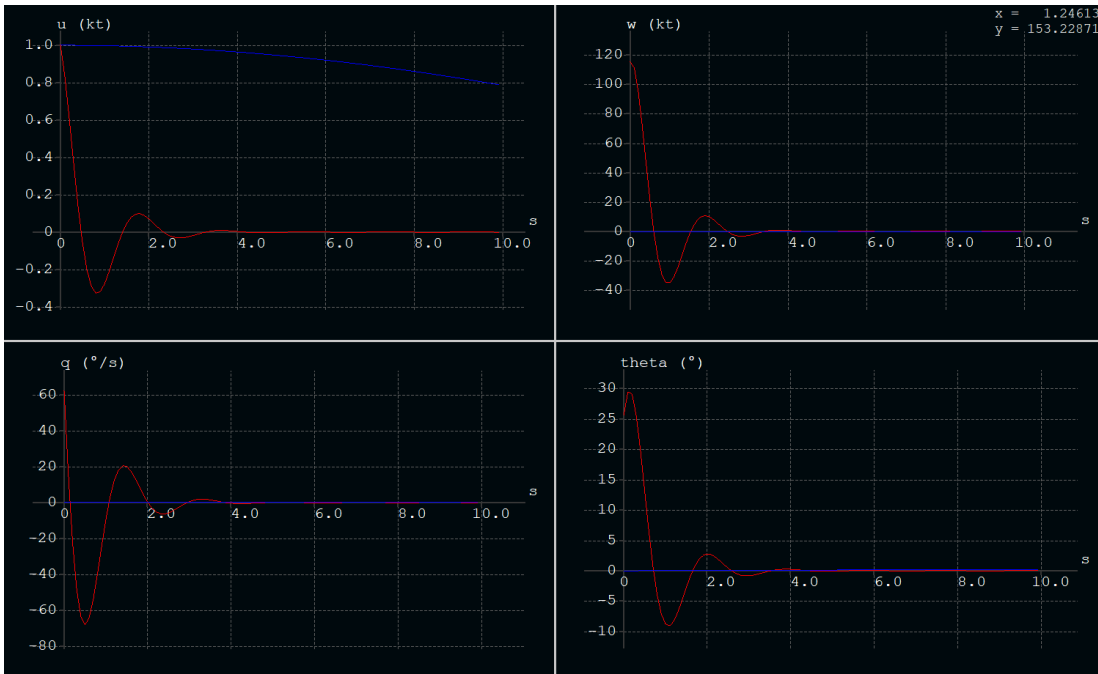
Figure 12.1 – Longitudinal stability analysis plot

Figure 12.2 – Longitudinal root-locus plot

Table 12.5 presents this mode's response times and frequencies for the lateral stability analysis. These values are then visualized in Figure 12.3. Both the roll mode and dutch-roll mode, when disturbed, returns to its initial position. The spiral mode steadily rises, indicating a slight instability in this mode when disturbed. Figure 12.4 presents the lateral root-locus plot.

Table 12.5 – Lateral mode values

	Roll Mode (Red)	Dutch-Roll Mode (Blue)	Spiral Mode (Green)
Natural Frequency (Hz)		0.530	
Damped Natural Frequency (Hz)		0.529	
Damping Ratio ζ		0.076	
Time to double t2 (s)	0.141		809.87
Time constant τ	0.203		--
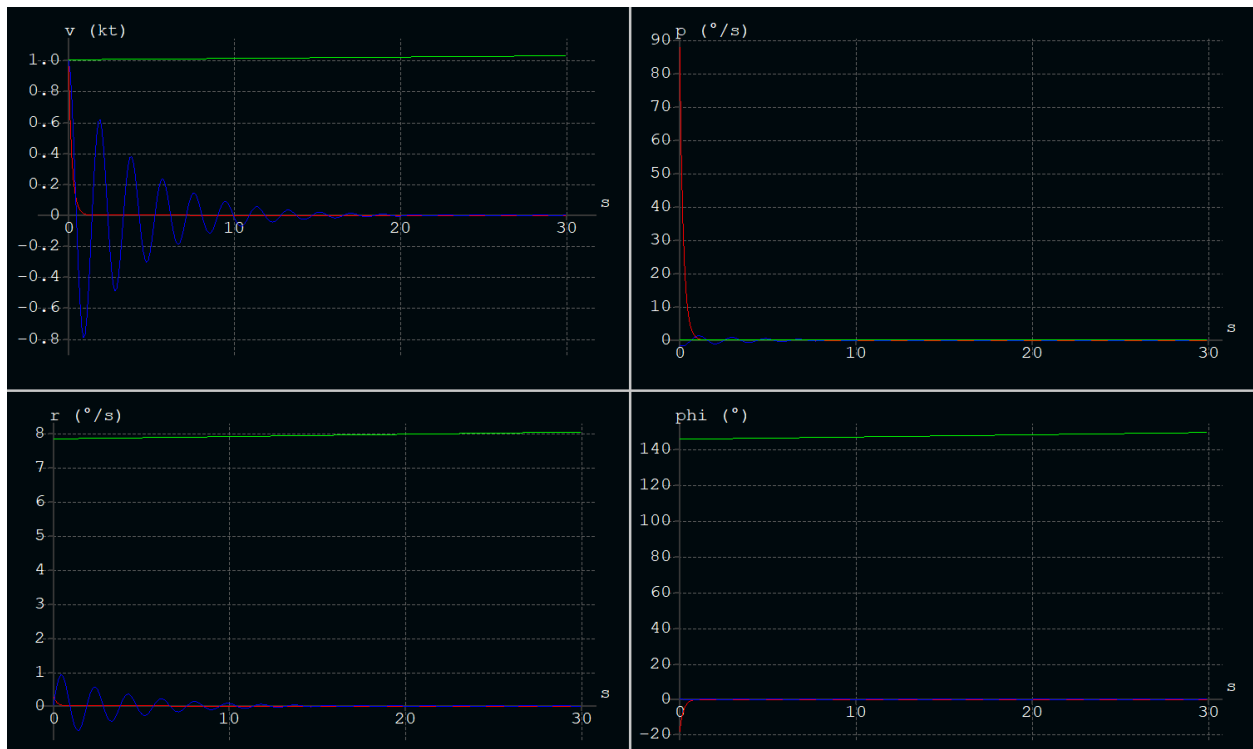
Figure 12.3 – Lateral stability analysis plot
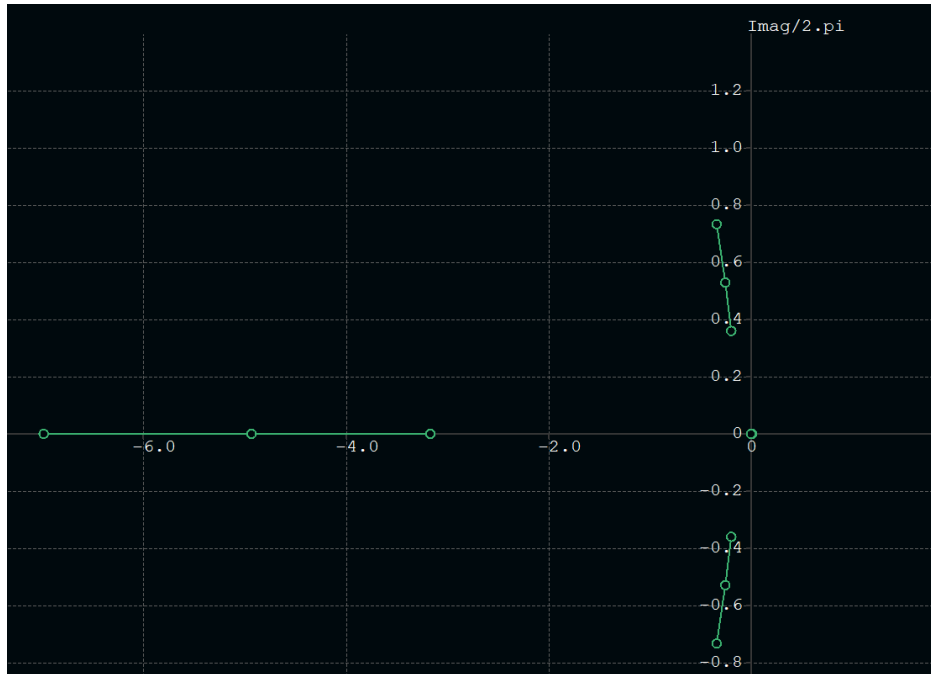
Figure 12.4 – Lateral root-locus plot

12.4   Conclusion

The YA-94 was determined to have a positive static margin. The moments of inertia were determined in two methods resulting in relatively similar results, but the analytical solution was chosen as the path forward since the analytical method is determined more accurate and there is much more confidence in the input values for the analysis.

The YA-94 is determined to be stable in the longitudinal direction when analyzing the aircraft's stability performance. As for the lateral direction, only two of the three modes are determined stable, and the spiral is currently displayed as slightly unstable as it has a very slight upward trend per Figure 12.3.

Chapter 13 – Drag Polar Estimation

13.1 Introduction

This chapter discusses the estimation of the YA-94's drag polar. Both Raymer and Roskam estimations were used to calculate the drag polar, and both methods are explained in the following sections. This chapter only estimates the overall drag of the aircraft unlike the drag breakdown which is presented in Chapter 19 – Drag Breakdown where the drag of all components is determined individually and later summed together. Therefore, this chapter presents an estimated drag value of the YA-94 and later further analyzed and refined in Chapter 19 – Drag Breakdown.

13.2 Drag Polar

13.2.1 Raymer Drag Estimation

The skin-friction coefficient (C_{f_e}) and wetted area ratio (S_{wet}/S_{ref}) were estimated using Table 13.1 and Figure 13.1. The skin friction coefficient of an air force fighter is used as an estimation, while the wetted area ratio is referenced around the F-4, estimated to be 4.5. These values can then estimate the zero-lift drag using equation (13.1).

$$C_{D_0} = C_{f_e} \frac{S_{wet}}{S_{ref}} = (0.0035)(4.5) = 0.0158 \tag{13.1}$$

Table 13.1 – Skin friction coefficient [9]

$C_{D_0} = C_{f_e} \left(\dfrac{S_{wet}}{S_{ref}} \right)$	C_{f_e}
Bomber	0.0030
Civil transport	0.0026
Military cargo (high upsweep fuselage)	0.0035
Air Force fighter	0.0035
Navy fighter	0.0040
Clean supersonic cruise aircraft	0.0025
Light aircraft – single-engine	0.0055
Light aircraft – twin-engine	0.0045
Prop seaplane	0.0065
Jet seaplane	0.0040
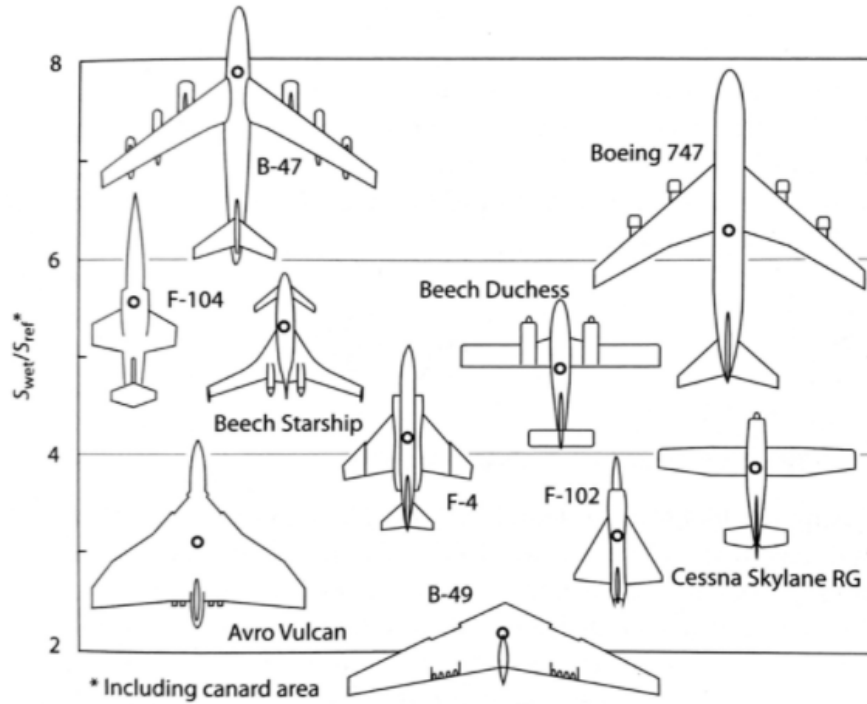
Figure 13.1 – Wetted area ratios

Using these given values, the drag polars for takeoff, landing, and clean configurations are then calculated and plotted in Figure 13.2. The inputs to generate these plots can be seen in Table 13.3. The C_{D_0} for takeoff and landing was determined by adding drag effects due to flap settings and landing gear, values suggested by Roskam in Table 13.2. Note also that the K value is determined with equation (13.2).

Table 13.2 – Estimated drag per component

Drag Component	C_{D_0}	Chosen C_{D_0}
Landing gear	0.015 to 0.025	0.02
Takeoff flaps	0.01 to 0.02	0.015
Landing flaps	0.055 to 0.075	0.065

$$K = \frac{1}{\pi A e} \tag{13.2}$$

where:
- A = Wing aspect ratio
- e = Oswald efficiency

Table 13.3 – Raymer – drag polar input and L/D outcome value

	C_{D_0} (Raymer)	AR	e	K	L/D max (Raymer)
Takeoff	0.0508	6	0.8	0.0698	8.4
Landing	0.1008	6	0.76	0.0737	5.8
Clean (subsonic)	0.0158	6	0.72	0.0663	15.5
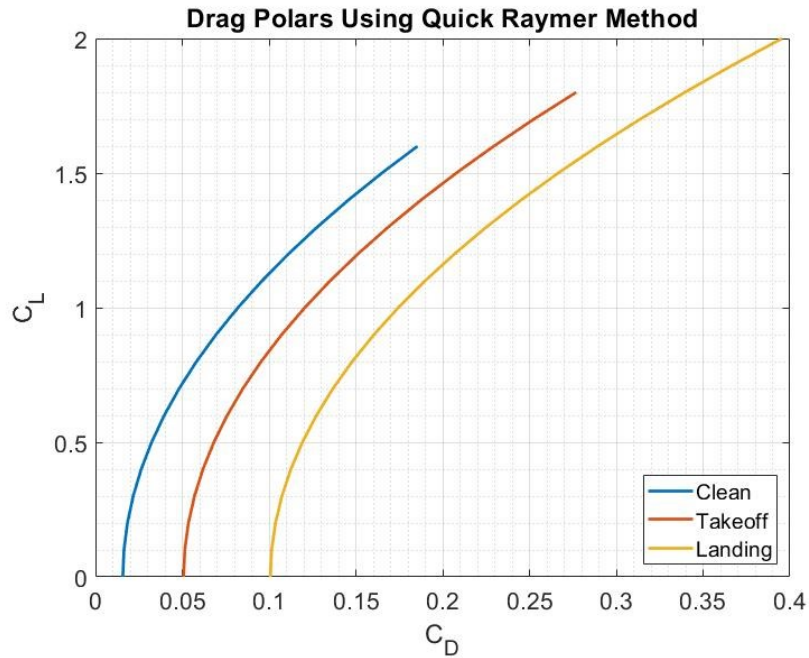
Figure 13.2 – Drag polar – Raymer's method

13.2.2 Roskam Drag Estimation

Roskam's method begins by calculating S_{wet} using Table 13.4 with the values of a fighter. S_{wet} is calculated with equation (13.3) where W_0 is the total takeoff weight of 50,000 lbs. This area was analyzed to be $2.613 * 10^3 \ ft^2$.

$$S_{wet} = 10^{c+dlog(W_0)} \tag{13.3}$$

Table 13.4 – Regression line coefficients for takeoff weight versus wetted area [38]

	c	d
Homebuilt	1.2362	0.4319
Single Engine Propeller Driven	1.0892	0.5147
Twin Engine Propeller Driven	0.8635	0.5632
Agricultural	1.0447	0.5326
Business Jets	0.2263	0.6977
Regionals Turboprop	-0.0866	0.8099
Jet Transports	0.0199	0.7531
Mil. Trainers	0.8565	0.5423
Fighters	-0.1289	0.7506
Mil. Transports, Bombers, and Patrol Airplanes	0.1628	0.7316
Flying Boats	0.6295	0.6708
Supersonics Cruise Airplane	-1.1868	0.9609

S_{wet} is then used to estimate the equivalent skin friction coefficient (c_f) referencing Figure 13.3. This was determined to be 0.0020, which is used in Table 13.5 to find the equivalent parasite area (f) using equation (13.4), resulting in $f = 1.477 * 10^5 \, ft^2$.

$$f = 10^{a+\log(S_{wet})} \tag{13.4}$$

Table 13.5 – Correlation coefficients for parasite area versus wetted area [38]

Equivalent skin friction coefficient, c_f	a	b
0.0090	-2.0458	1.000
0.0080	-2.0969	1.000
0.0070	-2.1549	1.000
0.0060	-2.2218	1.000
0.0050	-2.3010	1.000
0.0040	-2.3979	1.000
0.0030	-2.5229	1.000
0.0020	-2.6990	1.000
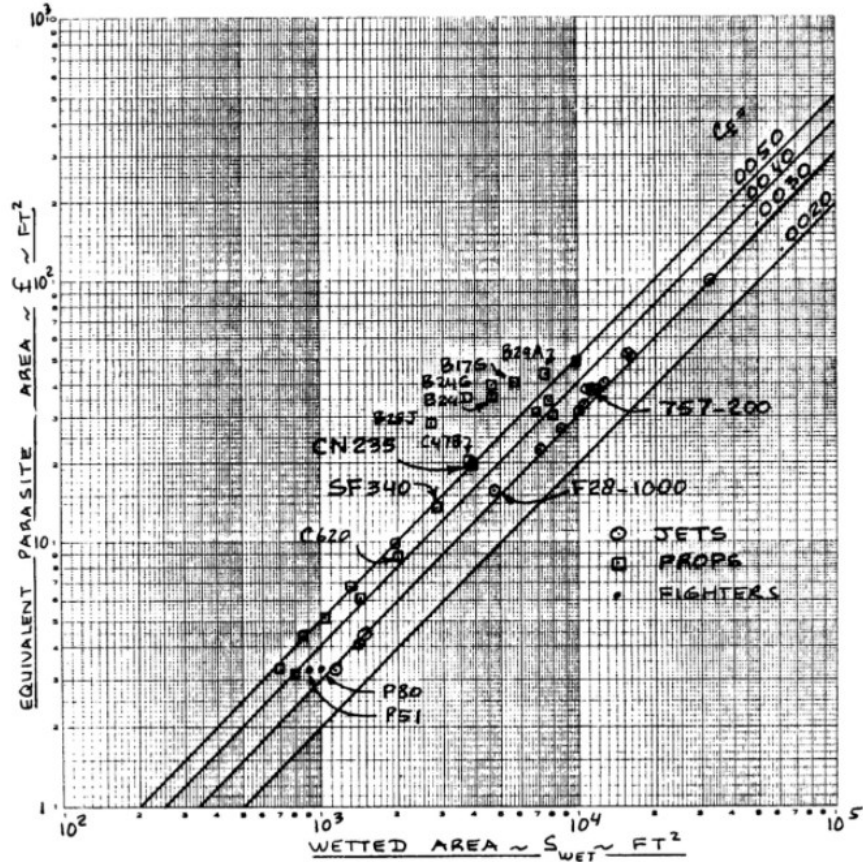
Figure 13.3 – Skin friction coeff. per wetted area

With f determined, the zero-lift drag can be calculated using equation (13.5) where S_{ref} is the reference wing area of $600 \, ft^2$. The drag polar is plotted in Figure 13.4 with other inputs, and the resulting L/D can be referred to in Table 13.6.

$$C_{D_0} = f/S_{ref} \qquad (13.5)$$

Table 13.6 – Roskam – drag polar input and L/D outcome value

	C_{D_0} Roskam	AR	e	K	L/D max Roskam
Takeoff	0.0475	6	0.8	0.0698	8.7
Landing	0.0975	6	0.76	0.0737	5.9
Clean (subsonic)	0.0125	6	0.72	0.0663	17.3
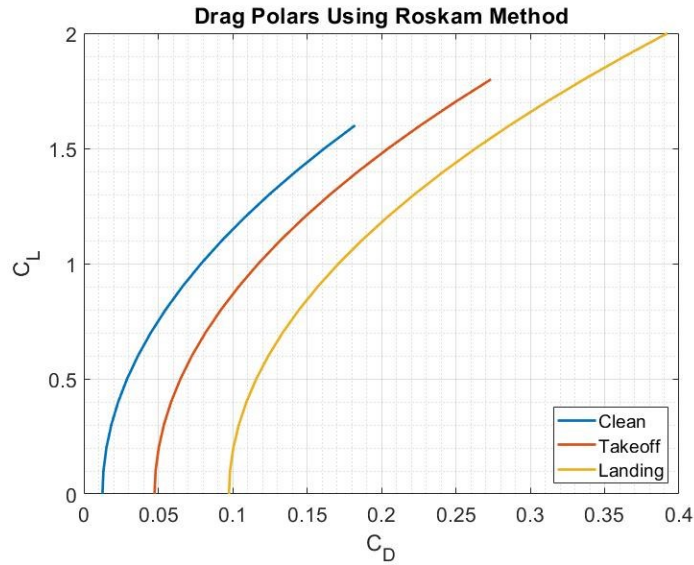
Figure 13.4 – Drag polar – Roskam's method

13.3   Conclusion

When using the Raymer and Roskam drag estimation, the clean cruise L/D was 15.5 and 17.3, respectively. During the initial estimation in chapter 3, L/D was assumed to be 15.0. Raymer's methods come close to the L/D, while Roskam's estimation is slightly over. These values are realistic since the L/D for the A-6 Intruder, in comparison, is about 15. In conclusion, both methods result in similar values of drag and L/D. A detail breakdown of this drag polar is further discussed in Chapter 19 – Drag Breakdown.

Chapter 14 – Economic, Environment, Safety, and Manufacturing

14.1   Economic Considerations

Currently, the USAF is looking for an affordable attack aircraft to replace the aging A-10 and use it in place for certain missions where the F-35 would be called in, costing thousands of dollars to operate. This design aims to provide a more modern aircraft designated for the attack role while achieving the same mission at a lower operational cost. Currently, the F-35 costs $42,000 per hour of flight while the A-10 only costs $19,000 to $20,000 per hour of flight [1]. This is a 50% difference in operational cost. The USAF suggests an aircraft at around $4,000 and $5,000 per hour. The YA-94 will not be able to achieve this price range as a jet fighter but will aim to achieve an operational cost between $12,000 to $15,000.

14.2   Environmental Considerations

The A-10 has been in service for almost 45 years using GE TF-34 engines. With today's engines, they are much more efficient and powerful. As of right now, the YA-94 plans to use the same engines as they are still far more fuel-efficient. However, it is expected that the YA-94 can carry a higher payload than the A-10. Therefore, the YA-94 aims to be more carbon-emission friendlier while providing additional performance. In addition, the life expectancy of the YA-94 would be aimed towards around 50 years in service, ensuring the aircraft must be fully modular, allowing updates to its systems.

14.3   Safety Considerations

The YA-94 is planned to include ejection seats for both crew members on board if the aircraft is shot down, saving both lives. The belly of the fuselage will need to be reinforced to allow emergency belly-landings if the landing gear fails to deploy. Finally, the YA-94's cockpit will be reinforced with a titanium "tub" to protect the pilots inside while engaging enemy targets at very low altitudes, which would be within range of small-arm fire.

14.4   Manufacturing Considerations

Additive manufacturing (AM) would be considered to allow faster lead times and lower production costs. However, these would need to be done for non-critical parts as AM is still a researched process. Most parts would need to be designed modularly to allow parts to be replaced with ease while also allowing system upgrades when new technologies are produced over time. Therefore, accessibility to certain aircraft areas will need to be considered during the design phase.

Chapter 15 – Structural Arrangements

This chapter presents the initial concept of the structural arrangement of the YA-94. It is estimated to have most of the primary structure made from aluminum with the skin and secondary structures made of composites to keep the aircraft light. Titanium will only be used to manufacture the "bathtub" surrounding and protecting the cockpit area. The below figure illustrates the internal structure and arrangement of the YA-94.
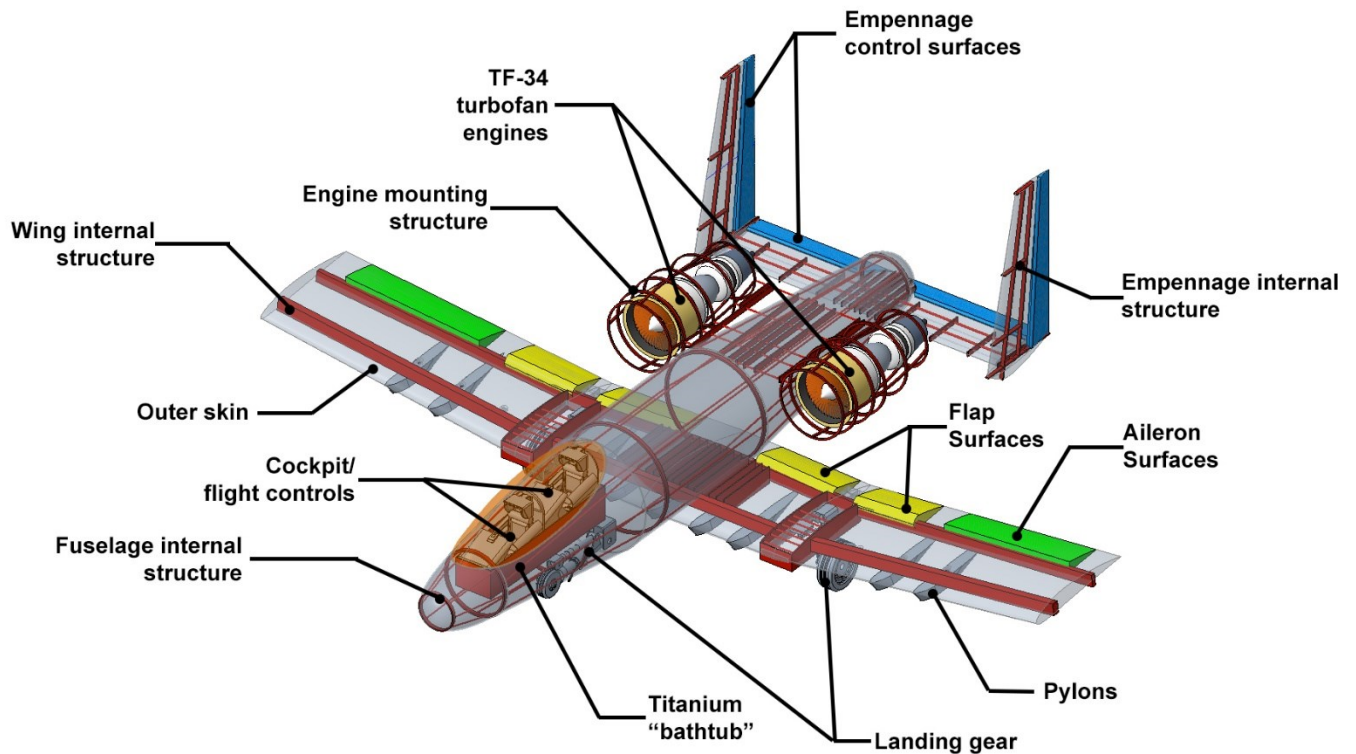
Figure 15.1 – YA-94 internal structure arrangement

To highlight some of the features, the main wing spar runs through the wing's quarter chord line as most of the lift force will be present along that location. Parts of the main landing are also attached to the main spar to absorb most of the impact loads due to landing. The hardpoint pylons are attached along the main spar to carry majority of the payload's weight.

The trailing edge spar primarily serves as attach points for secondary structures and mechanisms (flaps, ailerons, landing gear joints, etc.). Similar wing-like internal structures are used for the engine pylons and empennage including spars and ribbing. The internal structure for the fuselage consists of circular ribbing and cylindrical stingers to resist torsion and bending moments.

Chapter 16 – Subsystem Arrangement

16.1   Introduction

Chapter 16 presents the subsystem design and layout within the YA-94. The following subsystems are discussed:

- Flight controls
- Propulsion and fuel system
- Hydraulic system
- Electrical system
- Instruments and avionics
- Safety and survivability

16.2   Flight Controls System Layout Design

Fly-by-wire is the chosen control system for the YA-94. Therefore, a combination of hydraulic fluid and electrically powered actuators are used to operate the aerodynamic surfaces. Section 16.4 elaborates further on the hydraulic and electrical system layout. Figure 16.1 illustrates the control surfaces layout including locations of the actuators. An example of an actuator is shown in Figure 16.2.
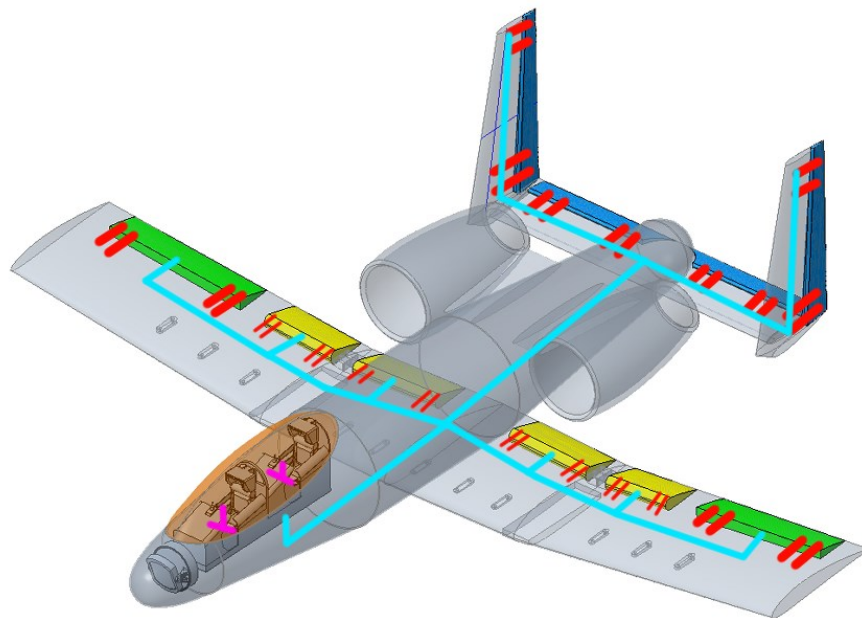
Figure 16.1 – Flight control system internal layout

Figure 16.2 – Hydraulic actuator [53]

Due to the threatening environment the YA-94 operates within, each control surface is operated by two sets of actuators. This is to ensure the aircraft remains controllable if one fails or becomes damaged during combat.

16.3 Propulsion and Fuel System Layout Design

Figure 16.3 illustrates the propulsion and fuel system layout. The YA-94 includes a total of four fuel tanks. Two of them are stored in the center of the fuselage while the other two are stored within the wing, close to the root. Overall, the tanks are closely placed together in the center of the aircraft surrounded by outside armor plating to provide the most protection in case of incoming enemy fire.
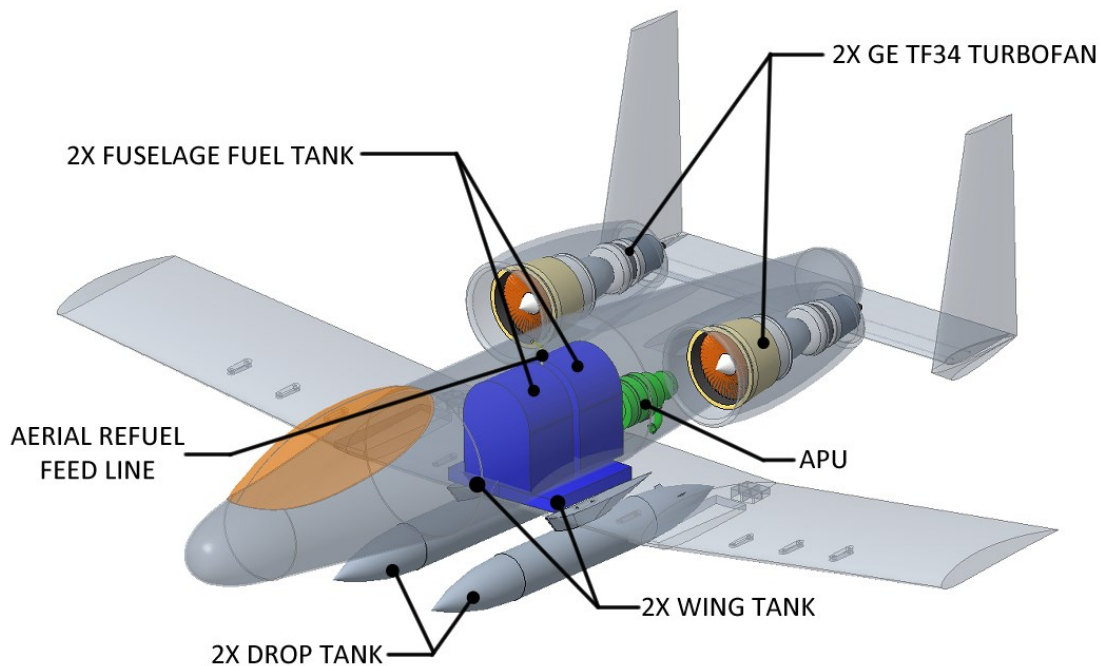
Figure 16.3 – Fuel system internal layout

Fuel lines are routed to the two engines in the aft end of the aircraft. Each engine is provided a dual feeding system. This is to provide redundancy in case if one fuel line fails or

become damaged. Therefore, two fuel pumps are also integrated for each engine to guarantee continuous fuel flow. The engines are also capable to start without an external power source. An onboard APU (green) is available to allow the pilots to start their engines without the assistance of another power source like other aircraft.

There are also fuel pumps located at the bottom of the aircraft, beneath the existing fuel tanks. This allows fuel to also be pumped from the external fuel pods if the pilots decide to use them. An additional fuel line is located between the two primary tanks, connecting the two tanks and routed to the top of the fuselage. This allows aerial refueling from a KC-135 Stratotanker if the mission requires continuous flight or no available runways are within reach for manual refuel. An example of this feature is shown in Figure 16.4.

Figure 16.4 – F-15 aerial refueling [54]

16.4   Hydraulic System Layout Design

Figure 16.5 presents the hydraulic system layout throughout the YA-94. Again, a dual system is used to ensure that sufficient hydraulic pressure is provided to the necessary subsystems, in this case the landing gear and control surfaces. If one hydraulic system fails, the other is able to compensate and ensure the aircraft remains in control.
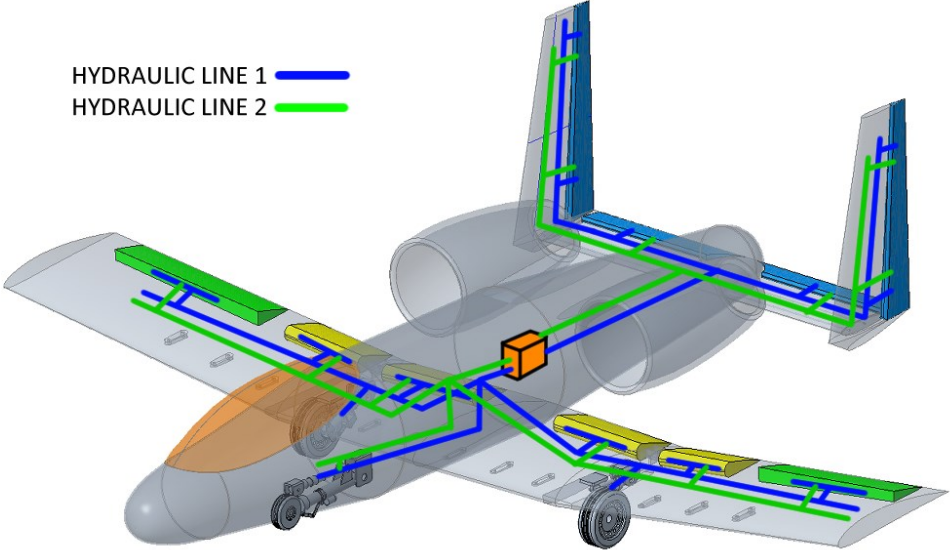
Figure 16.5 – Hydraulic system internal layout

16.5   Electrical System Layout Design

Figure 16.6 presents an electrical system diagram for the F-104 Starfighter connecting to critical subsystems on the aircraft. Like the YA-94, the F-104 includes a 2-pilot crew and is jet-engine driven. Therefore, it can be assumed the electrical system of the YA-94 is laid out similar to the F-104.
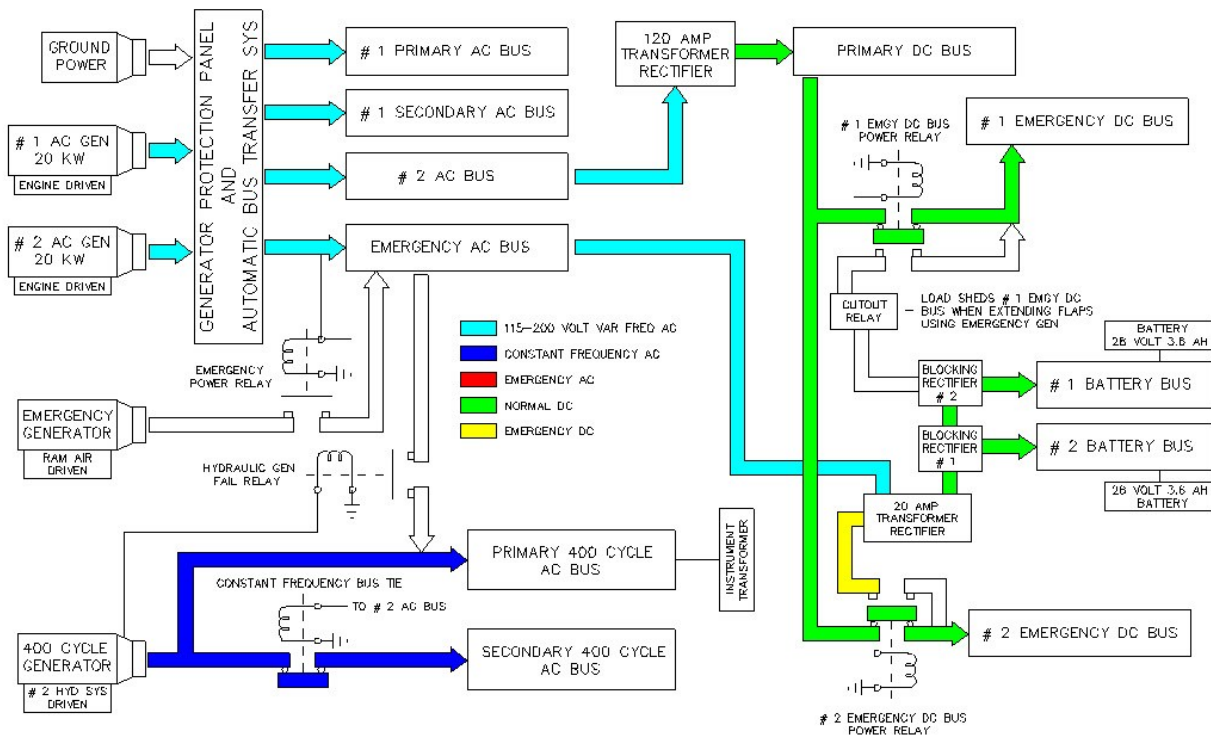
Figure 16.6 – General electrical system diagram [55]

As shown, there are redundant alternating current (AC) and direct current (DC) generators onboard in case any one generator becomes inoperative allowing the aircraft to remain operational. Two of the AC generators are engine driven providing high wattage to the primary and secondary AC electrical bus subsystem. From the primary AC bus, the current is divided and transformed into the primary DC bus subsystem. The below lists a sample of critical components that are powered by each bus subsystem on the aircraft.

The primary DC bus subsystem powers the following:
- Air data computer seat actuator
- Auto pilot cockpit spotlights
- Navigational light duct, anti-ice
- Electronic equipment test engine bypass flaps
- Taxi light engine inlet air temperature
- Radar accelerometer
- Voice recorder radar dehydrator

The secondary AC bus powers the following:
- Fuel boost pump intake duct anti-ice
- Fuel boot pump transfer pump

Finally, the primary AC bus powers the following:
- Air conditioning oxygen indicator
- Anti-icing valve pitot and AoA probes
- Fuel boost pump auto trandformer for landing lights
- Early warning system and radar system

16.6 Cockpit Instrumentation and Avionics Systems

Figure 16.7 showcases the flight controls and computers in the cockpit that the pilots operate, all surrounded by a titanium bathtub serving as protection from small-arms fire. A generic volume in the rear of the seating area presents the overall avionic systems and boxes used on the aircraft. Below the seating platform, an onboard oxygen generating system (OBOGS) is available to generate oxygen utilizing bleed air from the aircraft's engines. This is much more efficient than using a liquid oxygen system (LOX) which can be a limiting resource when flying. In addition to using bleed air, a heating, ventilation, and air conditioning system (HVAC) is used to provide environmental comfort in the cockpit. In front of the seating area is a radar system. This allows the pilots to detect targets from a great distance allowing them to plan before engaging. The specific radar system can be from any notable supplier (e.g., Honeywell or Raytheon).
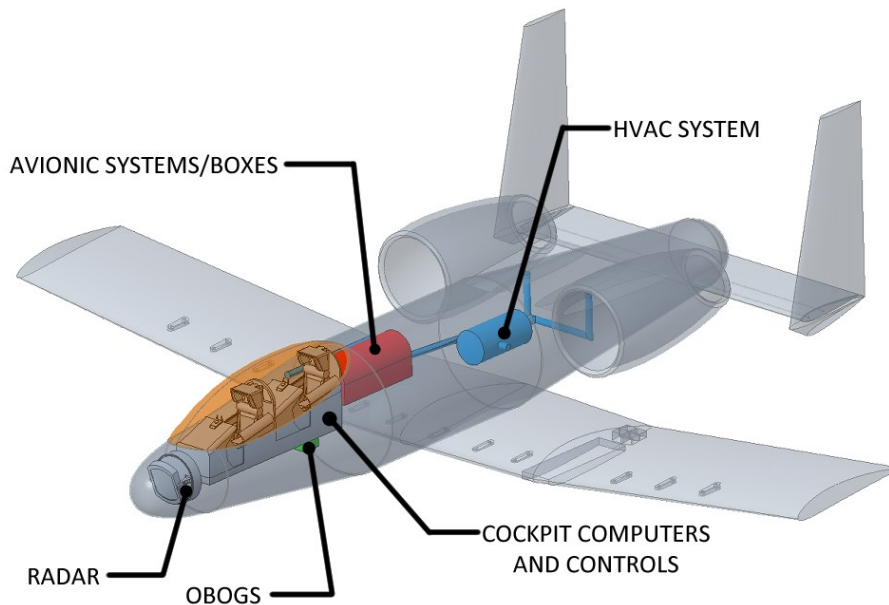
Figure 16.7 – Instrumentation and avionic system layout

16.7 Weapon System Integration

As stated before, the YA-94 will use the same GE GAU-8 gatling gun as found on the A-10. It is known to be an effective weapon against ground targets, especially armored ones. As presented in Figure 16.8, the cannon is placed centered in the nose to provide accuracy. The feeding belt is stretched along underneath the cockpit and attached to the ammo drum, located

behind the cockpit. The ammo drum is located near the center of the fuselage to ensure the highest protection and prevent premature detonation from incoming enemy fire.
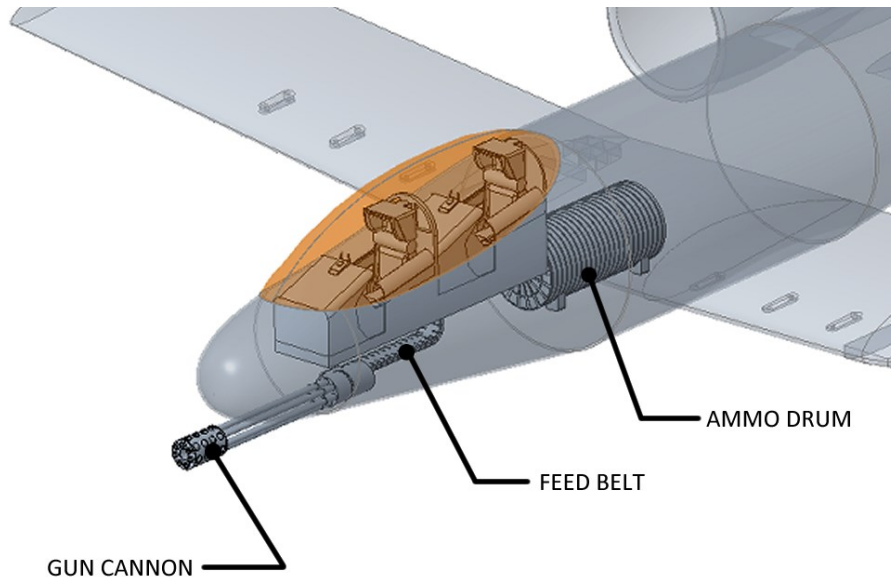
Figure 16.8 – GE GAU-8 integration layout

16.8   Safety and Survivability Considerations

One safety feature on the YA-94 includes ejection seats for both crew members onboard. The canopy is wired to small electro-explosive devices which would remove the canopy rapidly to allow the pilots to eject out of the cockpit safely midflight.

As mentioned before, to protect the pilots onboard during combat, the entire cockpit is covered in titanium plating. This will protect them from small-arms fire from the ground while also protecting critical computers onboard. The canopy is made of bullet-proof glass to protect the pilots giving them a full 360° area of protection.

The aircraft also features self-sealing fuel tanks. In case the tanks are punctured, the material surrounding the fuel tank can absorb the fuel, swell, and expand, plugging the hole in the process preventing additional fuel from leaking out during flight.

Another safety feature on the aircraft is self-locking landing gear. In case the aircraft loses significant hydraulic pressure, the gears are still able to deploy due to gravity and lock themselves into place due to air drag and ground friction when rolling on the runway. This guarantees much safer landings in case the YA-94 came back heavily damaged.

Chapter 17 – V-n Diagram

A V-n diagram, or flight envelope, was created to visualize the operational limits of the YA-94, presented in Figure 17.1. The listed equations below were used to determine and plot the limits of the aircraft per its speed and maximum load factors.
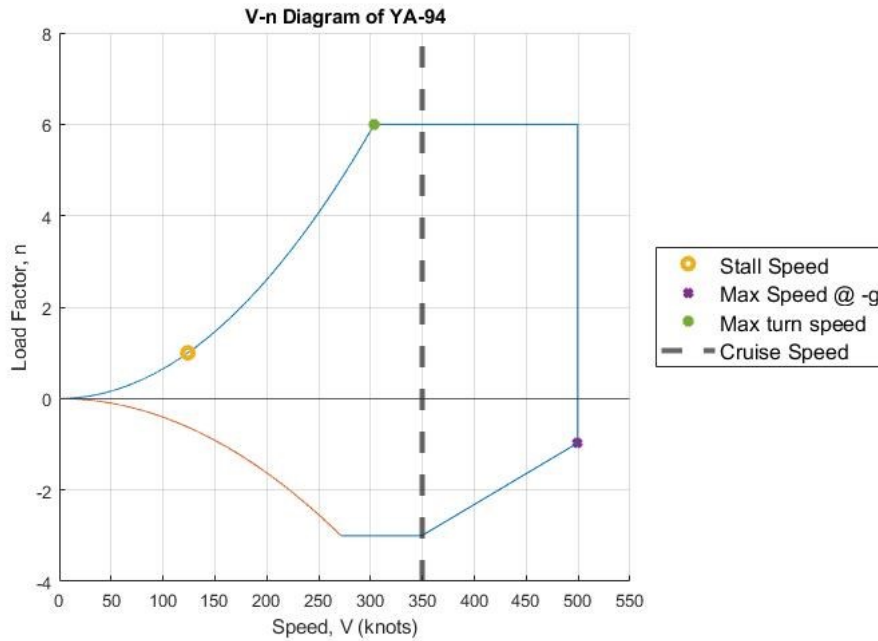
Figure 17.1 – YA-94 flight envelope diagram

Stall speed:

$$V_{stall} = \frac{\sqrt{2W_0}}{\rho S c_{L_{max,+}}}$$ (17.1)

where:
- W_0 = Gross weight
- ρ = Air density
- S = Reference planform wing area
- $c_{L_{max,+}}$ = Maximum lift coefficient at positive load

Corner speed:

$$V_a = V_{stall}\sqrt{n^+}$$ (17.2)

where:
- n^+ = Positive load factor

Corner speed load factor:

$$n^* = \frac{n^+}{V_a} * V \qquad (17.3)$$

where:
- V = Varying aircraft flight speed

Maximum speed at negative load:

$$V_{max,-} = \frac{\sqrt{2n^- W_0 g}}{\rho S c_{L_{max,-}}} \qquad (17.4)$$

where:
- n^- = Negative load factor
- $c_{L_{max,-}}$ = Maximum lift coefficient at negative load

Negative load factor:

$$n_{max}^- = \frac{n^-}{V_{max,-}} * V \qquad (17.5)$$

Maximum positive and negative stall factors:

$$n_{V+} = \frac{c_{L_{max,+}} \rho V^2 S}{2W_0} \qquad (17.6)$$

$$n_{V-} = -\frac{c_{L_{max,-}} \rho V^2 S}{2W_0} \qquad (17.7)$$

As shown, the aircraft can only operate within the defined boundaries to maintain structural integrity. The YA-94 has a maximum positive g-load of 6-Gs and a maximum negative g-load of -3-Gs. Only at cruise speed (350 knots) can the aircraft structure handle both maximum positive and negative loads. The maximum turn capability is done at 6-Gs with the aircraft travelling at 304 knots before overloading the structure. During negative load, such as diving, the aircraft can travel at 500 knots with the structure only experiencing no more than -1-G. Overall, the aircraft is very limited in the negative load with much more flexibility in the positive load.

Chapter 18 – Stability and Control Analysis, AVL

18.1   Introduction

Chapter 18 details the stability and control analysis of the YA-94, building upon what was presented in Chapter 12. The Athena Vortex Lattice (AVL) code is primarily used throughout this chapter to analyze various performance and control characteristics. It must be noted that the AVL model does not include the fuselage body. Thus, the additional effect from this body is not calculated and considered into this chapter but is assumed the produced values are close enough. The following characteristics are examined:

- Trim analysis
- Takeoff rotation
- One engine inoperative condition
- Roll performance

18.2   Trim Analysis

Figure 18.1 presents a trim crossplot diagram for the YA-94 cruising at various angles of attack (AoA) between -5 and 5 degrees. As shown, each line represents the elevator being deflected at three different states. Both moment and lift coefficient values were obtained through AVL using the described angle inputs and speed.
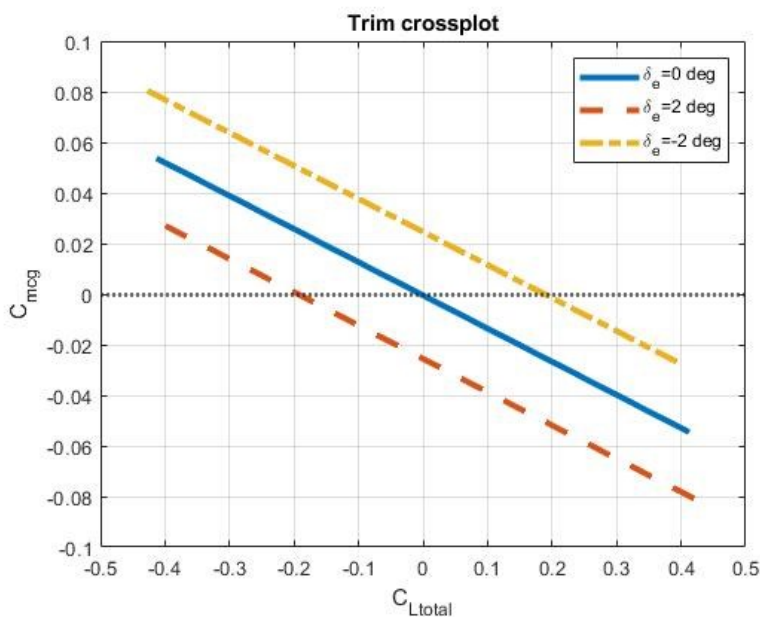
Figure 18.1 – Trim crossplot

The elevator was set dependent on a zero-pitching moment to determine the efficient trim elevator angle. When analyzing AVL, it was determined that the YA-94 would cruise at 350 knots, an AoA of 2.59 degrees (nose up) with an elevator deflection of -2.09 degrees (elevator up) for MTOW CG location.

18.3   Takeoff Rotation

The elevator must be sized and positioned correctly during takeoff to provide enough pitching moment to begin pitching the nose up. Equation (18.1) determines the required pitching moment coefficient the YA-94 must obtain at takeoff speed.

$$C_{m_{req}} = \frac{M_{req}}{\bar{q} S L_{elev}}$$
(18.1)

where:
- M_{req} = The total moment between the CG and the main landing gear
- $\bar{q}$ = dynamic pressure at takeoff speed
- L_{elev} = Moment arm between the landing gear and aerodynamic center of the horizontal stabilizer
- S = Wing planform area

Using the above equation and moving at 10% above stall speed, a pitching moment coefficient of 0.233 is required to pitch the nose upward during takeoff. To verify the design, the following constraints were applied to the AVL model:

- 10% above stall speed
- Flap deflection of 30° (flap down)
- elevator deflection of -25° (elevator up)

It must be noted that AVL can only model plain flaps, and the YA-94 is designed with fowler flaps which would only require 15°. Therefore, the flaps must be deflected much more in AVL.

A pitching moment coefficient of 0.226 was obtained when running this case with an achieved AoA of 12.3°. This is considered close enough to the required value determined above in equation (18.1).

18.4   Minimum Control Speed with Engine Out (OEI Analysis)

Due to the dangerous environment the YA-94 operates in, there will be scenarios where the aircraft will sustain heavy damage due to adversary fire while trying to remain airborne and either provide additional CAS or return home safely. One of these investigated scenarios is the one engine inoperative (OEI) condition. In this scenario, only one engine is operational while the other windmills, causing an induced yawing moment that must be counteracted to maintain directional flight.

The yaw moment caused by the operational engine is determined by equation (18.2), resulting in a yaw moment of 52,760 lbf-ft (71.5 kN-m). The windmilling drag effect by the inoperative engine is determined with equation (18.3) which generates an additional drag moment determined by equation (18.4). The minimum control speed in this scenario must be 10% above the aircraft's stall speed. The total yaw moment caused by the asymmetric thrust

resulted in 56,580 lbf-ft (79.2 kN-m). Therefore, the rudders must be adequately sized to counteract the induced yaw moment.

$$N_{T_1} = Ty_P = 7913.74lbf * 6.67ft = 52,760 \ lbf \cdot ft \qquad (18.2)$$

where:
- T = Thrust from operating engine
- y_p = Moment arm distance from operating engine thrust to aircraft midplane

$$D_{wm} = \frac{1}{2}c_{D_{wm}}\rho(v_{mc})^2 S \qquad (18.3)$$

where:
- $c_{D_{wm}}$ = Windmilling drag coefficient
- ρ = Air density
- v_{mc} = Minimum control speed, in this case, 10% above stall speed
- S = Wing planform area

$$N_{D_1} = D_{wm}y_p = 3,820 \ lbf \cdot ft \qquad (18.4)$$

$$N_{T_1} + N_{D_1} = 56,580 \ lbf \cdot ft \qquad (18.5)$$

AVL was used to model and analyze this effect. Per Roskam's requirement, a sideslip of 0° was applied in this scenario. Other applied constraints included the rudder deflected at 12.5°, flaps set to takeoff deflection of 30°, aileron deflection set to zero rolling moment, and elevator set to zero pitching moment. This produced a total yaw moment coefficient $C_{N_{tot}}$ of .02607. Equation (18.6) is used to determine the total yawing moment produced by the rudders, resulting in 58,960 lbf-ft (80 kN-m). Therefore, the rudders are correctly sized and capable of maintaining straight directional flight during an OEI scenario. In addition, the required rudder deflection is well under the maximum 25° of deflection.

$$N_{Tot} = C_{N_{tot}} * \frac{1}{2}\rho(v_{mc})^2 Sb = 58,960 \ lbf \cdot ft \qquad (18.6)$$

where:
- $C_{N_{tot}}$ = Total moment coefficient
- ρ = Air density
- v_{mc} = Minimum control speed, in this case, 10% above stall speed
- S = Wing planform area
- b = Wingspan

18.5   Roll Performance

For comparison, it was determined by users of Digital Combat Simulator (DCS) that the A-10 has a steady roll rate of roughly 130 degrees per second. Using AVL and inputting a maximum aileron deflection of 25°, the YA-94 produces a rolling rate coefficient (c_P) of 0.21599. This coefficient is used in equation (18.7) which determines the dimensional roll rate at 243 degrees per second.

$$P = \frac{c_P 2V}{b}$$ (18.7)

where:
- c_P = Rolling rate non-dimensional coefficient
- V = Flight speed
- b = Wingspan

This roll rate achieves the desired roll response but is very high compared to the A-10 and thus requires further analysis. Raymer's method was used next to determine the aircraft's roll rate, which was determined by equation (18.8).

$$P = -\left(\frac{C_{ld_a}}{C_{l_p}}\right)\delta a$$ (18.8)

where:
- C_{ld_a} = determined by equation (18.9)
- C_{l_p} = Roll damping parameter, defined by Figure 18.2
- δa = Aileron deflection angle
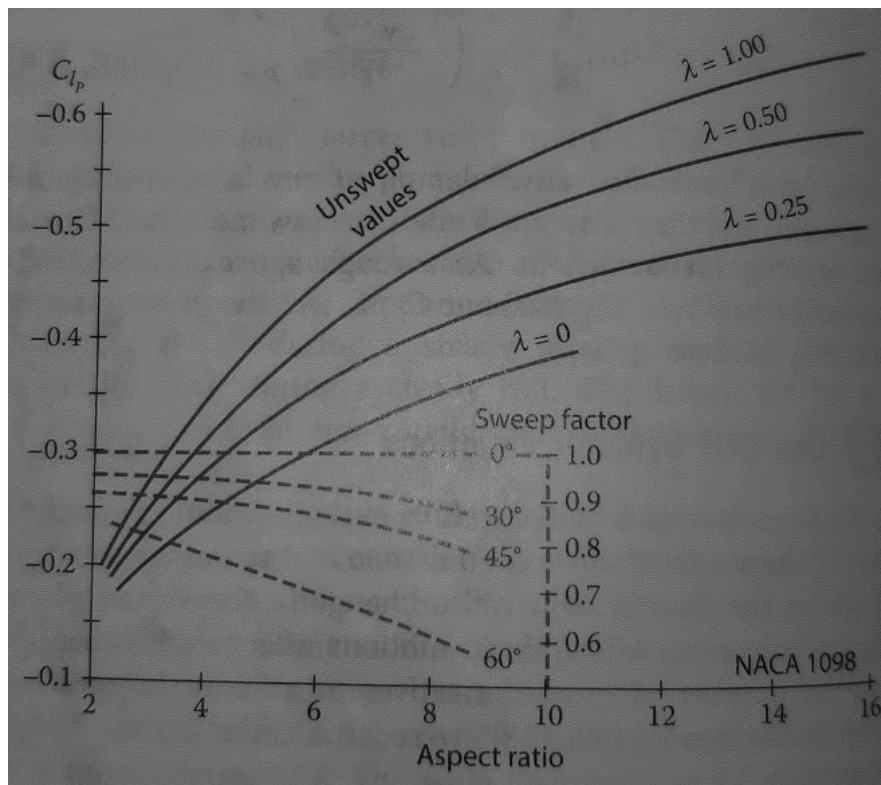
Figure 18.2 – Roll damping parameter [9]

119

$$C_{l_{d_a}} = \frac{2\left(\sum K_f \left(\frac{\partial C_L}{\partial \delta_f}\right)' Y_i S_i cos\Lambda_{HL}\right)}{S_w b}$$

(18.9)

where:

- K_f = defined in Figure 18.3
- $\left(\frac{\partial C_L}{\partial \delta_f}\right)'$ = Theoretical lift increment for plain flaps, defined by Figure 18.4
- Y_i = Aileron lift increment area location, defined by Figure 18.5
- S_i = Aileron lift increment area, defined by Figure 18.5
- Λ_{HL} = Aileron hinge line sweep angle
- S_w = Total wing planform area
- b = Wingspan
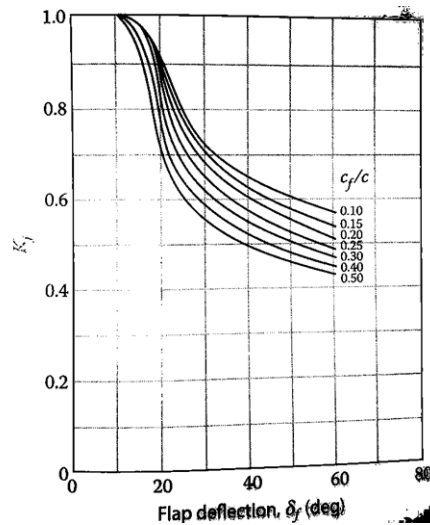
Figure 18.3 – Empirical correction for plain flap lift increment [9]
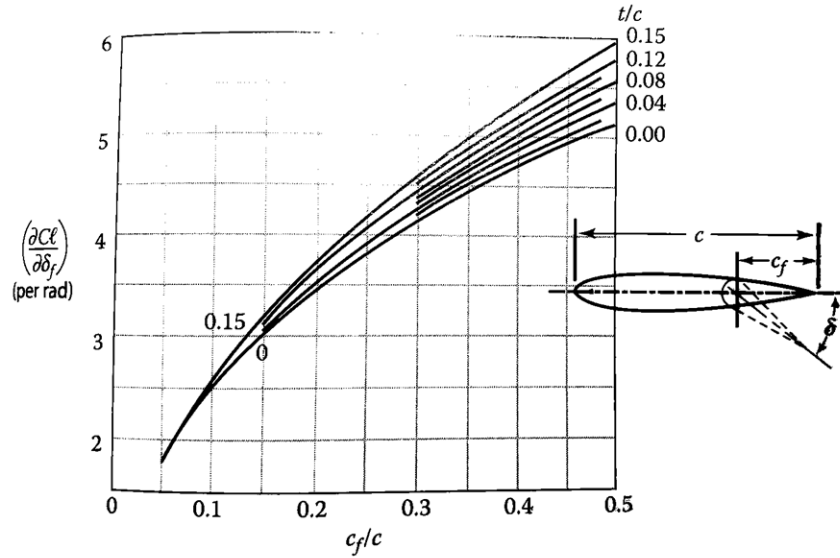
Figure 18.4 – Theoretical lift increment for plain flaps [9]
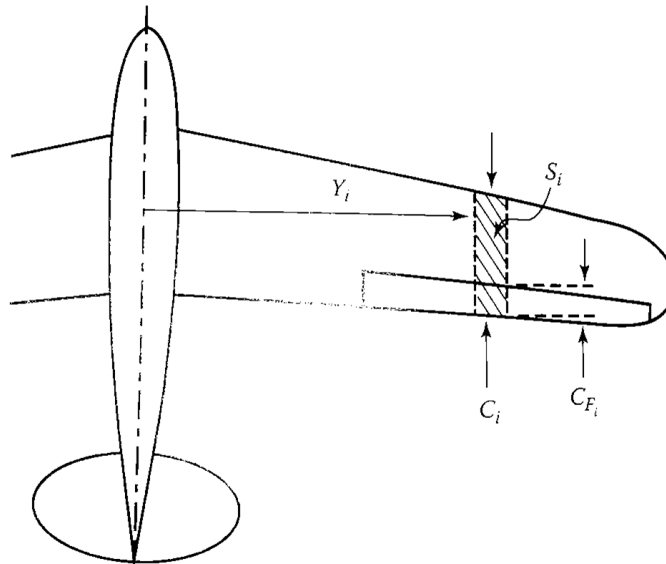
Figure 18.5 – Aileron strip geometry [9]

Using the provided figures above and the same aileron deflection of 25°, the estimated roll rate comes out to 23.76 deg/s. Referencing mil-spec MIL-F-8785 B, a typical attack fighter must achieve a roll angle of 90° in 1.3 seconds. With the determined roll rate, a roll angle of only 30.89° is achieved within the same time reference. This is much lower than the military requirement when using Raymer's method.

18.6   Conclusion

In conclusion, the YA-94 meets all critical stability and control conditions with some difficulties in the rolling requirement. AVL meets the required roll rate although it seems unrealistically high. Raymer seems to underestimate the roll performance and does not meet the desired roll angle per the mil-spec. However, it must be noted that the roll angle defined by the mil-spec includes roll acceleration due to the aircraft's mass inertia. This feature is not modeled within Raymer's calculation thus making this calculation inconclusive. The decision was made to go with the AVL result and conclude the design meets the roll rate requirement.

Chapter 19 – Drag Breakdown

19.1   Introduction

The drag breakdown is estimated and presented in this chapter using Raymer's method. The parasitic drag is determined using the equivalent skin-friction and component buildup methods. Unlike Chapter 13 – Drag Polar Estimation, this chapter determines the drag of each component of the aircraft, external payloads, and other discrepancies and later summed together to determine the total drag produced by the aircraft.

19.2   Parasite (Zero-Lift) Drag

19.2.1 Equivalent Skin-Friction Method

This method assumes a well-designed aircraft in subsonic cruise and will have parasite drag due to mostly skin friction and a slight separation pressure drag [9]. Equation (19.1) is used to estimate the parasite drag with Table 13.1 to reference for equivalent skin-friction coefficients C_{f_e}, in this case, an air force fighter.

$$C_{D_0} = C_{f_e} * \frac{S_{wet}}{S_{ref}} \tag{19.1}$$

where:
- C_{f_e} = Equivalent skin-friction coefficient
- S_{wet} = Wetted surface area of aircraft
- S_{ref} = Reference wing planform area

The estimated skin friction coefficient using this method comes out to 0.0220, including the aircraft and external payloads. The skin friction coefficient of the aircraft alone (clean configuration) comes out to 0.0172. It must be noted that S_{wet} was calculated using the concurrent CAD model of the YA-94.

19.2.2 Component Buildup Method

For a more accurate representation of the aircraft's parasite drag, the drag of each component on the aircraft must be individually determined at subsonic speed and later summed together to determine the overall drag. Equation (19.2) is used with its variables defined as follows.

$$\left(C_{D_0}\right)_{subsonic} = \frac{\sum\left(C_{f_c}FF_cQ_cS_{wet_c}\right)}{S_{ref}} + C_{D_{misc}} + C_{D_{L\&P}} \tag{19.2}$$

where:

- C_{f_c} = flat-plate skin-friction drag coefficient of the individual component
- FF_c = Form factor of the individual component
- Q_c = Interefence factor of the individual component
- S_{wet_c} = Wetted area of individual component
- $C_{D_{misc}}$ = Miscellaneous drags of unique features of the aircraft
- $C_{D_{L\&P}}$ = Estimated drag contributions for leakage and protuberances

Table 19.1 presents the breakdown of each drag component of the aircraft and the sum of the parasitic drag. The calculations for each component can be referenced in Appendix F.

Table 19.1 – Parasite drag component breakdown

Component	C_{D_0}
Fuselage	0.0038
Wing	0.0007
Nacelle	0.0029
Horizontal tail	0.0002
Vertical tail	0.0002
Miscellaneous (bombs, drop tanks, etc)	0.0047
L&P (e.g. gun cannon)	0.0003
Total parasite drag:	0.0128

It is much lower when comparing the total parasitic drag to the drag estimated in the previous method (0.0220).

19.3   Induced-Lift Drag Coefficient

In addition to the drag caused by the non-lifting bodies of the aircraft, the creation of lift causes an induced drag to the aircraft. This is determined through the Oswald span efficiency method presented by Raymer. The Oswald efficiency factor of a straight wing is estimated using equation (19.3) which is then used in equation (19.4) to solve the induced drag constant K, where A in both equations is the wing aspect ratio. Equation (19.5) can then be used to solve the induced drag based on the clean cruise lift coefficient, which comes out to be $C_{D_i} = 0.00099$.

$$e = 1.78(1 - 0.045A^{0.68}) - 0.64 \tag{19.3}$$

$$K = \frac{1}{\pi A e} \tag{19.4}$$

$$C_{D_i} = KC_L^2 \tag{19.5}$$

Therefore, with both the parasite and induced drag known, the total drag coefficient of the YA-94 comes out as $C_D = 0.0138$. This value can then be used in equation (19.6) to calculate the overall lift-to-drag ratio of the YA-94.

$$\frac{L}{D} = \frac{C_{L_1}}{C_{D_0} + C_{D_i}} = \frac{0.1274}{0.0138} = 14.6 \tag{19.6}$$

Recalling Chapter 13 – Drag Polar Estimation, the clean drag coefficient was predicted to be 0.0158 with an L/D of 15.5. Methods and values determined in this chapter closely align with the predicted values. Therefore, the drag breakdown method gave a much more accurate drag representation than the equivalent skin-friction method.

19.4   Conclusion

This chapter discussed the drag breakdown of each component found on the YA-94. The final determined values of the drag and lift-to-drag come close to the predicted values estimated in previous chapters. Therefore, the overall aerodynamics of the aircraft is suitable for its specified mission.

Chapter 20 – Critical Performance Requirements

20.1   Introduction

Chapter 20 presents the critical performance requirements of the YA-94. Performances are analyzed and confirmed compared to the mission specifications highlighted in chapter 2. Detailed calculations of the below aspects can be seen in Appendix G – Performance Calculations. The following performance criteria are listed as follows:

- Maneuverability
- Takeoff and landing distance
- Climb speed
- Range and Endurance

20.2   Maneuverability

Per the mission specifications, it was desired that the YA-94 have a minimum sustained turn at a load factor of 2Gs at 5°/sec, and the instantaneous turn must be at a minimum of 6Gs and 20°/sec. A maneuver diagram was generated using Raymer's and Roskam's methods to determine the required speed to obtain the desired turn rate and load factor before stalling. Refer to Appendix I – Turning Performance Calculation for plot generation. This diagram can be seen in Figure 20.1 where a maximum instantaneous turn rate of 23°/sec at 280 knots is achieved with the sustained turn envelope highlighted in yellow. It must be noted that these values were calculated at 5,000 ft altitude, standard atmosphere conditions.
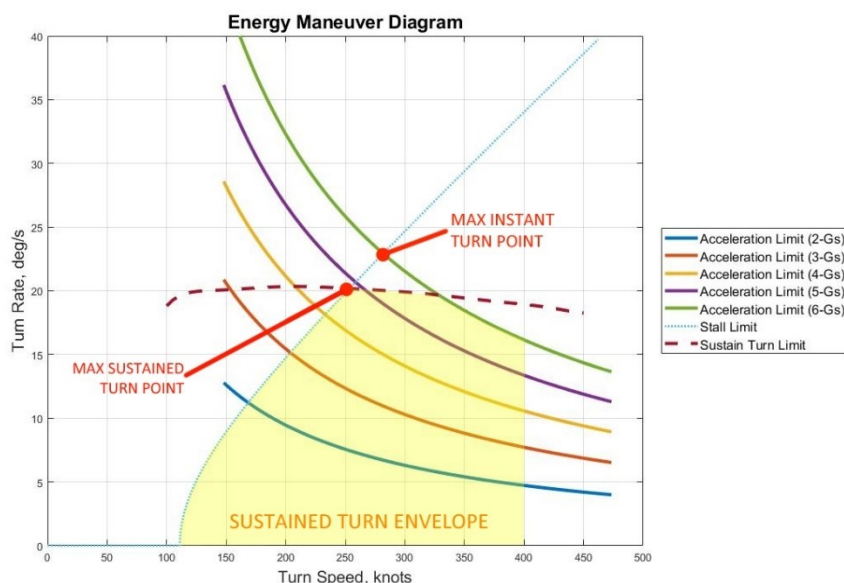
Figure 20.1 – Energy maneuver diagram

The YA-94 can perform a maximum sustained turn rate of 20°/sec while maintaining a load factor of 4.8Gs. During the instantaneous turn performance, the aircraft can turn at a rate of 23°/sec before stalling. Both turn performances are well above the required turn rate from the mission specifications.

Equations (20.1) and (20.2) can be used to analyze the corner speed and turn radius, respectively, at the desired turn performances. At the maximum turn rate, or instantaneous turn, the aircraft has a turn radius of 1,182 ft (360.3 m) with a corner speed of 280.94 knots. This speed is further confirmed in Figure 20.1.

$$V_{turn} = \frac{g\sqrt{n^2 - 1}}{\dot{\psi}}$$
(20.1)

where:
- n = load factor
- $\dot{\psi}$ = turn rate

$$R_{turn} = \frac{V_{turn}^2}{g\sqrt{n^2 - 1}}$$
(20.2)

When analyzing with RDSWin, Figure 20.2 was generated and shows the instantaneous turn rate is achievable at 6Gs while aligning closely with the hand-calculate graph in Figure 20.1.
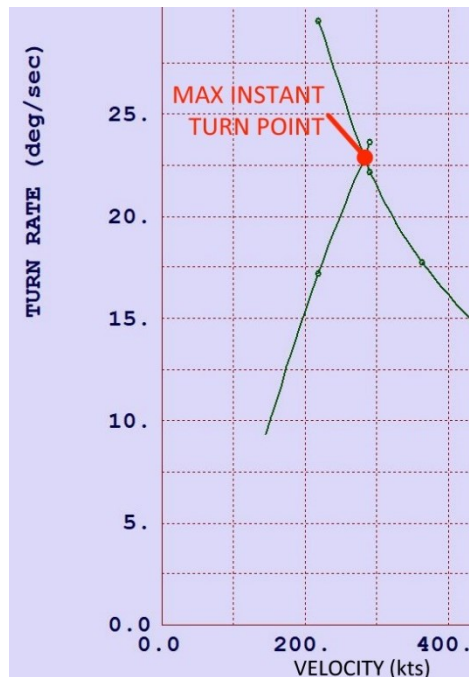
Figure 20.2 – Turn rate vs. tangential velocity

Equation (20.4) determines the required thrust during a sustained turn maneuver to confirm if the selected engine produces enough thrust for the mission profile. The following variables are defined as shown:

- c_{D_0} = Zero-lift drag coefficient
- $c_{L_{man}}$ = Lift coefficient during the maneuver
- A = Wing aspect ratio
- e = Oswald efficiency
- $\bar{q}$ = dynamic pressure
- S = Reference planar wing area

$$T_{reqd} = \left(c_{D_0} + \frac{c_{L_{man}}^2}{\pi A e} \right) \bar{q} S \tag{20.3}$$

A 4.8G load factor with a turn speed of 255 knots at 5,000 ft altitude resulted in a required minimum thrust of 16,850 lbf (75.0 kN), which is just below the calculated maximum installed thrust from Section 6.3.1. Therefore, the TF-34 is a suitable engine.

20.3 Takeoff and Landing Distance

Using equations (20.4) and (20.8) from Roskam, the total takeoff and landing distances required, including the ground and air running distances, can be determined for the YA-94. Equation (20.5) determines the ground distance alone for takeoff. As for landing, the air and ground segments can be determined separately with equations (20.6) and (20.7), respectively. Table 20.1 presents these distances, and when compared to the mission specs, the calculated distances are well under the requirements. The USAF requires a runway length of no more than 3,000 ft which is also obtained.

$$s_{TO} = f_{TO} h_{TO} \left[\left(\frac{1}{\gamma_{LOF}} \right) + \frac{\left(\frac{V_3}{V_{S_{TO}}} \right)^2 \left(\frac{W}{S} \right)_{TO} \left(\left(\left(\frac{\bar{T}}{W} \right)_{TO} - \mu' \right)^{-1} + 1.414 \right)}{\left(h_{TO} \rho g c_{L_{max_{TO}}} \right) (1 + 1.414 \gamma_{LOF})} \right] \tag{20.4}$$

where:
- f_{TO} = obstacle height factor
- h_{TO} = obstacle height
- $\frac{V_3}{V_{S_{TO}}}$ = Ratio of speed at obstacle height to stall speed during takeoff
- $\left(\frac{W}{S} \right)_{TO}$ = takeoff wing loading
- $\left(\frac{\bar{T}}{W} \right)_{TO}$ = mean thrust-to-weight ratio during takeoff
- μ' = total friction coefficient due to ground and drag
- γ_{LOF} = liftoff flight path angle

$$s_{TOG} = \frac{\left(\frac{V_{LOF}}{2g}\right)}{\left(\frac{\bar{T}}{W}\right)_{TO} - \mu'}$$

(20.5)

$$s_{air} = \left(\frac{1}{\bar{\gamma}}\right)\left(\frac{V_A^2 - V_{TD}^2}{2g + h_L}\right)$$

(20.6)

where:
- V_A = approach speed at the obstacle
- V_{TD} = speed when thrust equals drag
- $\bar{\gamma}$ = approach angle
- $h_L = 50\ ft$ obstacle height for all regulations

$$s_{LG} = \frac{V_{TD}^2}{2\bar{a}}$$

(20.7)

where:
- $\bar{a}$ = deceleration during ground run

$$s_L = s_{air} + s_{LG}$$

(20.8)

Table 20.1 – Running distances

	Imperial (ft)	Metric (m)
Ground run takeoff distance (s_{TOG})	1,092	333
Total takeoff distance (s_{TO})	1,550	472
Ground run landing distance (s_{LG})	1,760	536
Total landing distance (s_L)	3,050	930

20.4 Climb Rate

The desired climb rate of the YA-94 is to be a minimum of 4,000 ft/min (1,220 m/min) when travelling 30% above stall speed. Using equation (20.9), the aircraft has a climb rate of 5,180 ft/min (1,580 m/min). This is also well above the minimum climb rate performance requirement. Using the same equation at maximum speed of 400 knots, a ROC of 12,850 ft/min (3,900 m/min) is obtained, a lot higher than the ROC estimated in section 4.5.

$$RC = 60 * U_1 * \left(\left(\frac{T}{W}\right)_{clean} - \frac{1}{\frac{L}{D}}\right)$$

(20.9)

where:
- U_1 = steady speed, 30% above stall speed at $c_{L_{max}}$
- $(T/W)_{clean}$ = thrust-to-weight ratio during clean (no flaps) condition
- L/D = lift-to-drag ratio of aircraft

It must be understood, unlike a turboprop aircraft where thrust degrades overtime, a jet aircraft can maintain constant thrust with velocity throughout the climb duration. However, when increasing the aircraft's forward velocity, the power of the engines increases which in turn increases the aircraft's climb rate. Therefore, for a typical jet aircraft, the maximum climb rate performance occurs at the aircraft's maximum speed.

Figure 20.3 was generated using RDSWin to confirm the max climb rate capability. As illustrated, the YA-94 has a max capability of climbing a little over 10,000 ft/min (3,050 m/min). This is well above the requirement while exceeding the A-10's climb performance requiring the YA-94 to fly at maximum speed. When comparing to the analytical value, the climb rate is lower when taken at the same speed. For conservative purposes, the RDSWin estimate is used as the final ROC result. This confirms that the YA-94 meets the climb expectations outlined in the mission specs.
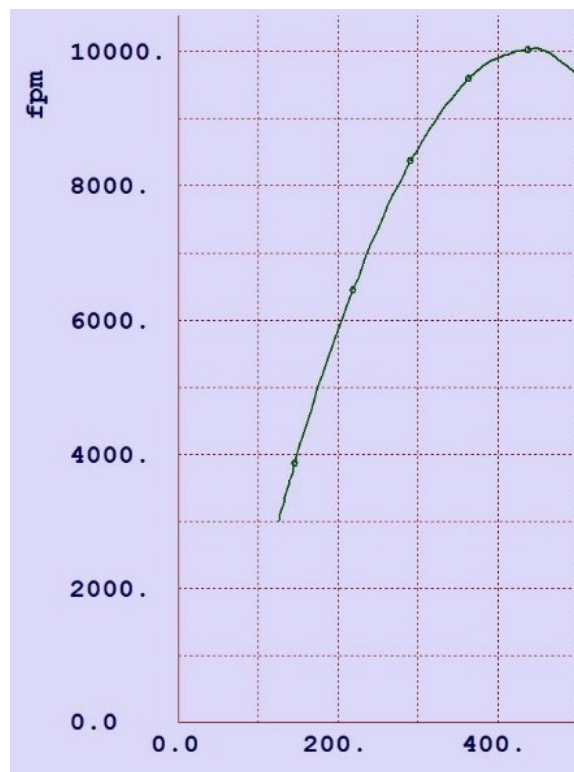
Figure 20.3 – RDSWin climb rate analysis

20.5   Range and Endurance/Loiter

In section 3.3.1, it was confirmed that the YA-94 has a capable range of 500 nmi as defined by the mission specifications. However, RDSWin does not consider payload drop. Therefore, in this section, the clean flight (fuel and pilots onboard only) is assumed to determine the aircraft's true range and endurance. Roskam's equations are used as the analytical method while confirming the calculations with RDSWin.

First, the range is determined by assuming the aircraft travels at a constant altitude. Equation (20.10) is used, assuming a constant altitude of 30,000 ft and an SFC of 0.556 as determined by RDSWin during cruise resulting in a total range of 1,700 nmi.

$$R_{alt} = \frac{f_{mj}}{SFC} \times \frac{1}{\sqrt{\rho_{cruise}S}} \sqrt{\frac{C_L}{C_{D_{cruise}}}} \times \left(\sqrt{W_{0_{clean}}} - \sqrt{W_{end}} \right) \tag{20.10}$$

where:
- f_{mj} = range factor, 1.677 if calculating range in nmi
- SFC = Specific fuel consumption during cruise
- ρ_{cruise} = Air density at cruise altitude
- C_L = Lift coefficient during cruise
- $C_{D_{cruise}}$ = Cruise drag coefficient at 90% of max L/D
- $W_{0_{clean}}$ = Clean total weight of aircraft, empty weight + 98% of fuel (32,430 lbs)
- W_{end} = Final weight at end of flight, empty weight + 10% of fuel (24,860 lbs)

During constant speed, equation (20.11) is used instead. In this case, a constant cruise speed of 350 knots is assumed, resulting in a total range of 2,250 nmi.

$$R_{speed} = \frac{V}{SFC} \times \frac{L}{D_{cruise}} \times \ln\left(\frac{W_{0_{clean}}}{W_{end}}\right) \tag{20.11}$$

where:
- V = Cruise speed
- SFC = Specific fuel consumption during cruise
- L/D_{cruise} = Lift-to-drag ratio, 90% of max L/D

During the RDSWin analysis, a range of 2,000 nmi at 30,000 ft was assumed with an endurance of 0.5 hrs. This resulted in a predicted gross weight of 32,400 lbs, close to inputted weight values used in the analytical solution. Therefore, this confirms that the YA-94 has a total range of around 2,000 nmi during its clean flight configuration.

As for the aircraft's total endurance, equation (20.12) is used resulting in a total flight time of 6.45 hrs regardless of travelling at constant speed or constant altitude. Loiter time can also be determined using the same equation but assuming 75% of the total fuel has been used after flying and right before landing. This resulted in 1.07 hrs of loiter time. This is double the inputted value of 0.5 hrs used in RDSWin. However, it must be realized that the analytical solution predicted a higher range value during constant cruise speed, lining up well with that estimation. Therefore, it is confirmed that the YA-94 can loiter for about 1 hour while capable of staying in the air for a little over 6 hours, excluding payloads.

$$R_{speed} = \frac{1}{SFC} \times \frac{L}{D_{cruise}} \times \ln\left(\frac{W_0}{W_{end}}\right) \tag{20.12}$$

20.6   Conclusion

In conclusion, all critical performance requirements met or exceeded expectations presented in Chapter 2 – Mission Specifications. It can be confidently confirmed that the YA-94 is a well-designed aircraft and could compete with the existing A-10 platform with the presented aspects above.

Chapter 21 – Final Concept Drawing
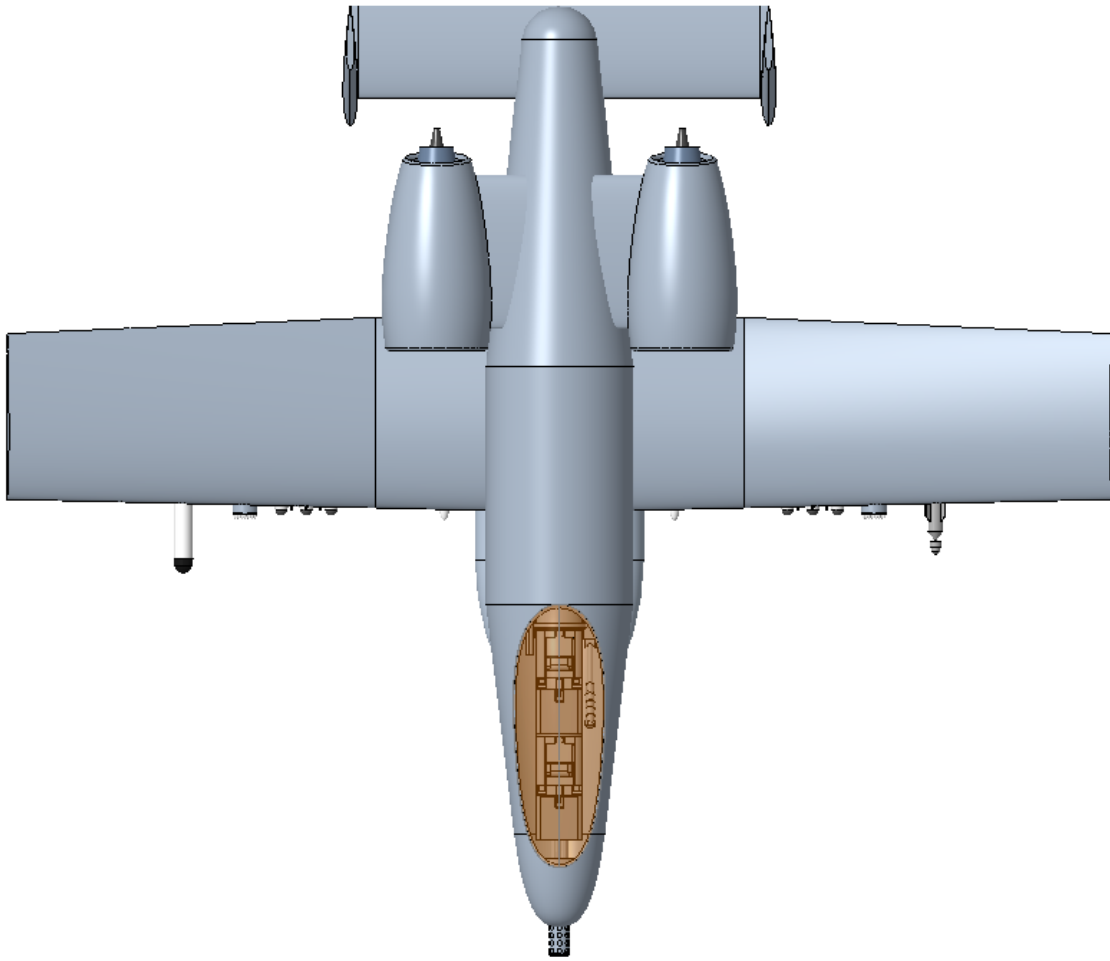
Figure 21.1 – YA-94 final design; top view

Figure 21.2 – YA-94 final design; front view
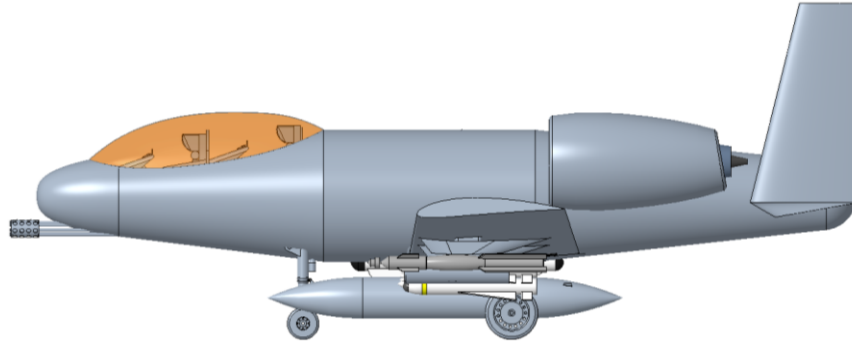
Figure 21.3 – YA-94 final design; right view

Table 21.1 – YA-94 final design specifications

Performance and Geometry	Imperial	Metric
Wingspan	60 ft	18.3 m
Length	50 ft	15.2 m
Wing aspect ratio	6	
Max takeoff weight	50,000 lbs	22,680 kg
Empty weight	24,000 lbs	10,890 kg
Max payload weight	16,820 lbs	7,630 kg
Max speed	400 knots	
Cruise speed	350 knots	
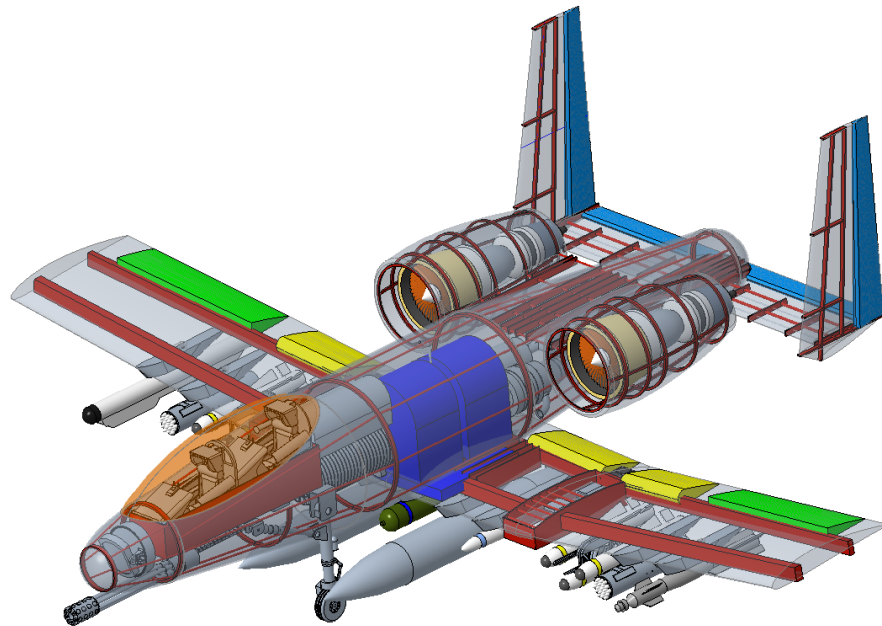
Figure 21.4 – YA-94 final subsystem layout diagram

Chapter 22 – Cost Analysis

22.1   Introduction

Chapter 22 presents the cost analysis of the YA-94. It is assumed that there will be 700 units built in the program, with JP-8 as the primary fuel type and expected 30-year service. Both Raymer (chapter 18 or Appendix H – Cost Analysis; Raymer Method) and Roskam (Part VIII) methods were used to estimate the detailed breakdown of the following cost categories:

- Design and development (RDTE)
- Manufacturing
- Operation

22.2   Design and Development Cost

Table 22.1 presents and compares the estimated RDTE cost from both methods. Roskam estimates slightly below what Raymer predicts, which may be due to different rate predictions between the two authors while compensating for inflation up to 2020.

Table 22.1 – RDTE cost estimation

Roskam Estimation	$2.91 billion
Raymer Estimation	$3.18 billion

22.3   Manufacturing Cost

Table 22.2 compares the manufacturing cost of the YA-94. This then allows calculating the cost of the acquisition unit cost, presented in Table 22.3.

Table 22.2 – Manufacturing cost estimation

Roskam Estimation	$22.2 billion
Raymer Estimation	$3.9 billion

Table 22.3 – Unit acquisition cost estimation

Roskam Estimation	$41.0 million
Raymer Estimation	$12.0 million

The A-10 has a unit cost of $17 million, and Raymer predicts roughly $5 million cheaper than the A-10.

22.4 Operation Cost

Table 22.4 compares the cost comparison of the aircraft's yearly and hourly operations costs. This assumes 216 missions per year, with each mission lasting about 1.5 hours. As for fuel cost, the price was set as $4.29 per gallon, quoted as of mid-2022 for JP-8 grade fuel.

Table 22.4 – Operations cost

Roskam Estimation	
$/hr	$13,931.00
$/yr	$4,514,000.00
Raymer Estimation	
$/hr	$4,165.00
$/yr	$1,350,000.00

For comparison, the A-10 operates $19,000 to $20,000 per hour. However, per USAF standard, two aircraft must fly per mission, resulting in at least $40,000 per mission. Since the YA-94 operates with two pilots onboard, both methods estimate well under the original operational cost of the A-10. The estimates between the two methods are quite different, however due to the possibility of differing inflation rates each method uses.

22.5 Conclusion

In conclusion, the YA-94 obtained a lower cost than the A-10 in both unit acquisition and operational costs. Although Raymer predicts lower values than Roskam, Roskam is more realistic. With composites being considered, it is impossible to obtain an acquisition cost, as analyzed by Raymer. In addition, Roskam's cost values are estimated closer for a jet-powered aircraft. Therefore, Roskam's values closely align with real world cost while still being cheaper than the A-10.

References

[1]   Hallion, R. P. "Battlefield Air Support: A Retrospective Assessment." *Airpower Journal*, Vol. 4, No. 1, 1990.

[2]   Hallion, R. P. *Strike From the Sky: The History of Battlefield Air Attack, 1910-1945*. University Alabama Press, 2010.

[3]   Spick, M. *The Great Book of Modern Warplanes Hardcover*. Chrysalis Books, 2000.

[4]   Keller, J. Fighter Pilot Turned Congresswoman Throws Wrench In Quiet Plans To Cut A-10 Squadrons. *Task & Purpose*. https://taskandpurpose.com/gear-tech/a-10-warthog-fleet-mcsally/. Accessed Jun. 14, 2022.

[5]   Goldfein, D. L. Close Air Support. 2014.

[6]   Pirnie, B. R., Vick, A., Grissom, A., Mueller, K. P., and Orletsky, D. T. *Beyond Close Air Support: Forging a New Air-Ground Partnership*. Santa Monica, 2005.

[7]   Weisgerber, M. "The Light Attack Aircraft." *AIR FORCE Magazine*, 2010, pp. 56–56.

[8]   Shohan, A. S., Khan, I., Shahriar, A., and Salam, A. "Design and Optimization of a Ground Attack Aircraft." *Journal of Mechanical and Civil Engineering*, Vol. 13, No. 3, 2016, pp. 104–110.

[9]   Raymer, D. P. *Aircraft Design: A Conceptual Approach*. American Institute of Aeronautics & Ast, Playa del Rey, 2018.

[10]   Textron Aviation. AT-6 Wolverine. https://defense.txtav.com/en/at-6#:~:text=The%20AT%2D6%20Wolverine%20covers,defense%20and%20civil%20support%20missions. Accessed Jun. 14, 2022.

[11]   AT-6 Wolverine Light-Attack Aircraft. *Airforce Technology*. https://www.airforce-technology.com/projects/6-wolverine-light-attack-aircraft/. Accessed Jun. 14, 2022.

[12]   Jackson, P. *Jane's All the World's Aircraft 2010-2011*. Janes Information Group, 2010.

[13]   Embraer. Super Tucano. *Embraer*. https://defense.embraer.com/global/en/super-tucano. Accessed Jun. 14, 2022.

[14]   Textron Aviation Defense. Scorpion. *Textron Aviation Defense*. https://scorpion.txtav.com/. Accessed Jun. 14, 2022.

[15]   Reid, L. Jr. A-29s Over Afghanistan. https://www.dvidshub.net/image/2822519/29s-over-afghanistan. Accessed Jun. 14, 2022.

[16]   Chen, P. Scorpion! *flckr*. https://www.flickr.com/photos/milchcow_peng/28008899366/. Accessed Jun. 14, 2022.

[17]   Lockheed Martin. *F-35 Lightning II Program Status and Fast Facts*. 2012.

[18]   Lockheed Martin. The Global F-35 Enterprise. *Lockheed Martin*. https://www.lockheedmartin.com/en-us/products/f-35/f-35-global-partnership.html. Accessed Jun. 14, 2022.

[19]   Fedor, L. Sukhoi Su-25 of the Russian Air Force Landing at Vladivostok.

[20]   Greer, W., and da Reporter. Boeing Delivers First A-10 Wing Set to US Air Force. https://www.defenseadvancement.com/news/boeing-delivers-first-a-10-wing-set-to-us-air-force/. Accessed Jun. 14, 2022.

[21]   "Gas Turbine Engines." *Aviation Week & Space Technology*, 2009, p. 119.

[22]   Gunston. *Anatomy of Aircraft*. Longmeadow Pr, 1989.

[23] General Electric Aviation. *TF34 Turbofan Engines*. Cincinnati, 2014.

[24] Langdon, L. S. "Fahrenheit 3,600." *Mechanical Engineering Magazine Select Articles*, 2007, pp. 34–37.

[25] Honeywell Aerospace. TFE731 Turbofan Engine. *Honeywell Aerospace*.

[26] MiG-21.de. Engines of the MiG-21. *MiG-21.de*. https://www.mig-21.de/english/technicaldataengines.htm. Accessed Jun. 14, 2022.

[27] US Air Force. F135 Engine during the JSF System Development and Demonstration (SDD) Phase.

[28] Pratt & Whitney. F135 - The World's Most Advanced Fighter Engine. *Pratt & Whitney*. https://prattwhitney.com/products-and-services/products/military-engines/f135. Accessed Jun. 14, 2022.

[29] Norris, G. "Power Plan." *Aviation Week & Space Technology*, 2015, pp. 13–26.

[30] Kundu, A. K. Aircraft Cost Considerations. In *Aircraft Design*, Cambridge University Press, Cambridge, 2010, p. 524.

[31] Kundu, A. K. Aircraft Cost Considerations. In *Aircraft Design*, Cambridge University Press, Cambridge, 2010.

[32] Boito, M., Keating, E. G., Wallace, J., DeBlois, B., and Blum, I. *Metrics to Compare Aircraft Operating and Support Costs in the Department of Defense*. Santa Monica, 2015.

[33] Mizokami, K. "One of These Three Light Attack Planes Could Help Replace the A-10." *Popular Mechanics*, 2017.

[34] Weisgerber, M. "Air Force Wants New Plane to Replace A-10, Fight ISIS." *Defense One*, 2016.

[35] Goebel, G. A-10: Development & Description. *Internet Archive: waybackmachine*. https://web.archive.org/web/20090925160942/http://www.vectorsite.net/ava10_1.html. Accessed Jun. 14, 2022.

[36] Global Security. TF34 Engine. *Global Security*. https://www.globalsecurity.org/military/systems/aircraft/systems/tf34.htm. Accessed Jun. 14, 2022.

[37] War is Boring. Pilots Plan Tomorrow's A-10. *Medium*. https://medium.com/war-is-boring/pilots-plan-tomorrows-a-10-833a05de6fae. Accessed Jun. 14, 2022.

[38] Roskam, J. *Airplane Design*. Roskam Aviation and Engineering Corporation, Ottawa, 1985.

[39] Thomas, R. H., Burley, C. L., and Olson, E. D. Status of Hybrid Wing Body Community Noise Assessment With Propulsion Airframe Aeroacoustic Experiments. 2010.

[40] Crane, D. *Dictionary of Aeronautical Terms*. Aviation Supplies & Academics, Inc., Renton, 1997.

[41] what-when-how. Tail Designs. *The-Crankshaft Publishing*. http://what-when-how.com/flight/tail-designs/. Accessed Jun. 14, 2022.

[42] Skill Lync. Why Do Different Aircraft Have Different Tails? Youtube, 2020.

[43] Hadingham, E. "Winner Take All." *Air & Space Magazine*, 2003, p. 2.

[44] Love, M. C. Groundloops. In *Better Takeoffs & Landings*, McGraw-Hill Professional, New York, 1995, pp. 75–76.

[45] Mentour Pilot. Why Are the Jet-Engines Placed There? Wings vs Tail. Youtube, 2018.

[46] Airforce Technology. Mako Advanced Trainer and Light Attack Aircraft. *Airforce Technology*. https://www.airforce-technology.com/projects/mako/. Accessed Jun. 14, 2022.

[47] Real Model Pilots. Pilot Seats. *Real Model Pilots*. http://realmodelpilots.co.uk/Accessories/Pilot-Seats. Accessed Jun. 14, 2022.

[48] Prakasa, A. "A Comparative Study Installation Arrangement of Primary Flight Display (PFD) in the Flight Deck's Regional Passenger Transport Aircraft." *AVITEC*, Vol. 1, No. 1, 2019.

[49] mholka. F-16 Canopy — Photo. *depositphotos*.

[50] Airbus. Are You Properly Seated. Airbus S.A.S., Blagnac Cedex, Jan, 2018.

[51] General Electric. Airborne and Surface Gun Systems. *Small Arms of the World*.

[52] The Goodyear Tire & Rubber Company. Aircraft Tire Data Book. *Global Aviation Tires*. goodyearaviation.com. Accessed Jun. 14, 2022.

[53] Moog Inc. Electromechanical Gun Elevation Actuator C116L422E. https://www.moog.com/products/actuators-servoactuators/defense/military-ground-vehicles-actuators/electromechanical-gun-elevation-actuator-c116l422e.html. Accessed Jun. 8, 2022.

[54] Hill Aerospace Museum. HOW DIFFICULT IS AERIAL REFUELING? *Hill Aerospace Museum*. https://www.aerospaceutah.org/how-difficult-is-aerial-refueling/. Accessed Jun. 8, 2022.

[55] Sobelman. Lockheed F-104 Starfighter. *The Airplane Driver's Network*. http://www.airplanedriver.net/study/f104.htm. Accessed Jun. 17, 2022.

[56] CFI Notebook. Electrical Systems. https://www.cfinotebook.net/notebook/operation-of-aircraft-systems/electrical. Accessed Jun. 9, 2022.

[57] F-16.net. Why Is the F-35 Replacing the A-10? *F-16.net*. https://www.f-16.net/forum/viewtopic.php?f=22&t=24483&start=1695. Accessed Jun. 14, 2022.

Appendix A – Standard A-10 Payload Loadout

The following is a loadout configuration example for an attack aircraft.

A-10A外部兵装搭載図 / EXTERNAL STORES

STA.No.	11	10	9	8	7	6	5	4	3	2	1
Mk.82	●	●	●	●	●		●	●	●	●	●
SNAKEYE / Mk.20 / SUU-30	●	●	⦿⦿⦿	●	●		●		⦿⦿⦿	●	
M117	●	●	⦿⦿⦿	⦿⦿⦿	◦◦		◦◦	⦿⦿⦿	⦿⦿⦿	●	●
GBU-8			●	●				●	●		
GBU-10			●	●				●	●		
GBU-12	●		●	●				●	●		●
Mk.84			●	●	●	●	●		●		
BLU-27		●	●	●	●		●	●	●	●	
AGM-65			⦿⦿⦿					⦿⦿⦿			
SUU-20				●	●		●	●			
SUU-23					●		●				
ALQ-119	●										●
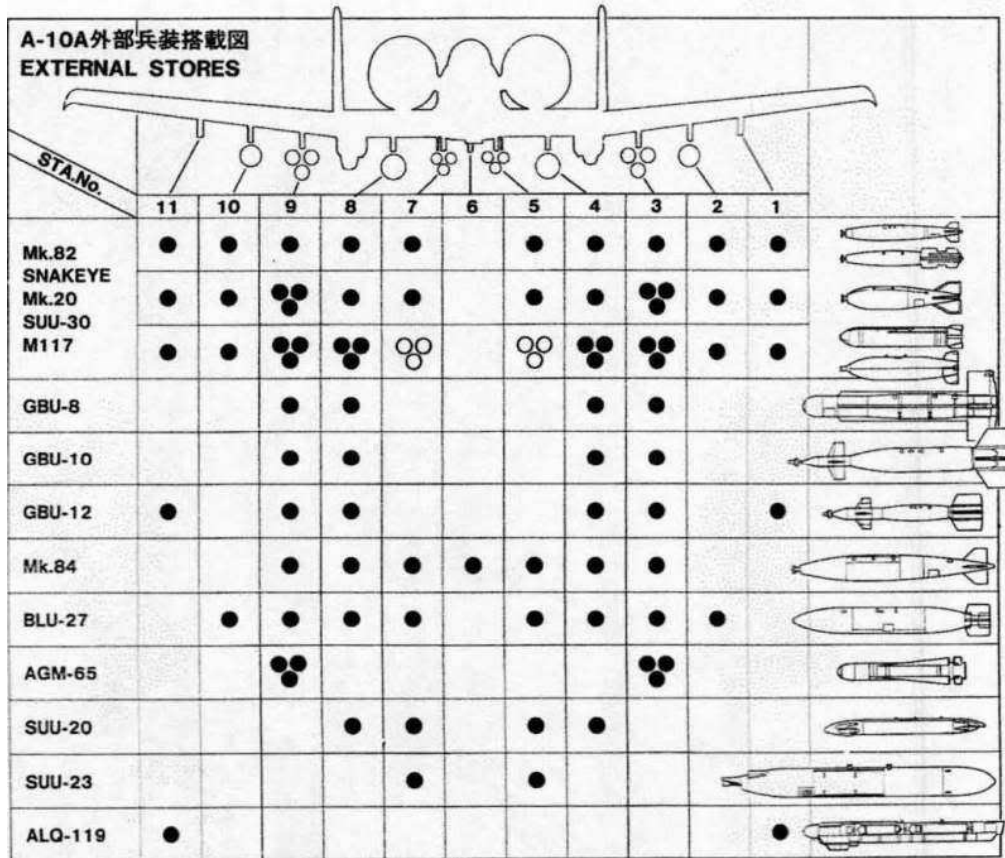
Figure A.1 – Loadout configure example [57]

Appendix B – RDSWin Analysis

B.1 RDSWin – Anti-Personnel Mission Analysis

The following is the text file export from RDSWin assuming an Anti-Personnel Mission.

```
-------------------------------------------------------------------------------

MISSION SIZING OR RANGE

 Seg.  4  CRUISE :     350.0   kts at    30000.0   ft        RANGE =    500.0    nmi

 Seg.  5  LOITER :     300.0   kts at    10000.0   ft     ENDURANCE =     0.50   hrs

-------------------------------------------------------------------------------

       TOTAL RANGE =    500.0        TOTAL LOITER TIME =     0.50

       FUEL WEIGHT =   3326.6          EMPTY WEIGHT =   19581.8

    USEFUL LOAD  (-Wf)=   9360.0      AIRCRAFT GROSS WEIGHT =   32268.5

-------------------------------------------------------------------------------
```

```
                AIRCRAFT DATA FILE :    YA-94_052022_AntiPerson.rdsdat

                  MISSION FILE :    YA-94_052022_AntiPerson.rdsdms

                      UNITS :    FPS

             Using ICAO Standard Atmosphere

          Empty Weight Sizing Coefficient C = -.13

       Service Ceiling defined by Rate Of Climb =  300     fpm

   Number of Steps for Cruise, Loiter, and Climb =  1

               Sizing Sensitivity = 0.0001

             Max # Sizing Iterations = 100

                Max Descent Angle = -30

           Maximum Landing Approach Angle = -3

   Optimal Climb Speed is used between input start & end speeds

        Sizing Calculation with 'Rubber' Engine
```

```
-------------------------------------------------------------------------------

Segment #1    TAKEOFF

-------------------------------------------------------------------------------
```

Altitude =   0.0

 Current Wt =   50000   W/S = 90.   T/W = 0.035

     C = 0.5565   Time = 0.233

MISSION SEGMENT WEIGHT FRACTION = 0.9955

Segment #2   TAKEOFF

 Altitude =   0.0

 Current Wt =   49773   W/S = 89.592   T/W = 0.3516

     C = 0.371   Time = 0.0167

MISSION SEGMENT WEIGHT FRACTION = 0.9978

Segment #3   CLIMB/ACCEL

 (Calculated at averaged altitude & acceleration-biased speed: V=.293*Vstart+.707*Vend)

 Start Alt =   0.0   End Alt =   30000

 Start VEL =   150.   End Vel =   350.

 Start Mach = 0.2269   End Mach = 0.5943

 Current Wt =   49665   W/S = 89.396   T/W = 0.3524

     CL = 0.4935   CD0 = 0.0172   K = 0.0663

     L/D = 14.789   C = 0.371

     Ps = 8408.5   fpm

 TIME TO CLIMB   =   4.095   min

 DISTANCE TRAVELED =   19.901   nmi

MISSION SEGMENT WEIGHT FRACTION = 0.9911

142

Segment #4   CRUISE

RANGE =   500.   CLIMB/DESCENT RANGE CREDIT =   19.901

Altitude =   30000   ft

Cruise Vel =   350.   kts

Mach =   0.5943

Current Wt =   49224   W/S = 88.602

T/W =   0.3377   (available)

T/W =   0.068   (required)

THRUST SETTING USED = 19.1   % of Dry (Continuous) Power

CL =   0.5702   CD0 =   0.0172   K =   0.0663

L/D =   14.703   CLmax =   2.   (usable)

C =   0.5565

SEGMENT CRUISE TIME =   82.244   min

SEGMENT CRUISE DISTANCE =   480.1   nmi

SPECIFIC RANGE (nmi/lb) =   0.188

MISSION SEGMENT WEIGHT FRACTION = 0.9494

Segment #5   LOITER

Loiter Time =   0.5

Altitude =   10000   ft

Loiter Vel =   300.   kts

Mach =   0.4703

Current Wt =   46735   W/S = 84.123   T/W =   0.3745   (available)

T/W =   0.0709   (required)

THRUST SETTING USED = 18.9   %

CL =   0.3733   CD0 =   0.0172   K =   0.0663

L/D = 14.108   CLmax = 2.   (usable)

  C = 0.5565

    SPECIFIC LOITER (sec/lb) = 1.953

MISSION SEGMENT WEIGHT FRACTION = 0.9805

Segment #6   DESCENT

 Current Wt =   45822   W/S = 82.48

  DISTANCE TRAVELED = 0.0

MISSION SEGMENT WEIGHT FRACTION = 0.9900

Segment #7   LANDING

 Current Wt =   45364   W/S = 81.655

MISSION SEGMENT WEIGHT FRACTION = 0.9950

RESERVE & TRAPPED FUEL ALLOWANCE=   1.06

   Sizing Iterations   Useful Load (less Wf)=9360

Iteration #	W0guess	We	Wfuel	W0calculated
1	50000.0	28662.9	5154.6	43177.5
2	44883.1	26093.3	4627.1	40080.4
3	32715.7	19817.7	3372.7	32550.5
4	32282.2	19589.1	3328.1	32277.1
5	32268.5	19581.8	3326.6	32268.5

RDS SIZING RESULTS   FPS

   AIRCRAFT DATA FILE: YA-94_052022_AntiPerson.rdsdat

      MISSION FILE: YA-94_052022_AntiPerson.rdsdms

         T/W = 0.350

         Thrust =   11294.0

         W/S = 90.00

      Wing Area =   358.5

      Wo as-drawn =   50000.0 lbs-m

   Sizing Calculation with 'Rubber' Engine

MISSION SEGMENT	MISSION SEGMENT WEIGHT FRACTION OR DROPPED WEIGHT	Wi/WO	FUEL BURN -SEGMENT (lbs-m)	FUEL BURN -TOTAL 32268.5	AIRCRAFT WEIGHT (end of Seg)
1 TAKEOFF SEGMENT	0.9955	0.9955	146.4	146.4	32122.0
2 TAKEOFF SEGMENT	0.9978	0.9933	70.0	216.4	32052.1
3 CLIMB and/or ACCEL.	0.9911	0.9845	284.7	501.1	31767.4
4 CRUISE SEGMENT	0.9494	0.9347	1606.1	2107.2	30161.3
5 LOITER SEGMENT	0.9805	0.9164	589.0	2696.2	29572.2
6 DESCENT SEGMENT	0.9900	0.9073	295.7	2992.0	29276.5
7 LANDING SEGMENT	0.9950	0.9027	146.4	3138.3	29130.1

                     Reserve & trap = 188.3

                     Total fuel = 3326.6

 Seg. 4 CRUISE :   350.0   kts at   30000.0   ft   RANGE =   500.0   nmi

 Seg. 5 LOITER :   300.0   kts at   10000.0   ft   ENDURANCE =   0.50   hrs

 (Ranges are reduced during analysis for climb/descent range credit)

       TOTAL RANGE =   500.0   TOTAL LOITER TIME =   0.50

FUEL WEIGHT =   3326.6   EMPTY WEIGHT =   19581.8

USEFUL LOAD (-Wf)=   9360.0   AIRCRAFT GROSS WEIGHT =   32268.5

------------------- RDS-Student Version win10.5a --------------------

B.2 RDSWin – Anti-Armor Mission Analysis

The following is the text file export from RDSWin assuming an Anti-Armor (Critical) Mission.

```
----------------------------------------------------------------------------------------
MISSION SIZING OR RANGE
 Seg.  4  CRUISE :      350.0   kts at     30000.0   ft         RANGE =     500.0    nmi
 Seg.  5  LOITER :      300.0   kts at     10000.0   ft      ENDURANCE =     0.50    hrs
----------------------------------------------------------------------------------------
          TOTAL RANGE =     500.0          TOTAL LOITER TIME =      0.50
          FUEL WEIGHT =    5226.5           EMPTY WEIGHT =   29010.2
       USEFUL LOAD  (-Wf)=   16460.0       AIRCRAFT GROSS WEIGHT =   50696.7
----------------------------------------------------------------------------------------


                       AIRCRAFT DATA FILE :    YA-94_052022_AntiPerson.rdsdat
                          MISSION FILE :    YA-94_052022_AntiPerson.rdsdms
                             UNITS :    FPS
              Using ICAO Standard Atmosphere
            Empty Weight Sizing Coefficient C = -.13
         Service Ceiling defined by Rate Of Climb =  300     fpm
     Number of Steps for Cruise, Loiter, and Climb =  1
                   Sizing Sensitivity = 0.0001
                  Max # Sizing Iterations = 100
                    Max Descent Angle = -30
                 Maximum Landing Approach Angle = -3
      Optimal Climb Speed is used between input start & end speeds
            Sizing Calculation with 'Rubber' Engine


----------------------------------------------------------------------------------------
Segment #1    TAKEOFF
----------------------------------------------------------------------------------------
  Altitude =   0.0
 Current Wt =   50000          W/S =  90.          T/W =  0.035
      C =  0.5565        Time =  0.233
MISSION SEGMENT WEIGHT FRACTION = 0.9955




----------------------------------------------------------------------------------------
Segment #2    TAKEOFF
----------------------------------------------------------------------------------------
  Altitude =   0.0
 Current Wt =   49773          W/S =  89.592         T/W =  0.3516
      C =  0.371        Time =  0.0167
MISSION SEGMENT WEIGHT FRACTION = 0.9978




----------------------------------------------------------------------------------------
Segment #3    CLIMB/ACCEL
----------------------------------------------------------------------------------------
```

(Calculated at averaged altitude & acceleration-biased speed: V=.293*Vstart+.707*Vend)

 Start Alt = 0.0   End Alt =   30000

 Start VEL = 150.   End Vel =   350.

 Start Mach = 0.2269   End Mach = 0.5943

 Current Wt =   49665   W/S = 89.396   T/W = 0.3524

     CL = 0.4935   CD0 = 0.0172   K = 0.0663

     L/D = 14.789   C = 0.371

     Ps = 8408.5   fpm

 TIME TO CLIMB   =   4.095   min

 DISTANCE TRAVELED = 19.901   nmi

MISSION SEGMENT WEIGHT FRACTION = 0.9911

Segment #4   CRUISE

     RANGE =   500.   CLIMB/DESCENT RANGE CREDIT =   19.901

  Altitude =   30000   ft

 Cruise Vel = 350.   kts

     Mach = 0.5943

 Current Wt =   49224   W/S = 88.602

     T/W = 0.3377   (available)

     T/W = 0.068   (required)

 THRUST SETTING USED = 19.1   % of Dry (Continuous) Power

     CL = 0.5702   CD0 = 0.0172   K = 0.0663

     L/D = 14.703   CLmax = 2.   (usable)

      C = 0.5565

         SEGMENT CRUISE TIME =   82.244   min

       SEGMENT CRUISE DISTANCE =   480.1   nmi

       SPECIFIC RANGE (nmi/lb) =   0.188

MISSION SEGMENT WEIGHT FRACTION = 0.9494

Segment #5   LOITER

Loiter Time =   0.5

  Altitude =   10000   ft

 Loiter Vel = 300.   kts

     Mach = 0.4703

 Current Wt =   46735   W/S = 84.123   T/W = 0.3745   (available)

     T/W = 0.0709   (required)

 THRUST SETTING USED = 18.9   %

     CL = 0.3733   CD0 = 0.0172   K = 0.0663

     L/D = 14.108   CLmax = 2.   (usable)

      C = 0.5565

       SPECIFIC LOITER (sec/lb) =   1.953

MISSION SEGMENT WEIGHT FRACTION = 0.9805

Segment #6   DESCENT

 Current Wt =   45822   W/S = 82.48
  DISTANCE TRAVELED =   0.0
MISSION SEGMENT WEIGHT FRACTION = 0.9900

Segment #7   LANDING

 Current Wt =   45364   W/S = 81.655
MISSION SEGMENT WEIGHT FRACTION = 0.9950

RESERVE & TRAPPED FUEL ALLOWANCE=   1.06

   Sizing Iterations   Useful Load (less Wf)=16460
 Iteration #   W0guess   We   Wfuel   W0calculated
     1   50000.0   28662.9   5154.6   50277.5
     2   50208.1   28766.7   5176.1   50402.7
     3   50696.7   29010.1   5226.5   50696.5

RDS SIZING RESULTS   FPS
  AIRCRAFT DATA FILE: YA-94_052022_AntiPerson.rdsdat
     MISSION FILE: YA-94_052022_AntiPerson.rdsdms
          T/W = 0.350
        Thrust = 17743.8
          W/S = 90.00
       Wing Area =   563.3
      Wo as-drawn = 50000.0 lbs-m
 Sizing Calculation with 'Rubber' Engine

   MISSION SEGMENT   MISSION SEGMENT   Wi/WO   FUEL BURN   FUEL BURN   AIRCRAFT WEIGHT
                        WEIGHT FRACTION   -SEGMENT   -TOTAL   (end of Seg)
                        OR DROPPED WEIGHT   (lbs-m)   50696.5
----
 1 TAKEOFF SEGMENT   0.9955   0.9955   230.1   230.1   50466.4
 2 TAKEOFF SEGMENT   0.9978   0.9933   109.9   340.0   50356.5
 3 CLIMB and/or ACCEL.   0.9911   0.9845   447.3   787.3   49909.3
 4 CRUISE SEGMENT   0.9494   0.9347   2523.3   3310.6   47385.9
 5 LOITER SEGMENT   0.9805   0.9164   925.4   4236.0   46460.5
 6 DESCENT SEGMENT   0.9900   0.9073   464.6   4700.6   45995.9
 7 LANDING SEGMENT   0.9950   0.9027   230.0   4930.6   45765.9
                          Reserve & trap =   295.8
                          Total fuel = 5226.4

 Seg. 4 CRUISE :   350.0   kts at   30000.0   ft   RANGE =   500.0   nmi

Seg. 5 LOITER :   300.0   kts at   10000.0   ft   ENDURANCE =   0.50   hrs
(Ranges are reduced during analysis for climb/descent range credit)

         TOTAL RANGE =   500.0   TOTAL LOITER TIME =   0.50
         FUEL WEIGHT =   5226.5   EMPTY WEIGHT =   29010.2
    USEFUL LOAD (-Wf)=   16460.0   AIRCRAFT GROSS WEIGHT =   50696.7

------------------- RDS-Student Version win10.5a -------------------

Appendix C – Weight Analysis Predictions

C.1   MATLAB – Mission Analysis Sample

The following is the MATLAB script sample using Roskam's method assuming an Anti-Personnel Mission.

Contents

```
clear
clc
```

Header--

```
Title: Conceptual Approach to Designing a New Attack Aircraft.

Date: May 2022

Graduate Student: Alexander H. Nuyn
Faculty Advisor: Professor Sean Montgomery

This project is in partial fulfillment of the requirments for the
degree Master of Science in Aerospace Engineering at San Jose State
University.

Purpose:    The following code calculates the empty, takeoff, and fuel
            weights of the conceptual YA-94 aircraft using similar
            methods derived by Roskam, "Part I: Preliminary Sizing of
            Aircraft" for fighter aircraft. This includes weight
            estimates during payload drop and ammo dispensation.
--------------------------------------------------------------------------
```

Known Values

Non-expandable payload weight W_pods = 2 * 205; % lbs, weight of 2 rocket pods

```
W_pods = 0; % lbs, not used during Anti-Armor missions
W_crew = 2 * 200; %lbs, 2 pilots
W_ECM = 540; % lbs

% Total expendable weapon weight
W_ammo = 3400; % lbs, Gun ammo weight

W_DT = 2 * 3880; % lbs, 2x drop tanks
W_bomb = 2 * 500; % lbs, 2x MK82 bombs
W_AGM = 2 * 1850; % lbs, 2x AGM racks
W_rocket = 13.6 * 19 * 2; % lbs | 2x pods, 19x rockets
W_cluster = 1000; % lbs, Cluster bombs
W_PW = 250; % lbs, Paveway laser-guided
W_flare = 116 * 2; % lbs, 2x flare set

% Total paload weight for Anti-Personnel mission, lbs
W_ext = W_rocket + W_cluster + W_PW + W_flare;

% Average paload weight for Anti-armor mission, lbs
% W_ext = W_DT + W_bomb + W_AGM + W_PW + W_flare + W_rocket;
```

Initial takeoff guess weight

```
W_TO = 50000; % lbs
diff = 1;
i = 0;
```

While loop to self iterate weights

Loop checks difference percentage if greater than .5% difference

```
while diff > .5
```

Empty Weight Fraction

```
A = 2.34;              % Table 3.1, Raymer
C = -0.13;             % Table 3.1, Raymer
K = 1;                 % Variable Sweep = 1.04, Fixed Sweep = 1.00
We_W0 = A * W_TO^C * K;
```

Phase 1 to 3 - Start-up and Takeoff

```
W3_WTO = .970; % Engine Start-up and Warm Up fraction
```

Phase 4 - Climb

```
W4_W3 = .985; % Climb fraction
```

Phase 5 - Cruise out

```
    R_cruise = 150;          % nmi, cruise range
    V_cruise = 350;          % kts, cruise speed
    SFC = 0.371;             % 1/hr, Specific Fuel Consumption
    LD_co = 15*.866;         % Lift-to-drag ratio, cruise

    % Cruise out weight fraction
    W5_W4 = exp(-R_cruise*SFC / (V_cruise*LD_co));
```

Phase 6 - Loiter

```
    LD_loiter = 15;      % Lift-to-drag ratio, loiter
    E = 0.5;             % hour, endurance time

    % Loiter weight fraction
    W6_W5 = exp(-E * SFC / LD_loiter);
```

Phase 7 - Combat Descent

Descent weight fraction

```
    W7_W6 = .990;
```

Phase 8 - Dash-out

```
    LD_do = 15;          % Lift-to-drag ratio, dash-out
    R_do = 100;          % nmi, dash-out range
    V_do = 300;          % knots, dash-out velocity
    SFC_do = 0.371;      % 1/hr, Specific Fuel Consumption during dash-out

    % Dash-out weight fraction
    W8_W7 = exp(-R_do*SFC_do / (V_do*LD_do));
```

Phase 9 - Drop payload

Payload drop weight fraction

```
    W9_W8 = 1.0;
```

Phase 10 - Strafe

```
    E_strafe = 5/60;     % hour; stafe time
    SFC_strafe = 0.371;  % 1/hr, Specific Fuel Consumption during strafe run
    LD_strafe = 10;      % Lift-to-drag ration during strafe run

    % Strafe weight fraction, non-corrected
    W10_W9_nc = exp(-E_strafe*SFC_strafe / LD_strafe);

    % Weight fraction so far from start-up to drop
    M_ff = W3_WTO * W4_W3 * W5_W4 * W6_W5 * W7_W6 * W8_W7 * W9_W8;

    W_ff = W_TO * (1-(1-M_ff)); % lbs, weight of aircraft PRIOR bomb-drop
    W_drop = W_ff - W_ext;      % lbs, weight of aircraft AFTER bomb drop
```

```
    % payload drop weight fraction
    W_correct = W_drop / W_ff;

    % Strafe weight fraction, corrected
    W10_W9 = (1 - (1 - W10_W9_nc) * W_correct);
```

Phase 11 - Dash-in

```
    LD_di = LD_do;  % lift-to-drag ratio, dash-in
    SFC_di = 0.371; % 1/hr, SFC dash-in
    R_di = 100;     % nmi, dash-in range
    V_di = 300;     % knots, dash-in velocity

    % Dash-in weight fraction, non-corrected
    W11_W10_nc = exp(-R_di*SFC_di / (V_di*LD_di));

    % Weight of aircraft AFTER strafe run due to fuel consumption, lbs
    W_strafe = W_drop - (1-W10_W9_nc)*W_drop;

    % Weight of aircraft AFTER ammo consumption
    W_fire = W_strafe - W_ammo; % lbs

    % Ammo expend weight fraction
    W_ammo_correct = W_fire / W_strafe;

    % Dash-in weight fraction, corrected
    W11_W10 = (1 - (1-W11_W10_nc) * W_ammo_correct);
```

Phase 12 - Climb out

Climb out weight fraction

```
    W12_W11 = W4_W3;
```

Phase 13 - Cruise in

```
    LD_ci = 15*.866;    % lift-to-drag ratio, cruise in
    R_ci = R_cruise;    % nmi, cruise in range
    SFC_ci = SFC;       % 1/hr, cruise in SFC, similar to Phase 5
    V_ci = 350;         % knots, cruise in speed

    % Cruise in weight fraction
    W13_W12 = exp(-R_ci*SFC_ci / (V_ci*LD_ci));
```

Phase 14 - Descent

Descent weight fraction

```
    W14_W13 = .99;
```

Phase 15 - Land and Taxi

Land and taxi weight fraction

```matlab
    W15_W14 = .995;
```

Final Weights

Final fuel weight fraction

```matlab
    Wf_W0 = 1-(M_ff * W10_W9 * W11_W10 * W12_W11 * W13_W12 * W14_W13...
        * W15_W14);

    % Final Fuel Weight, lbs
    W_fuel = Wf_W0 * W_TO;

    % Final Takeoff Weight, lbs
    W_TO_final = (W_crew+W_pods+W_ammo+W_ECM+W_ext) / (1-Wf_W0-We_W0);

    % Difference between W_TO guess and calculated, percent
    diff = abs(W_TO_final - W_TO) / W_TO *100;

    % New W_TO guess, lbs
    W_TO = W_TO_final;

    % while loop itertion counter
    i = i+1;
```

```matlab
end
```

Print results

```matlab
fprintf('Fuel Weight: %.3f lbs\n\n', W_fuel)
fprintf('Takeoff Weight: %.3f lbs\n\n', W_TO_final)
fprintf('Empty Weight: %.3f lbs\n\n', We_W0*W_TO)
fprintf('Takeoff Weight Differnce: %.3f%%\n\n', diff)
fprintf('Iteration count: %0.0f\n\n', i)
```

```
Fuel Weight: 3395.316 lbs

Takeoff Weight: 25950.212 lbs

Empty Weight: 16206.236 lbs

Takeoff Weight Differnce: 0.290%

Iteration count: 6
```

Published with MATLAB® R2021a

155

C.2 Roskam – Weight Calculation Iterative Sample

The following is a step-by-step first iterative process of calculating weight fractions per Roskam's methods [38], assuming an Anti-Personnel Mission.

Initial weight guess W_0 = 50,000 lbs

Empty weight fraction estimate A = 2.34
$\qquad\qquad$ C = -0.13
$\qquad\qquad$ K = 1
$\qquad\qquad$ $W_e/W_0 = AW_0^C K = 0.5733$

Phase 1 to 3 – Startup and Takeoff W_3/W_0 = .970

Phase 4 – Climb W_4/W_3 = .985

Phase 5 – Cruise Out
$$R_{cruise\ out} = 150\ \text{nmi}$$
$$V_{cruise\ out} = 350\ \text{knots}$$
$$SFC_{cruise\ out} = 0.5/\text{hr}$$
$$L/D_{cruise\ out} = 10 * .866 = 8.66$$
$$W_5/W_4 = e^{-\frac{R*SFC}{V*L/D}} = .9756$$

Phase 6 – Loiter
$$E = 0.5\ \text{hour}$$
$$L/D_{loiter} = 10$$
$$W_6/W_5 = e^{\frac{-E*SFC}{L/D}} = .9753$$

Phase 7 – Combat Descent W_7/W_6 = .9900

Phase 8 – Dash-out
$$R_{dash-out} = 100\ \text{nmi}$$
$$V_{dash-out} = 300\ \text{knots}$$
$$SFC_{dash-out} = 0.5/\text{hr}$$
$$L/D_{dash-out} = 10$$

$$W_8/W_7 = e^{-\frac{R*SFC}{V*L/D}} = .9835$$

Phase 9 – Drop Payload W_9/W_8 = 1.00

Phase 10 – Strafe

$$E_{strafe} = 5/60 \text{ hour}$$
$$SFC_{strafe} = 0.5/hr$$
$$L/D_{strafe} = 10$$

$$W_{10}/W_9 = e^{\frac{-E*SFC}{L/D}} = .9958$$

$$M_{ff} = \frac{W_3 W_4 W_5 W_6 W_7 W_8 W_9}{W_0 W_3 W_4 W_5 W_6 W_7 W_8} = .8851$$

$$W_{ff} = W_0 * \left(1 - \left(1 - M_{ff}\right)\right) = 44256 \; lbs$$

$$W_{drop} = W_{ff} - W_{ext} = 40021 \; lbs$$

$$W_{correct} = W_{drop}/W_{ff} = .9043$$

$$(W_{10}/W_9)_{corrected} = 1 - (1 - W_{10}/W_9) * W_{correct} = .9962$$

Phase 11 – Dash-in

$$R_{dash-in} = 100 \text{ nmi}$$
$$V_{dash-in} = 300 \text{ knots}$$
$$SFC_{dash-in} = 0.5/hr$$
$$L/D_{dash-in} = 10$$
$$W_{11}/W_{10} = e^{\frac{-E*SFC}{L/D}} = .9835$$

$$W_{strafe} = W_{drop} - (1 - W_{10}/W_9) * W_{drop}$$
$$= 39855 \; lbs$$

$$W_{fire} = W_{strafe} - W_{ammo} = 36455 \; lbs$$

$$W_{ammo,corrected} = W_{fire}/W_{strafe} = .9147$$

$$(W_{11}/W_{10})_{corrected} = 1 - \left(1 - \frac{W_{11}}{W_{10}}\right) * W_{ammo,correct} = .9849$$

Phase 12 – Climb Out

$$W_{12}/W_{11} = .9850$$

Phase 13 – Cruise In

$$R_{cruise\;in} = 150 \text{ nmi}$$
$$V_{cruise\;in} = 350 \text{ knots}$$
$$SFC_{cruise\;in} = 0.5/hr$$
$$L/D_{cruise\;in} = 10 * .866 = 8.66$$
$$W_{13}/W_{12} = e^{\frac{-E*SFC}{L/D}} = .9756$$

Phase 14 – Descent

$$W_{14}/W_{13} = .990$$

Phase 15 – Land and Taxi $\qquad$ $W_{15}/W_{14} = .995$

Final fuel weight fraction $\qquad$ $W_f/W_0 = 1 - M_{ff} * \dfrac{W_{10}W_{11}W_{12}W_{13}W_{14}W_{15}}{W_9W_{10}W_{11}W_{12}W_{13}W_{14}}$
$$= .1780$$

Final fuel weight $\qquad$ $W_{fuel} = W_f/W_0 * W_0 = 8897.6 \; lbs$

Final takeoff weight $\qquad$ $W_{0,final} = \dfrac{W_{crew} + W_{pods} + W_{ammo} + W_{ext}}{1 - \dfrac{W_f}{W_0} - \dfrac{W_e}{W_0}}$
$$= 33943 \; lbs$$

Final empty weight $\qquad$ $W_{empty} = \dfrac{W_e}{W_0} * W_0 = 28665 \; lbs$

Difference between guess and calculated $\qquad$ $\% \; diff = \dfrac{|W_{0,final} - W_0|}{W_0} * 100\% = 32.11\%$

With a 32% difference between the calculated and guess value, the process requires iteration until a difference of no more than 0.5% is accomplished. The calculated final takeoff weight would be designated as the next guess takeoff weight in the next iteration.

Appendix D – MATLAB Code: Wing-Loading and Thrust-to-Weight Ratio Relations

Contents

```
close all
clear
clc
```

Header---

```
Title: Conceptual Approach to Designing a New Attack Aircraft.


Date: May 2022


Graduate Student: Alexander H. Nuyn
Faculty Advisor: Professor Sean Montgomery


This project is in partial fulfillment of the requirments for the
degree Master of Science in Aerospace Engineering at San Jose State
University.


Purpose:     The following code calculates the optimal performance
             parameters for the YA-94. This includes the thrust-to-
             weight ratio, wing loading, takeoff conditions, stall
             speed, landing distance, turning rates, and etc.
-------------------------------------------------------------------------
```

Known Values

```
% Typical thrust-to-weight ratio for jet fighter, Raymer: Table 5.1
W0 = 50000;      % lbs, Max Takeoff Weight
W0_d = 32600;    % lbs, Design Takeoff Weight, w/o armament
W_f = 8600;      % lbs, total fuel weight
W_ext = 17000;   % lbs, external weapons weight
W_gun = 3110;    % lbs, ammo weight

M = 0.6;         % Max Mach speed
v_cruise = 590;  % ft/s, cruise speed @ 350 knots
v_stall = 210;   % ft/s, stall speed @ 120 knots

p_SL = 0.00238;  % slugs/ft3, density of air at SL
p_MT = 0.00189;  % slugs/ft3, density of air at 5000ft, hot day
```

159

```matlab
a = 0.244;            % Raymer, Table 5.3
C = 0.341;            % Raymer, Table 5.3
TW_est = a * M^C;     % Estimated T/W

g = 32.2;             % ft/s2, gravity acceleration

fprintf('Estimated Thrust-to-Weight per Max Mach: %.3f \n', TW_est)
fprintf('\n')
```

```
Estimated Thrust-to-Weight per Max Mach: 0.205
```

Stall Speed

```matlab
% From Roskam: Table 3.1
CL_max_FU = 1.6;      % Coeff of Lift @ Flaps Up,
CL_max_FLT = 1.5;     % Coeff of Lift @ Flaps Down, Takeoff
CL_max_FLL = 1.7;     % Coeff of Lift @ Flaps Down, Land

% Wing Loading with Flaps Up (lbs/ft2)
WS_FU_stall = 0.5 * p_SL * v_stall^2 * CL_max_FU;
fprintf('Wing-loading at CLmax 1.6: %.3f lbs/ft2\n', WS_FU_stall)

% Wing Loading with Flaps Down, Takeoff (lbs/ft2)
WS_FD_stall_TO = 0.5 * p_SL * v_stall^2 * CL_max_FLT;
fprintf('Wing-loading at CLmax 1.5: %.3f lbs/ft2\n', WS_FD_stall_TO)

% Wing Loading with Flaps Down, Landing (lbs/ft2)
WS_FD_stall_L = 0.5 * p_SL * v_stall^2 * CL_max_FLL;
fprintf('Wing-loading at CLmax 1.7: %.3f lbs/ft2\n', WS_FD_stall_L)

% Max Wing Loading Takeoff (lbs/ft2)
WS_stall = [WS_FU_stall WS_FD_stall_TO WS_FD_stall_L];
fprintf('Therefore, Wing-loading must be < %.3f lbs/ft2\n', min(WS_stall))
fprintf('\n')

figure(1)
grid on
hold on
xline(WS_FU_stall, 'r-', 'LineWidth', 2)        % CL = 1.6
xline(WS_FD_stall_TO, 'g--', 'LineWidth', 2)    % CL = 1.5
xline(WS_FD_stall_L, 'b:', 'LineWidth', 2)      % CL = 1.7
hold off
legend('Clean, C_{L}=1.6', 'Clean, C_{L}=1.5', 'Clean, C_{L}=1.7')
xlabel('Wing Loading (W/S), psf')
ylabel('Thrust-to-Weight (T/W)')
title('Thust-to-Weight vs Wing-Loading, Stall')
xlim([0 105])
```

```
Wing-loading at CLmax 1.6: 83.966 lbs/ft2
Wing-loading at CLmax 1.5: 78.719 lbs/ft2
Wing-loading at CLmax 1.7: 89.214 lbs/ft2
Therefore, Wing-loading must be < 78.719 lbs/ft2
```

Thust-to-Weight vs Wing-Loading, Stall
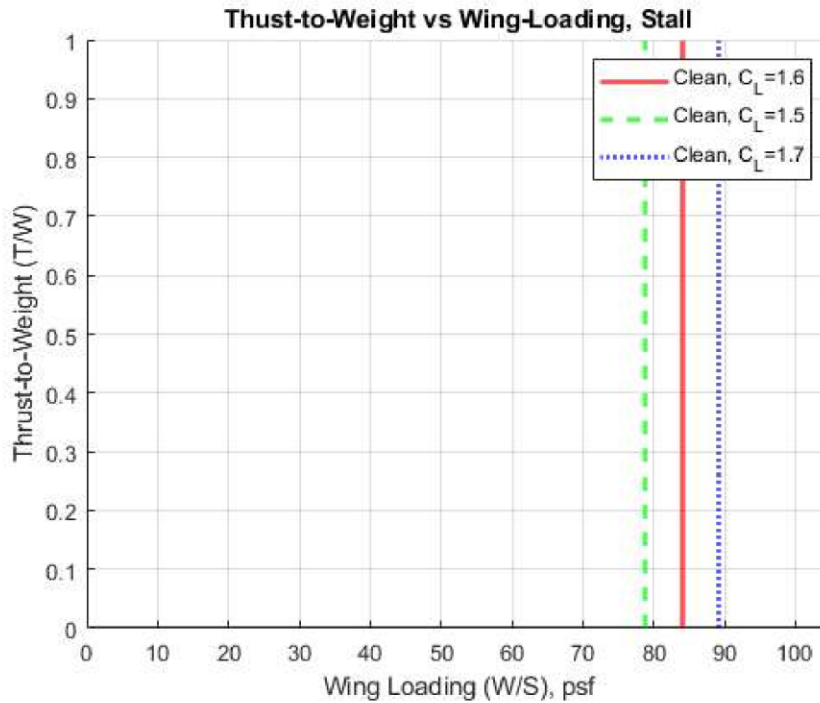
Takeoff Distance

```matlab
CL_max = [1.6 1.8 2.0]; % Max Lift Coefficient
sig = p_SL / p_SL; % air density ratio between landing and standard SL
TOP = 180; % lbs2/ft2, takeoff parameter @ 3700 ft takeoff distance

WS_TO = [10 20 40 60 80 100 120 140]; % Takeoff Wing-Loading

% Preallocation of T/W values
TW_TO = zeros(length(WS_TO), length(CL_max));

% Tabulate T/W values per W/S and CL @ Takeoff
for i_WS = 1:1:length(WS_TO)          % Wing-loading increment

    WS = WS_TO(i_WS);                             % W/S value

    for i_CL = 1:1:length(CL_max)     % Coeff of Lift increment
        CL = CL_max(i_CL);                        % Coeff. of Lift value
        TW_TO(i_WS,i_CL) = WS / (TOP * sig * CL);   % T/W value
        CL = CL_max(i_CL) + 1;
    end

    WS = WS_TO(i_WS) + 1;
end

fprintf('Tabulation of T/W variations due to W/S and CL @ takeoff:\n')
disp(TW_TO)

% Plot T/W vs W/S
figure(2)
xlim([min(WS_TO)-5 max(WS_TO)+10])
ylim([min(TW_TO(1,:))-.05 max(TW_TO(8,:))+.1])
grid on
```

161

```
hold on
plot(WS_TO , TW_TO(:,1), '-', 'LineWidth', 2)    % CL = 1.6
plot(WS_TO , TW_TO(:,2), '--', 'LineWidth', 2)   % CL = 1.8
plot(WS_TO , TW_TO(:,3), '-o', 'LineWidth', 2)   % CL = 2.0
hold off
legend('C_{L}=1.6', 'C_{L}=1.8', 'C_{L}=2.0')
xlabel('Wing Loading (W/S), psf')
ylabel('Thrust-to-Weight (T/W)')
title('Thust-to-Weight vs Wing-Loading, Takeoff')

fprintf('\n')
```

```
Tabulation of T/W variations due to W/S and CL @ takeoff:
    0.0347    0.0309    0.0278
    0.0694    0.0617    0.0556
    0.1389    0.1235    0.1111
    0.2083    0.1852    0.1667
    0.2778    0.2469    0.2222
    0.3472    0.3086    0.2778
    0.4167    0.3704    0.3333
    0.4861    0.4321    0.3889
```
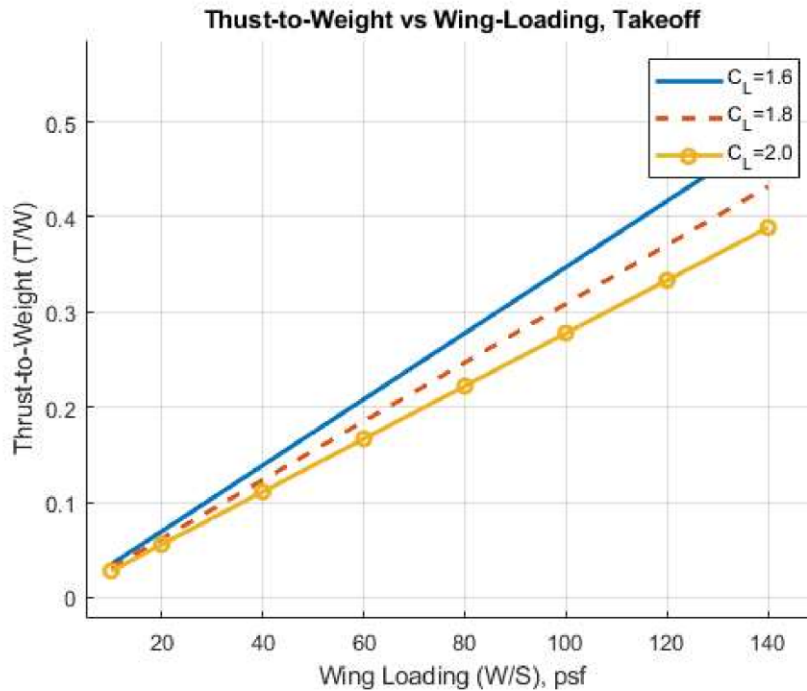

Landing Distance

```
W_land = W0 - W_ext - 0.75*W_gun - 0.50*W_f;  % lbs, Landing Weight

% Wing Loading at Landing (lbs/ft2)
WS_land = (v_stall^2 .* p_MT .* CL_max .* 0.5) .* W0/W_land;
```

162

```matlab
% Landing Distance
WS_stall = 90;
S_a = 450; % ft, obstacle-clearance distance, Raymer, Eq 5.11
S_land = (80 * (min(WS_stall)*W_land/W0) * 1./(sig .* CL_max)) + S_a;

fprintf('W/S variations due to vary CL @ landing:\n')
disp(WS_land)
fprintf('Minimum Landing Distance @ CL 1.6: %.3f ft\n', S_land(1))
fprintf('Minimum Landing Distance @ CL 1.8: %.3f ft\n', S_land(2))
fprintf('Minimum Landing Distance @ CL 2.0: %.3f ft\n', S_land(3))

figure(3)
grid on
hold on
xline(WS_land(1), '-b', 'LineWidth', 2)
xline(WS_land(2), '--r', 'LineWidth', 2)
xline(WS_land(3), ':k', 'LineWidth', 2)
hold off
legend('C_{L}=1.6', 'C_{L}=1.8', 'C_{L}=2.0')
xlabel('Wing Loading (W/S), psf')
ylabel('Thrust-to-Weight (T/W)')
title('Thust-to-Weight vs Wing-Loading, Landing')
xlim([0 230])

fprintf('\n')
```

```
W/S variations due to vary CL @ landing:
  126.4420  142.2473  158.0525

Minimum Landing Distance @ CL 1.6: 2823.075 ft
Minimum Landing Distance @ CL 1.8: 2559.400 ft
Minimum Landing Distance @ CL 2.0: 2348.460 ft
```
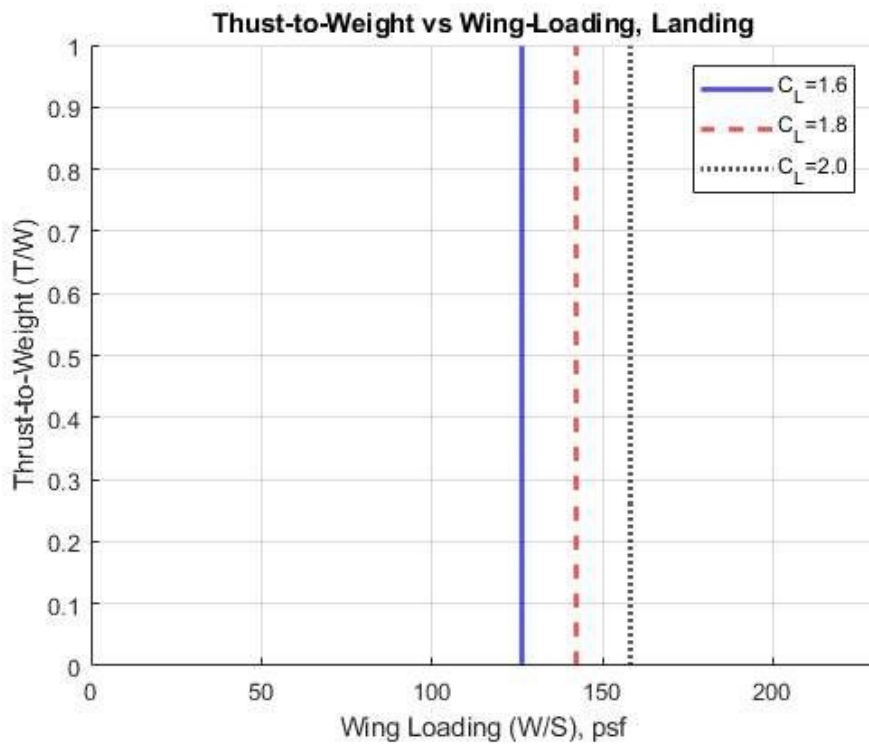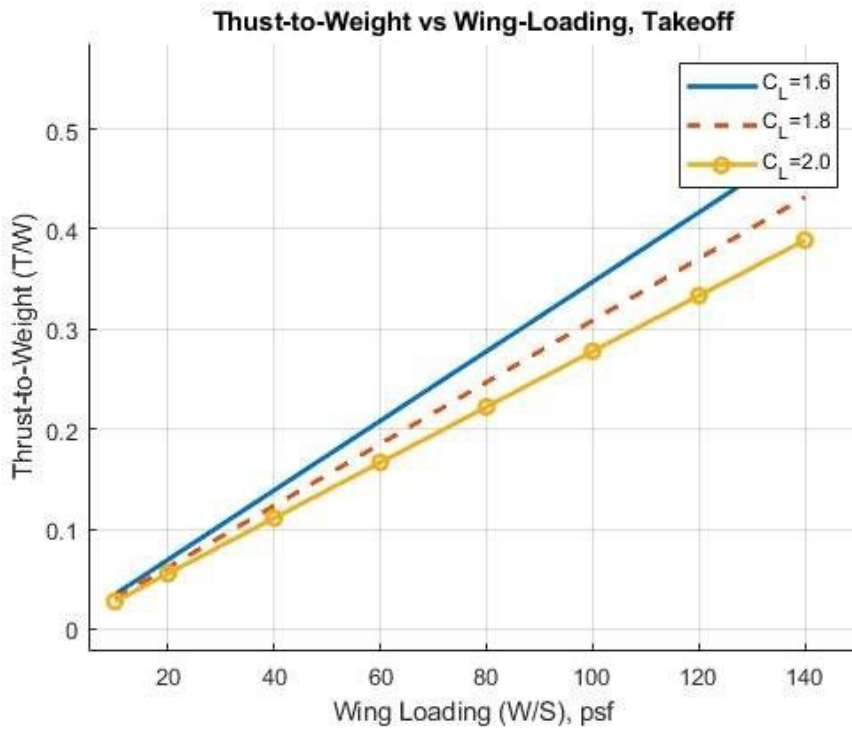
Drag Polar

```
C_D0 = 0.0148;        % Zero-lift drag coefficient
AR = 6;               % Wing Aspect Ratio
```

```matlab
% Oswald span efficiency,
e = [0.80;               % clean
     0.80*(1-.05);       % takeoff
     0.80*(1-.10)];      % landing

K = 1 ./ (pi*AR.*e);  % Constant Factor
C_L = 0:0.1:2.2;      % Coeff of Lift Range

% Coefficient of Drag
C_D = C_D0 + K .* C_L.^2;

% Maximum CL/CD
CL_CD_max_clean = max(C_L ./ C_D(1,:));
CL_CD_max_TO = max(C_L ./ C_D(2,:));
CL_CD_max_land = max(C_L ./ C_D(3,:));
CL_CD_max = [CL_CD_max_clean CL_CD_max_TO CL_CD_max_land];
fprintf('Max CL/CD @ clean = %.3f\n', CL_CD_max(1))
fprintf('Max CL/CD @ takeoff = %.3f\n', CL_CD_max(2))
fprintf('Max CL/CD @ landing= %.3f\n', CL_CD_max(3))

figure(4)
grid on
hold on
plot(C_D(1,:) , C_L , '-')
plot(C_D(2,:) , C_L , '-o')
plot(C_D(3,:) , C_L , '-.')
plot([0 C_D(1,:)] , CL_CD_max(1).*[0 C_D(1,:)], ':')
plot([0 C_D(2,:)] , CL_CD_max(2).*[0 C_D(2,:)], ':')
plot([0 C_D(3,:)] , CL_CD_max(3).*[0 C_D(3,:)], ':')
xline(min(C_D(1,:)), '--')
xline(min(C_D(2,:)), '--')
xline(min(C_D(3,:)), '--')
hold off
xlabel('C_{D}')
ylabel('C_{L}')
title('Drag Polar Plot')
legend('clean' , 'takeoff' , 'landing',...
       'Max C_{L}/C_{D}: clean' , 'Max C_{L}/C{D}: takeoff' ,...
       'Max C_{L}/C_{D}: landing' , 'Minimum Drag')

fprintf('\n')
```

```
Max CL/CD @ clean = 15.934
Max CL/CD @ takeoff = 15.503
Max CL/CD @ landing= 15.051
```

Thrust-to-Weight vs Wing-Loading, Landing

Drag Polar Plot
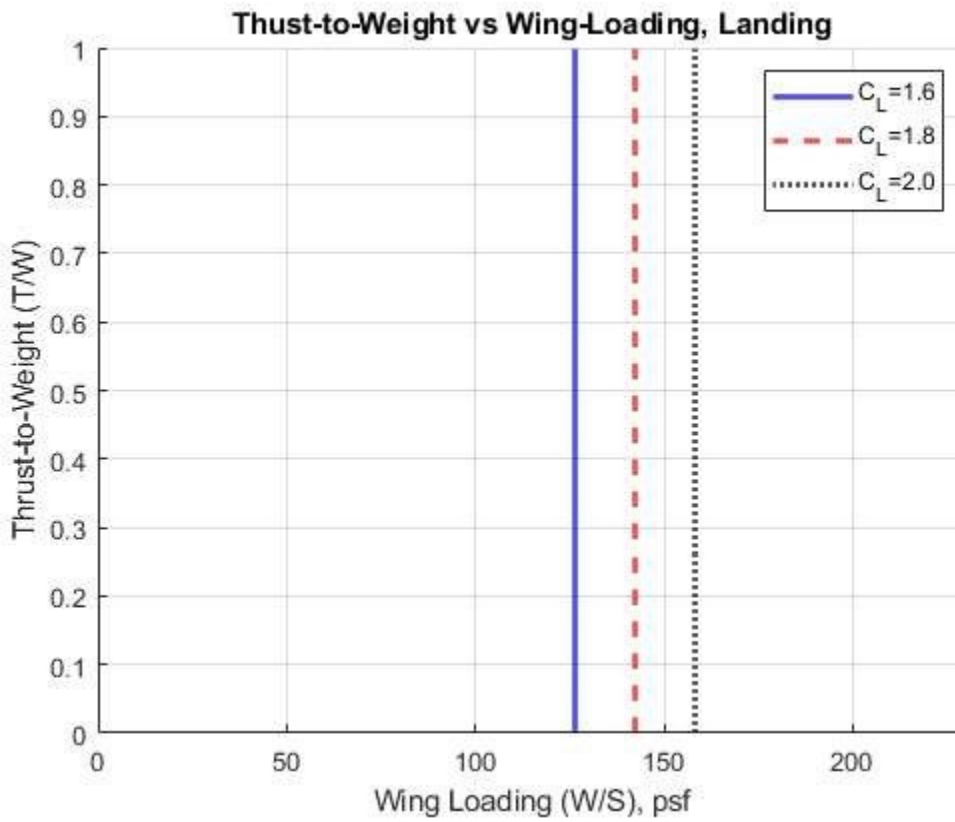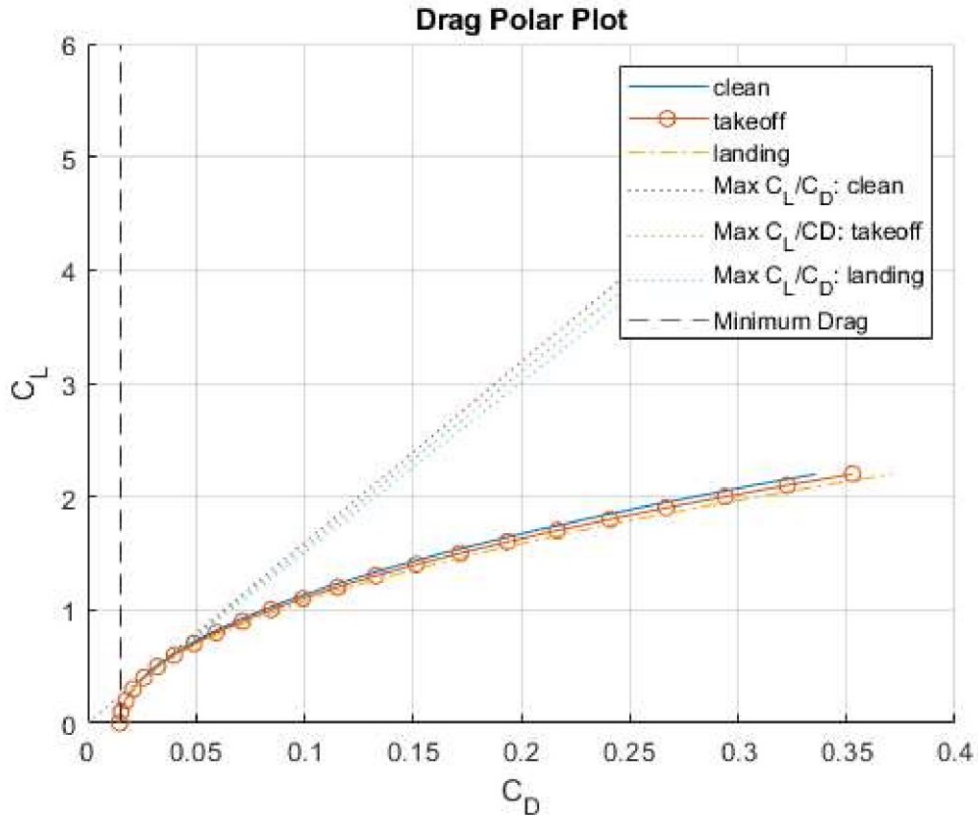
Climbing

```matlab
% Rate-of-climb velocities
RC_hor = v_stall * 1.30; % ft/s, Horizontal climb velocity
RC_vert = [4000; 5000; 6000] ./ 60; % ft/s, Vertical climb velocity

% Climb gradient
G = RC_vert ./ RC_hor;
q_climb = 0.5 * p_MT * (RC_hor)^2;        % lbs/ft-s, dynamic pressure
WS_range = (min(WS_TO):1:max(WS_TO)) .* [1;1;1];    % Wing-Loading range

% Thrust-to-Weight Ratio during Climb
TW_climb = (q_climb*C_D0 ./ WS_range + WS_range .*...
            1/(q_climb*pi*AR*e(1)))...
            + G;

figure(5)
hold on
plot(WS_range(1,:) , TW_climb(1,:) , '-', 'LineWidth', 2 ); % 5000 ft/min
plot(WS_range(1,:) , TW_climb(2,:) , '--', 'LineWidth', 2); % 6000 ft/min
plot(WS_range(1,:) , TW_climb(3,:) , '-.', 'LineWidth', 2); % 7000 ft/min
hold off
xlabel('Wing Loading (W/S), psf')
ylabel('Thrust-to-Weight (T/W)')
title('Thust-to-Weight vs Wing-Loading, Climbing')
legend('4000 ft/min' , '5000 ft/min' , '6000 ft/min')
grid on
ylim([0 .55])
```

Drag Polar Plot

Thust-to-Weight vs Wing-Loading, Climbing
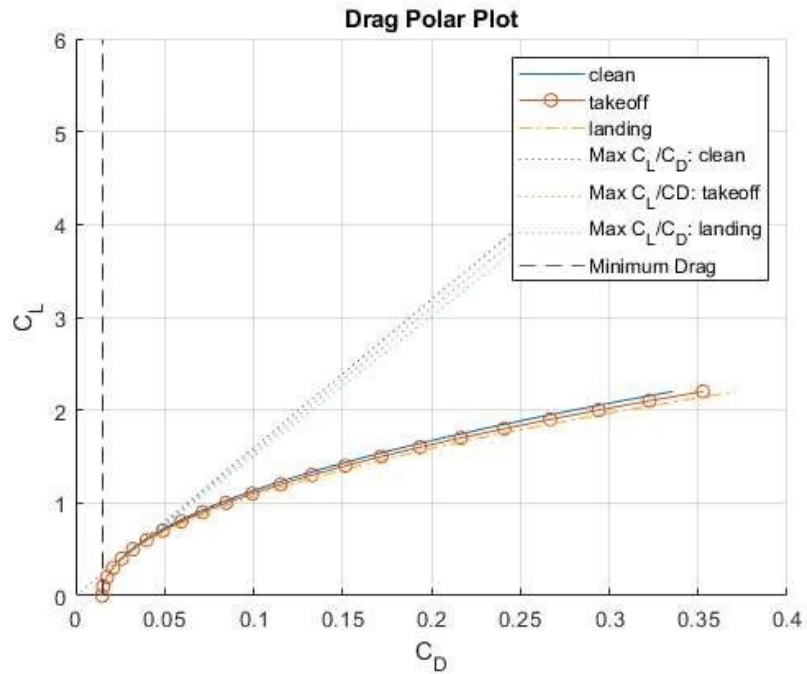
Cruising

```
p_cruise = 8.91e-4; % slugs/ft3, density of air at 30000 ft
q_cruise = 0.5 * p_cruise * v_cruise^2;
```

```
% Thurst to Weight Ratio during Cruise
TW_cruise = q_cruise*C_D0./WS_range(1,:) + ...
    WS_range(1,:)./(q_cruise*pi*AR*e(1));

figure(6)
hold on
plot(WS_range(1,:) , TW_cruise)
hold off
xlabel('Wing Loading (W/S), psf')
ylabel('Thrust-to-Weight (T/W)')
title('Thust-to-Weight vs Wing-Loading, Cruise')
grid on
ylim([0 .25])
```
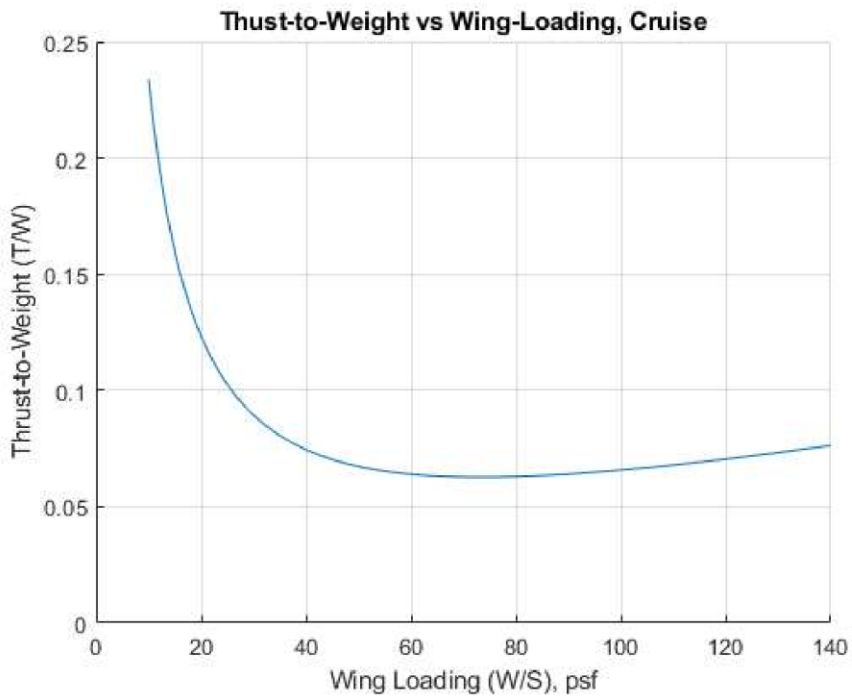

Turning

```
% g-loading
n = [2;      % sustain
     6];     % instant

% Sustained
e_sus = [e(1)*.70; e(1)*0.60; e(1)*0.50]; % Oswald Esfficieny during Turn
TW_sustain = 2*n(1) .* sqrt(C_D0 ./ (pi.*AR.*e));

% Instantaneous
W_com = W0 - W_ext;                  % lbs, Combat Weight
CL_turn = [1.5 1.6 1.7];             % Max CL during Turn
psid = 20 * pi/180;                  % rad/s, turn rate
v_turn = g*sqrt(n(2)^2-1) / psid;    % ft/s, heading velocity
q_turn = 0.5 * p_MT * v_turn^2;      % lbs/ft-s, dyanmic pressure
WS_instant = (q_turn .* CL_turn ./ n(2)) .* W0/W_com; % lbs/ft2
CL_instant = WS_instant(1)*n(2)/q_turn;
```

169

```
figure(7)
grid on
hold on
yline(TW_sustain(1) , 'r-', 'LineWidth', 2)
yline(TW_sustain(2) , 'b-', 'LineWidth', 2)
yline(TW_sustain(3) , 'g-', 'LineWidth', 2)
xline(WS_instant(1) , 'r-.', 'LineWidth', 2)
xline(WS_instant(2) , 'b-.', 'LineWidth', 2)
xline(WS_instant(3) , 'g-.', 'LineWidth', 2)
hold off
xlabel('Wing Loading (W/S), psf', 'Fontsize', 14)
ylabel('Thrust-to-Weight (T/W)', 'Fontsize', 14)
title('Thust-to-Weight vs Wing-Loading, Turning', 'Fontsize', 14)
legend('Sustain Turn @ 2-Gs, e_{70%} = 0.56',...
        'Sustain Turn @ 2-Gs, e_{60%} = 0.48',...
        'Sustain Turn @ 2-Gs, e_{50%} = 0.40',...
        'Instantaneous Turn @ 6-Gs, C_{L,max}=1.5',...
        'Instantaneous Turn @ 6-Gs, C_{L,max}=1.6',...
        'Instantaneous Turn @ 6-Gs, C_{L,max}=1.7', 'Fontsize', 14)
xlim([0 160])
ylim([0 .135])
```


170

Thust-to-Weight vs Wing-Loading, Turning

Legend:
- Sustain Turn @ 2-Gs, $e_{70\%} = 0.56$
- Sustain Turn @ 2-Gs, $e_{60\%} = 0.48$
- Sustain Turn @ 2-Gs, $e_{50\%} = 0.40$
- Instantaneous Turn @ 6-Gs, $C_{L,max} = 1.5$
- Instantaneous Turn @ 6-Gs, $C_{L,max} = 1.6$
- Instantaneous Turn @ 6-Gs, $C_{L,max} = 1.7$

X-axis: Wing Loading (W/S), psf
Y-axis: Thrust-to-Weight (T/W)
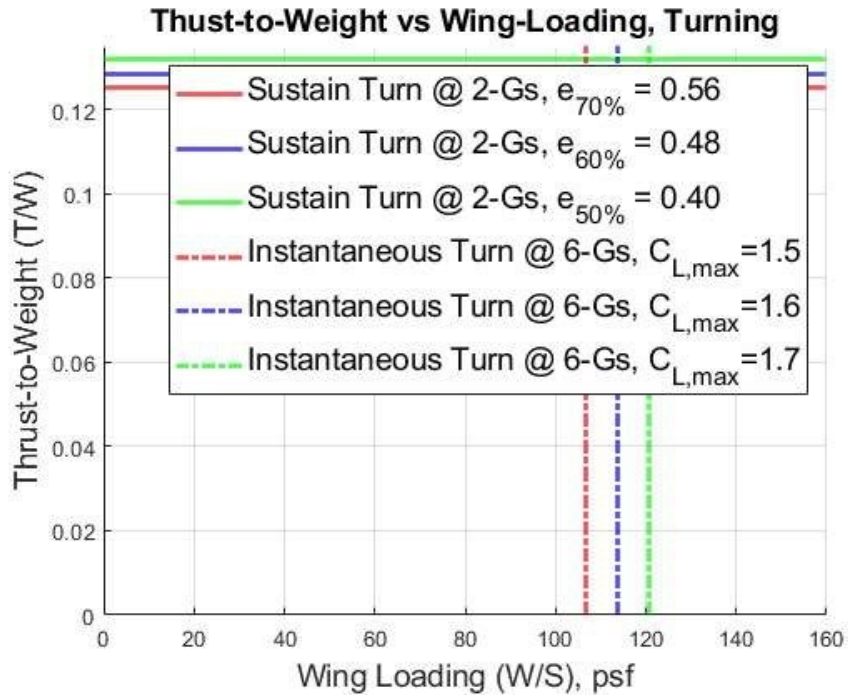
Matching Graph

```
close all
%
% figure(8)
```

```
% grid on
% hold on
%
% % Stall
% xline(min(WS_stall) , 'k')
%
% % Takeoff
% plot(WS_TO , TW_TO(:,1), 'r-+')    % CL = 1.6
% plot(WS_TO , TW_TO(:,2), 'g-x')  % CL = 1.8
% plot(WS_TO , TW_TO(:,3), 'b-o')  % CL = 2.0
%
% % Landing
% xline(WS_land(1), '--r')    % CL = 1.6
% xline(WS_land(2), '--g')    % CL = 1.8
% xline(WS_land(3), '--b')    % CL = 2.0
%
% % Climb
% plot(WS_range(1,:) , TW_climb(1,:) , 'r-*');  % 3000 ft/min
% plot(WS_range(1,:) , TW_climb(2,:) , 'g-*'); % 4000 ft/mi
% plot(WS_range(1,:) , TW_climb(3,:) , 'b-*'); % 5000 ft/mi
%
% % Cruise
% plot(WS_range(1,:) , TW_cruise , 'ro')
%
% % Turn
% yline(TW_sustain(1) , 'r-')      % Sustain, e @ 70%
% yline(TW_sustain(2) , 'b-')      % Sustain, e @ 60%
% yline(TW_sustain(3) , 'g-')      % Sustain, e @ 50%
% xline(WS_instant(1) , 'k-.')     % Instantaneous, CL = 0.6
% xline(WS_instant(2) , 'm-.')     % Instantaneous, CL = 0.7
% xline(WS_instant(3) , 'c-.')     % Instantaneous, CL = 0.8
%
% legend( 'Stall Speed, C_{L,max}=1.6',...
%          'Takeoff: C_{L,TO}=1.6', 'Takeoff: C_{L,TO}=1.8',...
%          'Takeoff: C_{L,TO}=2.0',...
%          'Landing: C_{L,L}=1.6', 'Landing: C_{L,L}=1.8',...
%          'Landing: C_{L,L}=2.0',...
%          'Climb: 3000 ft/min vertical',...
%          'Climb: 4000 ft/min vertical',...
%          'Climb: 5000 ft/min vertical',...
%          'Cruise Speed @ 350 knots',...
%          'Sustain Turn @ 2-Gs, e_{70%} = 0.56',...
%          'Sustain Turn @ 2-Gs, e_{60%} = 0.48',...
%          'Sustain Turn @ 2-Gs, e_{50%} = 0.40',...
%          'Instantaneous Turn @ 6-Gs, C_{L,max}=1.0',...
%          'Instantaneous Turn @ 6-Gs, C_{L,max}=1.2',...
%          'Instantaneous Turn @ 6-Gs, C_{L,max}=1.6')
%
% xlabel('Wing Loading (W/S), psf')
% ylabel('Thrust-to-Weight (T/W)')
% title('Thust-to-Weight vs Wing-Loading Plot')
% hold off
```

Matching Graph Simplified

```
figure(9)
grid on
hold on
```

```matlab
% Stall
xline(WS_FU_stall , 'r', 'LineWidth', 3)

% Takeoff
plot(WS_TO , TW_TO(:,2), 'g', 'LineWidth', 3)  % CL = 1.8

% Landing
xline(WS_land(3), 'b', 'LineWidth', 3)     % CL = 2.0

% Climb
plot(WS_range(1,:) , TW_climb(2,:) , 'r--', 'LineWidth', 3); % 6000 ft/min

% Cruise
plot(WS_range(1,:) , TW_cruise , 'g--', 'LineWidth', 3)

% Turn
yline(TW_sustain(3) , 'b--', 'LineWidth', 3)    % Sustain, e @ 50%
xline(WS_instant(2) , 'k--', 'LineWidth', 3)    % Instantaneous, CL = 1.6

legend( 'Stall Speed, C_{L,max}=1.6, 120 knots',...
        'Takeoff: C_{L,TO}=1.8, 3700 ft',...
        'Landing: C_{L,L}=2.0, 3000 ft',...
        'Climb: 6000 ft/min vertical',...
        'Cruise Speed @ 350 knots',...
        'Sustain Turn @ 2-Gs, e_{50%} = 0.40',...
        'Instant Turn @ 6-Gs, C_{L,max}=1.6', 'Fontsize', 12)

xlabel('Wing Loading (W/S), psf', 'Fontsize', 18)
ylabel('Thrust-to-Weight (T/W)', 'Fontsize', 18)
title('Thust-to-Weight vs Wing-Loading Plot', 'Fontsize', 18)
hold off
```
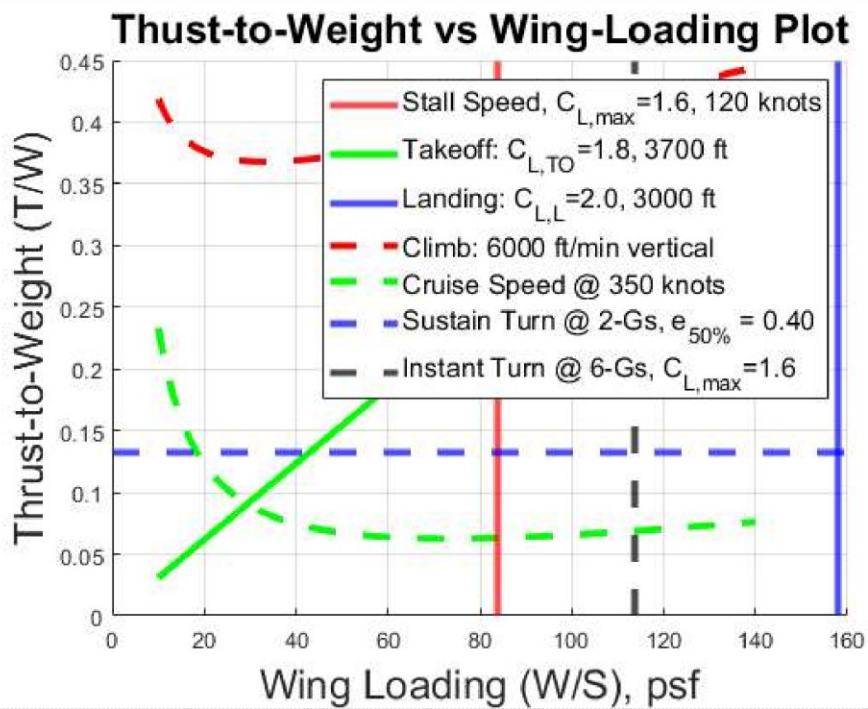
Appendix E – Weight Prediction Equations by Raymer [9]

Weight Component (lbs)	Equation
Wing	$W_{wing} = 0.0103 K_{dw} K_{vs} \left(W_{dg} N_z\right)^{0.5} S_w^{0.622} A^{0.785} (t/c)_{root}^{-0.4}$ $\times (1+\lambda)^{0.05} (cos\Lambda)^{-1.0} S_{csw}^{0.04}$
Horizontal Tail	$W_{HT} = 3.316 \left(1 + \dfrac{F_w}{B_h}\right)^{-2.0} \left(\dfrac{W_{dg} N_z}{1000}\right)^{0.260} S_{ht}^{0.806}$
Vertical Tail	$W_{VT} = 0.452 K_{rht} (1 + H_t/H_v)^{0.5} \left(W_{dg} N_z\right)^{0.488} S_{vt}^{0.718} M^{0.341}$ $\times L_t^{-1.0} (1 + S_r/S_{vt})^{0.348} A_{vt}^{0.223} \times (1+\lambda)^{0.25} (cos\Lambda_{vt})^{-0.323}$
Fuselage	$W_{fuselage} = 0.499 K_{dwf} W_{dg}^{0.35} N_z^{0.25} L^{0.5} D^{0.849} W^{0.685}$
Main Landing Gear	$W_{main\ gear} = K_{cb} K_{tpg} (W_l N_l)^{0.25} L_m^{0.973}$
Nose Landing Gear	$W_{nose\ gear} = (W_l N_l)^{0.290} L_n^{0.5} N_{nw}^{0.525}$
Engine Mounts	$W_{eng\ mount} = 0.013 N_{en}^{0.795} T^{0.579} N_z$
Firewall	$W_{firewall} = 1.13 S_{fw}$
Engine Section	$W_{eng\ section} = 0.01 W_{en}^{0.717} N_{en} N_z$
Air Induction System	$W_{air\ induct} = 13.29 K_{vg} L_d^{0.643} K_d^{0.182}$
Tailpipe	$W_{tailpipe} = 3.5 D_e L_{tp} N_{en}$
Engine Cooling	$W_{eng\ cool} = 4.55 D_e L_{sh} N_{en}$
Oil Cooling	$W_{oil\ cool} = 37.82 N_{en}^{1.023}$
Engine Controls	$W_{eng\ ctrl} = 10.5 N_{en}^{1.008} L_{ec}^{0.222}$
Starter (Pneumatic)	$W_{starter} = 0.25 T_e^{0.760} N_{en}^{0.72}$
Fuel System and Tanks	$W_{fuel\ sys} = 7.45 V_t^{0.47} \left(1 + \dfrac{V_i}{V_t}\right)^{-0.095}$ $\times \left(1 + \dfrac{V_p}{V_t}\right) N_t^{0.066} N_{en}^{0.052} \left(\dfrac{T \cdot SFC}{1000}\right)^{0.249}$
Flight Control	$W_{flight\ ctrl} = 36.28 M^{0.003} S_{cs}^{0.489} N_s^{0.484} N_c^{0.127}$
Instruments	
Hydraulics	$W_{hydraulics} = 37.23 K_{vsh} N_u^{0.664}$
Electrical	$172.2 K_{mc} R_{kva}^{0.152} N_c^{0.10} L_a^{0.10} N_{gen}^{0.091}$
Avionics	$W_{avionics} = 2.117 W_{uav}^{0.933}$
Furnishings	$W_{furnishing} = 217.6 N_c$
Air Conditioning and Anti-ice	$W_{air} = 201.6 \left[\dfrac{W_{uav} + 200 N_c}{1000}\right]^{0.735}$
Handling Gear	$W_{handling\ gear} = 3.2 \times 10^{-4} W_{dg}$

Variables	Definition	Values Used
$(t/c)_{root}$	Thick-to-chord ratio at root	0.18
A	Aspect ratio	6.00
A_{VT}	Vertical tail aspect ratio	3.44
B_h	Horizontal tail span (ft)	21.80
D	Fuselage diameter (ft)	8.00
D_e	Engine diameter (ft)	4.33
F_w	Fuselage width at HT intersection (ft)	4.17
H_t	HT height above fuselage (ft)	0.00
H_v	VT height above fuselage (ft)	12.20
K_{cb}	Cross beam constant	1.00
K_d	Duct constant	1.00
K_{dw}	Delta wing constant	1.00
K_{dwf}	Delta wing aircraft constant	1.00
K_{mc}	Mission completion required after failure constant	1.45
K_{rht}	Rolling horizontal tail constant	1.00
K_{tpg}	Tripod gear constant	0.83
K_{uht}	All-moving HT constant	1.00
K_{vg}	Variable geometry constant	1.00
K_{vs}	Variable sweep constant	1.00
K_{vsh}	Variable sweep wing constant	1
L	Fuselage length (ft)	50.00
L_a	Electrical routing distance from generators to avionics to cockpit (ft)	20.06
L_d	Duct length (ft)	0.00
L_{ec}	Routing distance from engine front to cockpit (ft)	16.48
L_m	Extended length of main gear (ft)	64.50
L_n	Extended nose gear length (ft)	96.00
L_s	Single duct length (ft)	0.00
L_{sh}	Length of engine cooling shroud (ft)	10.21
L_t	Tail length (ft)	0
L_{tp}	Length of tailpipe (ft)	5.00
M	Mach design number	0.60
N_c	Number of engines	2
N_{ci}	Number of crew equivalents	2
N_{en}	Number of engines	2
N_{gen}	Number of generators	2
N_l	Ultimate landing load factor	3.00
N_{nw}	Number of nosewheels	1.00
N_s	Number of flight control systems	2
N_t	Number of fuel tanks	4
N_u	Number of hydraulic utility function	18
N_z	Ultimate load factor	9.00

R_{kva}	System electrical rating (kVA)	135
S_{cs}	Total area of control surfaces (ft^2)	123.22
S_{csw}	Control surface area; wing mounted (ft^2)	56.53
S_{fw}	Firewall surface area (ft^2)	0.00
S_{ht}	Horizontal tail area (ft^2)	108.90
S_r	Rudder area (ft^2)	39.43
S_{vt}	Vertical tail area (ft^2)	120.60
S_w	Trapezoidal wing area (ft^2)	600.00
SFC	Specific fuel constant (lb/hr/lb)	0.371
T	Total engine thrust (lbf)	16000.00
T_e	Thrust per engine (lbf)	9065
V_i	Integral tanks volume (gal)	1515.15
V_p	Self-sealing protect tank volume (gal)	1515.15
V_t	Total fuel volume (gal)	1515.15
W	Total fuselage width (ft)	5.83
W_{dg}	Flight design gross weight (lbs)	40260.00
W_{en}	Engine weight, single (lbs)	1440.00
W_l	Landing gear gross weight (lbs)	33380.00
W_{uav}	Uninstalled avionic weight (lbs)	800
Λ	Wing sweep at 25% MAC	0.00
Λ_{vt}	VT sweep at 25% MAC	25.00
λ_{wing}	Wing taper ratio	0.82

Appendix F – Drag Breakdown Code

Contents

```
close all
clear
clc
```

Givens

```
W0 = 50000; % lbs, MTOW
W_clean = 32600; % lbs, clean TOW
AR = 6; % Wing aspect ratio
cL_max = 1.6; % max lift coeff., clean
l_fus = 50; % ft, fuselage length
l_n = 10.8; % ft, nacelle length
cbar = 9.65; % ft, wing mean geometric chord
cbar_h = 5; % ft, HT mean geometric chord
cbar_v = 5.15; % ft, VT mean geometric chord
sweep_25 = 0; % deg, wing sweep at quarter chord
sweep_h25 = 0; % deg, HT sweep at quarter chord
sweep_v25 = 15.11; % deg, VT sweep at quarter chord

U1 = 590; % ft/s, cruise speed
rho = 23.77e-4; % slugs/ft3, SL air density
mu = 3.737e-7; % slug/ft-s, dynamic viscosity of air
M_cruise = 0.52; % Cruise mach number
q_bar = rho * U1^2 / 2; % lbf/ft2, cruise dynamice pressure
```

Areas

Wing

```
Swet_w = 162664/144; % ft2, wing wetted area
Sref_w = 600; % ft2, wing ref area

% Fuselage
Swet_fus = (124638+13526.5) / 144; % ft2

% Horizontal tail
```

```matlab
Swet_h = 26340.4/144; % ft2

% Vertical tail
Swet_v = 2 * 18855.9/144; % ft2

% Nacelle
Swet_n = 60224.3/144; % ft2

% Misc.
Swet_clust = 5507.63/144; % ft2, cluster wetted area
Swet_tank = 2 * 20446.9/144; % ft2, drop tank wetted area
Swet_bomb = 2 * 2918.56/144; % ft2, bomb wetted area
Swet_agm = 2 * 21174.8/144; % ft2, 3x AGM w/ rack wetted area
Swet_rp = 2 * 4305.38/144; % ft2, rocket pod awetted area
Swet_ecm = 7431.9/144; % ft2, ECM wetted area
Swet_gbu = 7258.66/144; % ft2, GBU wetted area

% All component areas
Swetc = [Swet_fus Swet_w Swet_h Swet_v Swet_n];
```

Parasite drag prediction

```matlab
Swet_ac = sum(Swetc); % ft2, estimated total aircraft wetted area

cfe = .0035; % Equiv. skin-friction coeff., Raymer, Table 12.3, AF Fighter

cD0_est = cfe * ((Swet_ac+Swet_clust+Swet_tank+Swet_bomb+Swet_agm...
        +Swet_rp+Swet_ecm+Swet_gbu) / Sref_w);

cD0_est_clean = cfe * (Swet_ac/ Sref_w);

fprintf('Estimated total parasite drag coefficient: %.4f\n', cD0_est)
fprintf('Estimated parasite drag coefficient, clean: %.4f\n', cD0_est_clean)
fprintf('\n')
```

```
Estimated total parasite drag coefficient: 0.0220
Estimated parasite drag coefficient, clean: 0.0172
```

Flate-plate skin-friction coefficient, cf

```matlab
k = 2.08e-5; % ft, skin roughness, smooth paint, Raymer, Table 12.5

% Fuselage
Re_fus = rho * U1 * l_fus / mu;         % Re, reynolds number
Re_cut_fus = 38.21 * (l_fus/k)^1.053;   % Re, cutoff reynolds number
cf_fus = .455 / (log10(max([Re_fus Re_cut_fus]))^2.58 *...
    (1+.144*M_cruise^2)^.65); % skin-friction coeff.

% Wing
Re_w = rho * U1 * cbar / mu;     % Re, Wing reynolds number
cf_w = 1.328 / sqrt(Re_w); % skin-friction coeff.

% Horizontal tail
Re_h = rho * U1 * cbar_h / mu;      % Re, Horizontal tail reynolds number
cf_h = 1.328 / sqrt(Re_h); % skin-friction coeff.
```

```
% Vertical tail
Re_v = rho * U1 * cbar_v / mu;        % Re, Vertical tail reynolds number
cf_v = 1.328 / sqrt(Re_v); % skin-friction coeff.

% Nacelle
Re_n = rho * U1 * l_n / mu;          % Re, reynolds number
Re_cut_n = 38.21 * (l_n/k)^1.053;    % Re, cutoff reynolds number
cf_n = .455 / (log10(max([Re_n Re_cut_n]))^2.58 *...
    (1+.144*M_cruise^2)^.65); % skin-friction coeff.

% All component of skin friction
cfc = [cf_fus cf_w cf_h cf_v cf_n];
```

Form Factor, FF

```
xc_m = 0.3; % chordwise location of max thickness

% Fuselage
Amax_fus = 7672.14/144; % ft2, max x-section area, fuselage
f_fus = l_fus / sqrt((4/pi)*Amax_fus);
FF_fus = .9 + 5/f_fus^1.5 + f_fus/400;

% Wing
tc_wing = (.15+.18) / 2; % average wing max thickness per chord length
FF_w = (1 + .6/xc_m*tc_wing + 100*tc_wing^4) *...
    (1.34*M_cruise^.18*cosd(sweep_25)^.28);

% Horizontal tail
tc_hv = .12; % HT/VT max thickness per chord length
FF_h = (1 + .6/xc_m*tc_hv + 100*tc_hv^4) *...
    (1.34*M_cruise^.18*cosd(sweep_h25)^.28);

% Vertical tail
FF_v = (1 + .6/xc_m*tc_hv + 100*tc_hv^4) *...
    (1.34*M_cruise^.18*cosd(sweep_v25)^.28);

% Nacelle
Amax_nac = pi * (66.75/2/12)^2; % ft2, max x-section area, nacelle
l_nac = 130/12; % ft, nacelle length
f_nac = l_nac / sqrt((4/pi)*Amax_nac);
FF_nac = 1 + (.35/f_nac);

% All component of form factor
FFc = [FF_fus FF_w FF_h FF_v FF_nac];
```

Interference Drag, Q

```
Q_nac = 1.5;     % interference factor between nacelle and fueslage
Q_wing = 1.0;    % interference factor between wing and fueslage
Q_fus = 1.0;     % interference factor of fusealge
Q_tail = 1.08;   % interference factor between tail and fueslage

% All component interference drag
Qc = [Q_fus Q_wing Q_tail Q_tail Q_nac];
```

Miscellaneous Drag, cD_X

```
A_drop_tank = .25 * pi * (30/12)^2; % ft2, frontal area, drop tank
Dq_drop_tank = .7; % ft2, drag area, drop tanks
D0_drop_tank = Dq_drop_tank / Sref_w; % drag of drop tank


A_bombs = 6 * pi * .5^2; % ft2, frontal area, 6x bombs
Dq_bombs = 1.1; % ft2, drag area, bombs/rockets
D0_bombs = Dq_bombs/ Sref_w; % drag of bombs


A_mis = .25 * pi * (12.07/12)^2; % ft2, frontal area, missile
Dq_mis = .11; % ft2, drag area, missile and pylon
D0_mis = Dq_mis/ Sref_w; % drag of missiles


A_fuspy = (5*6) / 144; % ft2, frontal area, fuselage pylon
Dq_fuspy = .09; % fuselage store pylons
D0_fuspy = Dq_fuspy/ Sref_w; % drag of fuselage pylon


A_wpy = (5*12) / 144; % ft2, frontal area, wing pylon
Dq_wpy = .11; % wing store pylons
D0_wpy = Dq_wpy / Sref_w; % drag of wing pylon


cD0_misc = 2*D0_drop_tank + D0_bombs + D0_mis + D0_fuspy + D0_wpy;
```

Leakage and Protuberance Drag, cD0_LP

```
cD0_LP = 0.20 / Sref_w; % Drag of cannon port
```

Windmilling Engine Drag

```
A_eng = 15.2; % ft2, engine front face area
Dq_windj = 0.3 * A_eng; % ft2, drag area, windmilling jet engine
cD0_windj = 2 * Dq_windj / Sref_w; % engine windmill drag
```

Induced drag

```
e = 1.78 * (1-.045*AR^.68) - .64; % Oswald efficiency, straight wing
K = 1 / (pi*AR*e);
cL1 = .97*W_clean / (q_bar*Sref_w); % Coeff. of lift at clean cruise
cDi = K * cL1^2; % Induced drag coeff.
```

Total drag of aircraft

```
CD_fus = cf_fus*FF_fus*Q_fus*Swet_fus/Sref_w;
CD_wing = cf_w*FF_w*Q_wing*Swet_w/Sref_w;
CD_nac = cf_n*FF_nac*Q_nac*Swet_n/Sref_w;
CD_h = cf_h*FF_h*Q_tail*Swet_h/Sref_w;
CD_v = cf_v*FF_v*Q_tail*Swet_v/Sref_w;
CD_ac = CD_fus+CD_wing+CD_nac+CD_h+CD_v;


CD0_op = sum(cfc .* FFc .* Qc .* Swetc)/Sref_w + cDi + cD0_misc + cD0_LP;
CD0_wm = sum(cfc .* FFc .* Qc .* Swetc)/Sref_w ...
    + cDi + cD0_misc + cD0_LP + cD0_windj;
```

Ouput

```
fprintf('Fuselage parasite drag coefficient: %.4f\n', CD_fus)
fprintf('Wing parasite drag coefficient: %.4f\n', CD_wing)
fprintf('Nacelle parasite drag coefficient: %.4f\n', CD_nac)
fprintf('Horizontal tail parasite drag coefficient: %.4f\n', CD_h)
fprintf('Vertical tail parasite drag coefficient: %.4f\n', CD_v)
fprintf('Miscellaneous parasite drag coefficient: %.4f\n', cD0_misc)
fprintf('L&P parasite drag coefficient: %.4f\n', cD0_LP)
fprintf('Induced drag coefficient: %.4f\n', cDi)
fprintf('Clean aircraft parasite drag coefficient: %.4f\n', CD_ac+cD0_LP)
fprintf('Loaded aircraft parasite drag coefficient: %.4f\n', CD0_op-cDi)
fprintf('\n')
fprintf('Total parasite+induced drag coefficient: %.4f\n', CD0_op)
fprintf('Total parasite+induced drag coefficient w/ windmilling: %.4f\n'...
        , CD0_wm)
fprintf('\n')
fprintf('Clean, cruise coefficient of lift: %.4f\n', cL1)
fprintf('Clean, cruise L/D: %.4f\n', cL1/(CD_ac+cDi))
```

```
Fuselage parasite drag coefficient: 0.0038
Wing parasite drag coefficient: 0.0007
Nacelle parasite drag coefficient: 0.0029
Horizontal tail parasite drag coefficient: 0.0002
Vertical tail parasite drag coefficient: 0.0002
Miscellaneous parasite drag coefficient: 0.0047
L&P parasite drag coefficient: 0.0003
Induced drag coefficient: 0.0010
Clean aircraft parasite drag coefficient: 0.0081
Loaded aircraft parasite drag coefficient: 0.0128

Total parasite+induced drag coefficient: 0.0138
Total parasite+induced drag coefficient w/ windmilling: 0.0290

Clean, cruise coefficient of lift: 0.1274
Clean, cruise L/D: 14.5836
```

Appendix G – Performance Calculations

```
close all
clear
clc
```

Stall Speed

```
% Max Coeff. of Lift(s)
cL_max = [1.6 1.8 2.0];

% Givens
W0 = 50000;                 % lbs, total Weight
rho_stall = 23.77e-4;       % slugs/ft3, density of air at SL
% rho_stall = 20.48e-4;      % slugs/ft3, air density @ 5000 ft alt
S = 600;                    % ft^2, wing ref area
                            % Wing loading 98 > 90, wingspan 57.5 > 60 ft
AR = 6;                     % Wing aspect ratio
g = 32.2;                   % ft/s2, gravity
v_cruise = 590.7;           % ft/s, cruise speed
cD0 = [.0445 .0954 .0095];  % cD0 @ takeoff, land, clean
e = [.8 .76 .72];           % oswald efficiency @ takeoff, land, clean

% Calculate stall speeds
v_stall = zeros(1,length(cL_max)); % Pre-allocation
for i = 1:1:length(cL_max)
    v_stall(i) = sqrt(2*W0 / (rho_stall*cL_max(i)*S)); %ft/s
end

v_stall_kt = .592 .* v_stall;       % stall speed in knots
R_spec = 1716.49;                   % ft-lbf/slug-R
temp = 518.67;                      % R, temperature at SL
gamma = 1.4;                        % specific heat ratio for air
c = sqrt(gamma*R_spec*temp);        % ft/s, speed of sound
v_stall_M = v_stall ./ c;           % stall speed in Mach

fprintf('Stall speeds at CLmax of 1.6, 1.8, 2.0, respectively:\n')
fprintf('Stall speed in fps: %.2f, %.2f, %.2f\n',...
    v_stall(1), v_stall(2), v_stall(3))
fprintf('Stall speed in knots: %.2f, %.2f, %.2f\n',...
    v_stall_kt(1), v_stall_kt(2), v_stall_kt(3))
fprintf('Stall speed in mach: %.2f, %.2f, %.2f\n',...
    v_stall_M(1), v_stall_M(2), v_stall_M(3))
fprintf('\n')
```

```
Stall speeds at CLmax of 1.6, 1.8, 2.0, respectively:
Stall speed in fps: 209.34, 197.37, 187.24
Stall speed in knots: 123.93, 116.84, 110.85
Stall speed in mach: 0.19, 0.18, 0.17
```

Take-off distance

```
% Coefficients
f_TO = 1.0;
h_TO = 50;          % ft, obstacle clearance height
V3_V_STO = 1.15;    % ratio of speed at h_TO and stall speed (V3)in
                    % takeoff condition
WS_TO = 90;         % lbs/ft2, wing loading at takeoff
T_TO = 8500*2;      % lb, max static thrust at takeoff
lamda = 5;          % engine bypass ratio

% thrust-to-weight ratio at takeoff
T_bar = .75*T_TO * (5*lamda)/(4+lamda);
TW_TO = T_bar/W0;

mu_g = 0.02; % wheel-ground rolling friction coeff for concrete/asphault
cD_0 = .0445; % zero lift drag coeff.
gamma_LOF = 0.9*TW_TO - 0.3/sqrt(AR);
mu_prime = mu_g + .72*(cD_0/cL_max(2));

% Takeoff distance
s_TO = f_TO*h_TO*((1/gamma_LOF) + (V3_V_STO^2*WS_TO*(1/(TW_TO-mu_prime)...
        +1.414))...
        / (h_TO*rho_stall*g*cL_max(2)*(1+1.414*gamma_LOF)));

% Ground run distance
V_LOF = 1.1*v_stall(2);
s_TOG = (V_LOF^2/(2*g)) / (TW_TO-mu_prime);

fprintf('Takeoff distance: %.2f ft\n',s_TO)
fprintf('Ground run distance: %.2f ft\n',s_TOG)
fprintf('\n')
```

```
Takeoff distance: 1549.44 ft
Ground run distance: 1091.51 ft
```

Climb

```
U1 = 1.3 * v_stall(1); % ft/s, steady speed
U1_max = 675; % ft/s, max speed 400 knots
TW_clean = 0.3839; % thrust-to-weight ratio, clean config
L_D = 15; % Max lift-drag ratio
RC = 60*U1 * (TW_clean - 1/L_D);    % fpm, rate of climb
RC_max = 60*U1_max * (TW_clean - 1/L_D);    % fpm, rate of climb
CGR = TW_clean - 1/L_D;             % climb gradient

% Absolute ceiling
```

```matlab
h_abs = 50000; % ft, absolute altitude
t_cl_abs = 1/RC * h_abs; % min, time to climb to absolute altitude

% Service ceiling
h_serv = 45000; % ft, service altitude
t_cl_serv = 1/RC * h_serv; % min, time to climb to service altitude

% Combat ceiling
h_comb = 19500; % ft, combat altitude
t_cl_comb = 1/RC * h_comb; % min, time to climb to combat altitude

% cruise celing
h_cruise = 30000; % ft, cruising altitude
t_cl_cruise = 1/RC * h_cruise; % min, time to climb to cruise altitude

% Specific excess power
Ps = U1 * CGR; % ft/s

fprintf('Rate of climb: %.2f ft/min\n',RC)
fprintf('Rate of climb at 400 knots: %.2f ft/min\n',RC_max)
fprintf('Climb gradient: %.2f\n',CGR)
fprintf('Time to absolute ceiling: %.2f min\n',t_cl_abs)
fprintf('Time to service ceiling: %.2f min\n',t_cl_serv)
fprintf('Time to combat ceiling: %.2f min\n',t_cl_comb)
fprintf('Time to cruise ceiling: %.2f min\n',t_cl_cruise)
fprintf('Excess power: %.2f ft/s\n',Ps)
fprintf('\n')
```

```
Rate of climb: 5179.92 ft/min
Rate of climb at 400 knots: 12847.95 ft/min
Climb gradient: 0.32
Time to absolute ceiling: 9.65 min
Time to service ceiling: 8.69 min
Time to combat ceiling: 3.76 min
Time to cruise ceiling: 5.79 min
Excess power: 86.33 ft/s
```

Cruise and Range

```matlab
SFC = .5565; % lbm/lbf/hr, Specific fuel consumption
W0_clean = 24000 + .98*8600; % Total weight, fuel and aircraft only
% W0_clean = 50000; % MTOW

% Range at constant altitude
LD_cr = .9 * L_D;  % cruise lift-drag ratio
rho_cruise = 8.91e-4; % slugs/ft3, air density at 30k ft
f_mj = 1.677;
q_bar = rho_cruise * v_cruise^2 / 2; % lbf/ft2, cruise dynamice pressure
cL1 = W0 / (q_bar*S); % Coeff. of lift at cruise
cD_cr = cL1/LD_cr; % Cruise coeff. of drag
W_end = 24000 + .1 * 8600; % lbs, ending weight
% W_end = 50000-30000; % lbs, ending weight

R_alt = (f_mj/SFC)*1/sqrt(rho_cruise*S) * (sqrt(cL1)/cD_cr) * ...
    (sqrt(W0_clean) - sqrt(W_end)); % nm, Range at constant altitude

% nm, Range at constant speed
```

```
v_cruise_kt = 350; % knots, cruise speed
R_speed = (v_cruise_kt/SFC) * LD_cr*log(W0_clean/W_end);

fprintf('Range at constant altitude (30000 ft): %.2f nm\n',R_alt)
fprintf('Range at constant speed (350 knots): %.2f nm\n',R_speed)
fprintf('\n')
```

```
Range at constant altitude (30000 ft): 1702.77 nm
Range at constant speed (350 knots): 2256.47 nm
```

Endurance and Loiter

```
% Endurance at constant altitude/speed
E_true = (1/SFC) * LD_cr * log(W0_clean/W_end); % hrs
E = (1/SFC) * LD_cr * log((W0_clean-.75*8600)/W_end); % hrs

fprintf('Total endurance of aircraft (SFC=%.3f): %.2f hours\n',SFC,E_true)
fprintf('Loiter time before landing (SFC=%.3f): %.2f hours\n',SFC,E)
fprintf('\n')
```

```
Total endurance of aircraft (SFC=0.556): 6.45 hours
Loiter time before landing (SFC=0.556): 1.07 hours
```

Dive - No performance related requirements for military aircraft

Maneuvering

```
rho_turn = 20.48e-4; % slugs/ft3

% g-loading
n = [2;       % sustain
     6];      % instant

% turn rate, deg/s
psid = [5;        % sustain
        23];      % instant
psid = psid .* pi/180; % rad/s

R_t = zeros(length(n),1);
U_turn = zeros(length(n),1);
for i = 1:1:length(n)
    U_turn(i) = g*sqrt(n(i)^2-1) / psid(i);     % ft/s, turn speed
    R_t(i) = U_turn(i)^2 / (g*sqrt(n(i)^2-1));  % ft, turn radius
end

fprintf('Sustain turn ft @ 2Gs, 5 deg/s: %.2f knots\n',U_turn(1)*.592)
fprintf('Sustain turn radius @ 2Gs, 5 deg/s: %.2f ft\n',R_t(1))
fprintf('Instant turn speed @ 6Gs, 20 deg/s: %.2f knots\n',U_turn(2)*.592)
fprintf('Instant turn radius @ 6Gs, 20 deg/s: %.2f ft\n',R_t(2))
fprintf('\n')
```

```
Sustain turn ft @ 2Gs, 5 deg/s: 378.35 knots
Sustain turn radius @ 2Gs, 5 deg/s: 7323.55 ft
Instant turn speed @ 6Gs, 20 deg/s: 280.94 knots
Instant turn radius @ 6Gs, 20 deg/s: 1182.17 ft
```

185

Descent and glide - Range credit for descents by

subsonic military aircraft disallowed.

Landing

```
gamma_bar = .10;
V_A = 1.2 * v_stall(3); % ft/s, Approach speed
del_n = .10;
V_TD = V_A * sqrt(1-(gamma_bar^2/del_n));
h_L = h_TO; % ft, Obstacle height clearance
a_bar = 0.4*g; % ft/s2, decelaration for ground run

S_air = (1/gamma_bar) * ((V_A^2 - V_TD^2)/(2*g)+h_L); % ft, dist in air
S_LG = V_TD^2 / (2*a_bar); % ft, landing ground run distance to zero speed

S_L = S_air + S_LG; % ft, landing distance

fprintf('Total landing distance: %.2f ft\n',S_L)
fprintf('Roll landing distance: %.2f ft\n',S_LG)
fprintf('\n')
```

```
Total landing distance: 3047.71 ft
Roll landing distance: 1763.80 ft
```

Published with MATLAB® R2021a

186

Appendix H – Cost Analysis; Raymer Method

Contents

```
close all
clear
clc
```

Cost Rates, 2020

```
Re = 144;    % $/hr, Engineering cost
Rt = 148;    % $/hr, Tooling cost
Rq = 135;    % $/hr, Quality cost
Rm = 123;    % $/hr, Manufacturing cost
```

Aircraft inputs

```
W0 = 50000;                    % lbs, TOW
We = 24112;                    % lbs, empty weight
Wf = 8600;                     % lbs, fuel weight
V = 400;                       % knots, max speed
Vc = 350;                      % knots, cruise speed
Q = 10*12*5;                   % # of aircraft produced in 5 yrs
FTA = 5;                       % # of flight test aircraft
N_eng = 2;                     % # of engines per aircraft
T_max = 9065;                  % lbf, max thrust per engine
M_max = 0.6;                   % Max mach number of engine
T_turb_in = 3460;              % R, engine inlet temperature
C_avionics = (4000+8000)/2 * We;  % $, Cost of avionics
```

Hours calculation

```
He = 4.86*We^.777 * V^.894 * Q^.163; % Engineering hours
Ht = 5.99*We^.777 * V^.696 * Q^.163; % Tooling hours
Hm = 7.37*We^.82 * V^.484 * Q^.641;  % Mfg hours
Hq = .133; % QA hours
```

Other costs

```
CD = 91.3*We^.63 * V^1.3;                % $, Development support cost
CF = 2498*We^.325 * V^.822 * FTA ^1.21;  % $, Flight test cost
CM = 22.1*We^.921 * V^.621 * Q^.799;     % $, Mfg material cost
```

```
% $, Engine production cost
C_eng = 3112* (.043*T_max + 243.25*M_max + .969*T_turb_in - 2228);
```

$, Total RDTE and Flyaway Cost

```
RDTE_Flyaway = He*Re + Ht*Rt + Hm*Rm + Hq*Rq + CD + CF + CM + C_eng*N_eng;
```

Fuel cost

```
Hf = 216*1.5;        % hrs/yr/ac, Flight hours per year per aircraft
SFC = .371;          % lbm/lbf/hr, Specific fuel consumption
C_fuel = 4.29;       % $/gal, fuel cost per gallon
p_fuel = 6.74;       % lbs/gal, fuel density

% $/yr, Total fuel cost per year
C_tot_fuel = Q * Hf * (C_fuel/p_fuel) * SFC;
```

Crew cost

```
N_crew = 2; % Crew size per aircraft
N_serv = 1.1 * Q * N_crew; % Total # of crew members in service
Hc = 2080; % hrs, crew flight hours per year
C_serv = Re * 2080 * N_serv; % $, Total crew cost per yr
```

Maintenance Cost

```
Hmm = (10+15)/2; % Maintenance manhours per flight hour
Ca = (RDTE_Flyaway - (C_eng*N_eng)) / Q; % $, cost per aircraft w/o engine

% $/FH, Material cost per flight hour
C_mat_FH = (3.3*(Ca/(10^6))) + 14.2 + (58*(C_eng/(10^6))-26.1)*N_eng;

% $/yr, Total maintenance cost per year
C_main = C_mat_FH * Hf * Q;

C_op = (C_tot_fuel + C_main + C_serv) / Hf;
```

Display Results

```
fprintf('RDTE and Flyaway Total Cost: $%.2d\n',RDTE_Flyaway)
fprintf('Aircraft Unit Cost: $%.2d\n',RDTE_Flyaway/Q)
fprintf('Total fuel cost per year: $%.2d per year\n',C_tot_fuel)
fprintf('Total crew cost per year: $%.2d per year\n',C_serv)
fprintf('Total maintenance cost per year: $%.2d per year\n',C_main)
fprintf('Operational cost per year: $%.2d per year\n',C_op)
```

```
RDTE and Flyaway Total Cost: $7.23e+09
Aircraft Unit Cost: $1.20e+07
Total fuel cost per year: $4.59e+04 per year
Total crew cost per year: $395366400 per year
```

```
Total maintenance cost per year: $1.17e+08 per year
Operational cost per year: $1.58e+06 per year
```

Appendix I – Turning Performance Calculation

Contents

```
close all
clear
clc

W0 = .97*32600 + 3000; % lbs, Clean flight weight with ammo
S = 600; % Wing loading 98 > 90, wingspan 57.5 > 60 ft
g = 32.2; % ft/s2, gravity
U1 = 250:5:800; % ft/s, turn speeds
rho = 20.48e-4; % slugs/ft3, air density @ 5000 ft alt
cD0 = .0128;
AR = 6; % Wing aspect ratio
e = [.8 .76 .72]; %  oswald efficiency @ takeoff, land, clean

q_bar_turn = rho .* U1.^2 ./ 2; % lbf/ft2, cruise dynamic pressure
cL1 = W0 ./ (q_bar_turn.*S); % Lift coeff. @ specific turn speed
cL_max = 1.6; % Max coefficient of lift
```

Turn Speed Analysis, deg/s

```
n_instant = 6; % g-loading @ varying turn speed
psid_speed = zeros(n_instant, length(U1));  % deg/s,  Turn rate per speed
                                  % pre-allocation

for i = 1:1:n_instant
    for j = 1:1:length(U1)
        psid_speed(i,j) = g * sqrt(i^2-1) ./ U1(j); % rad/s, turn rate
    end
end
psid_speed = psid_speed .* (180/pi);    % deg/s, turn rate

V_D = 1.25 * 625; % ft/s, max dive speed
V = .1:.1:V_D; % ft/s, speed range
Vs = sqrt((2*W0) / (rho*S*cL_max));
ns = 1/Vs * V; % load factor at stall per speed
psid_stall = zeros(length(Vs), 1);    % deg/s,  Turn rate per stall
                                    % speed pre-allocation

for i = 1:1:length(ns)
    psid_stall(i) = g * sqrt(ns(i).^2-1) / Vs; % rad/s, turn rate
end
psid_stall = psid_stall .* (180/pi);    % deg/s, turn rate
```

Sustain Turn Power

K = 1 / (pi*AR*e(3)); % drag due to lift factor Ps = 86.33; % ft/s, excess power T_max = 590; % lbf, max thrust D = T_max; % lbs, max drag V_sus = sqrt(2*D / (rho*S*cD0)); % ft/s qbar_sus = rho * V_sus^2 / 2; %lbf/ft2, sustain dynamic pressure n_sus = qbar_sus*S*cL_max / W0; psid_sus = g * sqrt((n_sus.^2-1) ./ Vs); % rad/s, Turn rate per stall % speed pre-allocation psid_sus = psid_sus .* (180/pi); % deg/s, turn rate

fprintf('Sustained Turn Speed: %.2f ft/s\n', V_sus) fprintf('G-load during Sustained Turn: %.2f Gs\n', n_sus) fprintf('Turn Rate: %.2f deg/s\n', psid_sus)

```
cD0_sus = 0.0128; % drag coefficient
V_sus = (100:5:450) .* 1.69; % ft/s, sustain speed
n_sus = zeros(length(V_sus),1);
outputx = zeros(length(V_sus),1);
outputy = zeros(length(V_sus),1);
output_T = zeros(length(V_sus),1);
iter = zeros(length(V_sus),1);
T_avail = 17300; % lbf, Available thrust

for i = 1:1:length(V_sus)
    V_in = V_sus(i);
    n_in = 1;
    T_reqd = 0;
    j = 0;

    while T_reqd < T_avail
        j = j+1; % iteration counter
        output_T(i) = T_reqd; % lbf, Final thrust output per speed
        n_in = n_in + 0.1; % load-factor
        n_sus(i) = n_in;
        psid_sus = (g * sqrt(n_in^2-1) / V_in) * 180/pi; % deg/s, sustain
                                                  % turn rate
        cL_sus = 2*n_in*W0 / (rho*V_in^2*S); % sustain lift coeff of
                                        % speed and load
        qbar_sus = rho * V_in^2 / 2; % lbf/ft2-s, sustain dynamic pressure
        T_reqd = (.0128 + cL_sus^2/(pi*AR*.8)) * qbar_sus * S; % lbf, Thrust rerquired during sustain turn
    end

    iter(i) = j;
    outputx(i) = V_in / 1.69;
    outputy(i) = psid_sus;
end

p = polyfit(outputx, outputy, 10);
sustain_y = polyval(p, outputx);
```

```
Warning: Polynomial is badly conditioned. Add points with distinct X values,
reduce the degree of the polynomial, or try centering and scaling as described
in HELP POLYFIT.
```

Plot

```
figure(1)
for i = 2:1:n_instant
    plot(U1/1.69 , psid_speed(i,:), 'LineWidth', 3)
    hold on
end

plot(V/1.69 , psid_stall, ':', 'LineWidth', 2)
% plot(outputx, outputy, 'o')
plot(outputx, sustain_y, '--', 'LineWidth', 3)

xlabel('Turn Speed, knots', 'Fontsize', 15)
ylabel('Turn Rate, deg/s', 'Fontsize', 15)
```

```
title('Energy Maneuver Diagram', 'Fontsize', 17)
legend('Acceleration Limit (2-Gs)',...
    'Acceleration Limit (3-Gs)',...
    'Acceleration Limit (4-Gs)',...
    'Acceleration Limit (5-Gs)',...
    'Acceleration Limit (6-Gs)',...
    'Stall Limit',...
    'Sustain Turn Limit',...
    'Location', 'eastoutside', 'Fontsize', 12)
ylim([0 40])
grid on
hold off
```

Warning: Imaginary parts of complex X and/or Y arguments ignored.